Nanoindentation as a method to interrogate the mechanical properties of polymer coatings

Ekers, Tanya Wilhelmina

Nanoindentation as a Method to Interrogate the Mechanical Properties of Polymer Coatings

Tanya Wilhelmina Ekers

School of Engineering and Materials Science

Queen Mary, University of London

Supervised by Dr. Andy Bushby

Submitted in partial fulfilment of the requirements for the degree of Doctor of Philosophy from Queen Mary, University of London

Abstract

Polymer coatings are widely used in many industrial applications such as coatings on car bodies and refrigerators, and as varnishes on floor coverings and wood. As protective coverings polymer coatings are subject to wear and degradation making their mechanical properties a key performance indicator. Mechanical properties of non-polymeric coatings can be successfully determined using nanoindentation. However, the time-dependent nature of the mechanical properties of polymers requires a different approach to that used for time-independent materials. Spherical nanoindentation using a ramp and hold load method and creep analysis was compared to tensile testing and has produced results that fully characterise the time-dependent mechanical response. Using this method differences in mechanical properties between different polymers as well as the changes in mechanical properties due to degradation and aging were distinguished. In conventional instrumented indentation tests contact areas are calculated from the measured depth based on Hertzian contact mechanics. Finite element analysis has suggested that spherical indentation is indeed Hertzian for visco-elastic materials. Direct observations of the contact area of visco-elastic materials under load were made simultaneously with depth measurements by indenting transparent polymers at a macro-scale. This novel approach suggested that for some polymers spherical indentation can be non-Hertzian. It appears that the ramp load times as well as surface properties contribute to the non-Hertzian contact. Consequently, moduli obtained from nanoindentation tests may not always be directly comparable to moduli obtained from tensile tests. These results will support the development of standard nanoindentation test procedures for visco-elastic polymers.

Table of Contents

List of Figures

List of Tables

Acknowledgements

I would like to thank my supervisor, Dr. A. Bushby for his advice, support, expertise and for getting me here. Thank you so much. Thanks to EPSRC for funding. Thanks to Akzo Nobel (ICI) for sponsorship and particularly to Dr. P. Dooling and Dr. J. Carter for help and support. Big thanks to Bill Godwin for construction and help with the design of the macroindentation test rig. Thanks to Dr. M. Oyen for initial discussions and advice. Thanks for help and advice to Prof. D. Dunstan, to Dr. K. P'ng who also helped me to get started on the experimental work and to Dr. C. Walker. Thank you to Dr. M. Monclus at NPL for glass measurements. Thank you to Dr. W. Tu and Dr. J. Busfield for help with FEA, to Dr. N. Roohpour and Dr. E Bilotti for help with DMA and to all those at Queen Mary, University of London who have helped and assisted in so many ways. Not least, thanks also to my husband, Bob, for all your support and to all my family and friends, particularly my friends and colleagues Dr. T Zhu, Dr. X. Hou and Dr. J. Luo.

In memory of my father, H. J. C. van Veen, with love.

1 Introduction

Polymer coatings are very widely used, for example on floors, wood, glass, car bodies, appliances such as washing machines and refrigerators, and food containers. Coatings may be decorative as well as functional with a wide range of demands e.g. corrosion protection, abrasion protection, skid resistivity. Coatings are generally termed organic or inorganic, often with overlap as many consist of inorganic pigments in an organic matrix called the binder. The binder is the basis of the coating and it holds the constituents together. As well as containing pigments, many coatings are filled with other additives to change their properties.

Coatings that are not based on organic binders, such as enamel coatings, are not considered here. This work considers the organic binders, in particular unfilled coatings such as wood floor varnishes and basic polymer binders.

Varnishes and the majority of coatings during their time of service may be subject to small localised forces as rapid impact such as ‘knocks’ and dents, and to slow periodic deformations due to swelling and shrinking of the wood substrate according to atmospheric conditions. Consequently, it is important to have a full understanding of the mechanical properties and the age related and environmentally related behaviour and degradation of such coatings.

Continual exposure to air and water condensation on the coating surface leads to leaching of low molecular weight polymeric species and retained solvent or plasticizer. Degradation products may also leach and leave the coating more susceptible to brittle cracking.

The ultra violet radiation of light can promote various photolytic reactions and may result in the formation of free radicals and peroxides which, due to the resulting increase in cross-linking, increases the brittleness of the film.

Both solvent loss and cross-linking can lead to shrinkage of the polymer matrix, with the result that internal stresses build up within the film. Therefore results of testing a coating as a detached film may not be relevant when following age and environmentally related mechanical changes (Strivens 1999).

The traditional test to determine mechanical properties is conventional tensile testing. This is not possible for coatings attached to substrates nor is it relevant for the coating as a free standing film as mentioned above. For these reasons experimental techniques and analytical methods have been developed to enable mechanical properties to be obtained from nanoindentation.

Nanoindentation based on Hertzian contact mechanics has proved to be a useful technique for probing the surface of many elastic materials in bulk and as coatings on a substrate such that standard test methods have now been prescribed (ISO14577). However, when the same techniques are extended to polymers their visco-elastic mechanical response has led to problems that remain to be addressed. For some polymers the modulus values calculated from nanoindentation tests have been found to be higher than given literature values which are obtained from standard tensile tests. It is not clear whether polymers are subject to scaling effects under nanoindentation. The contribution of adhesion and surface forces may also be significant. It may be that Hertzian contact theory cannot cope with the time dependent response of polymers, or that it is applicable only under particular circumstances.

With regard to these issues this thesis will explore :-

- the theory describing the visco-elastic mechanical response of polymers
- instrumented indentation and the associated contact mechanics
- the application of nanoindentation as a technique to monitor age and environmental conditioning on polymer coatings
- the visco-elastic mechanical response of selected polymers under nanoindentation and compare this to the response to traditional tensile testing
- real measured contact parameters for polymers under spherical indentation and how these compare with assumed values
- modelled visco-elastic contact using finite element analysis.

2 Literature Review

2.1 Introduction

The mechanical properties of a polymer are dependent on its structure, so it is important to understand the structure-property relationship and how this determines the visco-elastic nature of a polymer. A brief overview of polymer structure and how this relates to mechanical properties, including creep, will be introduced in this chapter. A short description of some polymers commonly used as coatings will be given.

All polymers are visco-elastic, i.e. their response to stress is time dependent. This time dependent response to stress appears as creep. A description of creep will be given followed by a description of the mechanical models for visco-elastic behaviour and the derivation of the constitutive equations from these. A linearly visco-elastic response of a polymer is defined by the Boltzmann superposition principle which enables the behaviour of the polymer in response to a stress to be predicted at any time. This fundamental principle and its application to the experimental work presented in this thesis will be explained in this chapter as will elastic-visco-elastic correspondence theory and its usage in the analysis of the experimental work

Nanoindentation will then be reviewed with the emphasis on its application to polymer mechanics, the elastic-visco-elastic correspondence principle will be applied to spherical indentation and the suitability of nanoindentation testing for polymers will be examined.

2.2 Polymers

2.2.1 Polymer chemistry and structure relationship

A polymer molecule is a chain consisting of a series of repeated, linked, smaller units, called monomers. E.g 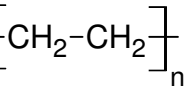 a simple ethylene monomer, where n is the number of ethylene monomers, in the region of 10^3 to 10^6.

The length, or degree of polymerisation, is proportional to the relative molecular mass, a longer chain has a greater average molecular mass and results in more chain entanglements. The structure of the polymer is dependent on that of its constituent monomers. The polymer chain may be linear, or have side branches or be cross-linked.

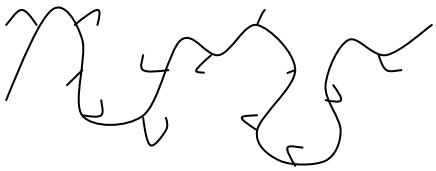

Figure 2.2-1Polymer chain with side branches

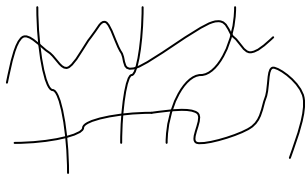

Figure 2.2-2 Cross-linked polymer network

A polymer may be composed of two or more different monomers, and termed a copolymer. These can be randomly arranged along the chain length or arranged in

blocks of like monomer units. Chains of one polymer type may be grafted onto a chain of the other. In this way polymers with different properties can be synthesised.

The shape of the polymer determines its packing efficiency. The packing of polymer molecules determines the structure of polymeric solids.

A polymer composed of linear molecules may have extensive secondary bond forces such as van der Waals forces and hydrogen bonding. These will act both intra-molecularly and inter-molecularly and affect packing. The side chains on a branched polymer reduce its packing efficiency and consequently its density. A cross-linked polymer may have covalent bonds between chains and form a three-dimensional network.

The orientation of the polymer chains to each other, and the strength of the intermolecular force between them, may result in chains ordered in three-dimensions. These regions are crystallites which are typically un-oriented and interspersed with amorphous regions. The degree of crystallinity has a significant affect on the properties of the polymer including the mechanical response. A semi-crystalline polymer will not be subject to the rules of linear visco-elasticity which apply to amorphous polymers. When a crystalline polymer is stressed the crystallites act as crosslinks in the polymer (Cowie 1991).

2.2.2 The free volume concept and molecular response to stress

A visco-elastic, polymeric, solid is a cohesion of flexible, threadlike molecules. Due to the great length of a polymer chain, it is possible for some of its sections to be in motion, so that it takes up more volume than its atomic dimensions. The mobility of the chain segments depends primarily on the degree of packing, or free volume.

The free volume concept of the mobility of particles in a packed system depends on the available free volume in which the particles can move, i.e. the degree of packing. As the packing increases, the transport mobility decreases. The decrease in mobility is initially slow but becomes more rapid so that at a critical packing level the mobility quickly falls towards zero.

For polymers, segmental mobility of the polymer chain is the equivalent to transport mobility. The flexibility of the chain controls the glass transition temperature and consequently the mechanical behaviour of a polymer.

At temperatures above the glass transition temperature a polymer behaves fluidly, segmental mobility is large so the free volume is large. As the polymer is cooled, the internal energy is reduced and both free volume and mobility decrease together.

When the glass transition temperature is reached, the mobility and free volume stop decreasing with decreasing temperature and this defines the glass transition temperature, T_g.

Below the glass transition temperature of the material the mobility becomes so small that free volume almost stops decreasing. The state of zero mobility can not be achieved as this would require zero free volume which depends on mobility.

However, due to the attraction between molecules, the presence of holes, or free volume, represents a state removed from equilibrium, *i.e.* an increase in internal energy with respect to the zero free volume state, so the free volume slowly continues to decrease and to approach the equilibrium state as the material ages.

Consequently, mechanical properties change with temperature and with aging of the material (Struik 1980).

An applied stress will move the entanglement of chains in the polymer network from its most energetically favourable arrangement. To enable the co-operative motion of the polymer chain segments in response to this stress there must be sufficient space, *i.e.* free volume, in which the segments can move. This movement, or flow, in sections of the chains builds up a back stress when the stress is held. When the original stress is removed, the back stress, after a period of time, will cause chain segments to diffuse back to their unstressed positions, i.e. recovery.

The slow continuous strain in response to stress is called creep, which together with elastic recovery defines visco-elasticity, a time-dependent mechanical response which will be discussed in Chapter 2.3. Conversely, the stress required to maintain an applied strain slowly decreases with time.

The movement of a chain through the entanglement of other moving chains has been described by a "reptation" model proposed by de Gennes (Cowie 1991). The chain is assumed to be in a hypothetical tube formed from the network of the other entangled chains. The chain within the tube undergoes conformational changes. Reptation is regarded as the movement of a kink in the chain along its length and imagined as a snake-like movement of the chain along the tube until it reaches the end and leaves it. The time taken for a chain to escape from its tube is termed the relaxation time, τ (Cowie 1991). Bulky, large side groups or monomer units can hinder segmental mobility and prevent the disentanglement of the polymer chain in response to an applied stress.

Typically, a linear amorphous polymer has five distinct regions of visco-elastic behaviour, determined by its molecular motion, which as described, depend on chain flexibility and temperature. See Figure 2.2-3.

Region **1**, the glassy state, is found at temperatures below the glass transition temperature; co-operative long range chain motion is in effect frozen. An applied stress may provide the necessary activation energy to enable side groups and limited sections of the chain to move or relax. Thus in region 1 movement is limited to short range vibrational motion and rotations. These are secondary relaxations and it has been suggested that these may improve the impact resistance of some materials (Cowie 1991). In this glassy state the polymer responds to an applied stress like an elastic solid, *i.e*. immediate strain in response to stress followed by recovery on removal of the stress as seen in Figure 2.2-3 (b).

As the temperature is increased the glass transition region **2** is reached and the modulus drops sharply, reflecting the constant increase in molecular motion as the temperature is increased above the glass transition temperature. At temperatures just above the glass transition temperature the chain movement is still slow and the polymer is said to have leathery properties as seen in the strain/time curves of Figure 2.2-3 (c).

Region **3** is at the flattening of the curve and the polymer is in a rubbery state.

As the temperature increases further the modulus again decreases, region **4**, and the state is rubbery flow. The stress response of the polymer in these states is instantaneous elastic followed by flow, shown in Figure 2.2-3 (d).

Above a certain temperature, region **5**, depending on the particular polymer there is a steady decrease in modulus with increasing temperature. The polymer exhibits very little elastic recovery and behaves like a viscous liquid. Figure 2.2-3 (e).

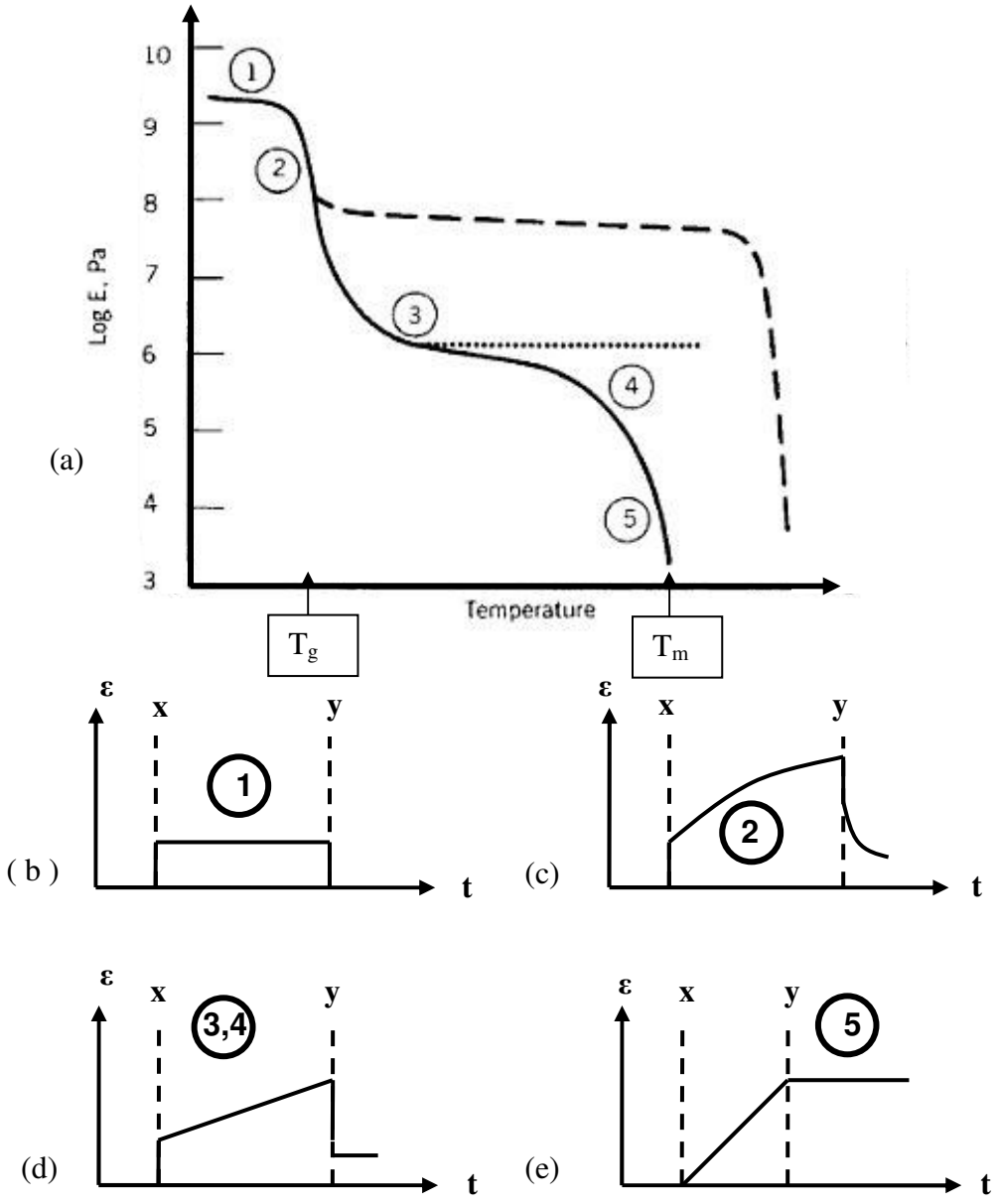

Figure 2.2-3 (a) Five regions of visco-elastic behaviour for a linear amorphous polymer also showing effects of crystallinity (dashed line) and cross-linking (dotted line) (Sperling 2006) with corresponding strain / time curves for stress applied at x and removed at y (b) glassy region; (c) leathery state; (d) rubbery state; and (e) viscous state (after Cowie 1991)

Cross-links between segments in the network of chains affect the mechanical behaviour of the polymer by acting as anchor points. Cross-links restrain slippage between chains and contribute to dimensional stability. They also affect the creep response and modulus at temperatures above the glass transition temperature, as seen

in Figure 2.2-3. Cross–linking has little effect on the mechanical behaviour below the glass transition temperature as the polymer chains are inherently frozen. Cross-linking enables a polymer to be fixed in a particular shape which is maintained on heating. The polymer is termed thermosetting. Polymers that soften on heating above their glass transition temperatures and are able to be re-shaped to cool and harden in their new form are termed thermoplastic.

Polymer mechanical properties are also affected by the presence of crystallites. Crystallites in a polymer matrix act as cross-links, however, as the temperature is raised segmental motion in the amorphous matrix is increased and melting does occur. Melting temperature is dependent on the degree of crystallinity.

2.2.3 Common polymers used in coatings

Most coatings are comprised of binder, which is the basis of the coating and holds the constituents together. The binder forms the film that coats the substrate and generally determines the properties of the film.

A solvent or volatile component is usually added to the binder which dissolves it, modifies the viscosity and enables the coating to be applied.

In addition, the coating may be filled with pigments which primarily provide colour and opacity to the film but also affect its properties.

Additives may also be included to affect the properties of the coating. Additives with a wide variety of chemistry and functions exist. The small quantities of the additives included may be catalysts for the polymerisation reaction, stabilizers, and flow modifiers. Plasticizers are frequently added to polymers; they dissolve in the polymer

and separate the chains thus making segmental chain movement easier. As a result the glass transition temperature is lowered, the rubbery plateau region modulus is lowered and, if the polymer is semi-crystalline, the melting temperature is lowered and, or, the amount of crystallinity is reduced.

However, the most important part of a coating is the binder. The coating name is based on the name of the binder. Slight changes in the chemistry of the binder can produce variation in physical and chemical properties of a coating.

The binder may be a copolymer with properties determined by the mutual solubility of the two covalently bonded homopolymers. If the component polymers are insoluble they exist as separate phases and two glass transition temperatures can be identified, *e.g.* polyurethane, in which there are hard and soft phases (Ward and Hadley 1996).

Polyurethane is a commonly used binder in which the size, interconnectivity and crystallinity of the hard domains, as well as the mixing of these in the soft phase, determines the mechanical response (Miller *et al.* 1985). Polyurethane based coatings are formed from an alcohol (R-OH) and an isocyanate (R-NCO). Aromatic and aliphatic isocyanates are commonly used. Polyurethane coatings based on aromatic isocyanates can be formulated to produce hard coatings with excellent chemical and heat resistance; however, exposure to sunlight leads to chalking of the coating and discolouration. Coatings based on aliphatic isocyanates have better weather and chemical resistance but they are slower to cure and are more expensive (Weldon 2001).

Examples of other commonly used binders relevant to this work are acrylics, alkyds, and epoxies :-

Acrylic based coatings are derived from acrylic acid (CH_2=CH-COOH). Acrylic polymers may contain acrylate and methacrylate esters in their structure. Acrylate monomers give soft properties and methacrylate hard properties to the polymer. They may be thermoplastic or thermosetting (Bentley 1991). Acrylic based coatings may also be split into three sub groups: - solution acrylics, thermosetting acrylics and acrylic latexes.

Acrylic latex coatings are widely used in the coatings industry. A latex is a dispersion of polymer particles in water and the film is formed by coalescence. The desired rheological properties of the acrylic latex coating usually require a large amount of additives to be added (Weldon 2001). The failure of these coatings is primarily related to water sensitivity or incompatibility with existing or subsequent coatings.

Alkyds are prepared by reacting polyols, dibasic acids and fatty acids. The oxidative curing process of an alkyd resin continues for many years so that over time the properties of the coating can be very different. Alkyd based coatings may have poor resistance to alkaline environmental conditions due to the hydrolysis of the backbone ester linkages, they are also susceptible to chemical and sunlight-induced attack at the remaining double bonds. Alkyd coatings are also susceptible to wrinkling which occurs when the surface of the coating dries at a faster rate than the interior.

The best known epoxy materials are based on pre-formed epoxy resins made from bisphenol A and epichlorhydrin. The stable carbon-carbon and ether links in the backbone chain contribute to good chemical resistance whilst the wide spacing between the reactive epoxide groups and in turn the hydroxyl groups contribute to their toughness. The polar hydroxy groups enhance adhesion through hydrogen bonding whilst the aromatic ring structure gives thermal stability and rigidity.

Despite these desirable properties however, epoxy resins do yellow so they are primarily used as undercoats and primers (Bentley 1999).

Although the components added to the organic binder will affect its mechanical properties to an extent, the mechanical response of a polymer coating will always be visco-elastic. This work considers the visco-elastic mechanical properties of the basic polymer binder.

2.3 Visco-elasticity

As a coating dries or cures it changes from being a viscous liquid to a visco-elastic solid. Visco-elastic behaviour is evident as time dependent behaviour in response to an applied stress. A visco-elastic material will behave elastically if stress loading is rapid enough. Elastic behaviour can be seen as an immediate strain when stress is applied followed by complete recovery on the removal of the stress, Figure 2.3-1 (a). Energy is stored and then released as in a Hookean spring. The response of a visco-elastic material to an applied stress is partly elastic and partly the flowing response of a liquid. When the stress is held at a constant value the visco-elastic material will exhibit a slow, continuous increase in strain and in this respect it behaves as a viscous liquid, Figure 2.3-1 (b). Recovery, on removal of stress, is also time dependent. When subject to constant strain, visco-elastic materials exhibit relaxation, that is, the stress necessary to hold the strain constant will decrease with time.

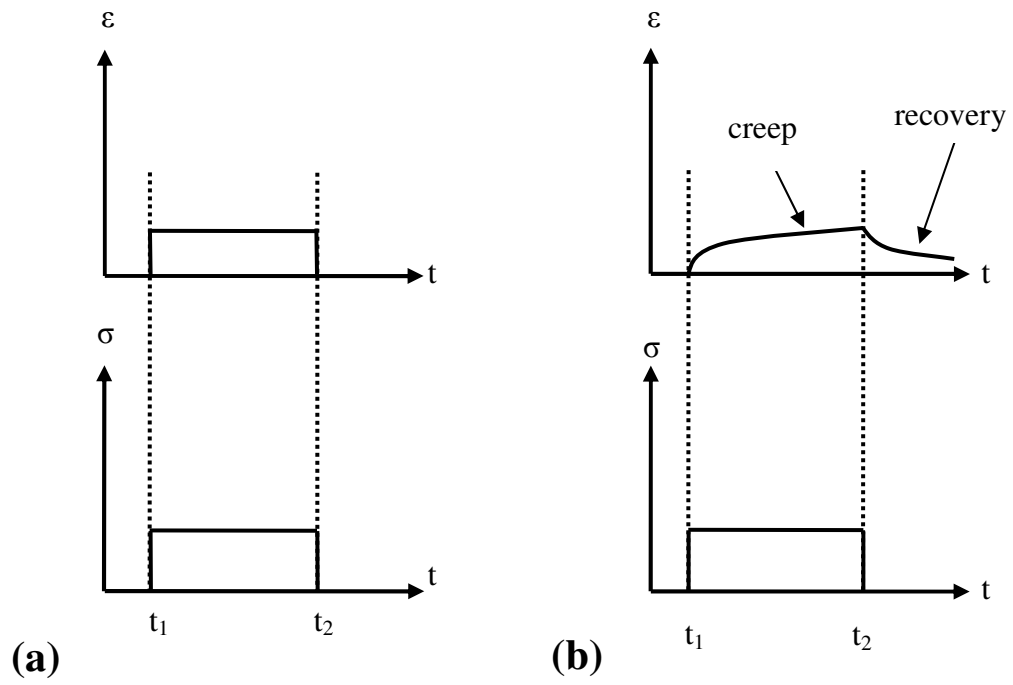

Figure 2.3-1 Schematic strain response to a stress applied at t1 and removed at t2 (a) elastic response (b) visco-elastic response.

2.3.1 Creep

The slow continuous strain exhibited by a visco-elastic material under constant stress is called creep and the reversal of strain upon removal of stress is called recovery. In a creep test, a step of constant stress, σ_0, is applied, and the time dependent strain, $\varepsilon_{(t)}$, is measured. When the strain at any given time is proportional to the applied stress at that time, the material is said to exhibit linear behaviour. This can be written as $\varepsilon_{(t)} = \sigma_0 J_{(t)}$ where $J_{(t)}$ is the creep compliance at that time, defined as the creep strain per unit of applied stress. When creep compliance is measured over decades it shows little or no time dependence at very short times and at long times (McCrum *et al.*, 1997).

As the time dependent behaviour of visco-elastic materials is phenomenological, the intrinsic characteristics of the material cannot be modelled by a single equation accurately describing it over a range of variables. For this reason, separate constitutive equations are used to provide a mathematical description of the ideal responses to a restricted range of variables. The observed behaviour of a material in response to an applied stress enables it to be described according to theoretically modelled materials. (*e.g*. Maxwell model, Kelvin model; described below in Section 2.3.2.) As creep compliance is a material property each material has its own value of creep compliance (Findley *et al.*1976).

A successful constitutive relationship will be able to describe the distinct features of the time dependent behaviour of the material.

2.3.2 Linear Constitutive Equations

In three dimensions, the constitutive equation for an isotropic, elastic, material, is

$$\sigma_{ij} = \lambda \varepsilon_{kk} \partial_{ij} + 2\mu \varepsilon_{ij} \qquad \textbf{Equation 2-1}$$

where λ and μ are the two independent Lamé elastic constants, ∂_{ij} is the Kronecker delta (1 if $i = j$, 0 if $i \neq j$) and $\varepsilon_{kk} = \varepsilon_{11} + \varepsilon_{22} + \varepsilon_{33}$. (The engineering constants can be extracted from the tensorial constants, λ and μ. Shear modulus, *G* is equivalent to μ.) The corresponding equation for an isotropic visco-elastic material is

$$\sigma_{ij}(t) = \int_0^t \lambda(t-\tau)\partial_{ij} \frac{d\varepsilon_{kk}}{d\tau} d\tau + \int_0^t 2\mu(t-\tau) \frac{d\varepsilon_{ij}}{d\tau} d\tau \qquad \text{(Lakes1999)} \qquad \textbf{Equation 2-2}$$

Linear constitutive equations have been developed based on the following models representing isotropic materials undergoing uni-axial stress. These can, however, be generalised to a multi-axial state of stress (Findley *et al.*1976).

2.3.3 Visco-elastic models

The elastic behaviour in response to a small applied stress is modelled by a Hookean spring. $\sigma = \frac{1}{C}\varepsilon$, where σ is stress, ε is strain and *C* is the spring compliance. In this system energy is stored and is recoverable. The viscous response to a small applied stress is modelled by a viscous liquid in a dashpot, according to Newton's law $\sigma = \eta \frac{d\varepsilon}{dt}$ where η is the coefficient of viscosity and $\frac{d\varepsilon}{dt}$ is the rate of stress (Cowie 1991). The dashpot represents loss of energy as heat and therefore deformation is non-recoverable. All materials behaving visco-elastically are modelled by various combinations of these spring and dashpot elements according to their response to an applied stress and to the method of investigation. The Maxwell model combines the spring and dashpot elements in series.

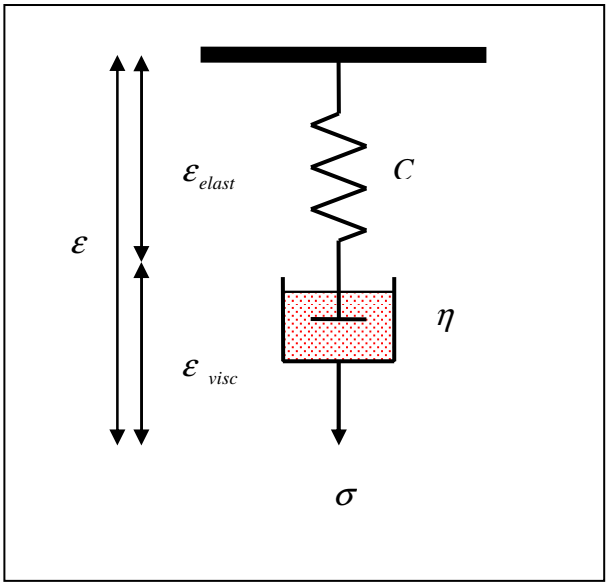

Figure 2.3-2 The Maxwell model

In the Maxwell model it is assumed that the contributions to strain are additive $\varepsilon = \varepsilon_{elast} + \varepsilon_{visc}$. For ε_{elast}, $\sigma = \frac{1}{C}\varepsilon_{elast}$ so $\frac{d\varepsilon_{elast}}{dt} = C\frac{d\sigma}{dt}$ and for ε_{visc}, $\sigma = \eta\frac{d\varepsilon_{visc}}{dt}$ so that $\frac{d\varepsilon_{visc}}{dt} = \sigma/\eta$.

Therefore

$$d\varepsilon/dt = C\frac{d\sigma}{dt} + \sigma/\eta \qquad \textbf{Equation 2-3}$$

Under constant strain $\frac{d\varepsilon}{dt} = 0$, so $\frac{d\sigma}{dt} = -\frac{1}{C}\frac{\sigma}{\eta}$. For the initial condition, where σ_0 is the stress immediately after stretching, $\sigma = \sigma_0$ so the solution is

$$\sigma = \sigma_0 \exp\left(\frac{-t}{C\eta}\right) \qquad \textbf{Equation 2-4}$$

From this it can be seen that when a Maxwell element is held at a constant strain the stress will relax exponentially with time so that at time $t = (C\eta)$ the stress will have reduced to $\frac{1}{e}$ times its original value. This time is called the relaxation time, τ_ε .

Equation 2 - 4 can be written as

$$\sigma = \sigma_0 \exp\left(\frac{-t}{\tau_\varepsilon}\right) \qquad \textbf{Equation 2-5}$$

Under constant stress a material that behaves according to the Maxwell model will respond initially by instantaneous elastic deformation followed by viscous flow but not at the decreasing rate that is seen in the primary stages of creep for many real materials.

The Voigt-Kelvin model combines a spring and a dashpot in parallel, thus the strain over the spring and the dashpot is equal and the stress is shared, additive.

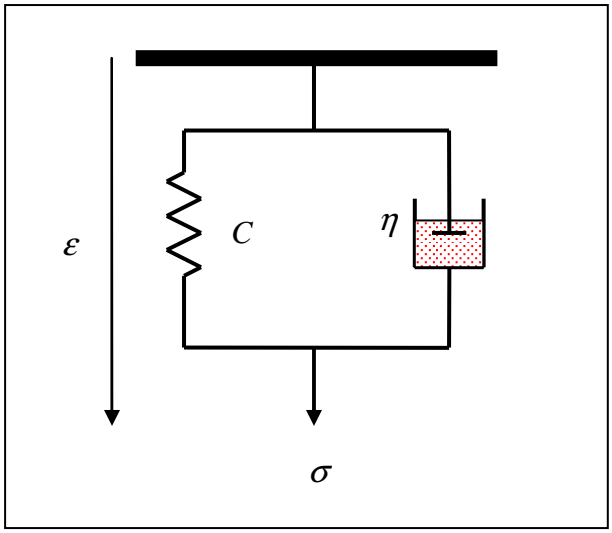

Figure 2.3-3 The Kelvin-Voigt model

The corresponding expression for strain is:-

$$\varepsilon(t) = \sigma C\left\{1 - \exp\left(\frac{t}{\tau_\sigma}\right)\right\} \qquad \textbf{Equation 2-6}$$

Where $\tau_\sigma = C\eta$ which is a measure of the time delay after imposition of stress and is called the retardation time (Cowie 1991). This model is useful for describing creep behaviour when stress is constant. However it does not show an instantaneous elastic response to an applied stress or a permanent strain after stress removal.

To obtain a better representation of real material behaviour a range of spring constants and a range of dashpot coefficients can be included by connecting either Maxwell models or Kelvin models in series to give a generalised Maxwell model and generalised Kelvin model respectively. One model can be converted to the other by including limiting values for η and for *C*. For example, a Maxwell model with zero compliance or a Kelvin model with infinite spring compliance becomes a dashpot (Findley 1976). As a result, the generalised models can represent a solid material or a liquid material.

Maxwell and Kelvin models can be combined to give a standard linear solid or Zener model, which shows elastic response, viscous flow and delayed elasticity. The standard linear solid model has two time constants, one for constant stress and one for constant strain. If a series of Kelvin elements are included a distribution of relaxation times will be represented so that all the significant characteristics of real materials can be represented.

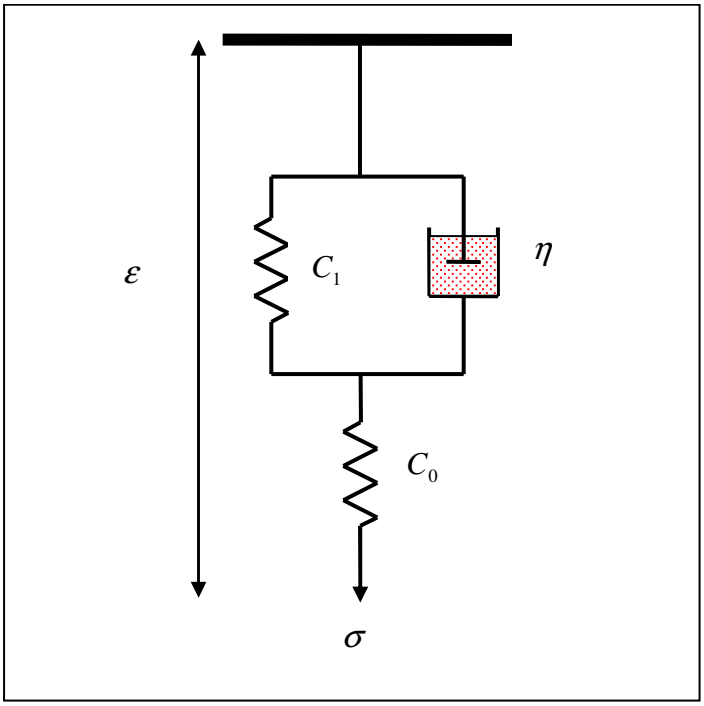

Figure 2.3-4 The standard linear model

This model leads to a linear equation in terms of stress and strain and their first time derivatives which may be regarded as the foundation of the theory (McCrum *et al.*,1997) written as

$$\varepsilon + (C_1\eta)\frac{d\varepsilon}{dt} = \sigma(C_0 + C_1) + ((C_0C_1)\eta)\frac{d\sigma}{dt}. \qquad \textbf{Equation 2-7}$$

With the time constants, relaxation time $\tau_\sigma = C_1\eta$ and retardation time $\tau_\varepsilon = C_0C_1\eta$ the relationship can be written as

$$\varepsilon + \tau_\sigma \frac{d\varepsilon}{dt} = (C_0 + C_1)\sigma + \tau_\varepsilon \frac{d\sigma}{dt}. \qquad \textbf{Equation 2-8}$$

The model for this equation shows all the significant characteristics of polymer relaxations although it is routinely extended to provide a better fit to experimental data.

2.3.4 Linear Constitutive Equation Solution for Creep

In a creep experiment a constant stress is applied at time t = 0, $\frac{d\sigma}{dt} = 0$, so from equation 2 - 8

$$\varepsilon + \tau_\sigma \frac{d\varepsilon}{dt} = \sigma_0 (C_0 + C_1) \qquad \textbf{Equation 2-9}$$

and the strain will relax to its equilibrium value of $\sigma_0 (C_0 + C_1)$ with time constant τ_σ.

The solution to (2 -9) is then

$$\varepsilon(t) = \sigma_0 (C_0 + C_1) - \sigma_0 ((C_0 + C_1) - C_0) \exp\left[-\frac{t}{\tau_\sigma} \right] \qquad \textbf{Equation2-10}$$

The creep compliance, $J_{(t),}$ at any time is given by $\frac{\varepsilon_{(t)}}{\sigma_0}$, (assuming linear behaviour).

So, dividing (2 -10) by σ_0 it can be seen that

$$J(t) = (C_0 + C_1) - ((C_0 + C_1) - C_0) \exp\left[-\frac{t}{\tau_\sigma} \right] \qquad \textbf{Equation 2-11}$$

This can also be written

$$J(t) = C_0 + C_1 \left\{ 1 - \exp\left[-\frac{t}{\tau_\sigma} \right] \right\} \qquad \textbf{Equation 2-12}$$

Thus it can be seen that the model has three parameters describing the material behaviour under a creep test. These are *(C_0)*, which corresponds to the instantaneous elastic response of the material as the stress is applied, (C_1) and τ_σ, which describe time dependent responses to the applied stress. The routine extension to this basic model is to include a distribution of relaxation times which gives a better representation of polymeric material behaviour as different slip processes in the polymer chains can cause a distribution of relaxation times due to material heterogeneity. The extension to the model is in the form of a series of *n* Kelvin – Voigt relaxation elements, i.e. spring – dashpot elements in parallel, each having a spring with compliance and a coefficient of viscosity in the dashpot such that the *i*th element has a relaxation time $\tau_i = (C_i)\eta_i$, the series is also referred to as a Prony series. Figure 2.3-5.

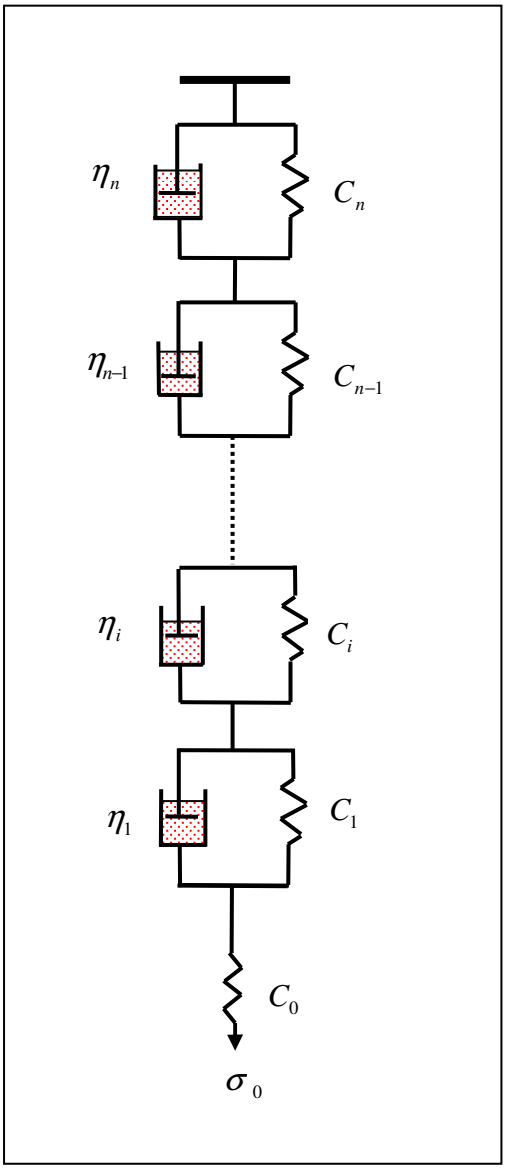

Figure 2.3-5 The extended Kelvin-Voigt model

When a constant stress is applied at $t = 0$, the spring with compliance, C_0, extends instantaneously and the corresponding strain is $\sigma_0 C_0$, the ith element and all other elements are also subject to σ_0 so that at time t, the time dependent creep compliance,

$$J(t) = C_0 + \sum_{i=1}^{n} C_i \left\{ 1 - \exp\left[-\frac{t}{\tau_i} \right] \right\} \qquad \textbf{Equation 2-13}$$

This can be written as

$$J(t) = C_0 - \sum_{i=1}^{n} C_i \exp\left[-\frac{t_i}{\tau_i}\right] \qquad \textbf{Equation 2-14}$$

taking this further, so that the continuous spectrum of relaxation times is represented by an integral it can be seen that, (McCrum *et al.* 1997).

$$J(t) = C_0 + \int_0^{\infty} \left\{1 - \exp\left[-\frac{t}{\tau}\right]\right\} C_i(\tau) d\tau \qquad \textbf{Equation 2-15}$$

However, in this work the summation with n = 2 is used, this corresponds to the model containing 2 Kelvin –Voigt elements as described above. So we have

$$J(t) = C_0 - C_1 \exp-\left[\frac{t}{\tau_1}\right] - C_2 \exp-\left[\frac{t}{\tau_2}\right] \qquad \textbf{Equation 2-16}$$

Equation 2 - 16 is used as the creep compliance function for this work.

2.3.5 Boltzmann Superposition Principle and Linearity

A visco-elastic material is behaving linearly if stress is proportional to strain at a given time, and if the sum of the strains resulting from separate stress components at a given time is the same as the strain that would result from the combined stress input at that time. This is the Boltzmann superposition principle and defines the linear behaviour of a visco-elastic material. See Figure 2.3-6.

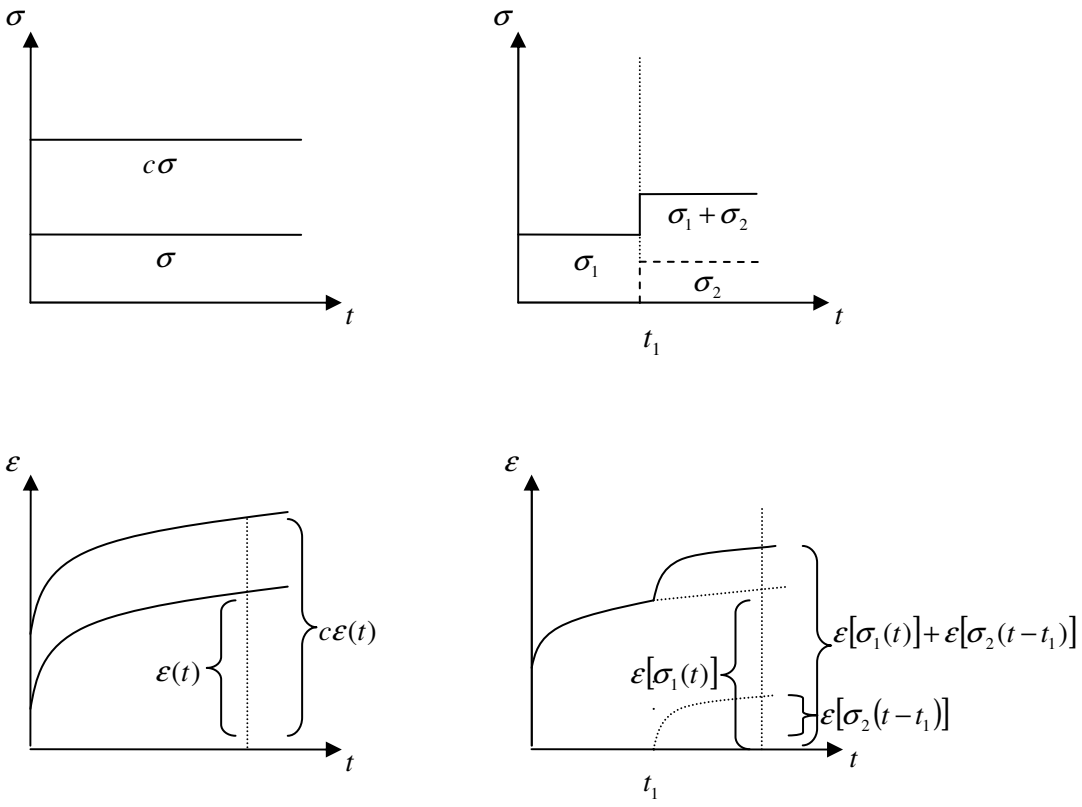

$$\varepsilon[c\sigma(t)] = c\varepsilon[\sigma(t)]$$

where *c* is a constant

$$\varepsilon[\sigma_1(t) + \sigma_2(t - t_1)] = \varepsilon[\sigma_1(t)] + \varepsilon[\sigma_2(t - t_1)]$$

Boltzmann superposition principle

Figure 2.3-6 Definition of Linearity

(from Findley 1976)

2.3.6 Integral Representation of the constitutive equations

The Boltzmann superposition principle, (BSP), enables the strain, resulting from any varying stress input, to be determined when the creep compliance function, *J*(t), is known.

It is seen that the strain resulting from a constant stress, σ_0, applied at t = 0 is $\varepsilon_0(t) = \sigma_0 J(t)$. When an additional stress, σ_1, is applied at time t_1 it results in an additional strain. The additional stress, σ_1, if it were acting alone, according to the Boltzmann superposition principle, would give a strain $\varepsilon_1(t)$ given by $\sigma_1 J(t - t_1)$. The Boltzmann superposition principle then states that if σ_0 alone results in a strain $\varepsilon_0(t)$ and σ_1 results in $\varepsilon_1(t)$ then σ_0 and σ_1 acting together, result in a strain [$\varepsilon_0(t) + \varepsilon_1(t)$].

Following this, it can be seen that if a series of stress pulses is applied the resulting strain is

$$\varepsilon(t) = \Delta\sigma_1 J(t - t_1) + \Delta\sigma_2 J(t - t_2) + \Delta\sigma_3 J(t - t_3) + \ldots\ldots \qquad \textbf{Equation 2-17}$$

If, instead of a series of pulses, the stress is changing continuously with time then equation 2-17 can be given in integral form. The strain at time t for a material, with no stress history, subject to a stress σ_u at time u is given by

$$\varepsilon(t) = \int_0^t (J(t-u)\frac{d\sigma}{du})du \qquad \textbf{Equation 2-18}$$

a Volterra type hereditary integral equation. (Volterra conceived the idea of a theory of functions which depend on a continuous set of values of another function in 1883. (O'Connor, Robertson 1996)).

The kernel function is $J(t-u)$, which is a hereditary, or memory, function describing the stress history dependence of strain (Findley *et al.* 1976). This method of using the BSP to describe the behaviour of visco-elastic materials is known as the integral form of the constitutive equation. The material constants and kernel function are determined by experiment.

Multi - axial stresses and the corresponding three dimensional strain responses are related by using the arguments above and considering the symmetry of the stress and strain tensors of the material.

$$\varepsilon_{ij}(t) = \int_0^t (J_{ijkl}(t-u)\frac{d\sigma_{kl}}{du})du \qquad \textbf{Equation 2-19}$$

Each component may have different time dependence. Cast glassy polymers, being approximately isotropic, can be described by two independent functions which correspond to the shear modulus and bulk modulus of purely elastic solids (Lakes1999).

If strains become greater than one or two percent most visco-elastic materials exhibit non linear behaviour. However, the corresponding non linear constitutive equations involve multiple integrals and become too mathematically complex for practical use. So the situations in which the equations are applied are usually simplified by restricting the stress or strain rates, restricting the loading conditions, considering only incompressibility, or by simplifying the material functions.

2.3.7 Elastic - visco-elastic correspondence analysis for tensile testing

The stress - strain behaviour of isotropic materials can be described in terms of shear *i.e*. deviatoric, strain as well as in changes in volumetric strain. As can be seen in equation 2.1 Section 2.3.2, the stresses $\sigma_{11,}$ $\sigma_{22,}$ $\sigma_{33,}$ $\tau_{12=21,}$ $\tau_{23=32}$, $\tau_{13=31}$ acting on any element in a material can be resolved into a mean component where $\bar{\sigma} = \frac{1}{3}(\sigma_{11} + \sigma_{22} + \sigma_{33})$ and the remainder, the corresponding deviatoric

stress, $s = \left(\sigma - \bar{\sigma} \right)$. The mean or hydrostatic stress is considered a stress invariant and is considered to be the component responsible for the uniform compression within the specimen, resulting in volume change. The remaining component is responsible for the distortion of the element producing a corresponding deviatoric strain, $d = \left(\varepsilon - \bar{\varepsilon} \right)$ where $\bar{\varepsilon} = \frac{1}{3}\left(\varepsilon_{11} + \varepsilon_{22} + \varepsilon_{33}\right)$ which is the mean normal strain (the elastic change in volume). For a visco-elastic material the analysis is simplified by describing the stress strain relationship in shear only. This is based on the common assumption that for an incompressible material $\nu = 0.5$, where ν is the Poisson's ratio and therefore volume does not change. Consequently, bulk deformation is assumed to be time-independent so that the time dependent deformation is shear deformation (Johnson 1985). Alternatively, it can be assumed that the Poisson's ratio remains constant with time so that the ratio between volumetric and shear deformations also remains constant.

For an isotropic elastic material under a tensile test, assuming incompressibility, *i.e.* $\lambda = \infty$, and $\varepsilon_{kk} = 0$, when stress is applied uni-axially the problem can be simplified to a two dimensional plane stress analysis and $\sigma_{ij} = \lambda \varepsilon_{kk} \partial_{ij} + 2G\varepsilon_{ij}$ can be written:-

$$\sigma_{11} = \lambda \varepsilon_{kk} + 2G\varepsilon_{11} \qquad \textbf{Equation 2-20}$$

this is solved by subtracting

$$\sigma_{22} = \lambda \varepsilon_{kk} + 2G\varepsilon_{22} = 0 \qquad \textbf{Equation 2-21}$$

because $\varepsilon_{22} = \varepsilon_{33} = -0.5\varepsilon_{11}$

$$\sigma_{11} = 2G(\varepsilon_{11} + 0.5\varepsilon_{11})$$

$$\sigma_{11} = s_{11} = 2G\left(\frac{3}{2}\varepsilon_{11}\right)$$ **Equation 2-22**

The corresponding visco-elastic equation is:-

$\sigma_{11} = \frac{3}{2}\int_0^t 2G(t-u)\frac{d\varepsilon_{11}(u)}{du}du$, inverting for strain gives:-

$$\varepsilon_{11} = d_{11} = \frac{2}{3}\int_0^t \frac{1}{2G}(t-u)\frac{d\sigma_{11}(u)}{du}du$$ **Equation 2-23**

This time dependent relationship between stress and strain in a uni-axial tensile test is a Boltzmann type integral and $\frac{1}{2G}$ can be replaced by the experimentally predetermined material creep function J , where

$J(t) = C_0 - C_1\exp\left(\frac{-t}{\tau_1}\right) - C_2\exp\left(\frac{-t}{\tau_2}\right)$ as described in section 2.3-4.

Based on Oyen's analysis (Oyen 2005) Equation 2.23 for the ramp to maximum load at time t_R, at constant ramp rate $\frac{ds_{ij}}{du} = k$, becomes

$$d_{ij}(t) = \frac{2}{3}\int_0^t J(t-u)\frac{ds_{ij}}{du}du \quad \text{for } 0 \le t \le tR$$ **Equation 2-24**

and for the peak load where $\frac{ds_{ij}}{du} = 0$

$$d_{ij}(t) = \frac{2}{3}\left[\int_0^t J(t-u)\frac{ds_{ij}}{du}du + \int_{t_R}^t J(t-u)0du\right] \quad \text{for } t \ge tR$$ **Equation 2-25**

the respective solutions are

$$d_{ij}(t) = \frac{2}{3}\left[C_0 kt - \sum C_i k\tau_i\left[1-\exp\left(\frac{-t}{\tau_i}\right)\right]\right], \qquad 0 \le t \le tR.$$ **Equation 2-26**

$$d_{ij}(t) = \frac{2}{3}\left[C_0 k t_R - \sum C_i k \tau_i \exp\left(\frac{-t}{\tau_i}\right)\left[\exp\left(\frac{t_R}{\tau_i}\right) - 1\right]\right], \qquad t \geq tR. \qquad \textbf{Equation 2-27}$$

Equation 2 - 27 is comparable to the relationship describing a step load, where $s_{ij}(t) = 0$, for t < 0 and $s_{ij}(t) = s_{ij\,\max}$, for t > 0, in which case $d_{ij} = s_{ij} J(t)$

the solution of which is

$$d_{ij} = s_{ij\,\max} \frac{2}{3}\left[C_0 - \sum C_i \exp\left(\frac{-t}{\tau_i}\right)\right] \qquad \textbf{Equation 2-28}$$

From this it can be seen that the only difference between ramp loading and step loading, is a constant factor scaling of each exponential decay term. This constant, a "ramp correction factor" is only dependent on the ratio of the material time constant to the experimental rise time (Oyen 2005).

$$RCF_i = \frac{\tau_i}{t_R}\left[\exp\left(\frac{t_R}{\tau_i}\right) - 1\right] \qquad \textbf{Equation 2-29}$$

Experimentally obtained creep curves can be fitted to a 2nd order exponential decay function (see Appendix 11.1) and from the resulting fitting parameters the amplitude coefficients, C_0, C_1 and C_2 and relaxation times, τ_1 and τ_2, can be calculated. See Appendix 11.1. From these the generalised creep function $J(t) = C_0 - C_1 \exp\left(\frac{-t}{\tau_1}\right) - C_2 \exp\left(\frac{-t}{\tau_2}\right)$ is determined. The compliance, and conversely the shear modulus, at any time can then be calculated so that at zero-time the (instantaneous) shear modulus, $G_{0,}$ can be calculated:-

$$G_0 = \frac{1}{2(C_0 - \sum C_i)}$$ **Equation 2-30**

And the relaxed or infinite-time shear modulus can be calculated as

$$G_\infty = \frac{1}{2C_0}$$ **Equation 2-31**

Due to different time patterns of creep and relaxation in visco-elastic materials the relationship between G(t) and J(t) is not simply reciprocal as it is in time independent elastic materials. But at time = 0 and at time = ∞ the viscosity is not involved so that at these time limits the relationship may be considered to be reciprocal (Ferry 1980). The ratio between G_0 and G_∞ provides a good general indication of the extent of visco-elasticity of the material. This ratio we define as the creep ratio, C_r, where

$$C_r = 1 - \frac{G_\infty}{G_0}$$ **Equation 2-32**

A material with a creep ratio of zero would be elastic, whilst a creep ratio approaching unity indicates a viscous material.

2.4 Nanoindentation / instrumented indentation testing

Nanoindentation is a technique whereby an indenter with a known tip shape and dimension is driven into a test material whilst the load is controlled and a high resolution sensor measures the resulting penetration.

Indents can be positioned to within about one micron so that the mechanical properties of very small volumes of material including thin films, coatings and surface layers can be determined, enabling specific areas to be mapped in terms of mechanics (Oyen *et al.* 2008).

At the start of data acquisition a very small initial force of 0.01mN is applied enabling the system to define zero displacement as the tip makes contact with the surface. The force is then held constant while a datum is established for the measurement of subsequent indenter displacements. Figure 2.4-1 inset.

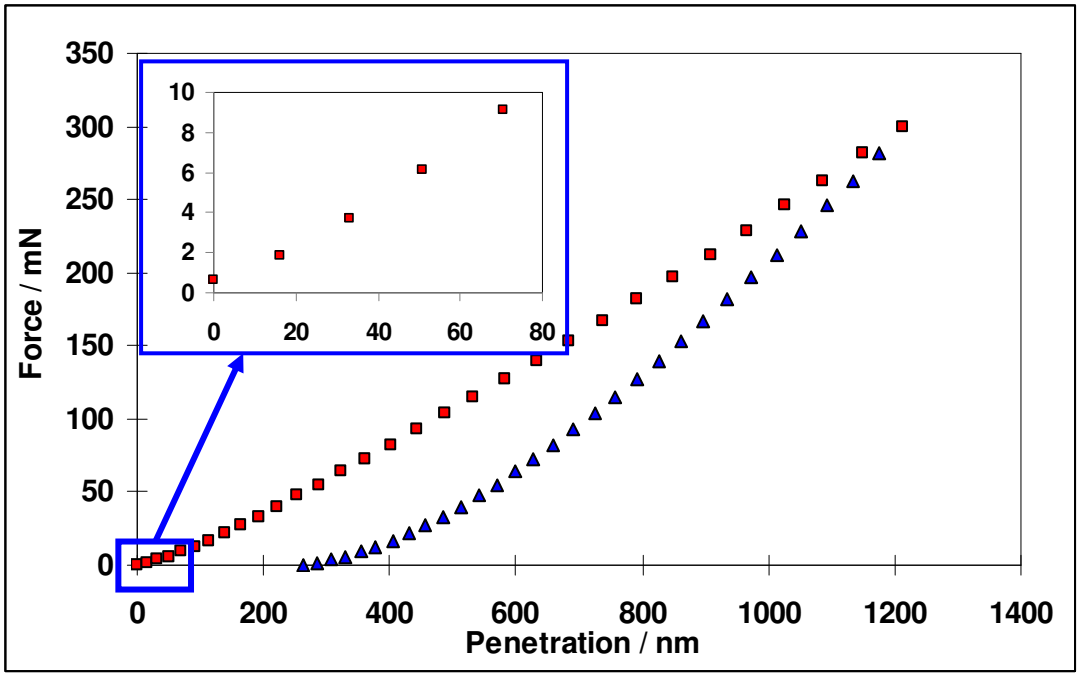

Figure 2.4-1 Glass nanoindentation showing steps in load - unload cycle and inset showing initial contact force at zero displacement

Nanoindentation tests consist of load - unload cycles with load applied as a sequence of steps to the chosen maximum load. The indenter is driven into the surface until a resistance equal to the set force is met and in a series of steps, at force equilibrium, the penetration and load are measured. Figure 2.4-1. Typical load cycles include loading to a set maximum load immediately followed by unload or partial unload; or, loading to a set maximum load which is held for a period of 120s and then decreased in the same steps to the starting value. The latter is the test used in this work for creep analysis.

Typical forces are in the range of 1 mN to a few Newtons, with depths reaching 1 to 20μm maximum (Bushby 2001). Current nanoindenter systems have sensing mechanisms capable of depth resolution < 0.01 nm and load resolution 50 nN (Agilent Technologies 2009) although in practice these are not achievable.

Particularly for polymeric materials, spherical indenter tips have the advantage over pointed indenters. The initial contact when using a spherical indenter is elastic, whereas pointed indenters at relatively lower loads produce plastic deformation. This is a problem when indenting polymers; it complicates the visco-elastic analysis as well as making the point of initial contact of the tip to the surface difficult to determine particularly when the polymer surface is compliant (Oyen 2006). For this reason only spherical indenters are considered in this work.

2.4.1 Nanoindentation: Theoretical Considerations

Whilst studying optical interference rings between two glass lenses in contact Hertz proposed the first satisfactory analysis of the stresses between two spheres in contact. Hertz hypothesised that the contact area between two elastic solids having profiles of solid bodies of revolution, is, in general, elliptical. To facilitate the calculation of the

local deformations he treated each body as an elastic half space loaded over a small elliptical region of its plane surface. For this to be justified two conditions must be met. The first condition is that the dimensions of the contact area must be small compared with the dimensions of each body. This ensures that any boundaries of the body do not affect the calculated stress field. The second condition is that the dimensions of the contact area should be small compared to the relative radii of curvature of the surfaces, thus ensuring that the surfaces outside the contact region can be approximated as the plane surface of a half space and that the strains are small enough to be within the scope of the linear theory of elasticity. Additionally, the surfaces are assumed to be frictionless so that the only pressure between them is normal (Johnson 1985).

For two elastic spherical bodies in contact, the contact area is circular, with contact radius, a, and this defines the surface boundary wherein pressure gives rise to normal displacements. Hertz relates a to the load, P, as

$$a = \left(\frac{3PR^*}{4E^*} \right)^{\frac{1}{3}} \qquad \textbf{Equation 2-33}$$

where R^* is the relative radius of curvature of the spheres given by

$$\frac{1}{R^*} = \frac{1}{R_1} + \frac{1}{R_2} \qquad \textbf{Equation 2-34}$$

and E^* is the reduced modulus derived from the moduli of both materials and given by

$$\frac{1}{E^*} = \frac{\left(1 - v_1^2\right)}{E_1} + \frac{\left(1 - v_2^2\right)}{E_2} \qquad \textbf{Equation 2-35}$$

E_1 and E_2 are the elastic moduli of the materials and v_1 and v_2 are the Poisson's ratios.

The mutual approach of distant points in the two solids, δ, is given by

$$\delta = \frac{a^2}{R^*} \qquad \textbf{Equation 2-36}$$

The spherical indentation of a flat elastic half space, Figure 2.4-2, is simply a special case of Hertzian contact theory for two spheres in contact. The flat elastic half space has radius infinity so that R^* becomes the radius of the indenter, R and the distance of mutual approach becomes the penetration into the half space, h.

Providing the same conditions are met, i.e. the surfaces are continuous and non-conforming, $a << R$; the strains are small, $a/R < 0.3$ (Johnson 1985); and frictional effects can be ignored it can be seen from the above, that for indentation with a spherical indenter, load is related to depth as

$$h = \left(\frac{3P}{4R^{1/2}E^*} \right)^{2/3} \qquad \textbf{Equation 2-37}$$

and

$$a = \left(\frac{3PR}{4E^*} \right)^{1/3} \qquad \textbf{Equation 2-38}$$

Using Hertzian theory for elastic contact together with the relationships developed by Sneddon (1965) for indenting a flat elastic half space with tips of different axisymmetric shapes, including $h_c = \frac{h}{2}$, where h_c is the depth at which the area of contact occurs, the analysis of the load versus penetration data obtained from an indentation test is frequently based on the work by Oliver and Pharr (Van Landingham *et al.*2000) Sneddon derived relationships between load, displacement

and contact area for any punch that can be described as a solid of revolution of a smooth function (Oliver and Pharr 1992).

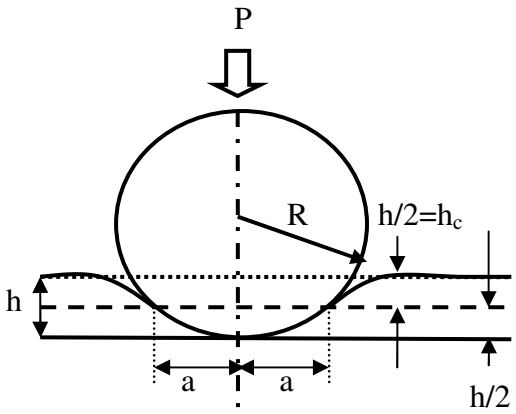

Figure 2.4-2 Schematic diagram of the deformation and definition of the contact dimensions of an elastic surface by a sphere

As the indenter is made from a material with high hardness to minimise its potential plastic deformation during a test, it is difficult to produce a perfectly spherical tip. Consequently, the effective radius, R is generally a function of the depth of penetration in contact with the spherical indenter, h_c , see Figure 2.4-2. By indenting into a series of reference materials the tip shape function can be determined (Bushby and Jennett 2001, Zhu, Bushby and Dunstan 2008).

Oliver, Hutchings and Pethica suggested that contact areas be measured from load displacement curves and knowledge of the indenter area function rather than the difficult and time consuming direct imaging of impressions (Oliver and Pharr 1992).

Doerner and Nix put together these ideas and developed a comprehensive method for determining hardness and modulus from indentation load displacement data. This was based on the observation that, for some materials, during the initial stages of unloading, the unloading curves were linear, that is, the elastic behaviour of the

indentation contact is similar to that of a flat cylindrical punch (Doerner and Nix 1986). The contact area was determined by extrapolating to zero load the initial linear portion of the unloading curve and using the extrapolated depth with the indenter shape function to determine the contact area.

Oliver and Pharr subsequently extended the method proposed by Doerner and Nix to account for the fact that for a large number of materials their experiments showed non linear unloading even during the initial stages.

Using the method of Oliver and Pharr, from one cycle of loading and unloading, mechanical properties can be determined from measurements of the maximum applied load and maximum penetration depth. From the resulting load/displacement curve of a nanoindentation test, the contact stiffness, $S = dP/dh$, is obtained from the initial part of the unloading curve. Contact depth, h_c, is then related, according to the tip shape, to the intercept of this tangent, h_i, with the x – axis, Figure 2.4-3.

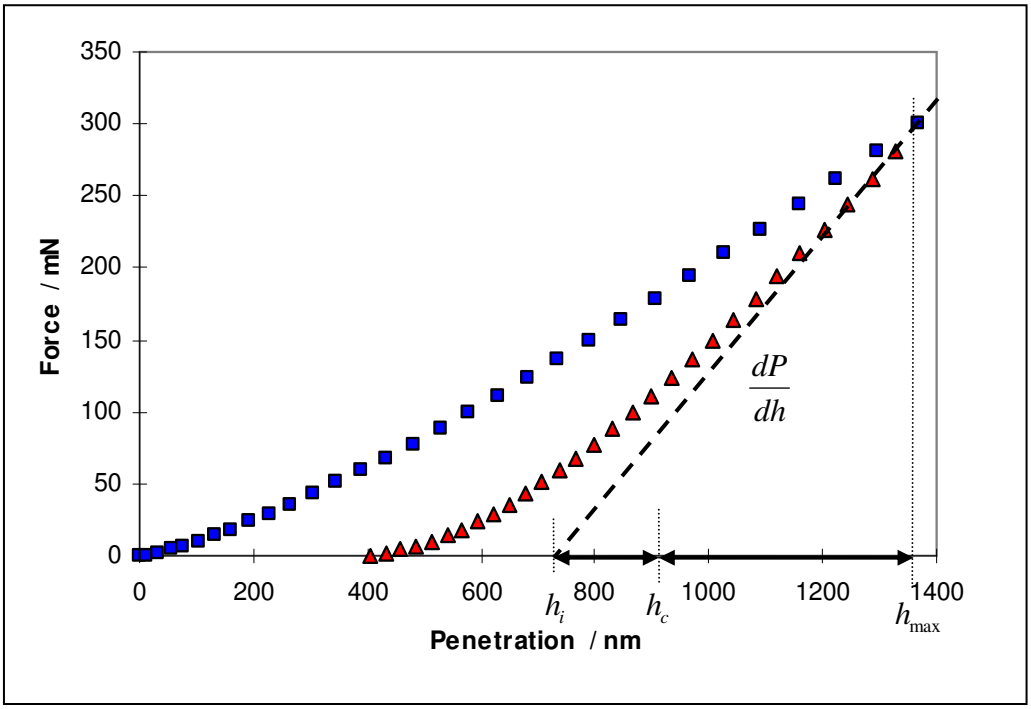

Figure 2.4-3 Glass nanoindentation example showing contact stiffness and contact depth from load – unload cycle

Based on displacement equations from Sneddon's analyses for spherical tipped indenters $h_c = h_{\max} - 0.75\frac{P_{\max}}{S}$ (Sneddon 1965,Van Landingham 2003)

Hardness, *H*, is determined from the equation $H = P/A$, where *A* is the contact area calculated as a function of contact depth. The elastic modulus is determined from the reduced modulus E^*, where $E^* = \left(\sqrt{\pi \cdot S}\right)/2\beta\sqrt{A}$ and β is a constant that depends on the geometry of the indenter, for spherical tips $\beta = 1$.

Generally, the relationship between depth of penetration, *h*, and load, *P*, is given as

$$P = \alpha(h - h_f)^m \qquad \textbf{Equation 2-39}$$

where α contains geometric constants, the sample elastic modulus, the sample Poisson's ratio, the indenter elastic modulus, and the indenter Poisson's ratio, h_f is the final depth after unloading and *m* is a power law exponent that is related to the indenter geometry, for a spherical tip *m* = 3/2. Final depth after unloading is relevant for elastic-plastic indentation and analysis methods have been described fully (Field and Swain 1993), (Oliver and Pharr 2004).

2.4.2 Visco-elastic correspondence with a spherical indentation analysis

The load – penetration, *P-h* , traces resulting from a nanoindentation test enable values of elastic modulus, *E* , and hardness, *H*, to be determined and the Oliver and Pharr method as outlined above is now widely used in the mechanical analysis of time-independent materials. However, the interpretation of *P-h* curves obtained from indenting time dependent materials is problematic due to a continued increase in the contact area during initial unloading. This affects the slope of the unloading curve and appears as what is frequently termed as "a nose" on the unloading curve, this

consequently affects the values for stiffness, S, where $S = \frac{dP}{dh}$ (Van Landingham 2000). To minimise the creeping effect on the unloading curve a typical procedure is to hold the indenter at the maximum load for a time long enough to allow the material to reach mechanical equilibrium before starting the unload (Briscoe *et al.* 1998).

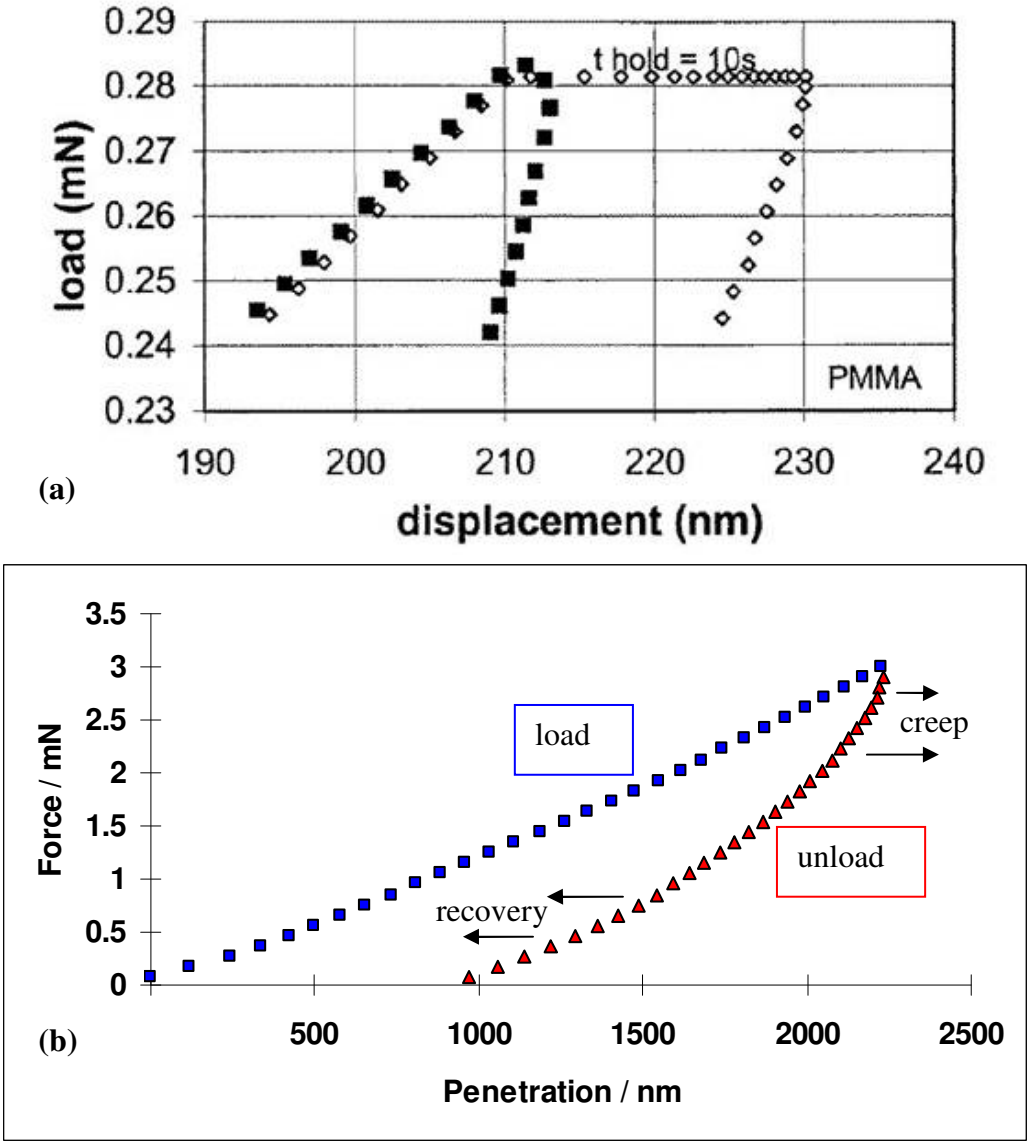

Figure 2.4-4 The "nose" problem: (a) PMMA nanoindentation experimental results (Briscoe *et al.* 1998); (b) PVC nanoindentation data showing creep during unload

It has also been proposed that when the initial unloading slope is used as a means to determine the instantaneous modulus, a fast unload is essential and this may eliminate the need to hold before unloading (Cheng *et al.* 2005). Both of these methods attempt to exclude the visco-elastic nature of the material and therefore useful information that fully characterise the material properties is lost.

Elastic – visco-elastic correspondence allows the creep behaviour to be analysed. The correspondence principle states that if the solution to the linear elastic problem is known, the solution to the corresponding visco-elastic problem can be determined. One method of applying this principle is by using a Laplace transformation with respect to time for each time dependent term in the governing equation. The problem becomes an associated elastic one and the solution is then inverse transformed to give the required solution. However, in a nanoindentation test the contact region varies with time so that for some points on the surface neither the traction nor the displacement is known throughout the history of the problem and a Laplace transform can not be applied. Lee and Radok have presented a solution for the visco-elastic counterpart of the Hertz elastic problem for spherical contact in which visco-elastic operators replace the elastic constants in the relationship between normal contact pressure and surface displacement. This can be applied so long as the contact area does not decrease (Lee & Radok 1960).

Using Hertzian contact mechanics, the elastic relationship is

$$h^{3/2} = \frac{3}{4}\left(\frac{1}{R}\right)^{1/2} \frac{P(1-\nu^2)}{E} \qquad \textbf{Equation 2-40}$$

where ν is the Poisson's ratio of the material and E is the elastic modulus.

As in the tensile analysis, sect.2.3.7, only the time dependent shear strain is considered as it is assumed that $\nu = 0.5$.

Using the fundamental relationship $G = \frac{E}{2(1+\nu)}$ it can be seen that the equation relating depth to load in a standard indentation test can be written

$$h^{3/2} = \frac{3}{4}\left(\frac{1}{R}\right)^{1/2} \frac{[P]}{4G} \qquad \textbf{Equation 2-41}$$

where G is the shear modulus.

In an indentation test it can be seen that when Poisson's ratio is 0.5, G is related to indentation modulus, $E^{'}$, as

$E^{'} = 4G$.

Lee and Radok's solution to the corresponding visco-elastic problem is the replacement of $[P/2G]$ by a visco-elastic operator for creep to give the Boltzmann type integral equation (derived from the interpretation of contact as the linear superposition of small changes in radial pressure distribution resulting from infinitely small step changes in load).

$$h^{3/2}(t) = \frac{3}{8}\left(\frac{1}{R}\right)^{1/2} \int_0^t J(t-u)\frac{dP}{du}du \qquad \textbf{Equation 2-42}$$

where u is the dummy variable of integration for time and J(t) is the material creep function.

Using Oyen's (2005) analysis of Lee and Radok

Equation 2.43 must be solved for the ramp from zero load to peak load during the time $0 \leq t \leq t_R$, and for the peak load at $t \geq t_R$ where $\frac{dP}{du} = 0$.

$$h^{3/2}(t) = \frac{3}{8}\left(\frac{1}{R}\right)^{1/2} \int_0^t J(t-u)\frac{dP}{du}du \qquad \text{for } 0 \le t \le t_R \qquad \textbf{Equation 2-43}$$

and for the peak load where $\frac{dP}{du} = 0$

$$h^{3/2}(t) = \frac{3}{8}\left(\frac{1}{R}\right)^{1/2}\left[\int_0^t J(t-u)\frac{dP}{du}du + \int_{t_R}^t J(t-u)0du\right] \quad \text{for } t \ge t_R \qquad \textbf{Equation 2-44}$$

The solutions depend on the material creep function, which is determined by fitting creep curves obtained experimentally.

The creep function used in this work is :- (from sect 2.3-4 equation 2 -16)

$$J(t) = C_0 - C_1 \exp(-\frac{t}{\tau_1}) - C_2 \exp(-\frac{t}{\tau_2})$$

Letting the constant ramp rate equal k, the solution for equation 2 - 44 is

$$h^{3/2}(t) = \frac{3}{8}\left(\frac{1}{R}\right)^{1/2} C_0 kt - \sum C_i k\tau_i\left[1 - \exp\left(\frac{-t}{\tau_i}\right)\right], \qquad 0 \le t \le t_R. \qquad \textbf{Equation 2-45}$$

Whilst for the hold period, the solution for equation 2 - 45 is

$$h^{3/2}(t) = \frac{3}{8}\left(\frac{1}{R}\right)^{1/2} C_0 kt_R - \sum C_i k\tau_i \exp\left(\frac{-t}{\tau_i}\right)\left[\exp\left(\frac{t_R}{\tau_i}\right) - 1\right], \quad t \ge t_R. \qquad \textbf{Equation 2-46}$$

Equation 2 - 47 is comparable to the relationship describing a step load where $P(t) = 0$, for $t < 0$ and $P(t) = P_{\max}$, for $t > 0$ in which case:

$h^{3/2} = \frac{3}{8}\left(\frac{1}{R}\right)^{1/2} P_{\max} J(t)$ the solution of which is

$$h^{3/2} = \frac{3}{8}\left(\frac{1}{R}\right)^{1/2} P_{\max}\left[C_0 - \sum C_i \exp\left(\frac{-t}{\tau_i}\right)\right] \qquad \textbf{Equation 2-47}$$

As described in Chapter 2.3-7, to correct for the ramp loading the ramp correction factor, Equation 2-29, is applied (see Appendix 11.1).

Remembering that under spherical indentation displacement is proportional to load $^{2/3}$, the experimental creep curves, as depth$^{(3/2)}$ versus creep time at constant load, can be fitted to a second order exponential decay function as in Chapter 2.3-7 (Appendix 11.1) and the resulting creep function (Chapter 2.3-4 Equation 2 -16) is obtained. The zero-time (instantaneous) shear modulus, G_0, can then be calculated using the creep function parameters from Equation 2.30, the infinite-time shear modulus G_∞, can be calculated from Equation 2.31 and C_r from Equation 2.32 as in tensile tests.

2.4.3 Suitability of nanoindentation for testing visco-elastic polymers as coatings

For compliant polymers the determination of the initial point of contact of the indenter tip to the surface is difficult, such that the penetration of the tip could already be significant relative to the measured maximum, h_{max}. This difficulty may be overcome by nanoindentation using a dynamically oscillating load. As in dynamic mechanical analysis (DMA), a sinusoidal input is applied and the amplitude and phase lag of the output is used to calculate the contact stiffness and the storage and loss moduli. This method has been successfully used in various studies. Dynamic nanoindentation and standard DMA studies by Herbert *et al.* (2008) found agreement to within 15% between the two methods on a highly plasticised polyvinyl chloride (PVC) sample. Dynamic nanoindentation was used in the measurement of the loss tangent of low density polyethylene at two different temperatures to determine the activation energy of the α relaxation (Loubet *et. al*. 2000) also in the mechanical

characterisation of polytetrafluoroethylene (PTFE) films on silicon substrates in the 0.5 to 15 μm thickness range (Lucas *et.al.*1998). However, the assumptions made in the analysis which relate storage and loss moduli to the storage and loss components of the mechanical impedance of the tip – sample contact are found to have significant limitations with regard to high loss polymers. Storage and loss moduli are assumed to be directly related to the storage and loss portions of the tip-sample mechanical impedance and the assumptions of linear visco-elasticity remain unchecked (Van Landingham *et al.* 2000) (Van Landingham 2003). Moreover, the application of a load oscillating at high frequencies or at greater frequencies than the coating would naturally experience can only result in less pertinent information regarding its mechanical properties.

When dealing with polymers as coatings there are further considerations to be made. For both time-dependent and time-independent materials it is necessary to be aware of the effects of the substrate when thin films and coatings are indented (Sakai 2009) (Zhang *et al*.2004). Studies of titanium films on a sapphire substrate have shown that when very thin films (up to 400 nm) plastically deform under indentation load, the interaction of the plastic field with the substrate results in an apparent increase in the hardness value of the film (Fabes *et al*. 1992). Saha and Nix found that compared to hardness measurements, elastic modulus measurements of thin films are more affected by the substrate. This is because the elastic field of the indenter is a long range field that extends into the substrate. This results in the substrate stiffness having an influence on the measured contact stiffness (Saha, Nix 2002). Consequently, it is difficult to estimate the film modulus from nanoindentation data when there is a large elastic mismatch between the film and the substrate and impossible from a single measurement. Studies of various methods to determine the

elastic modulus of various film/substrate combinations using multiple load experiments have been made by Mencik and co-workers (1997) and multilayer films were investigated by Chima-Okereke et al. (2006), recommendations for these methods were proposed and test methods are now standardised in ISO 14577.

For polymers, the methods to extract the modulus of the film from the composite modulus of a layered film composite has been successful for films with low geometric confinement but problems arise when films are very thin and indentation depth approaches the magnitude of the film thickness. In this case geometric confinement is high, characterised by high hydrostatic pressures to which many polymers are sensitive (Gacoin *et al*. 2006).

Lucas *et al*. (1998) found that for PTFE films of thickness 0.5 μm to 15 μm, substrate effects were only significant at depths greater than 5 – 10% of the film thickness. However, modulus values were found to be 2.4 to 3 times higher than those obtained using tensile testing or DMA. Additionally, in a study by White *et al* (2005) the modulus of a soft, compliant poly(di-methyl siloxane PDMS) derived from dynamic nanoindentation using a Berkovich tip was found to be a factor of two times higher than that measured using a rheological solids analyzer .

Whilst various indenter geometries have been successfully used to determine mechanical properties of elastic and visco-elastic materials, there may also be viscoplastic deformation when indenting with sharp indenter tips such as Berkovich tips. Any plastic deformation included in the measured total displacement must then be subtracted (Yang 2004). Work by Tweedie *et al.* (2006) has concluded that nanoscale contact creep experiments in which sharp and/or conical indenters are used on polymeric surfaces cannot be interpreted accurately using current linear visco-elastic analyses. However a visco-elastic-plastic model for sharp indentation

originating from linear visco-elasticity has been developed by Oyen and Cook (2002). Elements constructed from springs for elastic response, dashpots for viscous response and sliders for plastic response are combined to describe a range of visco-elastic-plastic behaviour during sharp indentation.

Provided the maximum strains are less than the elastic strain limit, spherical indenters are better suited to enable a linear visco-elastic response. Large radius spherical indenters are preferable (Oyen 2006). Spherical tips naturally have better geometrical accuracy than conical indenter tips. Tip defects on conical indenters have been found to make considerable contributions to initial depth calculations compared to spherical tips, in indentation tests on poly methylmethacrylate, PMMA (Briscoe and Sebastian 1996). However, nanoindentation studies on PMMA, and polycarbonate, PC, using both Berkovich tips and spherical indenter tips and elastic correspondence have produced results in which there is good agreement in creep compliance data with data from tensile tests and shear tests (Lu *et al.* 2003). Also, spherical indentation studies of PMMA on a larger scale (Brinell - tip radius 5mm) have shown good agreement to uniaxial tensile test results although the authors comment that the resulting shear relaxation function value, in the region of 0.6 GPa, was considerably lower than expected (Larsson and Carlson 1998). Young's modulus values given for commercially available PMMA are between 1.8 and 3.1 GPa and 2.4 to 3.3 GPa for cast PMMA (http://www.matbase.com/material/polymers/commodity/pmma/properties).

Investigations into stress fields around spherical indentations into PMMA, with the emphasis on yield stress, have shown yield stress to be sensitive to strain rate and hydrostatic pressure (Puttick *et al.* 1977). Values obtained for yield stress have been found to be higher than those obtained by traditional compression tests by a factor

1.8 to 2.2. The localised confining pressure and the compressibility index of the materials appear to be the significant contributory parameters (Kourtesis *et al.* 1997). Further studies into the mode of deformation during indentation have suggested that frictional effects are influential (Kent 1981). This highlights the influence of strain rates and hydrostatic pressures as well as friction on the mechanical response of polymers whether it is elastic or plastic and these should be kept in mind.

Problems occur in the determination of contact area. Depth-sensing indentation at macroscopic dimensions has indicated that pile-up occurs around the indenter in ductile materials such that over a range of materials there is a range in total depth to contact depth ratio (work done on non-polymeric materials with a Vickers tip) (Thurn *et al.* 2002). Analysis of nanoindentation load/displacement data and finite element analysis of contact area, using a conical indenter, has shown that contact area is affected by radial displacements resulting in the underestimation of the load when using Sneddon's solutions, but when Poisson's ratio, $\nu = 0.5$, the radial displacements vanish and the shape of the surface is consistent with the indenter (Hay *et. al* 1999). Bolshakov and Pharr (1998) have used finite element simulation to investigate the influence of pile up on the accuracy to which elastic modulus and hardness can be calculated using indentation. When pile up is large true contact areas are underestimated from the load-displacement data which leads to overestimation of the elastic modulus and hardness.

Furthermore, contact areas larger than those predicted using Hertzian contact mechanics have been seen in smooth rubber spheres in contact and in glass spheres in contact at low loads, this was attributed to adhesion due to attractive surface forces although these become less significant at high loads (Johnson *et al.* 1971).

The problem of unknown contact areas may be overcome by the use of flat ended punches which produce known contact areas however the behaviour of the stresses and strains close to the contact boundary produces non-linearities (Larsson and Carlson 1997) in addition there are difficulties involved in aligning the flat surface horizontally to the sample surface (Cheng *et al.* 2005).

Indentation of polymers appears to produce results that both agree and disagree with given literature values and the reasons for this are unclear.

True contact conditions need to be known to enable the correct interpretation of load -displacement data from spherical indentation tests.

2.4.4 Summary and Rationale

Polymers as coatings are widely used, it is therefore necessary to fully understand their mechanical properties. The standard tensile test is not appropriate for polymers as coatings and nanoindentation appears to be a suitable substitute.

The methods and analysis applied to the nanoindentation of time independent, or elastic, materials are not suitable for time dependent visco-elastic materials.

Models for the time-dependent mechanical response of polymers can be understood in terms of springs and dashpots. Linearity of response, associated creep functions and time-dependent shear moduli are underpinned by the Boltzmann superposition principle. This enables a stress to be applied over a finite ramp loading time and the instantaneous and relaxed shear moduli to be derived from the creep response. The assumption being that shear modulus is related to deformation of the material and is time dependent whereas bulk modulus is related to volume change and is time independent.

When indenting polymers, spherical indenter tips are preferable; this is to ensure that the material response can be wholly visco-elastic rather than viscoplastic. Spherical indentation can be understood using the Hertzian theory of elastic contact and the elastic visco-elastic correspondence principle with further interpretation by Lee and Radok.

When indenting polymers as coatings, to avoid substrate effects, and to keep within the linear visco-elastic regime as well as to comply with the Hertzian conditions, contact areas and depth of penetration must be kept very small. However linearity should be determined independently and not simply assumed from lack of residual impressions as Lu *et al.* (2003) have done, post indentation recovery does not imply that the response to loading was linear.

Nanoindentation using Hertzian contact analysis and elastic correspondence with the method and analysis as described appears to be the most suitable method for characterising the mechanical properties of polymers, it enables a full characterisation of the visco-elastic nature of the mechanical response rather than eliminating creep to derive a single instantaneous modulus value. Whilst this has proven to be a valid technique to determine the mechanical properties of many polymeric materials (Oyen 2007, Cheng 2005) for some polymers there still appears to be a difference in the moduli values derived from the test results and the literature values (Oyen 2007).

It is not known why these differences occur and possible reasons include:- a nonlinear visco-elastic response of the material, adhesion effects, size effects, and/or an incorrect assumption in the contact conditions.

For the characterisation of new materials in which a literature value is unknown it is essential that the method and analysis is fully understood. The circumstances under

which Hertzian theory can be applied to visco-elastic polymers must be established. How and when the differences in moduli arise should be known. In addition, and particularly important for polymers as coatings, the method and analysis should also be sensitive enough to distinguish chemical and physical differences that may occur during natural environmental conditioning.

With these issues in mind this work:-

1) uses nanoindentation creep to distinguish between various polymer coatings and monitors environmentally induced changes in their mechanical properties. The mechanical properties of four different coatings are investigated with regard to their chemical properties. The coatings are ranked according to their mechanical properties and to any changes in these as a response to exposure to weather. Mechanical properties are used and monitored in degradation studies as an alternative to the currently used accelerated weathering testing which is severe and destructive to the coatings.

2) uses creep and elastic visco-elastic correspondence as described and directly compares nanoindentation testing using a spherical tip to tensile testing as a benchmark for the nanoindentation of polymers;

3) provides further information on the contact conditions during ramp loading and a period of creep by direct observation of the actual contact areas during spherical indentation of various polymers and compares the results with those predicted using Hertzian theory;

4) further examines the contact conditions during visco-elastic indentation with a spherical indenter using FEA.

3 Materials and methods

Most polymer indentation studies have been of well known, well characterised, industrially prepared samples with known modulus values, *e.g*. PMMA, and polycarbonate, PC, (Lu *et al.* 2003, Oyen 2007, Cheng 2005) and generally there has been some agreement in modulus values obtained from these indentation tests. In this work, various materials, both known and unknown were used to provide examples of thermoplastic, thermo-set, cross-linked and amorphous polymers with varying glass transition temperatures. These studies were thought to be of more use to the development of nanoindentation as a technique suitable for the research and development of polymer coatings industry.

3.1 Materials

3.1.1 Coatings supplied by ICI

Samples were prepared by ICI Strategic Technologies division, (ICI is now Akzo Nobel) and supplied as standard glass microscope slides coated with un-named, numbered coatings, with exact chemistry known to ICI. The coating information is presented in Table 3.1-1.

The approximate thickness of the coatings was determined by deducting the slide thickness from the slide plus coating thickness.

As the coatings were also supplied as small samples of free-standing, thin (0.04 -0.07 mm), spread films, to provide an indication of their glass transition temperatures, T_g, the films were tested using dynamic mechanical analysis, DMA, (Q800 Dynamic Mechanical Analyzer, TA Instruments Ltd.). The films were tested using temperature

sweep mode in tension at mechanical oscillation frequency 1Hz. A peak in tan delta occurs at the glass transition temperature see Figure 3.1-1.

The coating material characterisation, T_g, and information is given in Table 3.1-1.

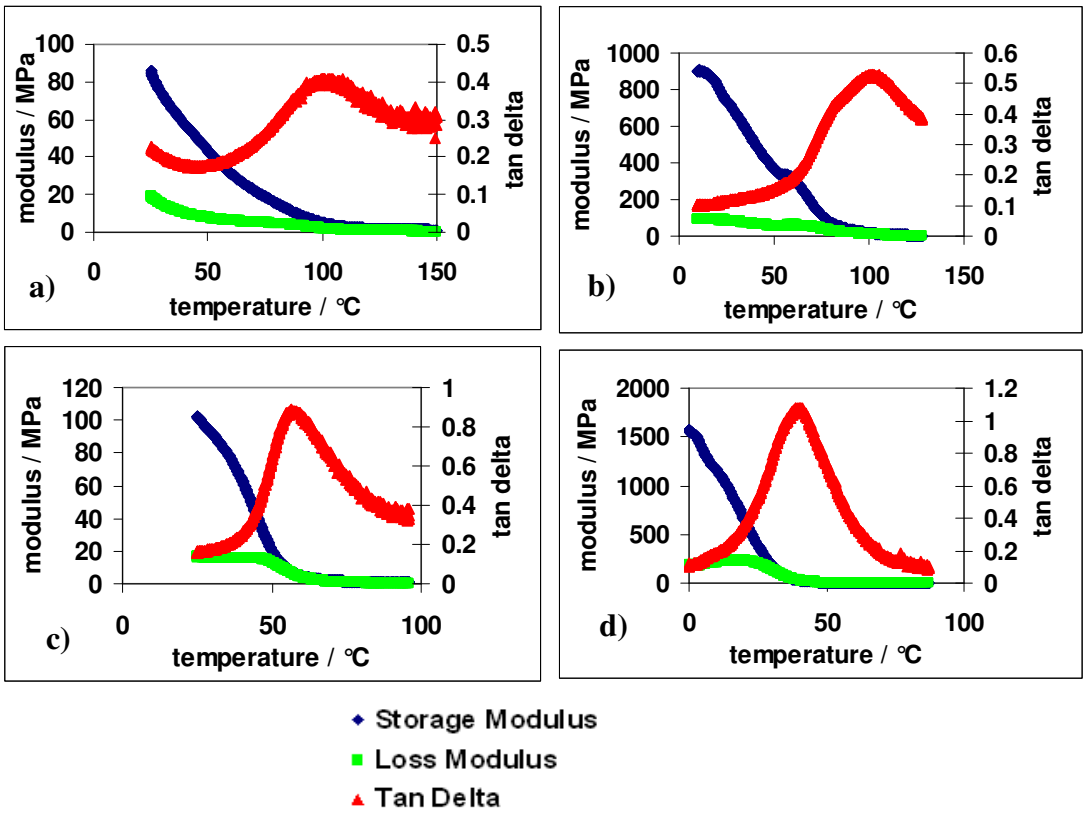

Figure 3.1-1 The glass transition temperature given by a peak in tan delta is shown for :- a) coating 1 , b) 2, c) 3, d) 4.

Table 3.1-1 Coating materials characterisation

Coating	coating thickness	code number	base of coating and given information	Tg approx./°C
1	40 - 80 µm	R11080/18/1	soft, durable, aliphatic polyurethane methyl acrylate (PUMA) latex.	101°C
2	40 - 80 µm	R11080/18/2	hard, interior, aromatic PUMA latex	94°C
3	40 - 80 µm	R11080/18/3	widely used, exterior grade acrylic latex	57°C
4	70- 130µm	R11080/18/4	alkyd	40°C

3.1.2 Epoxy

Epoxy samples were prepared using epoxy cold embedding resin, Epofix kit (Struers Ltd.) at room temperature. The epoxy resin is a bisphenol-A and epichlorhydrine reaction product which is cured with the addition of triethylenetetramine hardener. The hardener was added to the epoxy in various ratios to produce materials with varying amounts of cross-linking. The resulting samples gave examples of thermoset polymers with varying degrees of visco-elasticity. The samples were also cured, whilst in the mould, in an oven set at 50^{o}C for an hour thus ensuring that the chemical reaction would near completion. Tensile thermal DMA 1Hz on a free standing film of epoxy in the standard mix gave the glass transition temperature at approximately 40°C. Tensile samples had gauge length 70mm, width 13mm and thickness 2mm. Nanoindentation samples were small pieces approx 5 mm x 3 mm cut from tensile sample.

3.1.3 Cool-lok

Samples were made from Cool-lok (COOL-LOK® 34-250A), a hot melt adhesive which is a clay treated composition of paraffin waxes and petroleum, manufactured

by National Starch and Chemical Company Adhesives Division a member of the Akzo Nobel, (formerly ICI) group. (Tg 0° C DMA freq. 1 Hz) This is an isotropic, amorphous, thermoplastic polymer from which samples for testing can be easily prepared.

For all test conditions all Cool-lok samples were one day old.

Tensile samples gauge length 70mm, width 13mm and thickness 2mm. Nanoindentation samples were small pieces approx 5 mm × 3 mm cut from tensile sample.

3.1.4 Polymethylmethacrylate (PMMA)

The PMMA samples were cut from a 2.85mm thick sheet of Perspex (ICI, now Akzo Nobel). With a further PMMA sample supplied (Alternative Plastics Ltd, UK) as a 50 × 50mm cast sample of thickness 3mm. Samples for tensile testing were 25 – 26 mm wide 2.85mm thick with gauge length 250mm. The glass transition temperature literature value is between 95- 106°C.

The literature value quoted for the Young's elastic modulus of PMMA is 3.2GPa (Alternative Plastics Ltd.).

3.1.5 Glass

As a control material in the macroindentation study glass was also used. This was a 6mm thick standard soda-lime glass cut to produce a 50 x 60mm rectangular sample. The modulus, E, of the glass sample was 73.6GPa with a Poisson's ratio, ν, of 0.22, determined courtesy of National Physical Laboratories using a surface acoustic wave reflection technique.

3.1.6 Epoxy and Cool-lok sample preparation

Epoxy was mixed with hardener in the ratio 15:2 epoxy to hardener, (the standard mix), as well as in the ratios of 15:1 and 15:4. Due to the formation of bubbles which could potentially result in anisotropic samples, the mixture was poured into a small funnel, which was stopped until the bubbles had risen, (approximately one hour later). The mixture was then carefully poured from the bottom of the funnel into a dog bone shaped PTFE mould, to fill one mould at a time, a strip of Melinex (Melinex®), a polyester film, was immediately placed over the single mould and rolled over with a hard rubber printing roller. Once all moulds were filled a large sheet of Melinex was placed over the entire mould and the whole covered with a weighted sheet of glass. This method produced smooth, apparently bubble free, samples of uniform dimensions which were suitable for tensile testing. That is, samples having gauge length 70mm, width 13mm and thickness 2mm. Due to observed changes in the mechanical properties of the samples with time, all tests were carried out on samples that were aged for one week.

For macro indentation testing epoxy samples were prepared in the same way using a picture frame mould of set Express 2 Putty Soft (3M ESPE AG Dental Products Germany) clamped between supported Melinex sheets which resulted in rectangular samples approximately 50 x 60mm with 6mm thickness.

For the preparation of Cool-lok samples the dog bone shaped PTFE mould was used. Supplied pellets of Cool-lok were melted (approx.130° C) then poured into the mould at this temperature, still hot so that the melt flowed. The mould was slightly under-filled towards the grip edges of the mould but the gauge length part was filled evenly. As above, each mould was filled and covered with a strip of Melinex and

rolled over with a hard rubber printing roller (Figure3.1-2). Individual filling of moulds enabled more control over the even production of samples.

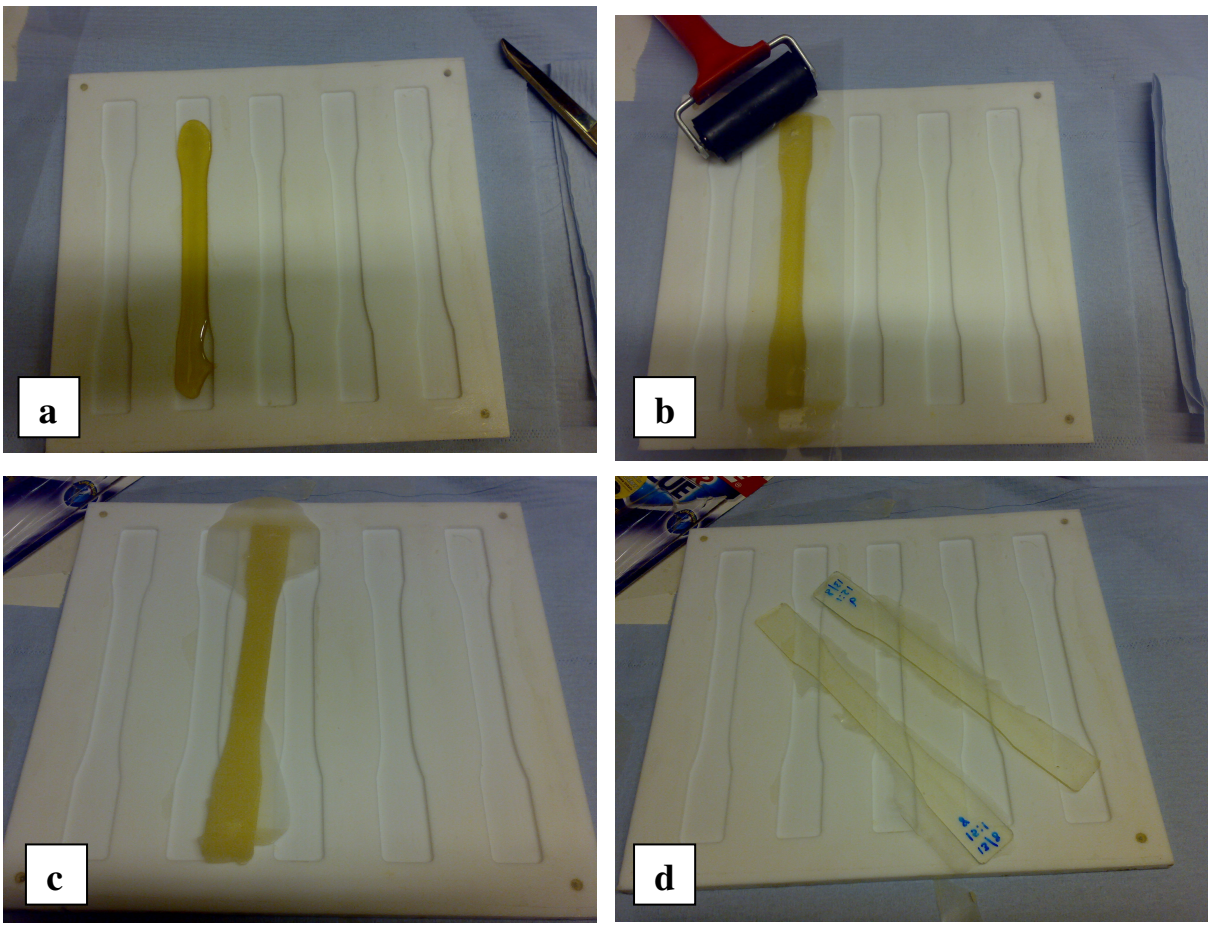

Figure 3.1-2 Sample preparation: the pictures show, a - melted Cool-lok poured into mould, b - Cool-lok flattened to fill mould, c - cooled Cool-lok sample, d - cured epoxy samples

3.2 Tensile tests

Tensile tests were performed using an Instron 5584 load frame (Norwood, MA, USA) with a 1kN load cell, resolution ± 0.05 N, and 2kN load cell, resolution ± 0.1N. The samples were tested using a ramp and hold loading protocol. The load as a

stress was linearly ramped to a maximum stress $P_{max.}$ over a rise time period, t_R, and then held at the constant maximum stress for a hold period of 150s, Figure 3.2-1.

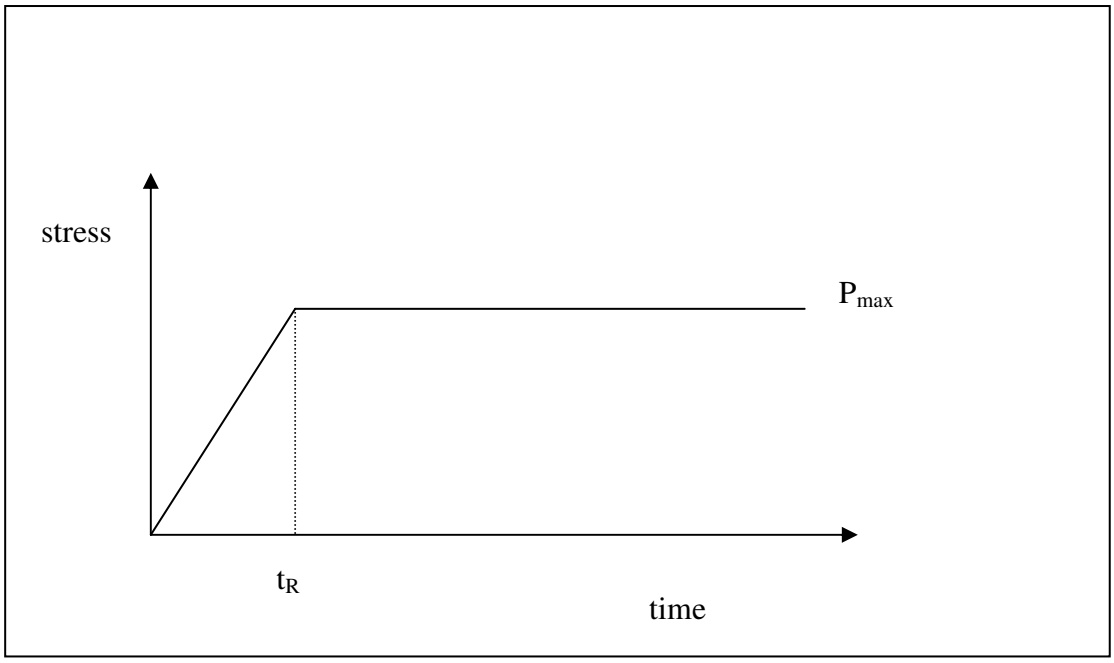

Figure 3.2-1 Schematic load time loading procedure for creep tests

Resulting strain creep curves were fitted using Origin® 7SR2 (OriginLab Corporation MA, USA.), see Appendix 11.1, and the obtained fitting constants were used to determine values for the creep function parameters $C_{0,}$ $C_{1,}$ and $C_{2.}$ The fitting procedure also produced values for time constants τ_1 and $\tau_{2.}$ These were then put back into equations 2 - 26 and 2 - 27 to check the quality of fit. From the creep function parameters G_0 and G_∞ were obtained as well as the creep ratio, C_r. (Chapter 2.3-7).

The values calculated for G_0 and G_∞ were calculated from results assuming $\nu = 0.5$, when the correct Poisson's ratio is known corrections to these values can be made.

When $\nu = 0.5$ the tensile modulus $E = 2G(1+\nu) = 3G_t$ where G_t is the experimentally determined shear modulus from the tensile test.

The correction to obtain shear modulus, G, from the tensile shear modulus, G_t calculated from tensile experimental results assuming $\nu = 0.5$, when the real Poisson's ratio, ν_k, is known is $G = G_t \frac{3}{2(1+\nu_k)}$.

3.3 Nanoindentation

Nanoindentation tests were performed using a UMIS (ultra micro-indentation system) -2000 nanoindenter (CSIRO, Lindfield, Australia).

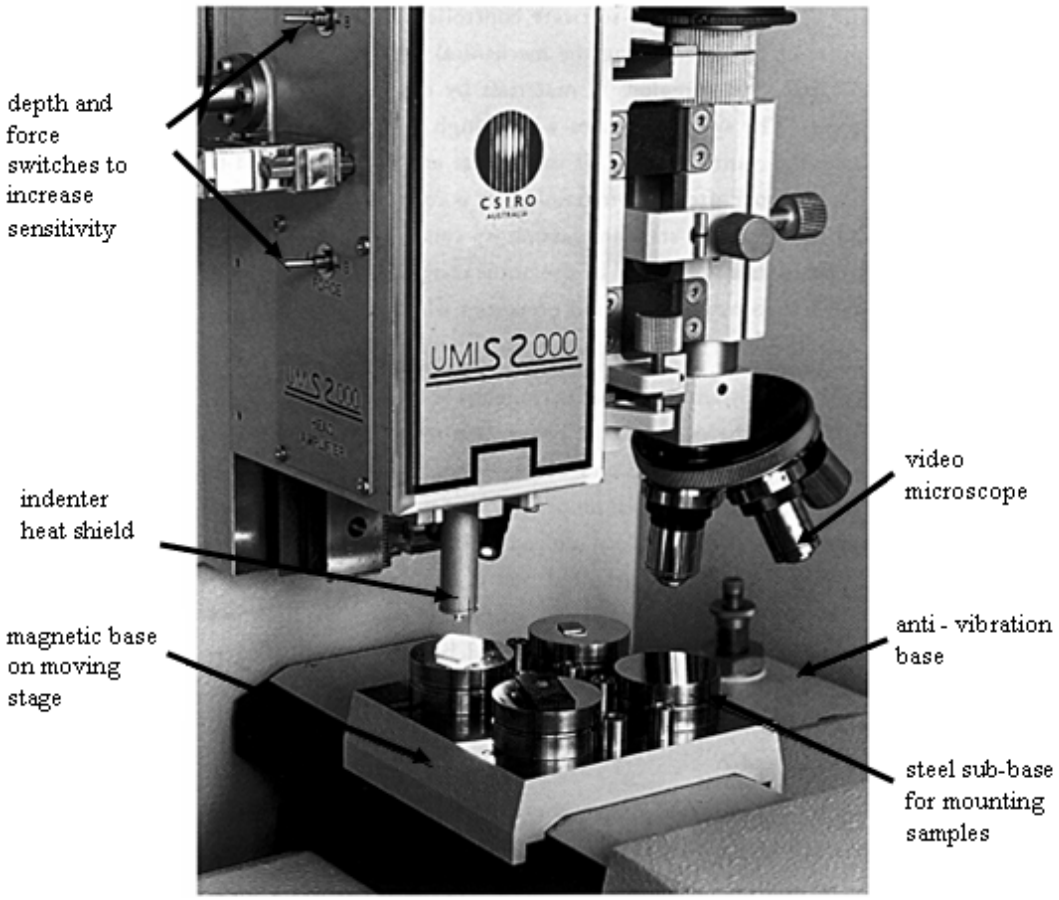

Figure 3.3-1 General view of UMIS 2000

The system is computer controlled. Force and displacement detection is based on linear variable differential transformers (LVDT). To reduce the effects of thermal fluctuations and vibrations the instrument is enclosed in a cabinet on an anti - vibration table. After setting up the tests and before the first test started the system was left to equilibrate at room temperature for 45 minutes to minimise mechanical and thermal fluctuations and keep within a thermal drift rate of less than 0.05 nm/s.

Samples were mounted to a hardened steel sub-base and attached to the magnetic base. Figure 3.3-1.

At the start of data acquisition a very small initial force of 0.1mN was applied enabling the system to set the zero point as the tip made contact. The force was then held constant while a datum for the measurement of subsequent indenter displacements was established.

The indenter was then driven into the surface until a resistance equal to the set force was met and in a series of steps, at force equilibrium, the penetration was measured. The load was applied as a sequence of linear steps to the chosen maximum load, which was held for a period of 120s and then decreased in the same steps to the starting value.

Nanoindentation force resolution was 0.2 μN and displacement resolution was 1-2 nm.

Remembering that for spherical indentation load is proportional to depth$^{3/2}$, the resulting displacement creep data were raised to the power 3/2 then fitted in the same way as tensile creep see Appendix 11.1. Resulting fitting constants were used to determine values for the creep function parameters C_0, C_1, and C_2. Values for time constants τ_1 and τ_2 were also obtained. The validity of the fit was checked by putting these parameters back into equations 2 - 46 and 2- 47. From the creep function the

parameters G_0 and G_∞ and creep ratio, $C_{r.}$ were calculated. Equations 2.30, 2.31 and 2.32.

In spherical indentation the indentation modulus is $E^* = \frac{1-\nu^2}{E} = \frac{1-\nu^2}{2G(1+\nu)} = \frac{1}{4G_i}$

when $\nu = 0.5$, and G_i is the experimentally determined instantaneous shear modulus.

The correction to obtain shear modulus, G, from indentation modulus, G_i is $G = G_i 2(1-\nu_k)$ with known ν_k (Oyen 2006).

3.4 Macroindentation

Large scale indentation was performed using an Instron 5564 load frame (Norwood, MA, USA) with a 1kN, and 100N load cell.

Loads were applied using displacement control of the crosshead at two rates to maximum load followed by a 120s hold load period.

The spherical indenter used was a polycrystalline alumina ball of radius 4.99 mm with literature value elastic modulus 380GPa and Poisson's ratio 0.22 (Auerkari 1996). The ball was held in a purpose built holder directly attached to the load cell.

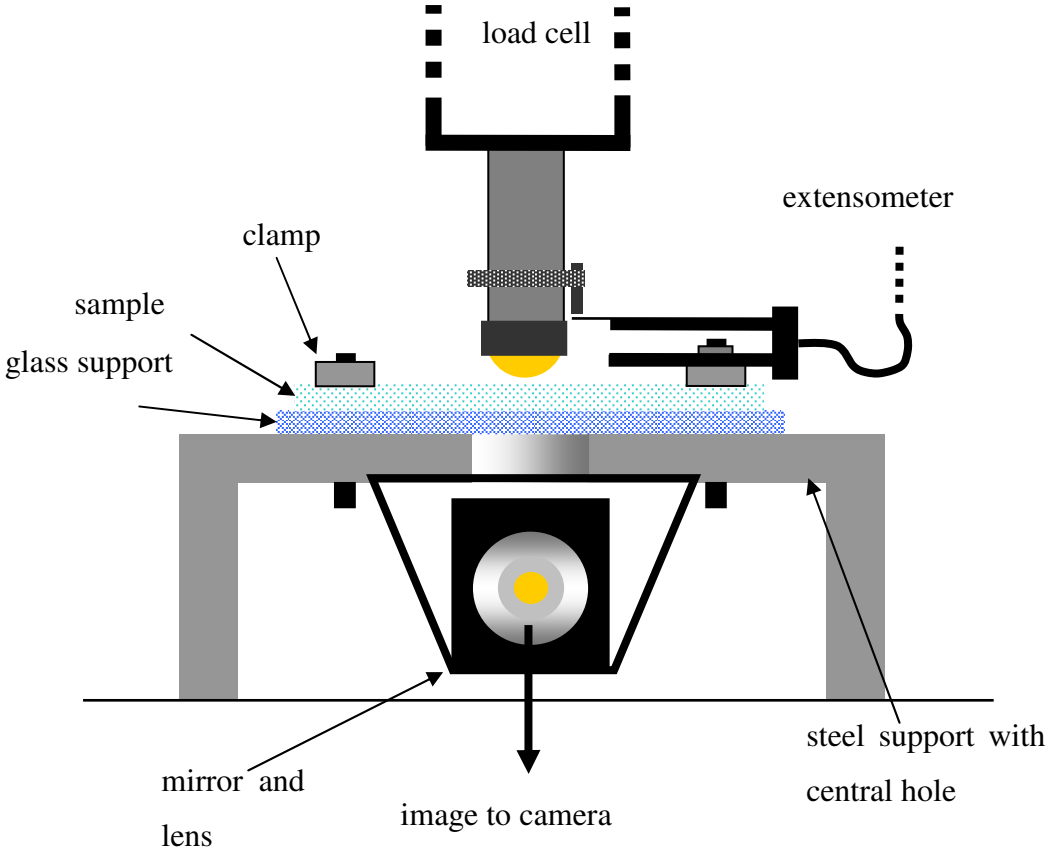

Figure 3.4-1 Schematic of indentation rig and set up

Figure 3.4-2 Photographs of experimental set up

A purpose built test rig of hardened steel was used. This incorporated a mirror such that *in situ* observation of the contact area was possible throughout the indentation (see Figures 3.4-1 and 3.4-2). Samples under investigation were supported on a 5mm thick piece of glass and clamped to the rig.

An image of the contact area, time, strain of extensometer (subsequently converted to displacement), and applied load were simultaneously recorded at intervals throughout the test.

To increase the reflectivity of the surface under contact and thereby improve the contrast of the images, the samples were coated with carbon using a Balzers CED 030 carbon thread evaporation unit. The standard procedure for coating samples for scanning electron microscopy was used. This resulted in a coating thickness approximately 10 to 15 nm, which had no effect on the indentation displacement results but significantly improved the observation of the contact area.

Images of the contact areas were photographed with a Canon EOS 450D digital camera with a macro lens capable of 1:1 magnification. The camera was securely mounted, and before the start of each test the lens was manually focussed on a loupe graticule placed in direct contact with the sample surface for the purpose of measuring pixels and calibrating the image scale. Thereafter the camera focus was not changed nor the camera moved until the test completed.

The photographic images of the contact area were processed and the contact area measured in pixels using Image J image processing freeware. (See Appendix 11.2 for details). The image scale was calibrated for each material to eliminate any errors due to the variation in refractive index between the materials.

Contact area measurements in pixels were then converted into contact areas in micrometres. Average values for the radius of the contact area, *a*, were also calculated. ($a = \sqrt{\pi A}$).

Using the experimentally obtained contact area radius value, *a*, the reduced indentation modulus, *E** was calculated from the Hertzian relationship $E^* = \frac{3PR}{4a^3}$.

The design of the test rig was such that displacement data was collected as directly as possible to the actual displacement of the indenter ball so that the effects of frame compliance on displacement measurements were minimised. Depth measurements were made by means of converting the strain measured with an extensometer of gauge length 13mm into displacement.

The extensometer was positioned such that the gauge length was between the surface to be indented and a screw specially attached to the ball indenter holder designed to push the extensometer as the penetration depth increased with load. (This can be seen in Figure 3.4-1)

The compliance of the experimental frame was determined by treating the total compliance, C_t, as the sum of the sample compliance, C, plus the frame compliance, C_f, $C_t = C_f + C$. Using $h = h_m - h_0 - C_f P$, where h is the depth of the indenter displacement, h_m is the measured depth, h_0 is the initial displacement at the start of the test and P is the applied load the frame compliance was determined.

Corrections were made to the measured displacement and load by subtracting the initial displacement of the extensometer and the corresponding load Figure 3.4-3.

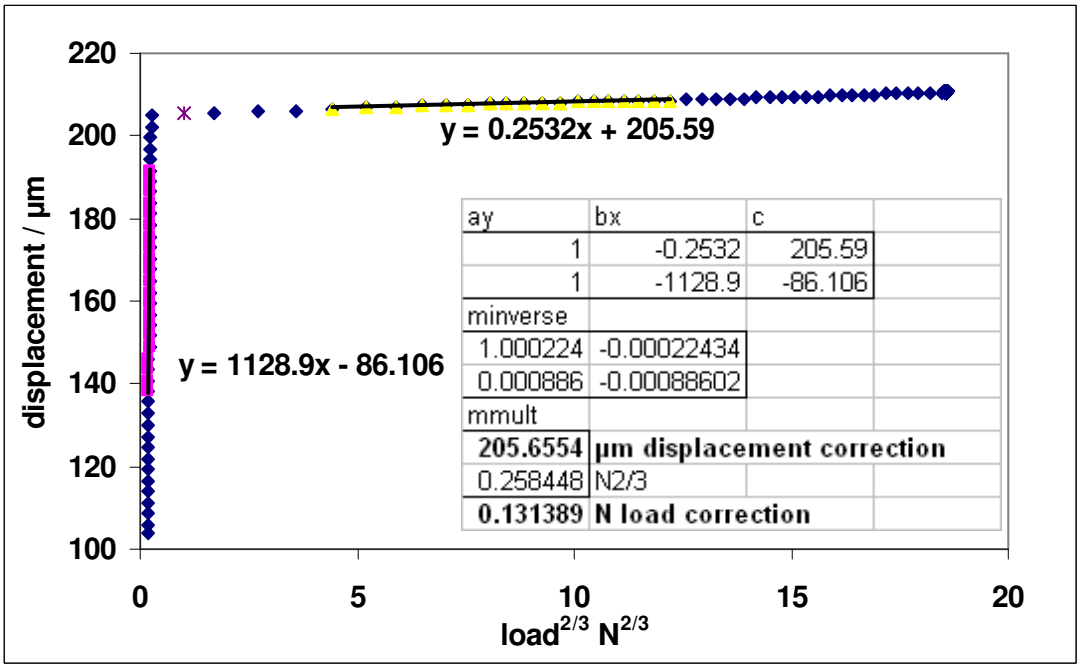

Figure 3.4-3 Showing raw displacement vs load$^{2/3}$ to determine initial contact corrections from simultaneous equations

A plot of measured depth, $h_m^{3/2}$, versus load, P, was constructed from the indentations on glass and a theoretical data set, $h_t^{3/2}$, using $h_t^{3/2} = \frac{3}{4}\frac{1}{E^*}\frac{P}{\sqrt{R}}$ was plotted alongside a proposed corrected depth data set, $h^{3/2}$, using the experimental load values. The parameter C_f was then adjusted until the corrected data set for the depth gave the best fit to the theoretical set. Values for C_f were less than 0.02 µm/N.

This method is based on the reasonable assumption that the contact is Hertzian for spherical indentation into glass. The value used for the modulus, E, of glass was 73.6GPa with a Poisson's ratio, ν, of 0.22, these values were determined independently using a surface acoustic wave reflection technique, courtesy of National Physical Laboratories.

4 Aging and weathering study: Polymer coatings on glass slides

4.1 Introduction

UV irradiation in a reactive atmosphere such as air generates radicals at the polymer surface. Gao *et al.* have seen in polyethylene terephthalate, PET, that such surface reactions have a strong effect on the surface chemical composition, morphology, adhesion, thermo-mechanics and stiffness/modulus, although specifically visco-elastic behaviour was not studied (Gao *et al.* 2005). Surface wetting due to rain or dew condensation causes rapid expansion and contraction of the polymeric material, and elevated relative humidity and temperature will enhance photolytic degradation (Burch *et al*.2002). Physical aging occurs throughout the bulk of the material as free volume and mobility of chains decrease, however chemical aging starts at the surface, and this has been seen in various polycarbonate films when elastic modulus and hardness have been investigated using nanoindentation (Boersma *et al.* 2004).

In this study nanoindentation was used to investigate the mechanical properties of four coatings supplied by Akzo Nobel (formerly ICI). Using nanoindentation the coatings were ranked according to their mechanical properties and to changes in these in response to exposure to natural weathering. The aim of this study was to determine whether nanoindentation is sensitive to changes in the mechanical properties of commercially based, newly developed coating samples rather than selected "well-behaved" polymers. It was required that any changes, both chemical and physical, would be naturally occurring and in real time. This would enable the development of a nanoindentation method and analysis to examine coatings after

periods of natural weathering. This technique could be used as an alternative to the currently used accelerated weathering testing which is severe and destructive to the coatings.

4.2 Methods

Coatings 1 to 4 as described in Chapter 3 Table 3.1-1 were indented as supplied, *i.e.* as coated glass slides, using the UMIS 2000 nanoindenter with a 100 μm radius spherical diamond tip, using the ramp and hold method.

The load procedure was:- maximum load, P_{max}, 0.2mN, ramped in 10 linear increments (*i.e.* t_R was approximately 20s) The maximum load was then held for a period of 120s. Each batch of tests consisted of 30 indents 50μm apart in a linear array across the sample surface.

As an initial control test, two samples of each coating were indented. Approximate h_{max} values were 650 nm for coating 1, 260 nm for coating 2, 470 nm coating 3 and 1500 nm for coating 4.

One slide of each coating type was then placed on a raised grid shelf, in a tray, covered with a clear polystyrene, propagator lid (Homebase Ltd. UK) and left in an environmentally exposed area (exposed, south facing, first floor window sill in south east Essex) for subsequent testing. The remaining one slide of each coating type was left covered, unexposed in a drawer, in a temperature controlled but not humidity controlled laboratory for subsequent testing.

Tests were performed on both exposed and unexposed samples after one week, three weeks, seven weeks, twenty-two weeks, twenty-five weeks, thirty-nine weeks sixty-six weeks and ninety weeks.

4.3 Results

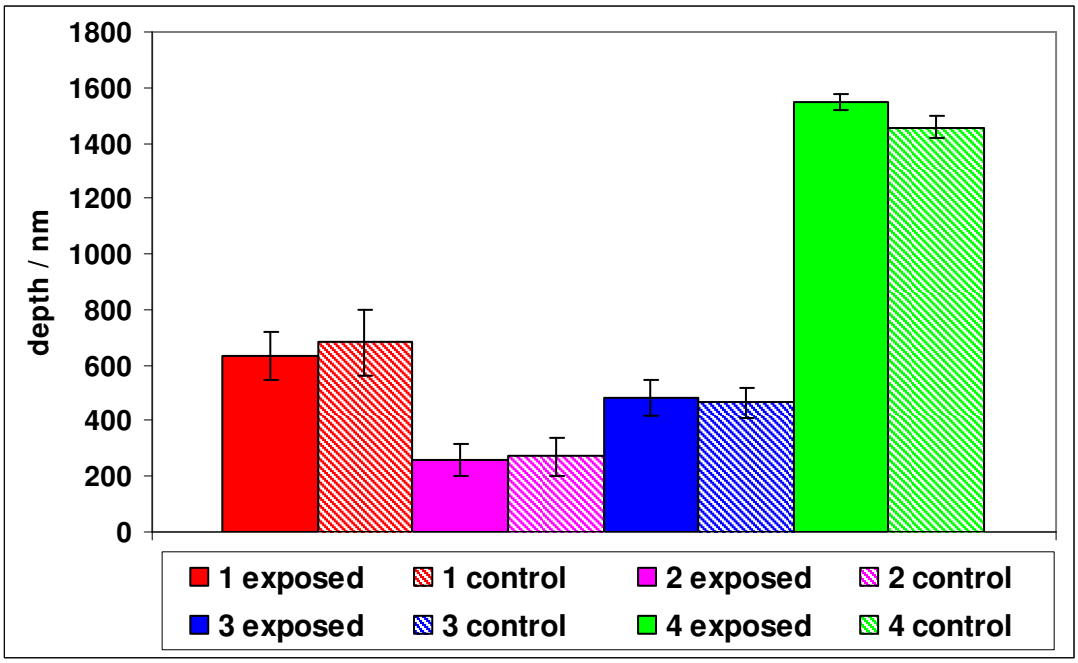

Figure 4.3-1 At the start of the test and before any exposure, maximum penetration depths show no differences between coatings of the same type but significant differences between coating types.

error bars at 95% confidence

All measured maximum penetration depths appear to be small compared to the film thickness, less than 2.5% of the film thickness, thus substrate effects are minimised.

The initial, control, tests showed that the four coating materials behaved differently in response to the same indentation test procedure. The measured maximum depth of penetration for each coating type is different, but for slides coated with the same material there is a good agreement in measured maximum penetration depth, Figure 4.3-1.

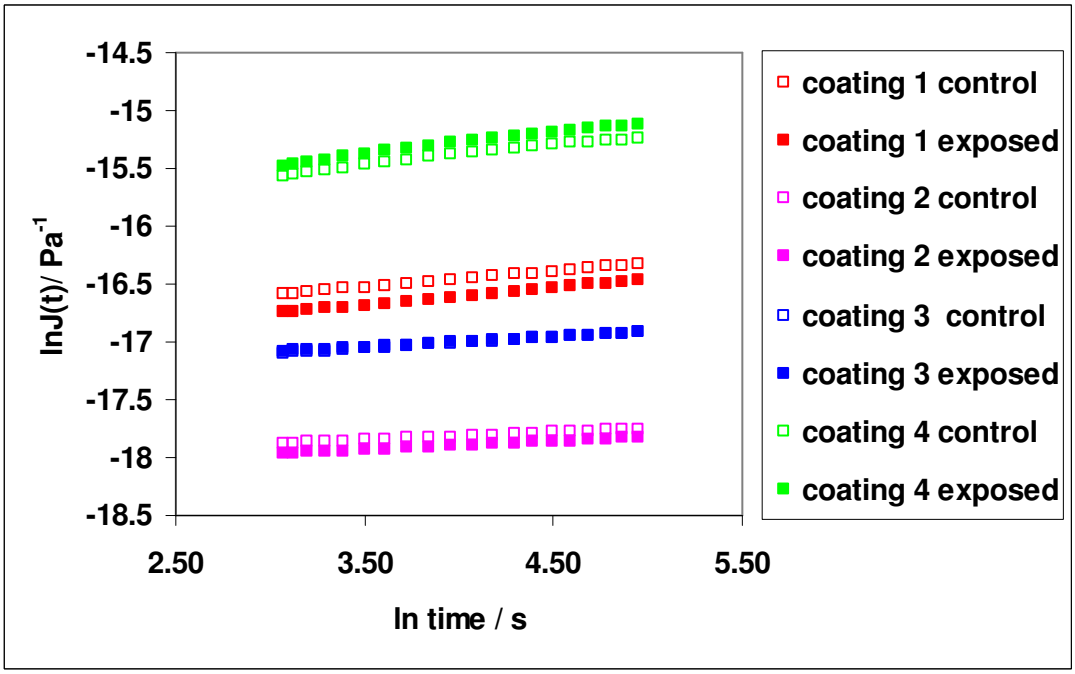

Figure 4.3-2 Averaged lnJ(t) versus ln time for all samples at start of experiment shows differences between coating types.

The creep response of each different coating type was also different and the coatings were distinguished by the creep function ln J(t) versus ln time plots (Figure 4.3-2). Figure 4.3-2 shows the differences between coatings in terms of creep function, differences in gradient as well as differences in values can be seen. In addition the variation within each coating type can be observed.

From the creep function of the material, instantaneous and long-time shear moduli were determined, and the creep ratio which is derived from these gives an indication of the visco-elasticity of the coatings. Two materials may have similar instantaneous moduli for example but their creep ratios may be different.

Differences were evident in the percentage relative creep as well as the calculated creep ratio values, C_r , $C_r = 1 - \frac{G_\infty}{G_0}$. Using the creep ratio values statistical t – tests were done before any exposure, the differences between the two slides of the same

coating were found to be insignificant. Analysis of variance tests showed that the differences between coating types, however, were significant, (see Appendix 11.3).

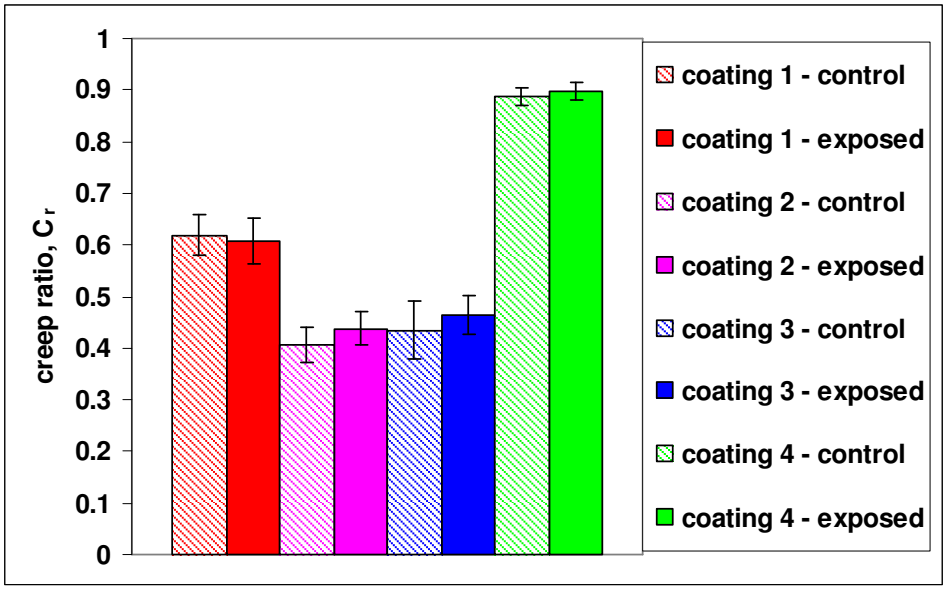

Figure 4.3-3 At the start of the tests differences in creep ratio, C_r, can be seen between coating types but not between slides having the same coating type.

error bars at 95% confidence

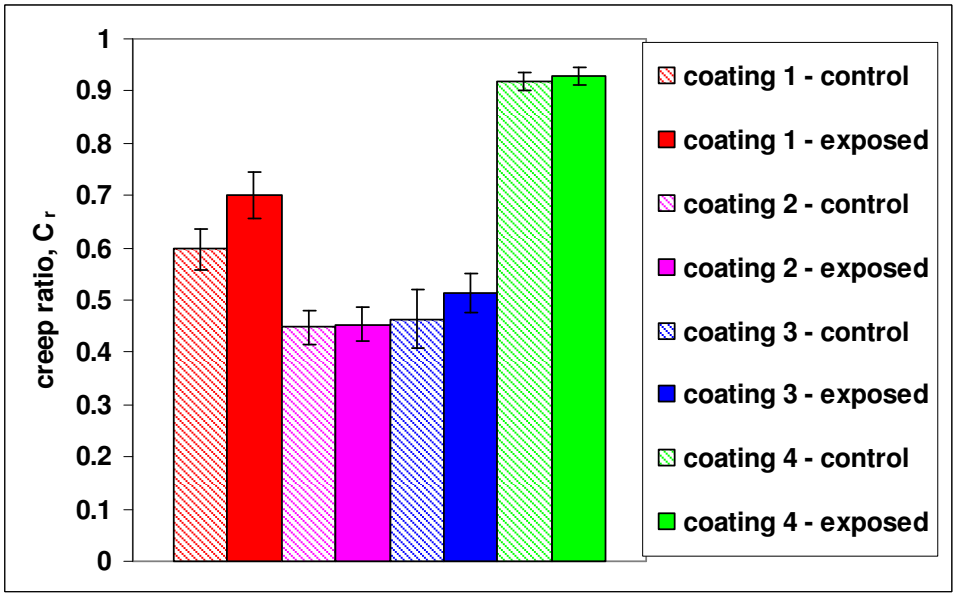

Figure 4.3-4 After 1 week a difference in creep function is seen in the exposed coating 1.

After 1 week, differences were seen in the response of the exposed coating 1, the aliphatic PUMA latex. More creep occurs in the exposed sample and this can be seen as an increase in creep ratio which is statistically significant, Appendix 11.4-1.

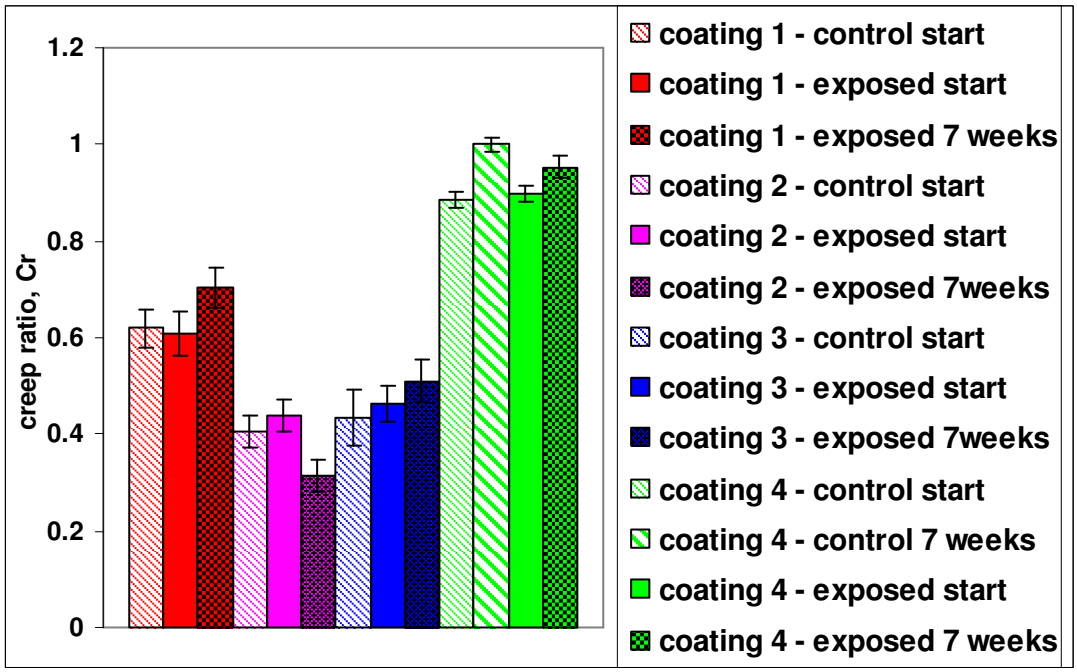

Figure 4.3-5 After 7 weeks differences in creep function are seen in the exposed coatings of all coating types and in both the control and exposed coating 4

Although not so clear from the calculated mean values of creep ratio after 7 weeks compared to the initial values for creep ratio (Figure 4.3-5), statistical tests using calculated creep ratios performed after 7 weeks suggest that the exposed slides for coatings 1, aliphatic PUMA, 2, aromatic PUMA, and 3, acrylic, have all changed significantly from the initial condition. (Statistical analysis results can be seen in Appendix 11.4-2).

At 7 weeks both samples of coating 4, alkyd based, had also changed. The model used in the analysis of the data is no longer suitable. Calculations using the amplitude coefficients resulted in moduli with negative values. The creep response may be non

linear and the experimentally observed creep behaviour may be better described by another model; further investigations need to be made.

Any changes in the creep curves that can be disregarded as scatter, possibly due to surface roughness, are evident in plots of creep versus log time appearing as a parallel shift in the slope of the data. Real changes in mechanical response due to changes in the material as a result of environmental conditioning would be seen as change in gradient of the data as the material creep response changes.

In plots of raw creep displacement versus log time at the start of the experiment and after 25 weeks, Figures 4.3-6 to 4.3-9, changes between plots (a) and (d), (the exposed coating), would be expected if environmental conditioning had caused changes in mechanical response. Plots (b) and (c) would be expected to be similar as these are plots of the unexposed coatings at the start and after 25 weeks. It can be seen that in addition to changes in scatter there is also evidence of changes in material response apparent as change in gradient of the data of some of the test results in a batch of tests. This is evident in the exposed coating 1 and in both samples of coating 4 which change gradients from being initially non linear to linear after 25 weeks. In addition, the exposed coating 4 shows some further steep gradient changes.

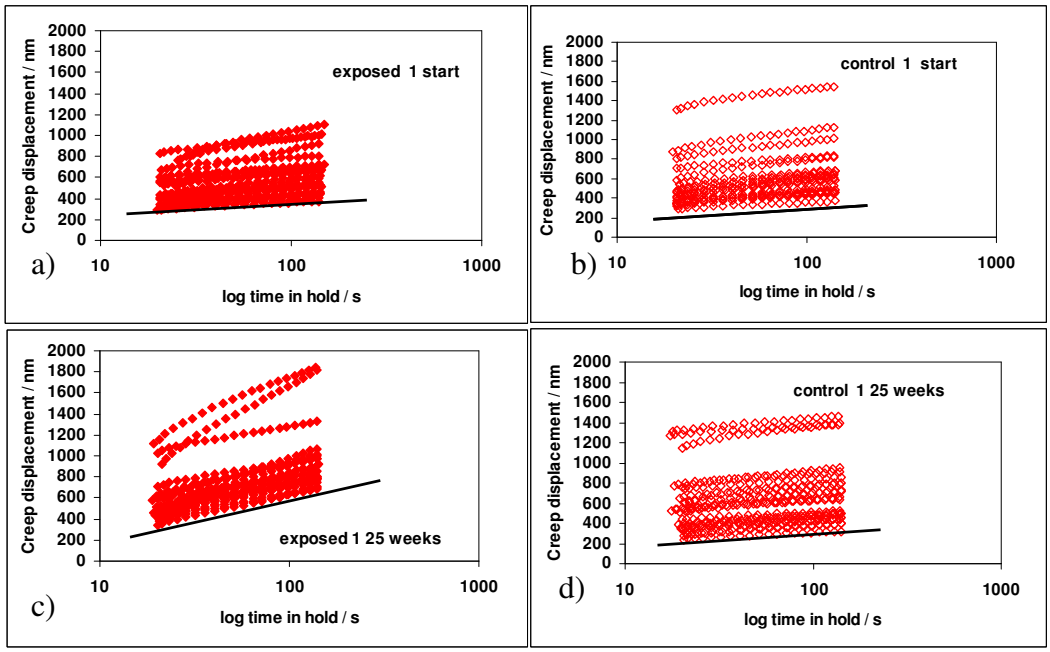

Figure 4.3-6 Creep displacement/log hold time aliphatic PUMA coating.; the exposed coating shows changes in gradient from start to 25 weeks a) to c), whereas no change is shown for the control coating b) to d)

(black line is a guide to eye)

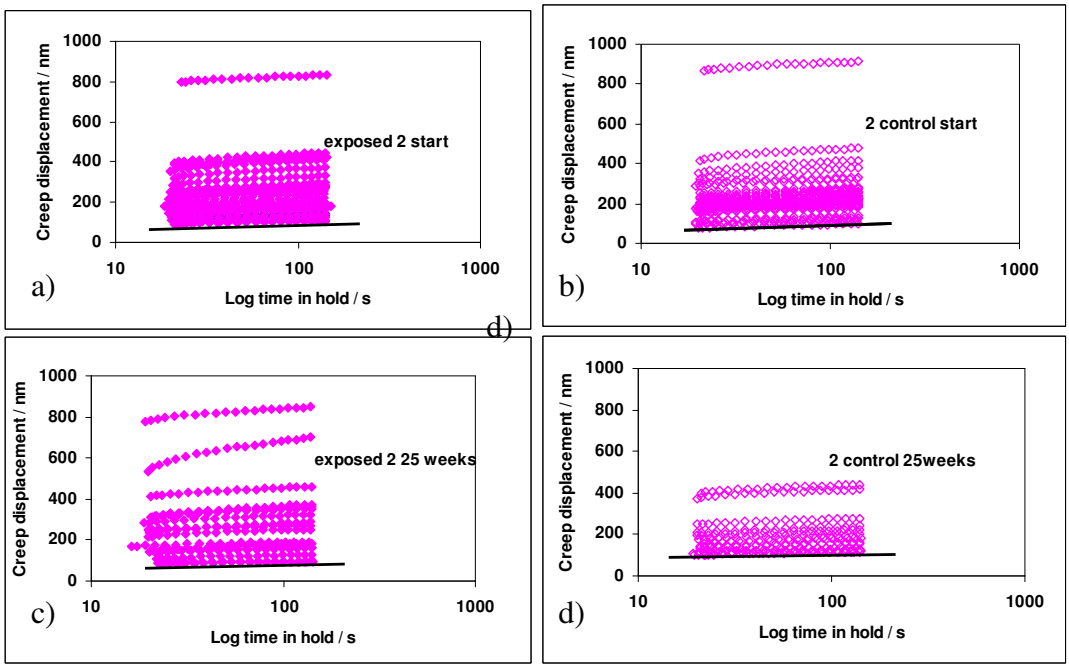

Figure 4.3-7 Creep displacement/log hold time coating 2; no changes can be seen in the exposed coating from start to 25 weeks a) to c) or the control coating b) to d)

(black line is a guide to eye)

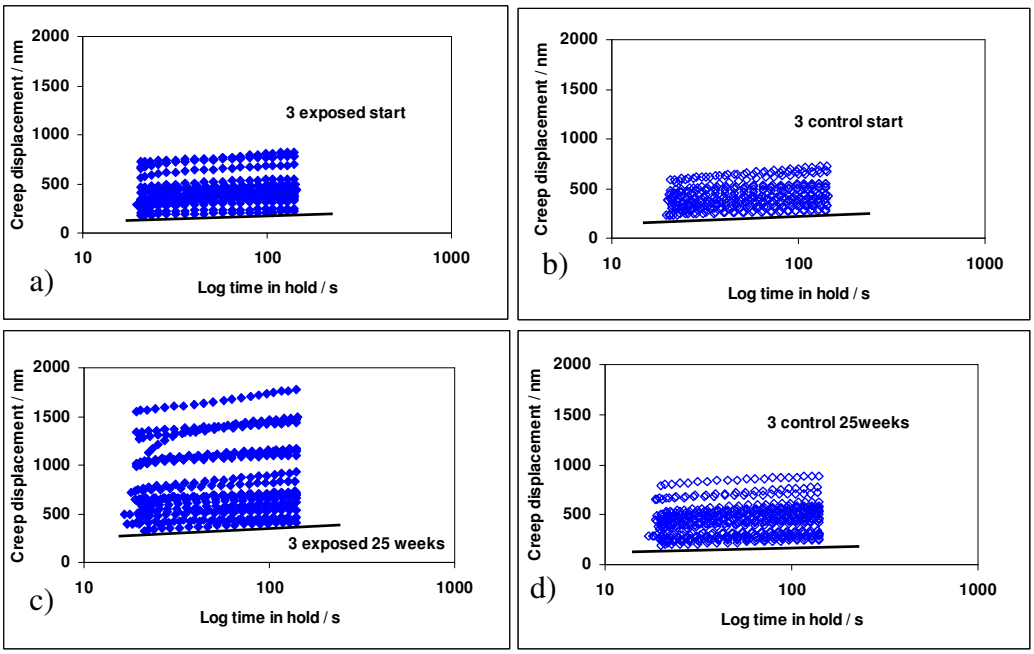

Figure 4.3-8 Creep displacement/log hold time for acrylic latex based coating 3; no changes can be seen in the exposed coating from start to 25 weeks a) to c) or the control coating b) to d)

(black line is a guide to eye)

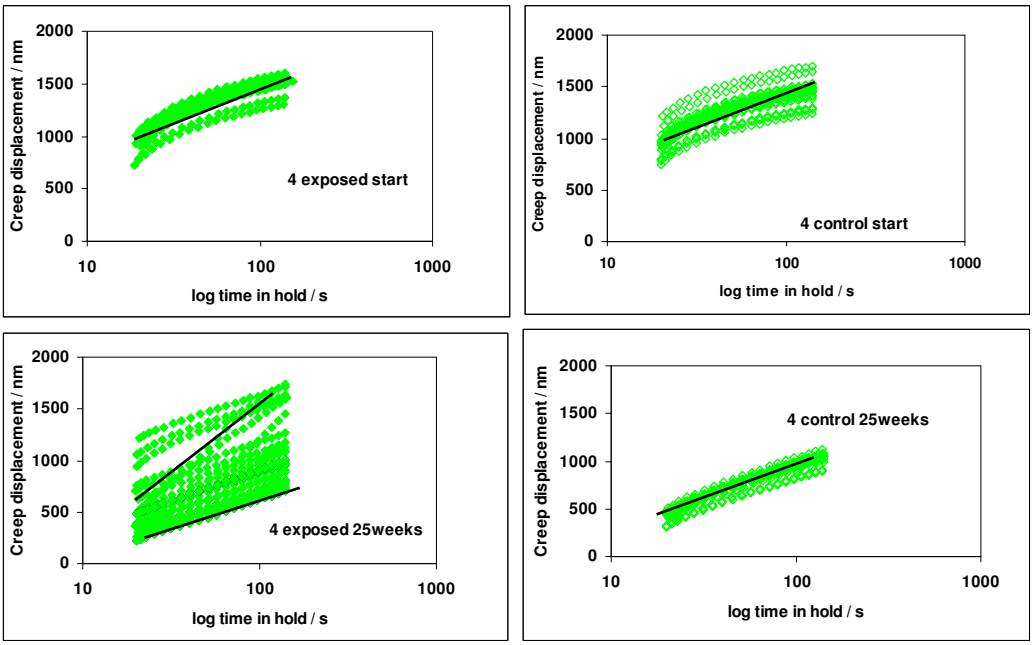

Figure 4.3-9 Creep displacement/log hold time for alkyd based coating 4; changes can be seen in both the exposed coating and the control from start to 25 weeks a) to c) and b) to d) curves become linear the exposed coating also shows some steep gradient changes

(black line is a guide to eye)

As sampling of the surface was done as a line of 30 indents 50 μm apart, the changes in the slope of creep displacement versus log time apparent in only some of the indents of coatings 1 and 4 could suggest that the material is changing in some regions of the surface and not in others.

Due to the failure of the analysis to produce valid modulus values and consequently creep ratios, it was no longer possible to use these to follow any changes in mechanical properties. Subsequently, the mean value of the normalised raw creep at the end of the creep time period was used. *i.e.* displacement at t_{creep} =120s/ displacement at t_{creep} =0. This effectively normalises for the scatter in the ramp load displacement as does the gradient in plots of raw creep displacement versus log time but mean normalised raw creep is simpler to calculate from the raw data produced.

Figures 4.3-10 to 4.3-13 show the changes in the normalised raw creep from the start of the test to the finish 90 weeks later.

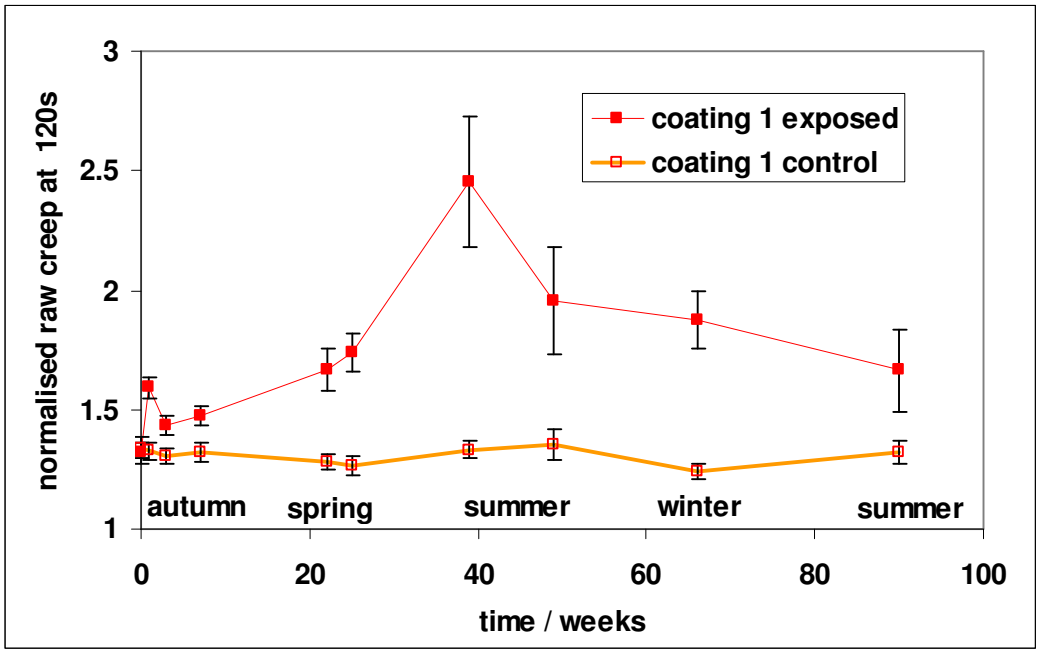

Figure 4.3-10 Coating 1 creep response changes with length of exposure, control coating shows no age related changes

error bars at 95% confidence

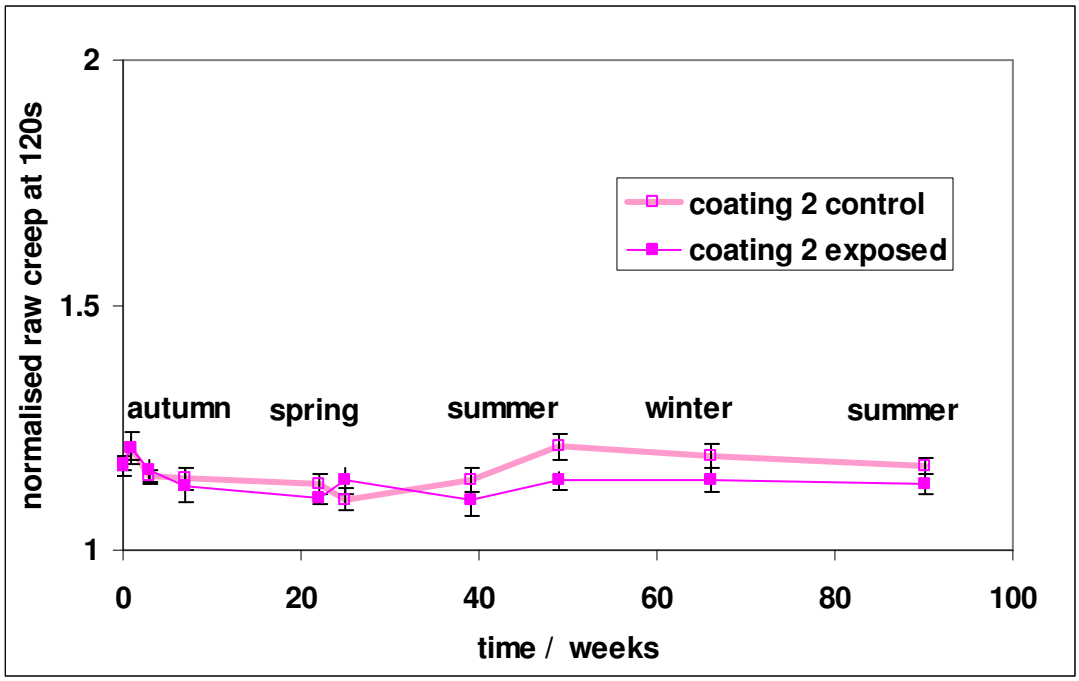

Figure 4.3-11 Coating 2 creep response shows no clear trend with exposure, no age related change can be seen

error bars at 95% confidence

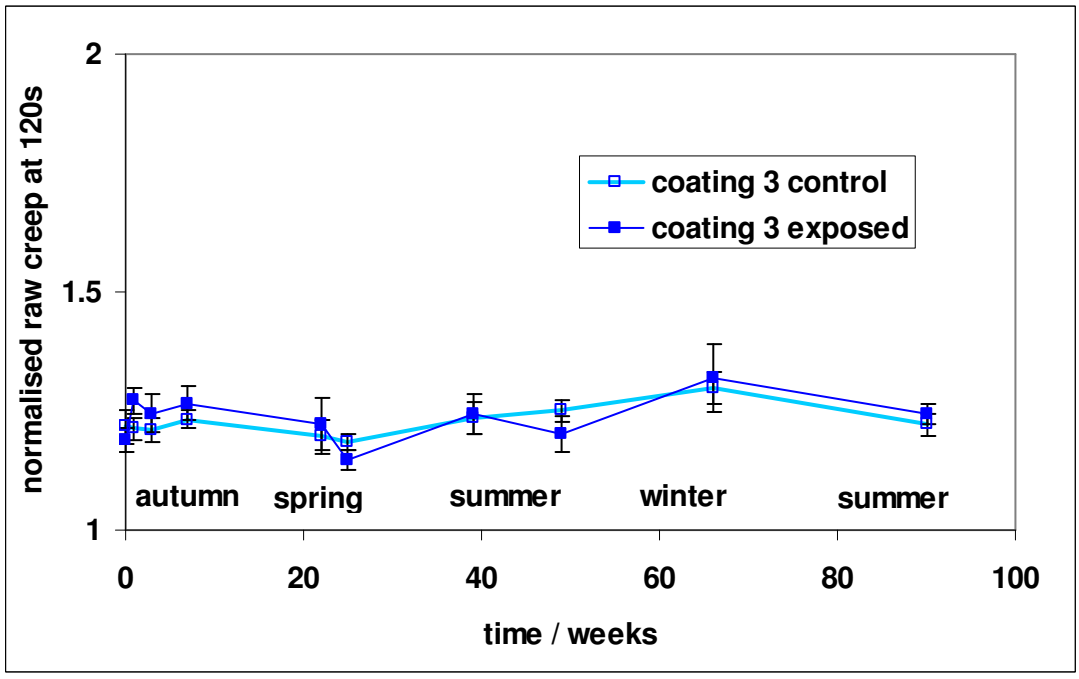

Figure 4.3-12 Coating 3 creep response of exposed and control fluctuate together no age or exposure related changes can be seen

error bars at 95% confidence

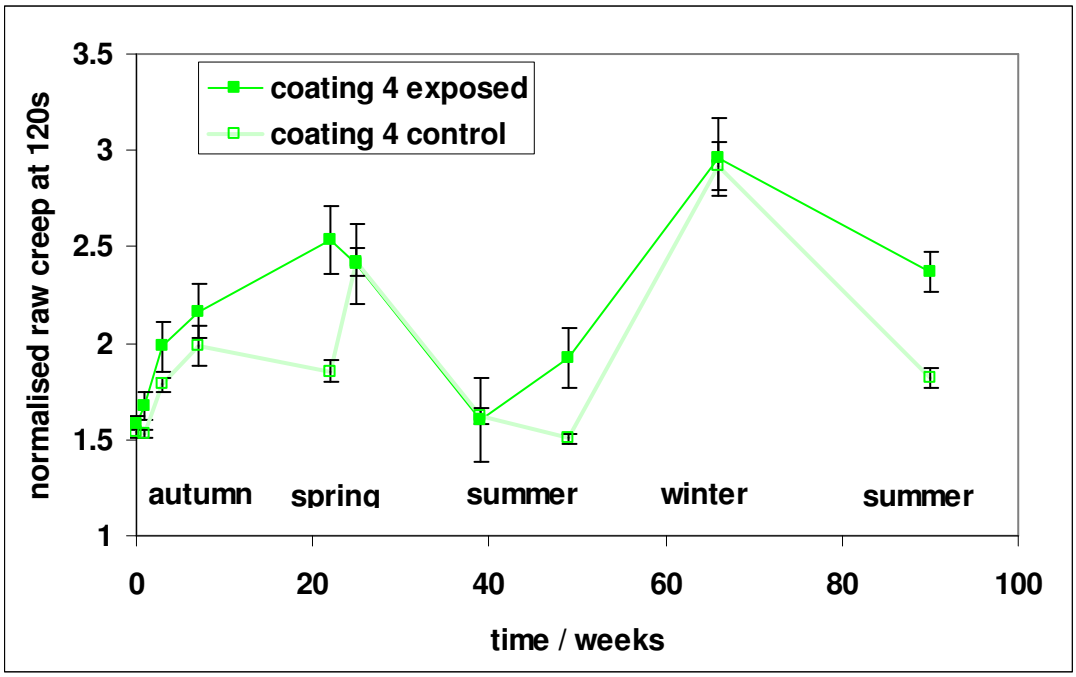

Figure 4.3-13 Coating 4 creeps more with age and with exposure, both exposed and control creep response fluctuate seasonally

error bars at 95% confidence

At the end of the 90 week test period the different responses of the coatings to natural weathering were clearly seen in the changed creep response, Figures 4.3-10 to 4.3-13.

Coating 1 shows the most significant changes. There appears to be a trend of increasing relative creep with increasing exposure. This behaviour appears to support the description “soft and durable” as given by Akzo Nobel Table 3.1-1

Coating 2 shows no clear trend with increasing exposure, and no obviously discernable trends with aging.

Whilst it should be remembered that the composition of the coatings includes the alcohol as well as any additives which also contribute to its properties the changes

seen might be expected as the phenyl group in coating 2 provides more chemical stability and is therefore more likely to resist sunlight induced reactions compared to the aliphatic PUMA based coating 1.

Coating 3, acrylic, both control and exposed coatings appear to behave very similarly, no clear trends are evident with age or exposure. As this coating is described as a widely used exterior grade coating these results are not surprising.

Coating 4, alkyd based, appears to creep much more as it ages, the trend is generally an increasing percentage relative creep with age. The exposed sample also appears to creep more than the unexposed. Both coatings appear to have similar variations in mechanical response. The increasing creep with age gave rise to invalid modulus values, as the material response was no longer described by the linear visco-elastic model used.

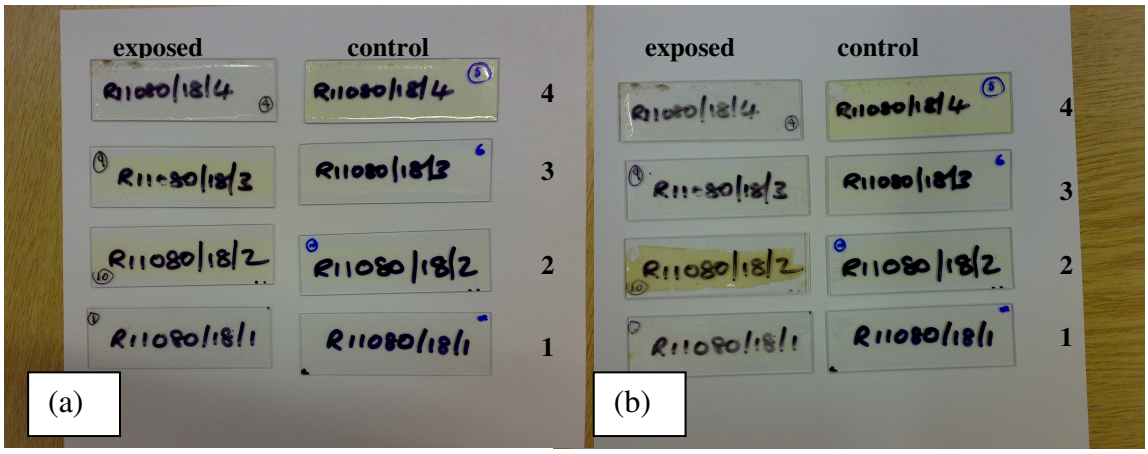

((a): photographs taken 22 weeks after initial tests, (b):photographs taken 49 weeks after initial tests

Figure 4.3-14 Coatings show changes in colour with age and exposure

As well as changes in creep, some of the sample slides showed a marked change in colour. This was apparent after 22 weeks from the start of the experiment. Coating 2 and 3 yellowed with exposure relative to the colour of the unexposed sample slide. Figure 4.3-14. Yellowing is expected in coatings based on aromatic isocyanates. On

the contrary coating 4 yellowed with age and the exposed coating became clearer. No obvious changes were seen in coating 1.

After 49 weeks the exposed coating 2, hard interior aromatic based, began to detach from the glass substrate and showed more yellowing in colour. The exposed alkyd based sample had lost the slight yellow colour it had at the start.

The changes in colour as well as the changes in mechanical response indicate that chemical changes were occurring in the material and preliminary investigations suggest that it is possible to determine these changes using attenuated total reflectance Fourier transform infra red, (ATR FTIR), spectroscopy. However due to the complexity of the resulting spectra and unknown details of the exact chemistry of the coatings this was not pursued in this work

4.4 Summary

Although the results show that the nanoindentation ramp and hold load method and accompanying analysis was suitable for probing the mechanical properties of the films, the resulting modulus values were questionable. The validity of the calculated modulus values is not known.

As tensile testing is widely accepted as a standard method for determining modulus values, in the following chapter the modulus values obtained from nanoindentation tests are compared with those obtained using a similar method and analysis in tensile tests.

5 Comparison between tensile and nanoindentation testing for the determination of visco-elastic properties and shear moduli

5.1 Introduction

The problems associated with testing a time dependent material can be overcome by using the ramp and hold method and analysis to determine a full mechanical characterisation as previously discussed in Chapter 2. Tensile testing is recognised as the standard method to determine the mechanical properties of a material. By performing the same method and analysis on the same material in both tension and nanoindentation, which is the only suitable method for coatings, a comparison can be made and the validity of nanoindentation test results can be examined.

As seen in the previous chapter the mechanical response to the same test may be different for different types of polymers. For this reason different types of materials, amorphous, thermoplastic, and thermoset with varying degrees of cross-linkage, were tested over different loads at different load rates.

Considerations should be given to the inevitable differences between nanoindentation testing and tensile testing. Stress in a tensile test is through the bulk of the sample whereas indentation will test only a very small area and volume of the sample. In addition, in indentation testing when load is controlled and held constant the resulting stress under the indenter depends on the contact area and is non-uniform

unlike the resulting stress in tensile loading which is explicit and uniform. Consequently in indentation, due to the increasing contact area, the normal component of stress is not constant.

However, as previously discussed, both nanoindentation and tensile testing can provide valid results from which visco-elastic properties and shear moduli can be derived. As these are assumed to be material properties a direct comparison between these tests should produce the same results.

A correlation between nanoindentation test results and results obtained from the widely accepted tensile test would confirm the suitability of using nanoindentation as a valid method to obtain the mechanical properties of coatings whilst attached to their substrate using creep and visco-elastic correspondence analysis as mentioned in previous chapters.

5.2 Methods

Both tensile tests (Chapter 3.2) and nanoindentation tests (Chapters 2.4 and 3.3) were performed on poly-methylmethacrylate, (PMMA), epoxy with varying degrees of cross-linking, and COOL-LOK® 34-250A (Cool-lok) samples.

For nanoindentation testing, pieces of epoxy and PMMA samples were mounted to the sub base using a very small amount of cyanoacrylate adhesive (Superglue). Cool-lok pieces were mounted to the base by heating the base sufficiently to allow the Cool-lok to just melt and on cooling be securely attached.

In tensile tests nine samples of PMMA, Cool-lok and nine samples of each of three different epoxy-hardener mixtures were ramped to three maximum stresses, $P_{max,}$ in three rise times, t_R , see Tables 5.2-1 to 5.2-3.

Nanoindentation testing was done using a similar ramp and hold method as in tensile testing, *i.e.* three maximum loads, P_{max} after three different rise times, approximately 8 s, 22 s, and 32 s according to the set 1 increment, 10 increments and 20 increments to maximum load, of the UMIS operating system. (Tables 5.2-1, 5.2-2 and 5.2-3). The creep hold period was 120 s in both tensile and indentation tests. The radius of the spherical indenter tip was 21 μm. After setting up the tests and before the first test started the system was left to equilibrate at room temperature for 45 minutes to minimise thermal fluctuations and keep within a thermal drift rate of less than 1nm/m.

Tensile tests on PMMA were performed, primarily, to ascertain the validity of the tensile procedure, as the PMMA was the only sample tested with a modulus value that was known in advance. (Given by supplier as 3.2GPa. see Chapter 3.1-4). For this reason the PMMA sample was tested under fewer loading conditions than the epoxy and Cool-lok samples.

Test parameters were chosen in an attempt to minimise the resulting strains consequently test parameters vary between the different materials.

Table 5.2-1 Loading procedures for Epoxy :Tensile and nanoindentation

Tensile				**Indentation**			
sample number	rise time t_R (s)	load rate (MPa/s)	maximum stress P_{max} (MPa)	increments of load	rise time t_R (s) approx.	load rate (mN/s) approx.	maximum load (mN)
1	2	2	4	1	9	0.3	3
2	2	4	8	1	11	0.9	10
3	2	8	16	1	13	2.3	30
4	20	0.2	4	10	20	0.15	3
5	20	0.4	8	10	25	0.4	10
6	20	0.8	16	10	27	1.1	30
7	50	0.08	4	20	31	0.09	3
8	50	0.16	8	20	37	0.3	10
9	50	0.32	16	20	42	0.7	30

Table 5.2-2 Loading procedures for Cool-lok : Tensile and nanoindentation

Tensile				**Indentation**			
sample number	rise time t_R (s)	load rate (MPa/s)	maximum stress P_{max} (MPa)	increments of load	rise time t_R (s) approx.	load rate (mN/s) approx.	maximum load (mN)
1	2	0.25	0.5	1	9	0.03	0.3
2	2	0.5	1	1	21	0.03	0.6
3	2	0.75	1.5	1	32	0.03	1
4	10	0.05	0.5	10	9	0.03	0.3
5	10	0.1	1	10	22	0.03	0.6
6	10	0.15	1.5	10	33	0.03	1
7	20	0.025	0.5	20	9	0.03	0.3
8	20	0.05	1	20	21	0.03	0.6
9	20	0.075	1.5	20	32	0.03	1

Table 5.2-3 Loading procedures for PMMA : Tensile and nanoindentation

Tensile				**Indentation**			
sample number	rise time t_R (s)	load rate (MPa/s)	maximum stress P_{max} (MPa)	increments of load	rise time t_R (s) approx.	load rate (mN/s) approx.	maximum load (mN)
1	2	2	4	10	20	0.01	0.3
2	2	4	8	10	20	0.03	0.6
3	20	0.2	4	10	20	0.04	0.9
4	20	0.4	8	10	21	0.14	3

5.3 Results: Epoxy

During tensile testing the load resolution was ± 0.1 N which for these samples corresponds to ± 0.005 MPa approximately. The displacement resolution was 0.2 μm. For tensile tests, 5 samples, each from a different mould poured from the same mixture and subject to the same test procedure, showed uncertainties in strain between 4 and 6 % as determined from the standard error in strain over the ramp and hold load period. For the nanoindentation test 30 repeats were performed on one sample and displacement uncertainties were also approximately 5%. Nanoindentation force resolution was 0.2 μN and displacement resolution 1nm.

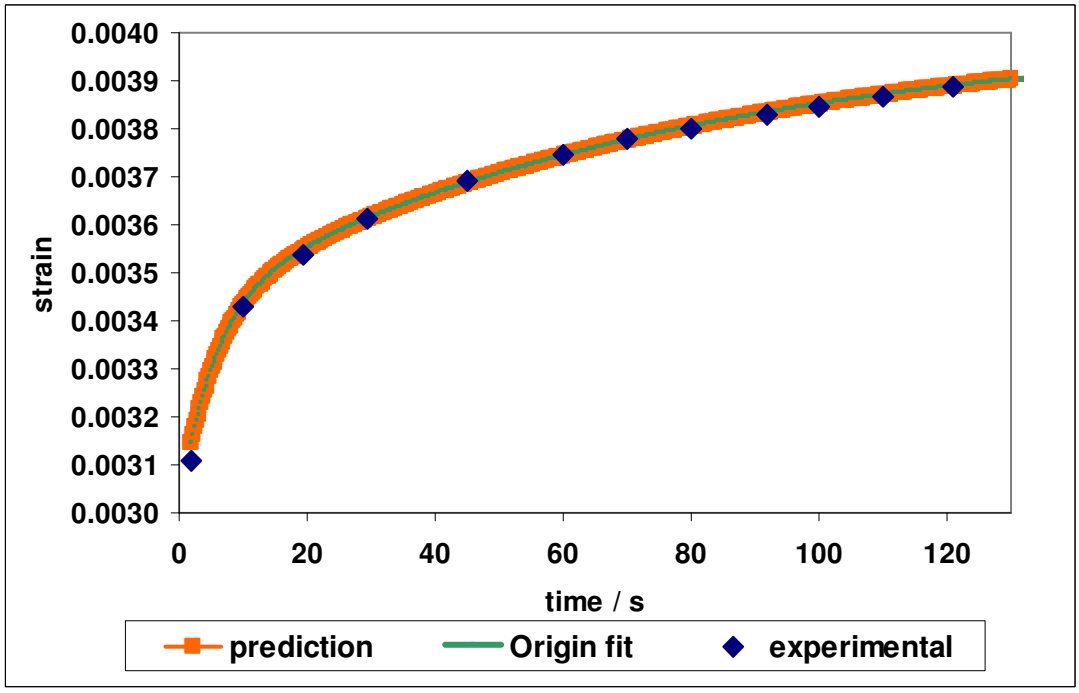

Figure 5.3-1 Typical creep curve obtained from epoxy samples in tensile test during hold load period. Showing experimental data, fit results and prediction using resulting coefficients and time constants (Shown here after 2s rise time to creep stress 4 MPa for 15:2 mixed sample)

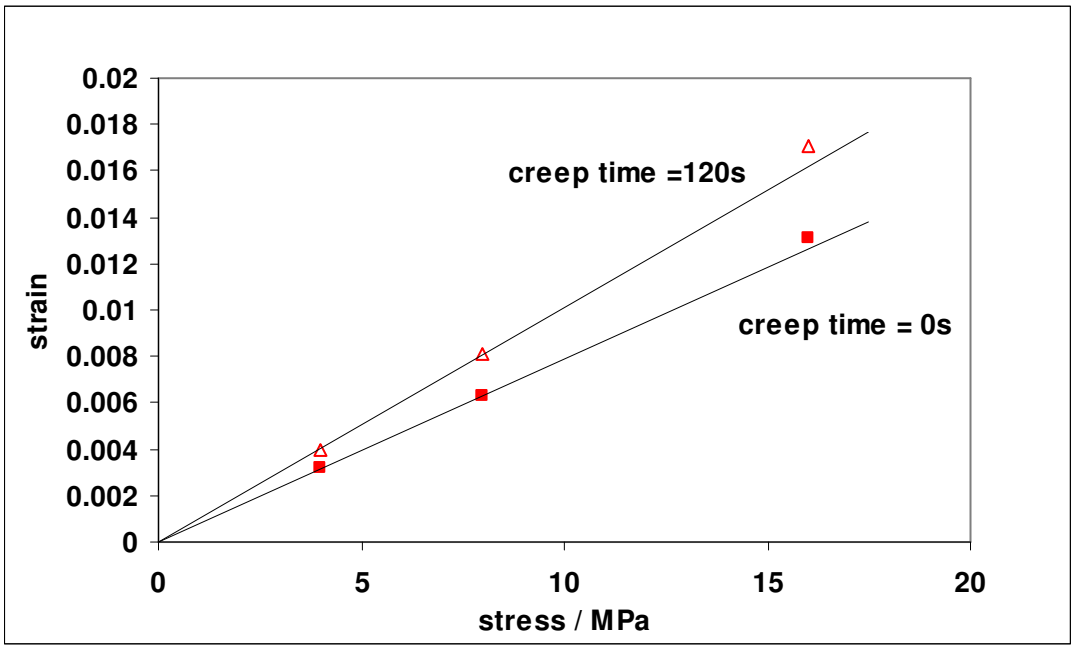

Figure 5.3-2 Epoxy 15:2 standard mix Tensile isochronal strain versus stress plot based on BSP after 2 s ramp load showing non-linearity of response at higher stress

solid lines at t=0approx.and t=120s approx. are linear regression through the two low stress data points

Isochronal stress plots of tensile strain were also made to check the linearity of the response and to verify the validity of the Boltzmann superposition principle, BSP. Figure 5.3-2 shows the isochronal plot for the standard epoxy mix sample. It was found that at 16 MPa stress the response was no longer within the linear visco-elastic regime. However at 4 MPa and 8 MPa maximum stress the response is linear and this can also be seen in the strain / time plot Figure 5.3-3.

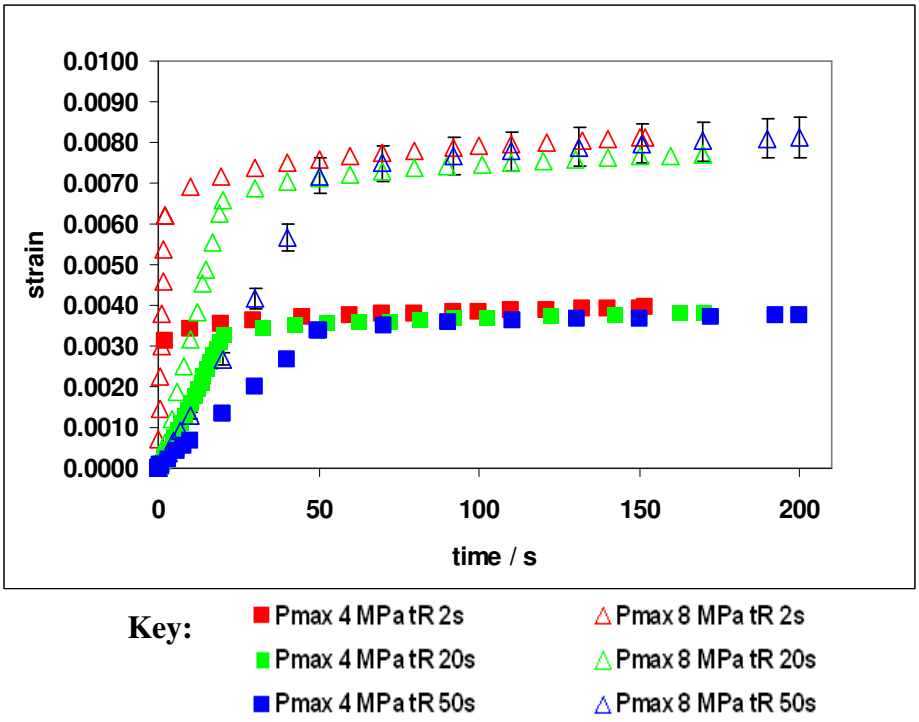

Figure 5.3-3 Epoxy 15:2 standard mix. Tensile strain response over ramp load and hold load period shows linearity of response

(5% error bars indicate the standard error in strain)

The plot shows that although the strain response is different immediately after reaching the maximum stress, during the period of creep the strain data are coincident and follow the same creep pattern, within experimental error. It can also be seen that more creep occurs following a rapid ramp load.

Isochronal checks for linearity in indentation response were not as useful as the load control of the indenter system gave different rise times for the different maximum

loads because, due to the system control, load is applied in increments of load rather than in ramp rise times. Ten increments of load for a 3mN load results in a shorter rise time and a different ramp rate to ten increments of load for a 30mN maximum load. However an indication of linearity of the creep response in the nanoindentation test results is given by the normalised creep compliance function plot. This can be seen for epoxy standard mix in Figure 5.3-4 in which the normalised creep compliance function resulting from tensile tests is included for comparison.

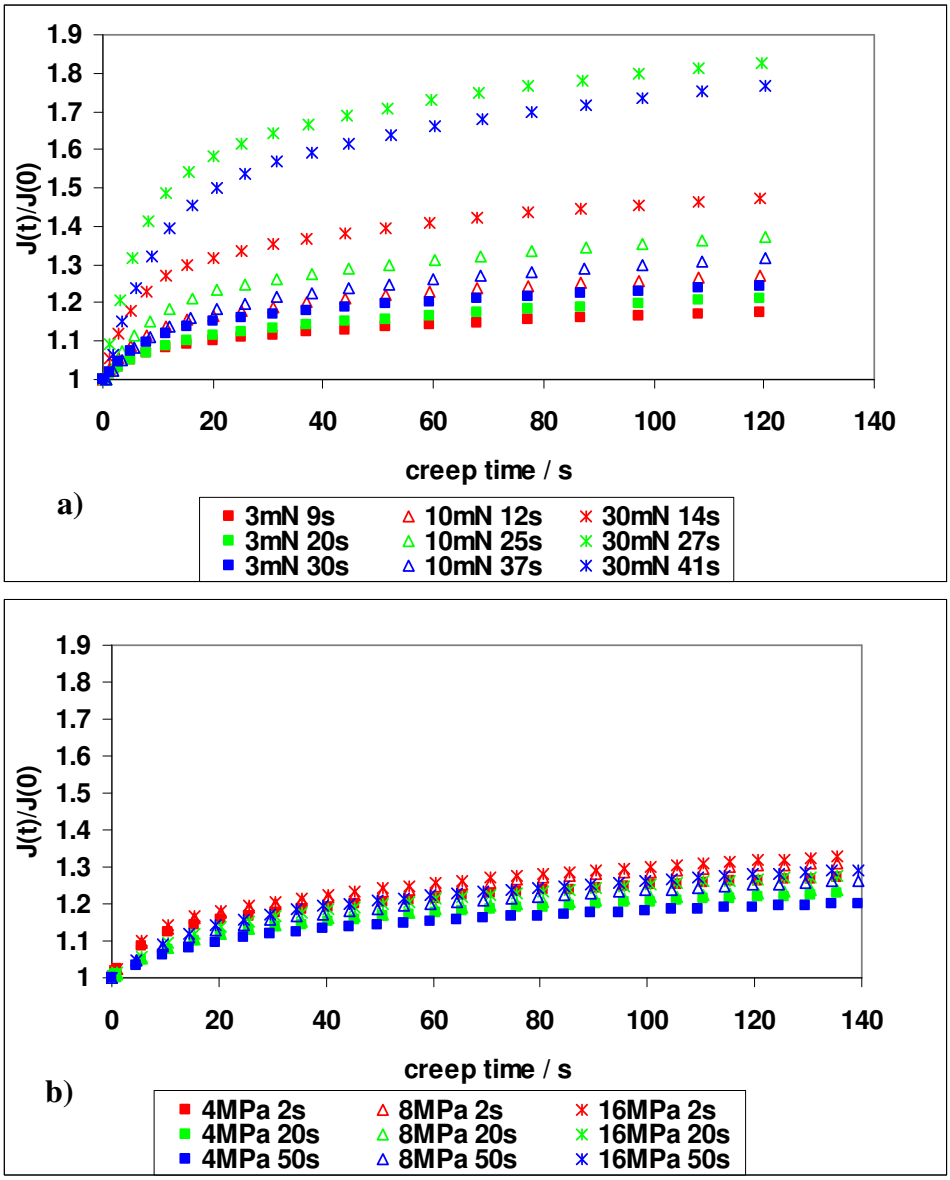

Figure 5.3-4 Epoxy 15:2 standard mix a) Nanoindentation results (b) tensile results. Normalised creep plots show non - linearity of visco-elastic response during nanoindentation creep. Nanoindentation creep is more affected by ramp load time.

It can be seen from Figure 5.3-4 that the nanoindentation creep response of the epoxy standard mix was non linear and creep displacement was affected by ramp load time. An indication of the linearity of the response during ramp loading can be seen in Figure 5.3-5, where it is evident that the response at 3 mN and 10mN was linear but at 30mN load the response was no longer linear. Non linearity could be due to the higher strain and the variation in ramp load times and rates. It can also be seen that the displacement was less than the displacement predicted by the Hertzian relationship using the modulus value obtained as a result of tensile testing. The degree of scatter in the displacement over a set of repeated tests is also evident.

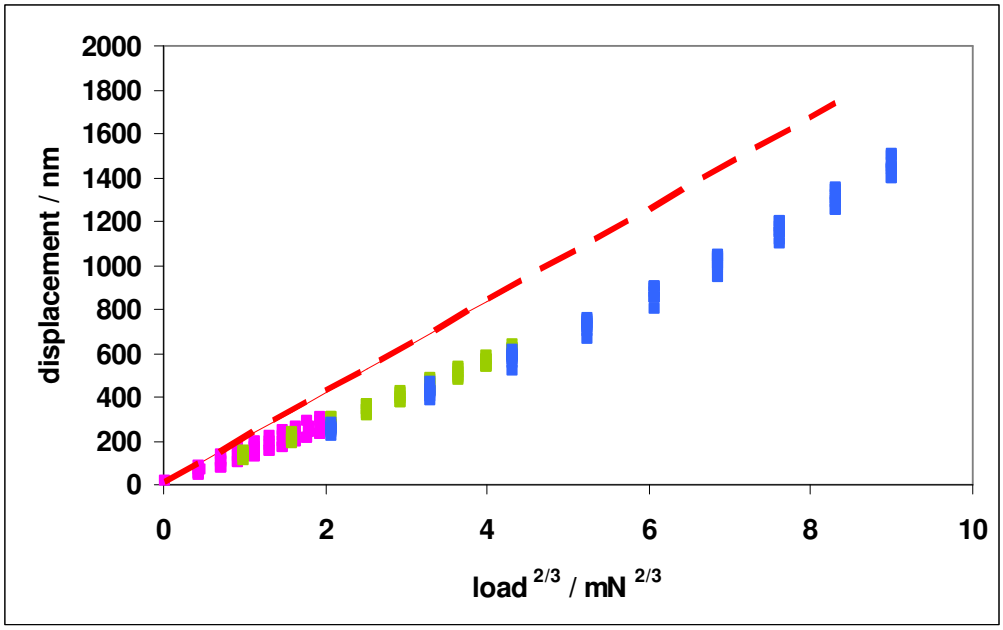

Key: pink = ramp load to 3mN, green = ramp load to 10mN, blue = ramp load to 30mN dashed red line = Hertzian response using averaged modulus value obtained from tensile creep

Figure 5.3-5 Epoxy 15:2 mix :- displacement vs. load $^{2/3}$ ramp loading to 3mN, 10mN and 30mN, the non linearity can be seen at the 30mN load

From the creep compliance function the instantaneous and long-time shear moduli of the material were determined as described in Chapters 2.3-7 and 2.4-2 and Appendix 11.1. The creep ratio, which is derived from these, gives an indication of visco-elasticity.

The effects of varying parameters such as creep stress and ramp load time can be seen for all three mixes of epoxy in Figures 5.3-6 to 5.3-11.

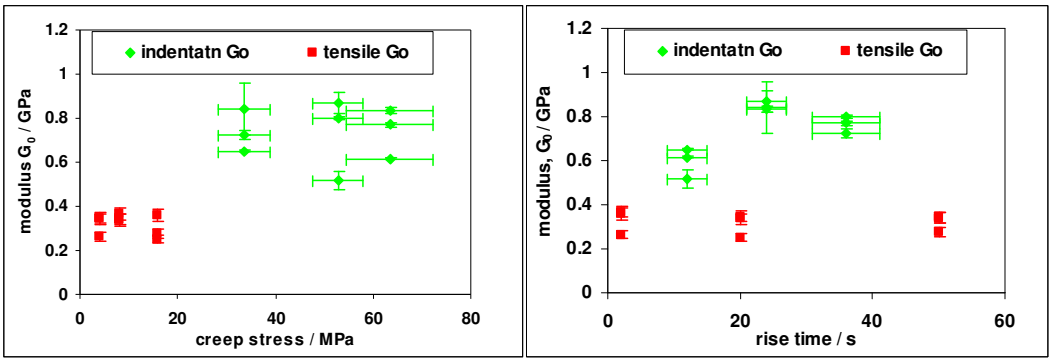

Figure 5.3-6 Epoxy 15:1 mix modulus value vs. maximum creep stress and vs rise time shows no clear trends Modulus error bars at 95% confidence. Indenter tip R = 21µm.

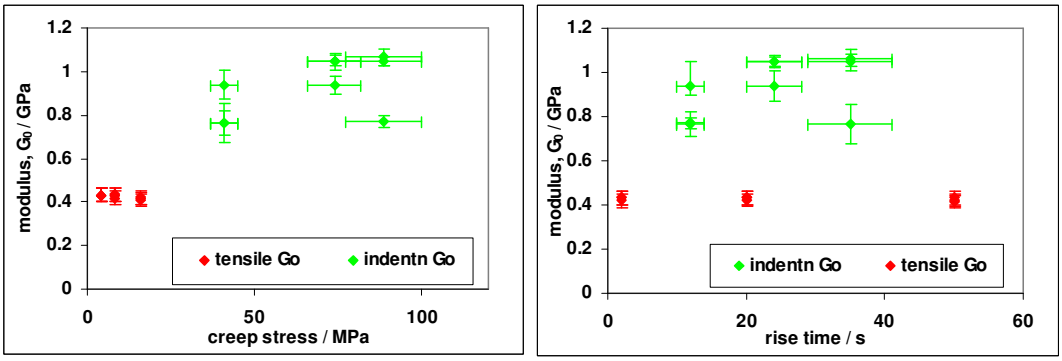

Figure 5.3-7 Epoxy mix 15:2 modulus value vs. maximum creep stress and vs. rise time ; shows possible slight decrease in modulus with both increasing rise time and creep stress in tensile tests; no clear trends in nanoindentation Modulus error bars at 95% confidence. Indenter tip R = 21µm

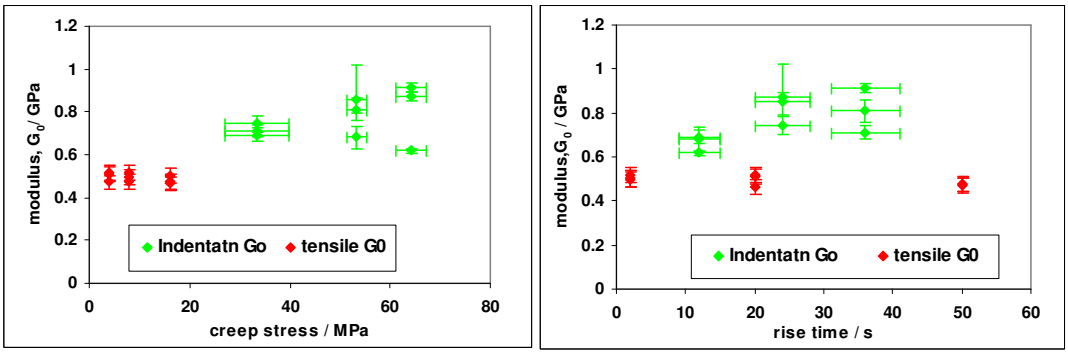

Figure 5.3-8 Epoxy 15:4 mix modulus value vs. maximum creep stress and vs rise time : possible very slight decrease in modulus with increasing creep stress and increasing rise time in tensile tests; possible increase in G_0 with increasing creep stress and rise time in indentation Modulus error bars at 95% confidence Indenter tip R = 21µm

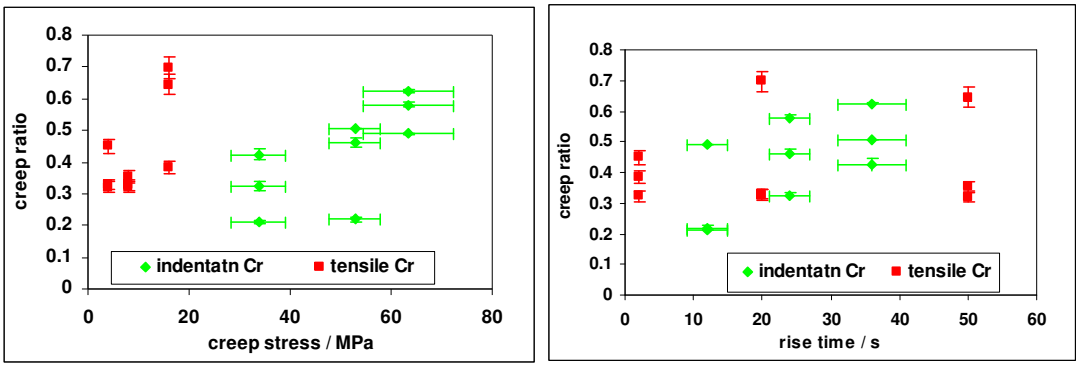

Figure 5.3-9 Epoxy 15:1 creep ratio vs. creep stress : mix shows creep ratio increases with creep stress in both tensile and indentation tests ; creep ratio increases with increasing rise time in indentation tests only creep ratio error bars at 95% confidence Indenter tip R = 21µm

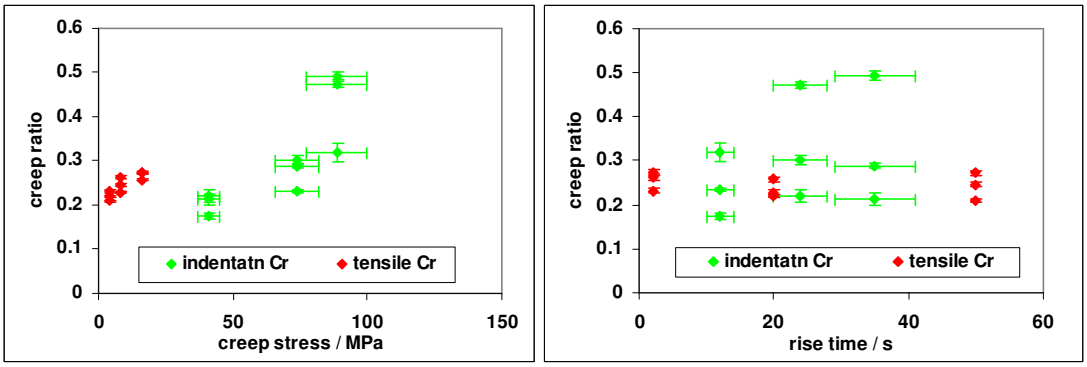

Figure 5.3-10 Epoxy 15: 2 mix; creep ratio vs. creep stress, creep ratio clearly increases with creep stress in both indentation and tensile tests creep ratio error bars at 95% confidence Indenter tip R = 21µm

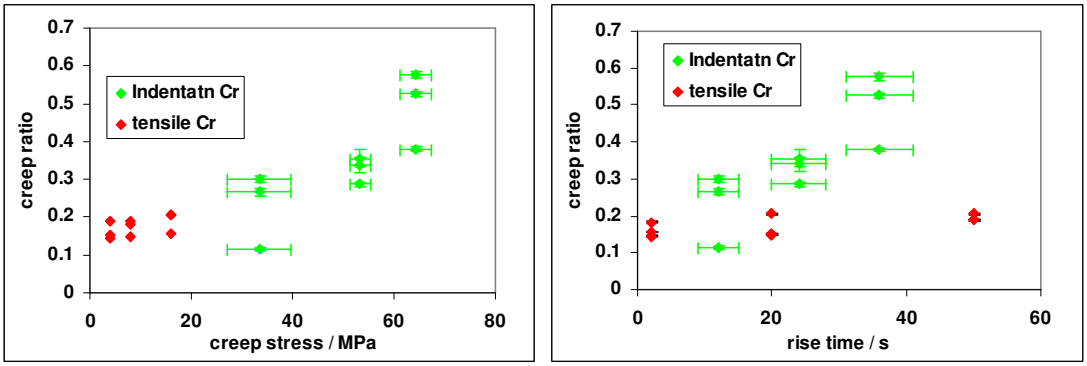

Figure 5.3-11 Epoxy 15:4 mix; creep ratio vs. creep stress, creep ratio increases with both increasing creep stress and increasing rise time in both indentation and tensile tests. creep ratio error bars at 95% confidence Indenter tip R = 21µm

To enable direct comparisons between tensile and indentation tests, the stress corresponding to the applied load in the indentation test was used. This was calculated from the mean pressure, $P_m = \frac{P_{\max}}{\pi a^2}$ and used as $\frac{P_m}{3}$ in accordance with Tabor's analogy between indentation and tensile results (Tabor 1951).

The large x axis error bars in rise time and creep stress reflect the range of rise times resulting from 1, 10 and 20 increments of load and the range of creep stress resulting at each different maximum load.

Despite the scatter in the results in both test methods trends were evident in the ranking of epoxy with increased amounts of hardener. As expected, increasing the amount of triethylenetetramine hardener increased the modulus of the epoxy as more cross-links can be formed between the amine groups and the epoxide groups.

The creep ratios provide a good indication to the changes in mechanical properties due to increasing the amount of hardener in the epoxy mix. As expected the mix with the least hardener produced the more visco-elastic material. As creep stress was increased the creep ratio also increased in both indentation and tensile tests. As rise time was increased the creep ratio of the 15:1 and 15:4 mixed epoxy samples also appeared to increase. The results for all the epoxy samples are summarised in table 5.3 -1.

Experimental results show that the calculated modulus values from the indentation test, range from 2 to 3 times higher than those calculated from the tensile test.

Table 5.3-1 Summary of tensile and nanoindenation results: epoxy

	Epoxy 15:1	Epoxy15:2	Epoxy 15:4
G_0 (GPa) tensile	range 0.26-0.37	approx. 0.43	range 0.46-0.511.5
G_0 (GPa) indentatn.	range 0.6-0.9	range 0.7-1.0	approx. 0.9
G_∞ (GPa) tensile	range 0.06-0.26	approx. 0.32	range 0.37-0.44
G_∞ (GPa) indentatn.	range 0.3-0.6	range 0.5-0.7	approx 0.6
C_r tensile	range 0.3-0.7	range 0.22 - 0.26	range 0.15-0.2
C_r indentation.	range 0.2-0.65	range 0.2-0.5	range 0.15-0.6
Timeconstant,t_1(s) tensile	range 6-16	range 5-13	range 4-13
Time constant,t_1(s) indentatn.	range 5-11	range 5-10	range 5-9
Time constant,t_2 (s) tensile	range 77-237	range 77-132	range 66-144
Time constant,t_2 (s) indentatn.	range 75-154	range 64-115	range 66-140

5.4 Results: Cool - lok

The analysis procedure for Cool-lok was the same as for the epoxy samples, *i.e.* creep curves obtained from the hold at a constant stress period were fitted in Origin (as described in Chapters 2.3-7 and 2.4-2 and Appendix 11.1). Isochronal stress versus strain was plotted to ascertain that the creep was linear in tensile tests.

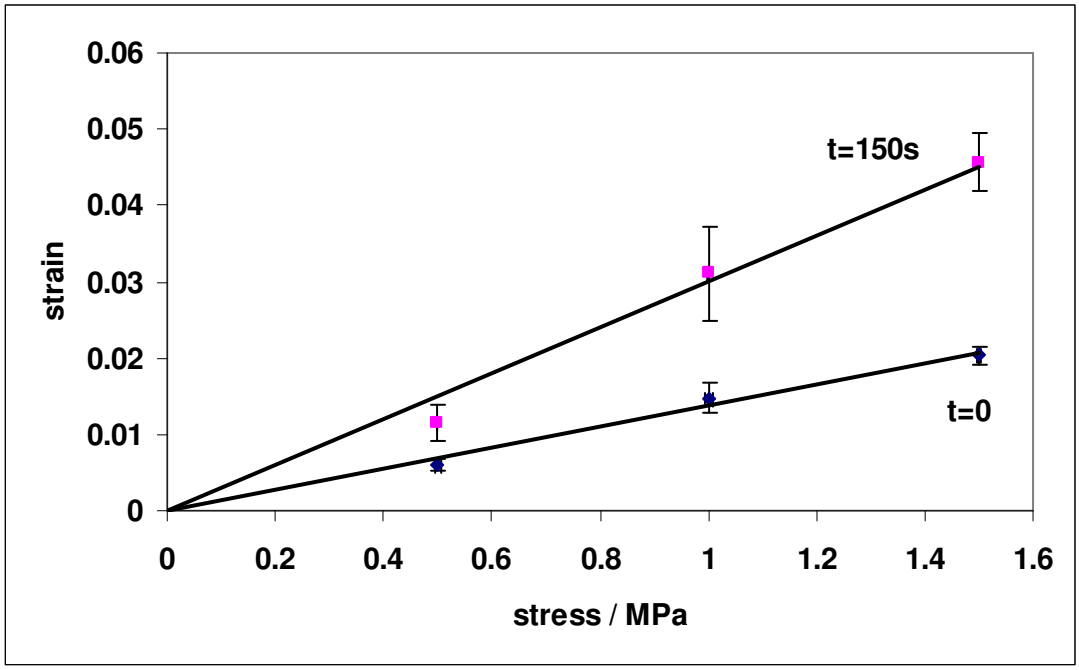

Figure 5.4-1 Isochronal plot of creep strain after 2s rise time to show linearity of creep behaviour in response to applied stress whilst tensile testing Cool-lok.

solid lines at t=0approx.and t=120s approx. are linear regression in Excel; error bars at 95% confidence

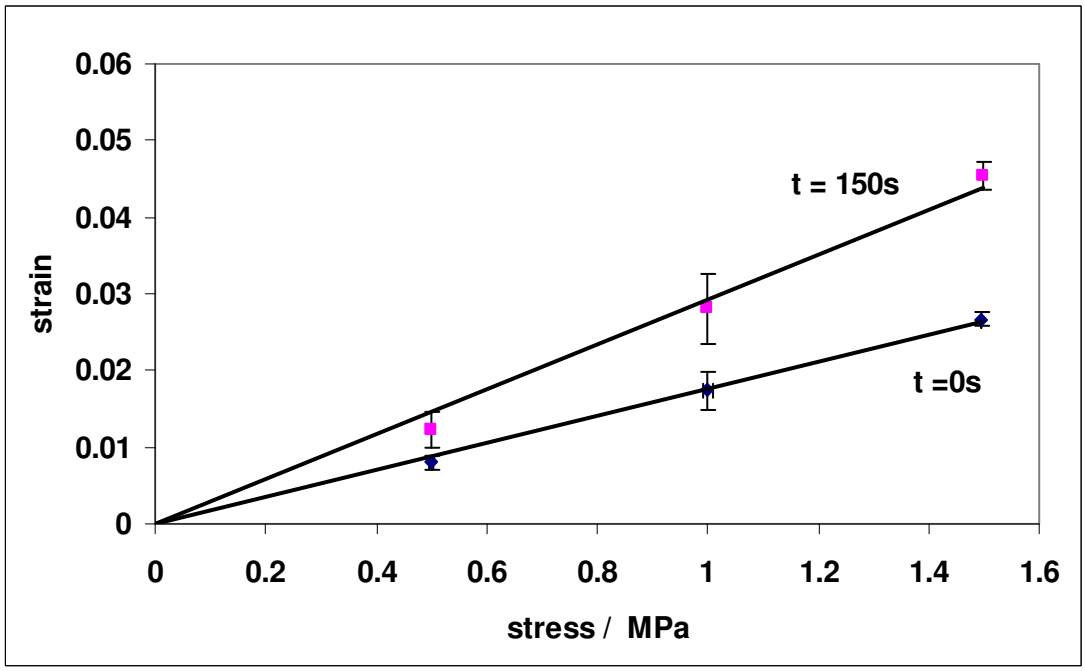

Figure 5.4-2 Isochronal plot of creep strain after 10s rise time to show linearity of creep behaviour in response to applied stress whilst tensile testing Cool-lok.

solid lines at t=0approx.and t=120s approx. are linear regression; error bars at 95% confidence

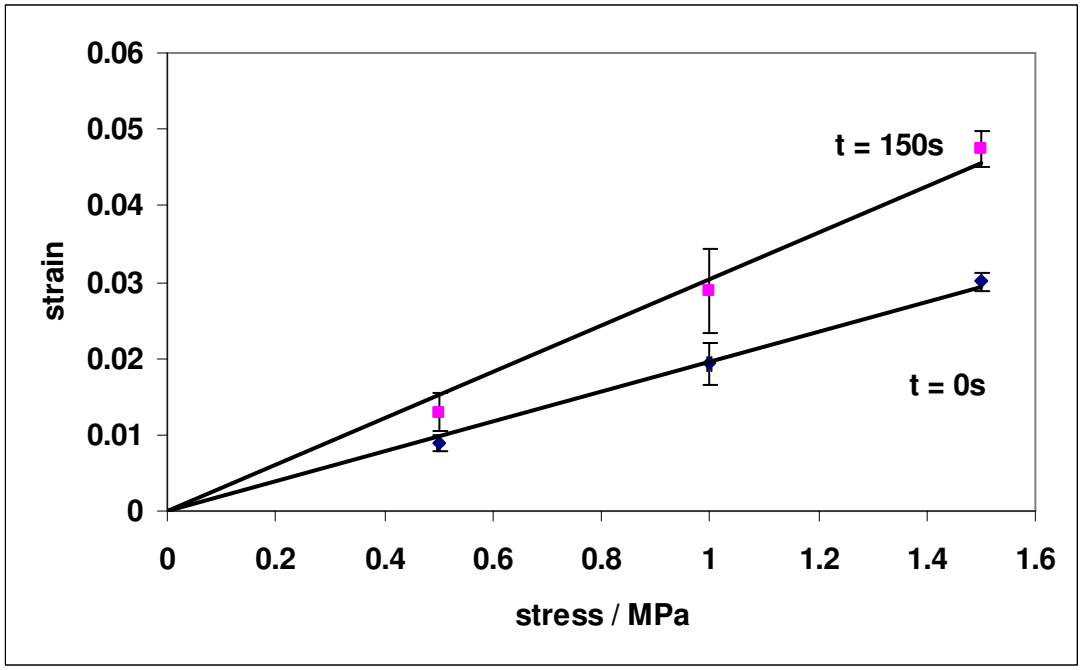

Figure 5.4-3 Isochronal plot of creep strain after 20s rise time to show linearity of creep in response to applied stress whilst tensile testing Cool-lok

solid lines at t=0approx.and t=120s approx. linear regression; error bars at 95% confidence

Isochronal plots suggest that the strain response to ramp loading in tensile tests was linear, this can be seen in the t = 0 fit lines at the start of creep Figures 5.4 -1 to 5.4 -3. The response to increased stress appeared linear as defined by the Boltzmann superposition principle. At the end of the period of hold load, at creep time = 150s the creep response, as the stress was increased, was not so clearly linear Figures 5.4 -1 to 5.4 -3 as indicated by the line fitted to t = 150s strain data.

The linearity of the creep response can be observed as agreement of the averaged normalised creep function over the three different loads. It can be seen by the agreement of the data coloured red in Figure 5.4-4 that a linear creep response in tensile testing resulted only after the 2s rise time. The creep response after a 10s rise time and a 20s rise time appeared to be non linear at higher stress. When looking at isochronal plots and the normalised creep function plots together (Figures 5.4 -1 to

5.4-4) it seems that disproportionately more creep occurred at higher stress after slower rise times.

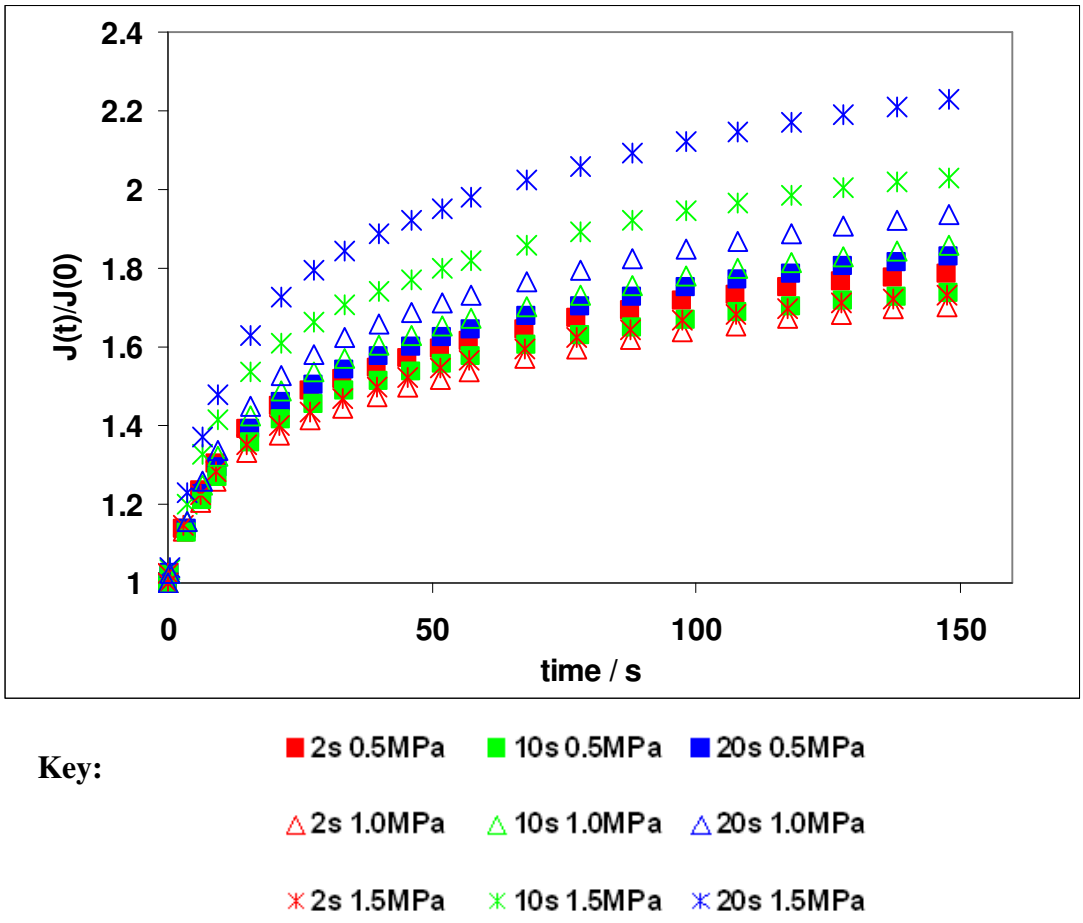

Figure 5.4-4 Cool-lok tensile : normalised averaged creep function at different rise times and different creep stress

During ramp loading in nanoindentation tests the displacement response appeared non linear Figures 5.4-5 to 5.4-7. This was evident even at the faster rise times where less creep was expected during the ramp loading. The material can be seen to be creeping during ramp loading in Figures 5.4-6 and 5.4-7 as the displacement does not increase linearly with load$^{2/3}$. For comparison, Figures 5.4-6 to 5.4-7 also show the expected displacement during ramp loading using Hertzian contact with the modulus calculated from tensile creep and assuming no time dependence.

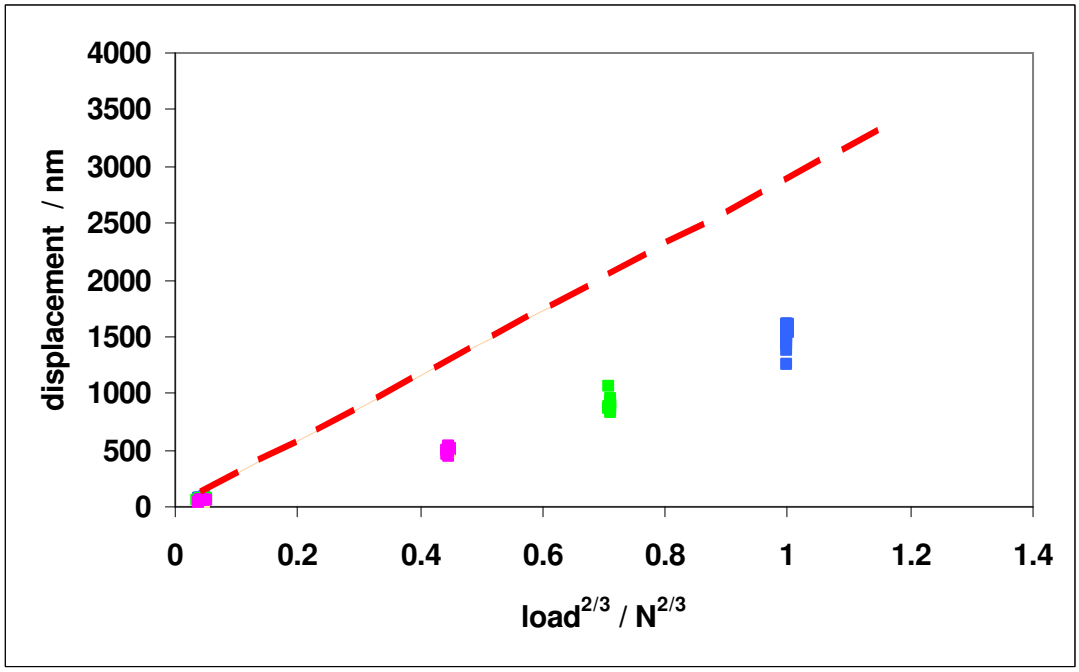

Figure 5.4-5 Cool-lok nanoindentation displacement vs. load$^{2/3}$ showing data from 30 repeated tests during 1increment (t_R = 8 - 9 s) ramp loading to maximum loads 0.3mN. 0.6mN and 1mN : shows non linear ramp loading and scatter in displacement

Key ; pink = 0.3mN max. load, green = 0.6mN max. load blue = 1mN max load, red dashed line Hz predictn using tensile modulus

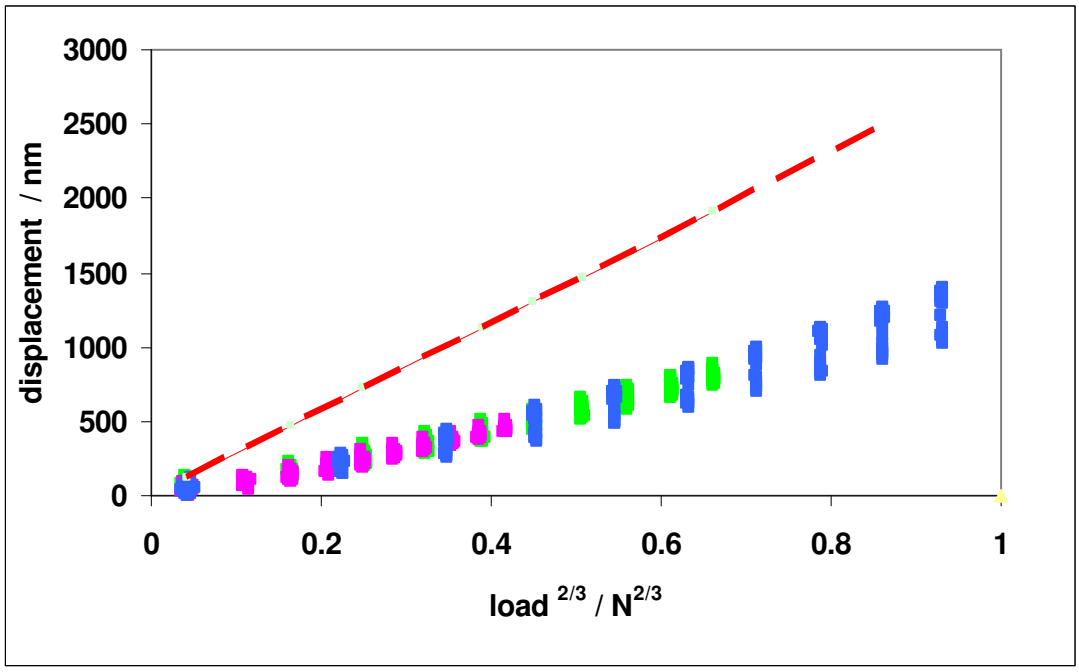

Figure 5.4-6 Cool-lok nanoindentation displacement vs. load$^{2/3}$ showing data from 30 repeated tests during10 increment (t_R = 18 - 20 s) ramp loading to maximum loads 0.3mN. 0.6mN and 1mN : shows non linear ramp loading and scatter in displacment

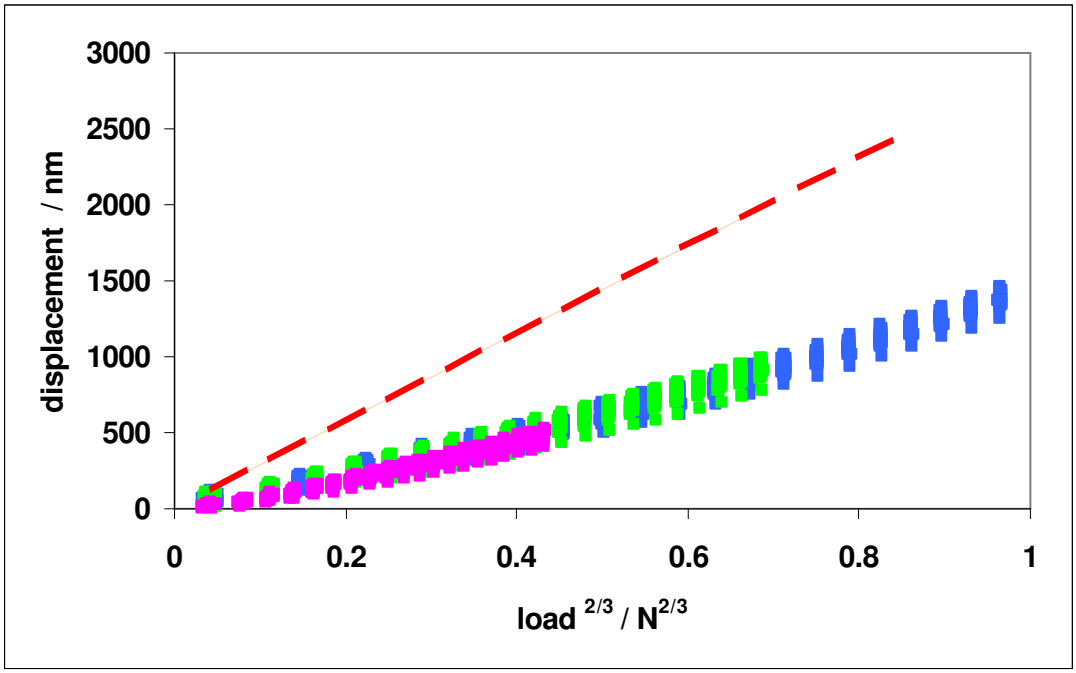

Key ; pink = 0.3mN max. load, green = 0.6mN max. load blue = 1mN max load, red dashed line Hz predictn using tensile modulus

Figure 5.4-7 Cool-lok nanoindentation displacement vs. load$^{2/3}$ showing data from 30 repeated tests during 20 increment (t_R = 29 - 32 s) ramp loading to maximum loads 0.3mN. 0.6mN and 1mN : showing non linear ramp loading and scatter in displacment

The normalised creep curves obtained from indentation testing again show the significance of the rise time, agreement is seen between creep function curves at different maximum loads when the rise time was similar, see Figure 5.4 -8 *i.e.* the creep function *J*(t) appears independent of stress over the stress range applied after a similar ramp loading time. This confirms the importance of rise time in creep analysis, nanoindentation appears particularly sensitive to rise time. However, unlike tensile creep, in which normalised creep appears greater at higher stress after slow rise times, in nanoindentation normalised creep appears less at higher loads after slower rise times.

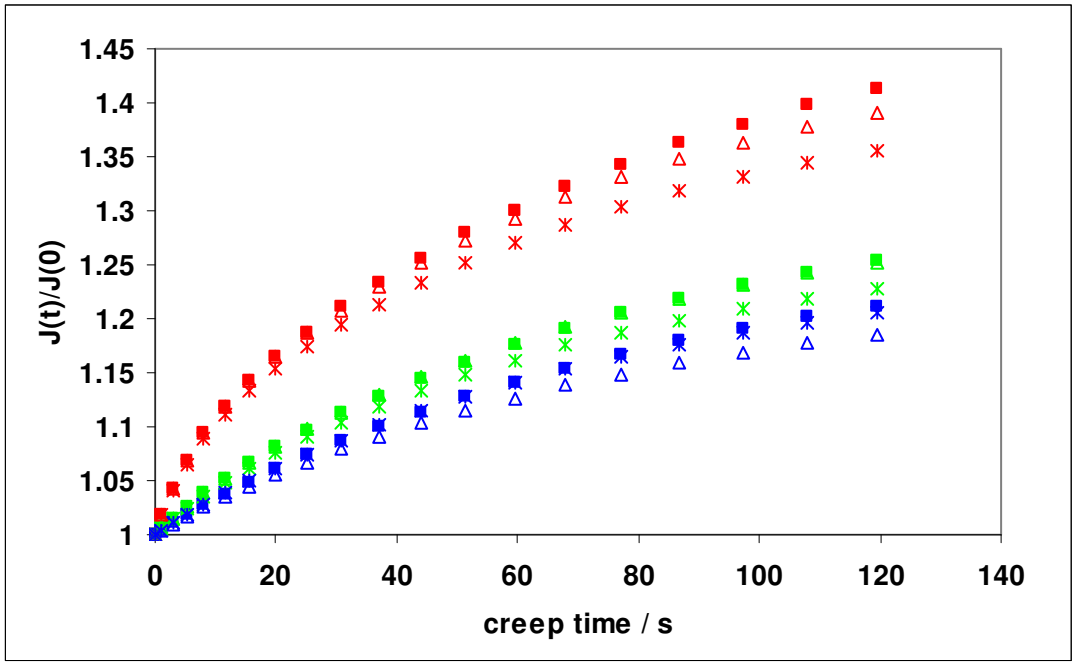

Key:

■ 1 inc 0.3mN	■ 10inc 0.3mN	■ 20 inc 0.3mN
△ 1 inc 0.6mN	△ 10inc 0.6mN	△ 20inc 0.6mN
✳ 1 inc 1mN	✳ 10 inc 1mN	✳ 20 inc 1mN

Figure 5.4-8 Cool-lok indentation: averaged normalised creep function where 1 inc = 8s ±1s, 10inc = 22s ±1s, 20 inc =32 ±1s showing significance of ramp load rise time to linearity of creep response

When looking at the normalised creep response resulting from tensile tests and nanoindentation tests together, Figure 5.4-9, it can be seen that much less creep occurs in the nanoindentation test over all conditions. This may be due to creep already having occurred during the ramp loading. However, the moduli are calculated from the creep response and nanoindentation creep appears significantly less than tensile creep.

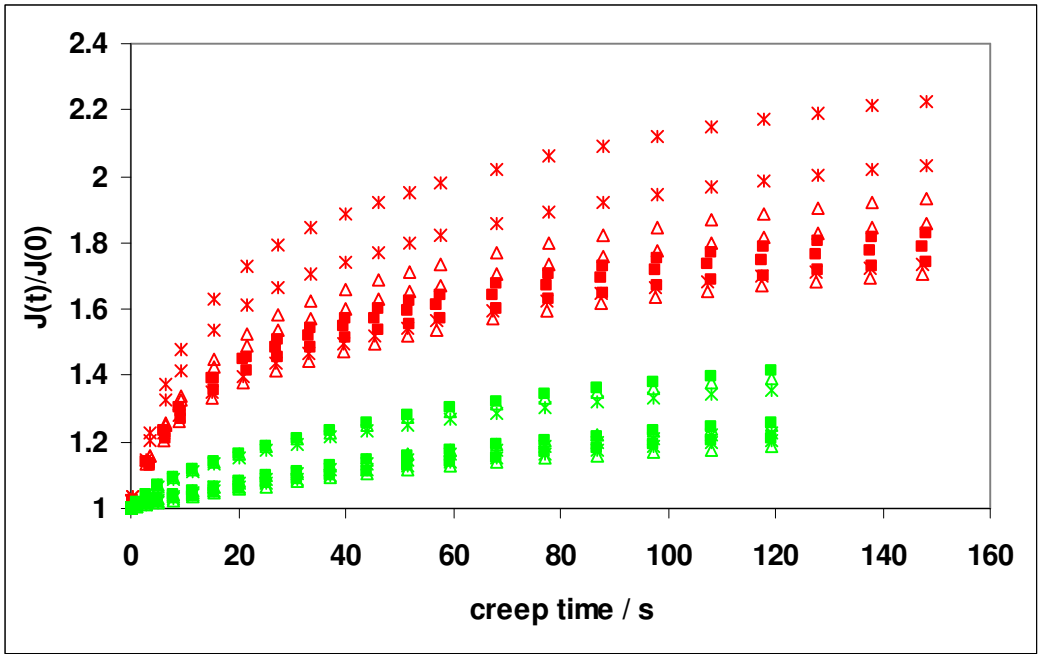

Key: Red : Tensile results Green : Indentation results

Figure 5.4-9 Cool-lok :Normalised creep curves over all test conditions in tensile and nanoindentation tests suggest that creep is constrained in nanoindentation

When incompressibility is assumed the material is assumed to flow visco-elastically so as to maintain constant volume. In an indentation test the flow of the material under the indenter is restricted by the surrounding bulk material. However, it may be possible that the material flows up and around the indenter tip thus increasing the assumed contact area and this will be investigated in Chapter 6.

Averaged modulus values calculated from the creep function obtained from both tensile and nanoindentation tests were compared and the effects of changing test parameters on these can be seen in Figures 5.4-10 and 5.4 -11.

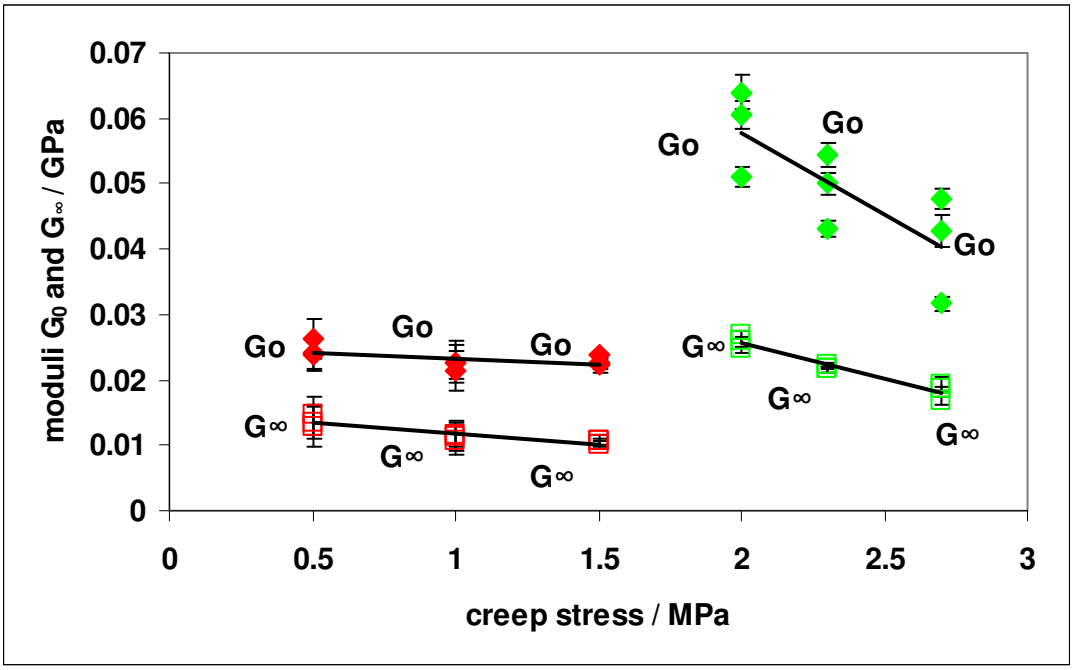

Key: Red : Tensile results Green : Indentation results (error bars at 95% confidence) black lines are linear regression

Figure 5.4-10 Cool-lok: moduli decrease in indentation with increased creep stress; in tensile tests only slight trend

Figure 5.4 -10 shows that both calculated moduli G_0, and G_∞, appear to decrease when creep stress was increased in indentation tests also, but to a lesser degree, in tensile tests. From the gradients it appears that the decrease in instantaneous modulus, G_0, with increasing creep stress in indentation is approximately 10 times the corresponding decrease in G_0 with increasing creep stress in tensile tests; whilst the decrease in G_∞ with increasing creep stress in indentation is 3 times the corresponding decrease in tensile tests.

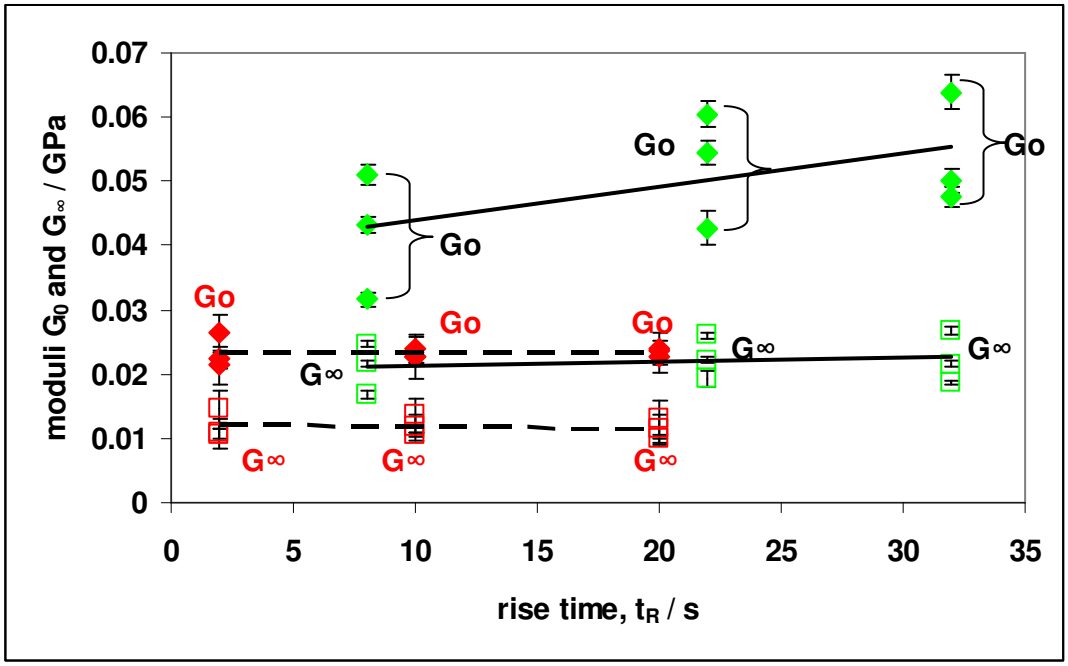

Key: Red : Tensile results Green : Indentation results (error bars at 95% confidence)
black lines solid and dashed are linear regression

Figure 5.4-11 Cool-lok : moduli versus rise time showing moduli from nanoindentation tests are greater that those from tensile tests, also showing moduli derived from nanoindentation are sensitive to rise time

Calculated instantaneous modulus values, $G_{0,}$ appear to increase as rise time is increased in indentation tests. Other trends with increased rise time are unclear. Figure 5.4 -11.

Calculated creep ratios C_r, are similar, approximately 0.5, when calculated from both tensile and indentation test results, although this also appears to be affected by rise time, more so in indentation tests, as well as by creep stress in which the tensile results appear more sensitive. Figures 5.4 -12 and 5.4 -13.

The results show that the creep response of Cool-lok was dependent on stress and rise time in both tensile and indentation tests. The creep response during indentation testing was particularly sensitive to rise times.

Time constants appeared to be in agreement over the two test methods. Figures 5.4-14 and 5.4-15.

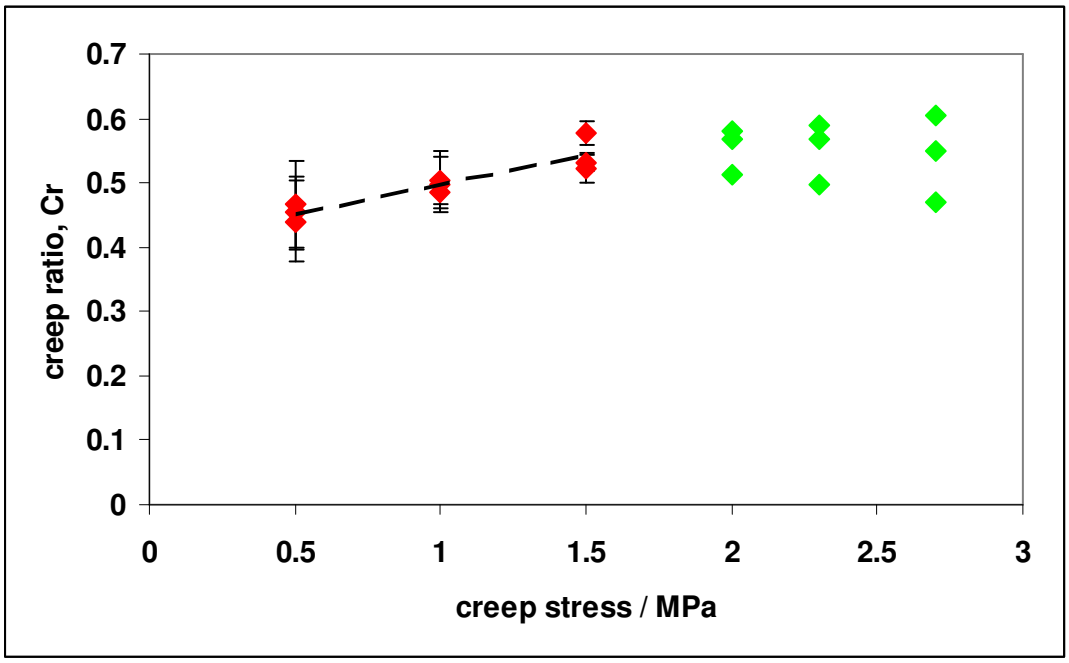

Key: Red: Tensile results Green : Indentation results black lines dashed are linear regression

Figure 5.4-12 Cool-lok:Tensile and indentation results show creep ratios are in agreement and sensitive to creep stress

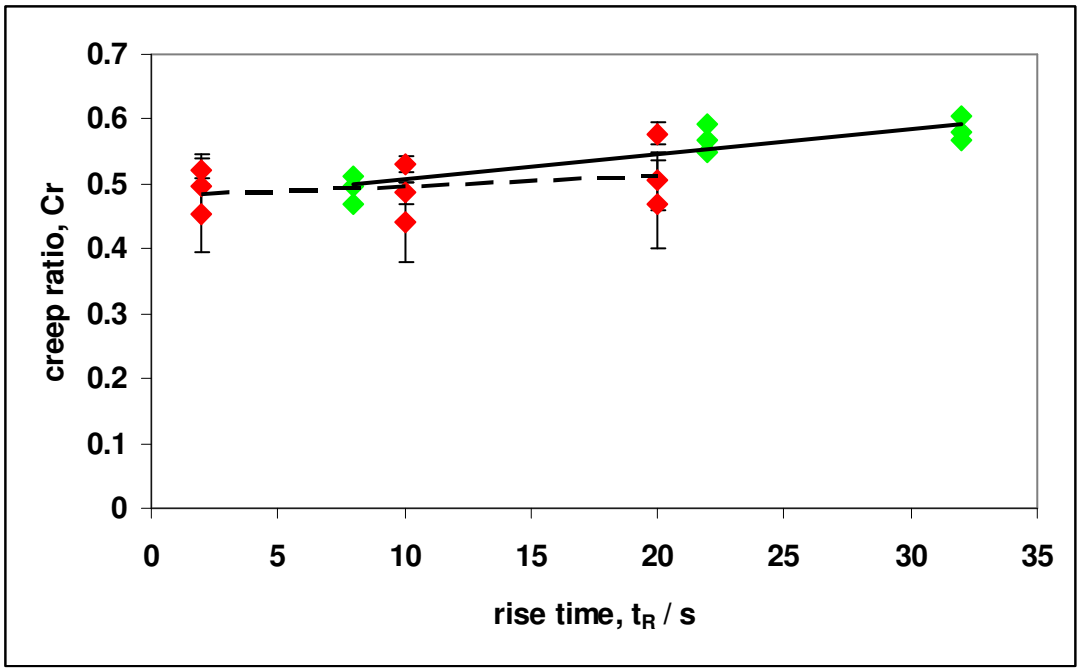

Key: Red : Tensile results Green : Indentation results black lines solid and dashed are linear regression

Figure 5.4-13 Cool-lok; creep ratio shows agreement in results between methods and creep ratio appears to increase with increasing rise time.

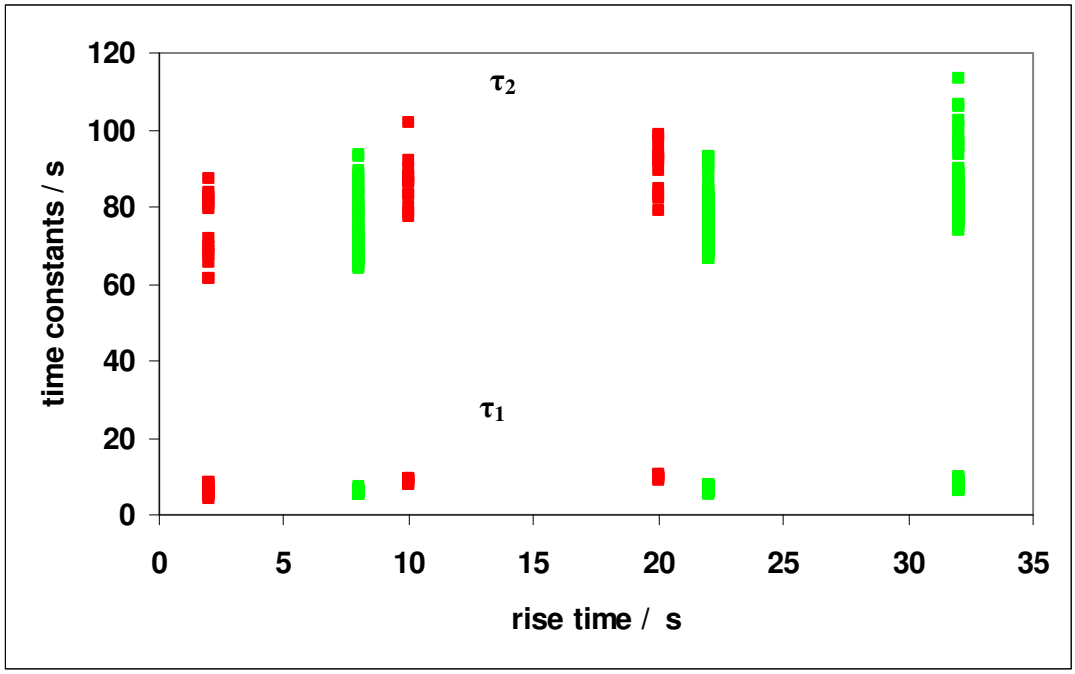

Key: Red: Tensile results Green : Indentation results

Figure 5.4-14 Cool-lok; time constants versus rise time, tensile and indentation results show agreement in ranges of time constants and no sensitivity to rise time

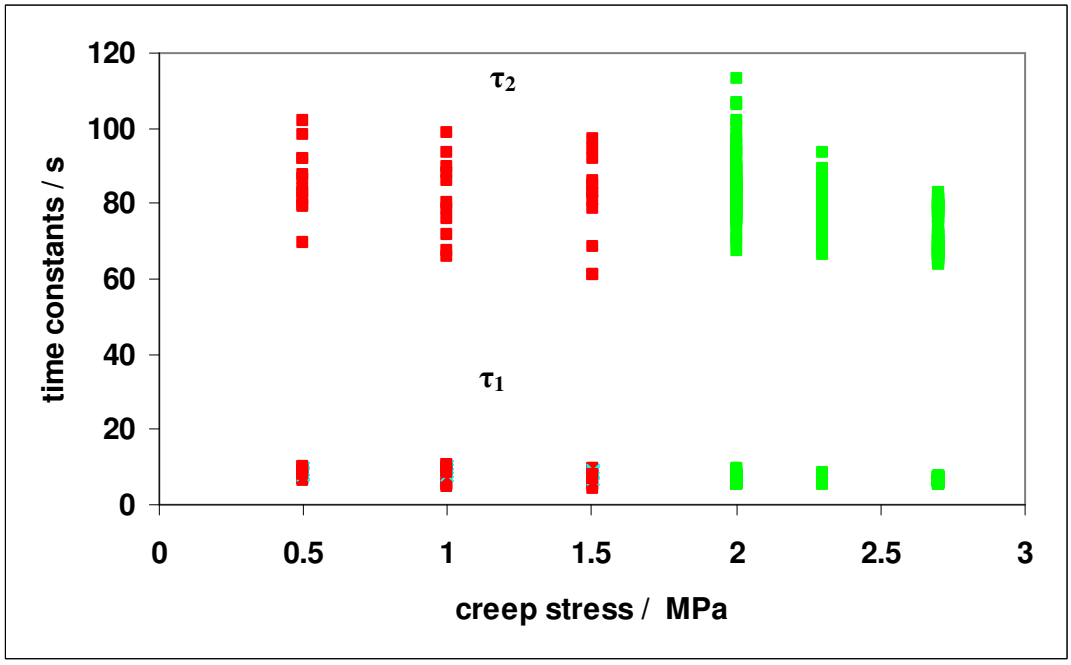

Key: Red: Tensile results Green : Indentation results

Figure 5.4-15 Cool lok; time constants versus creep stress. tensile and indentation results show agreement and no sensitivity to creep stress

Table 5.4 -1 summarises the parameters obtained from the results of the 2 test methods.

Table 5.4-1 Comparison of the values which characterise the mechanical behaviour of Cool-lok obtained from tensile and indentation testing averaged over all test conditions

Test method	tensile	indentation
Time constant, t1 (s)	8.24 ± 0.02	6.49 ± 0.05
Time constant, t2 (s)	83 ± 1.4	77.5 ± 0.5
Amplitude coefficient, C0 (Pa^{-1})	4.42E-08 ± 1.3E-09	2.35E-08 ± 3E-10
Amplitude coefficient, C1 (Pa^{-1})	9.49 E-09 ± 4.1E-10	5.82E-09 ± 9E-11
Amplitude coefficient, C2 (Pa^{-1})	1.29E-08 ± 5.8E-10	6.99E-09 ± 6E-11
Instantaneous shear modulus, G0 (GPa)	0.0233 ± 0.0004	0.0492 ± 0.0006
Long-time shear modulus, G∞ (GPa)	0.0118 ± 0.0004	0.02188 ± 0.0002
Creep ratio	0.498 ± 0.009	0.5484 ± 0.003

The modulus values calculated from the two methods differ by a factor of 2, approximately.

5.5 Results: PMMA

PMMA results were processed with the same analysis as in epoxy and Cool-lok studies. (Described in Chapters 2.3-7 and 2.4-2 and Appendix 11.1) For the slower ramp load rise time the tensile creep response was non linear but the faster ramp load produced a linear visco-elastic creep response as seen in Figure 5.5 -1.

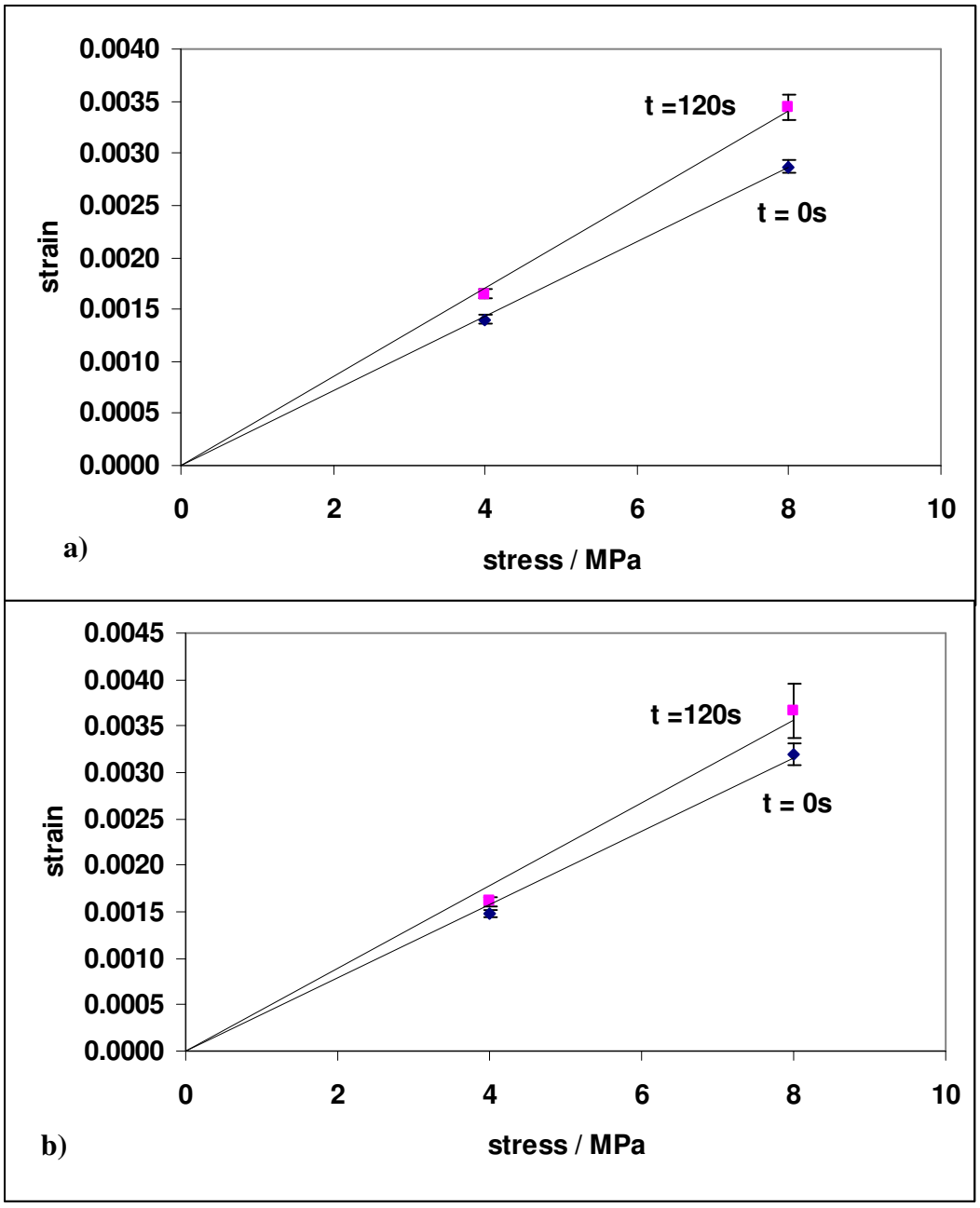

Figure 5.5-1 PMMA; Isochronal plots at 4MPa and 8MPa loads: a) shows linearity after a 2s ramp load time b) shows a non-linear visco-elastic response after a 20s ramp load time

solid lines at t=0approx.and t=120s approx. are linear regression (error bars at 95% confidence level)

Tensile stress – strain data from 5 individual tests is presented in Figure 5.5 -2. A linear regression to the data gives a Young's modulus between 2.7 GPa and 2.9 GPa. This validates the tensile test method, as a value in this region is in agreement with the literature value especially considering that values can differ between different PMMA suppliers and at different temperatures and of course, being visco-elastic, at different strain rates. The Young's modulus of PMMA has range 1800 MPa – 3100 MPa and cast PMMA has range 2420 – 3300 MPa Poisson's ratio 0.35-0.4. (http://www.matbase.com/material/polymers/commodity/pmma/properties) http://www.goodfellow.com/E/Polymethylmethacrylate.html

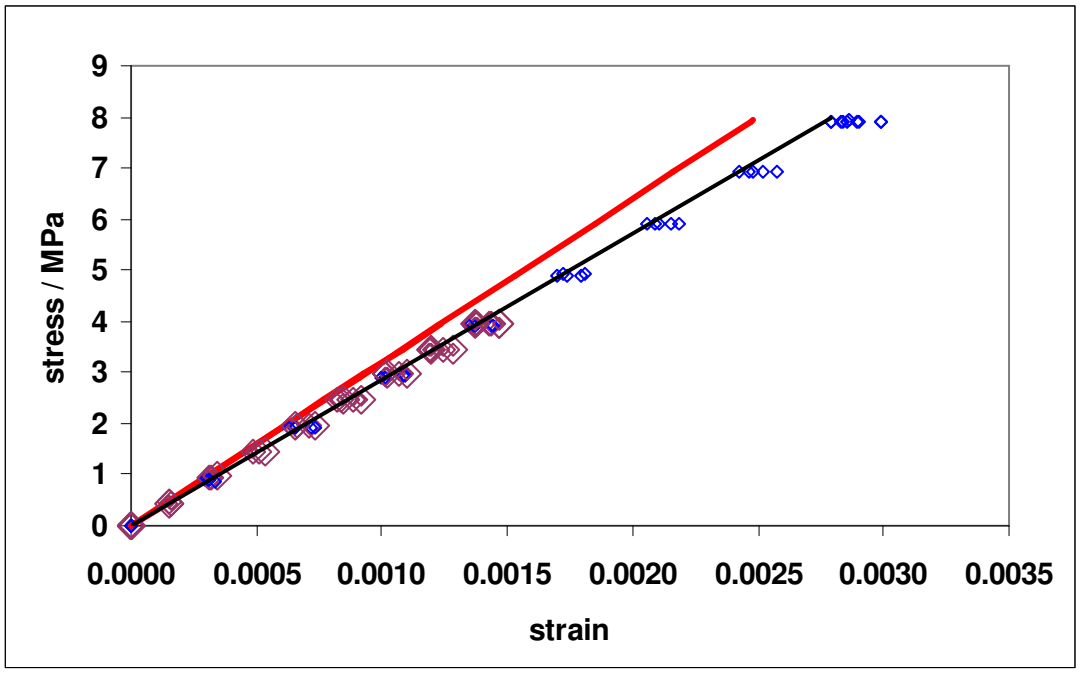

Key: red line = response predicted by literature value given by supplier = 3.2 GPa, black line = linear regression giving Young's modulus approx. 2.8GPa

Figure 5.5-2 PMMA tensile response to stress during ramp loading is approximately as predicted by the literature value of the elastic modulus

Figure 5.5 -3 presents the G0 and G∞ values calculated from creep at constant load after different rise times from both tensile and nanoindentation tests. The data points

represent the average of 5 tests under the same conditions in tensile testing and, similarly, approximately 30 tests in indentation. The error bars in the creep stress represent the range of creep stress as a consequence of the range of contact areas resulting from constant load applied in the nanoindentation test. There appears to be an increase in modulus value with increasing creep stress in indentation.

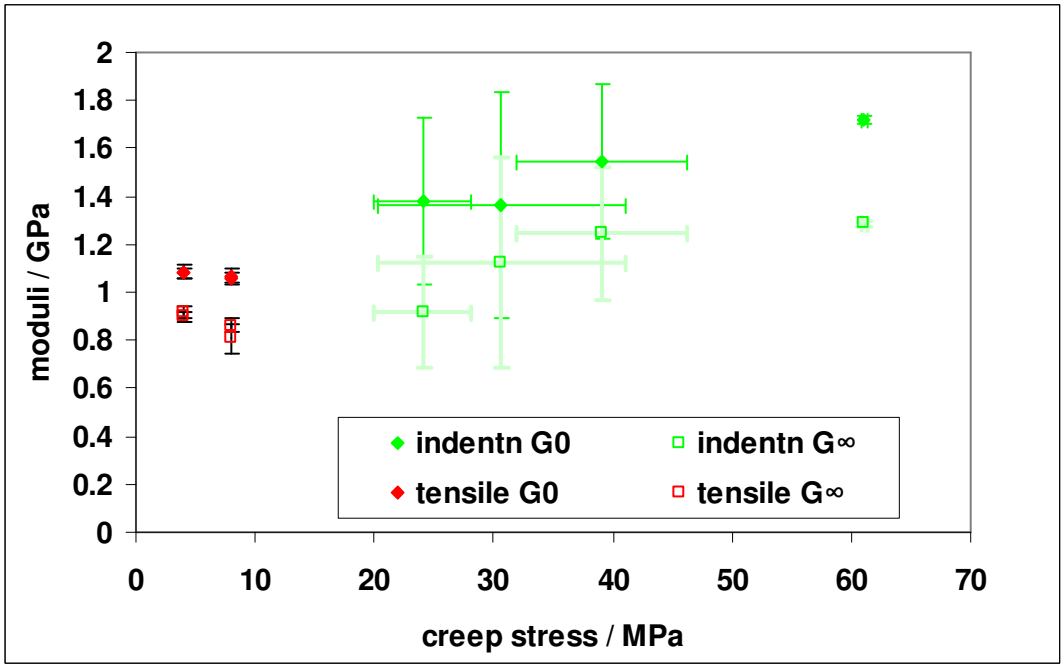

Figure 5.5-3 PMMA moduli vs. creep stress : moduli calculated from indentation creep are greater than those calculated from tensile creep (modulus value error bars at 95% confidence level)

After correction for the Poisson's ratio 0.35 for PMMA, (see Chapter 3.2), the values of the instantaneous shear modulus calculated from the tensile creep curves are in good agreement with the literature value calculated from the relationship

$G = \dfrac{E}{2(1+\nu)} = 1.18$ GPa when $E = 3.2$ GPa and $\nu = 0.35$.

Indentation results produced averaged modulus values approx 1.5 times greater than those obtained from tensile testing.

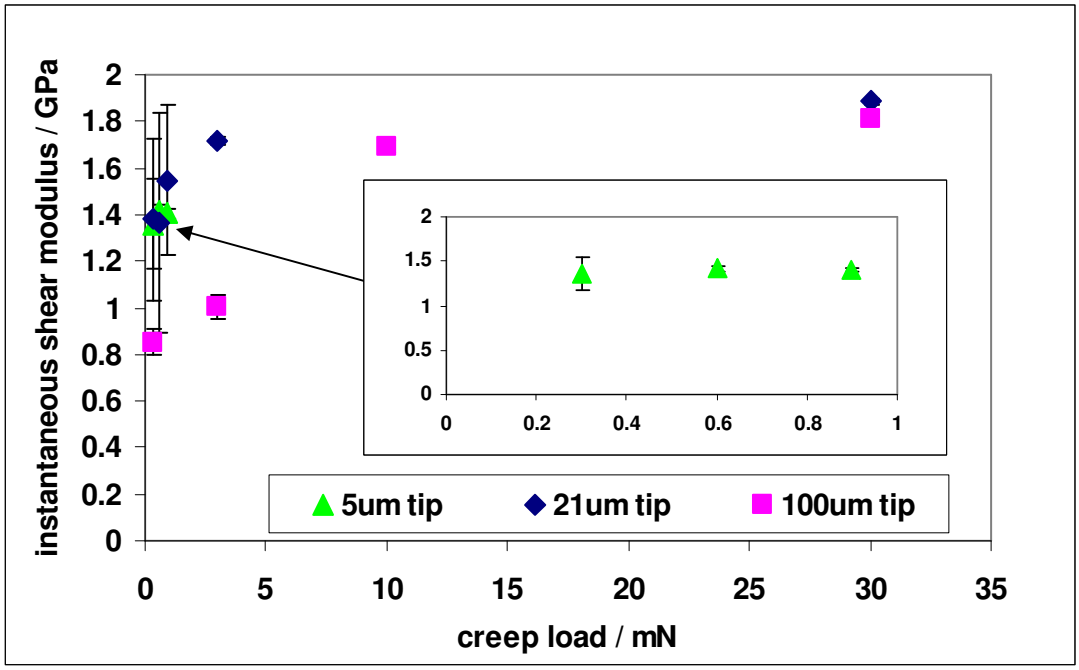

Figure 5.5-4 PMMA modulus vs. creep load: indentation with spherical tips of 3 different radii at different maximum loads, shows that calculated modulus values vary with load.
(inset 5 µm tip results shown again for clarity)
(Error bars at 95% confidence level)

Figure 5.5-4 shows the results of further indentation tests at different maximum loads using spherical indenter tips of different radii. It appears that the modulus values are sensitive to the maximum load applied. The modulus values increase with increasing load and appear to level off at a modulus value of approximately 2GPa.

When loads are converted to average mean pressures using contact areas predicted from indentation depths assuming Hertzian contact, the effect of pressure on the modulus value can be seen, Figure 5.5 -5. Calculated modulus values appear to increase with mean pressure up to a maximum pressure dependent on tip radius. Representative strain according to Tabor (1951), *i.e.* representative strain = *a/R*, can also be calculated and Figure 5.5 -6 shows the changes in modulus with increasing strain.

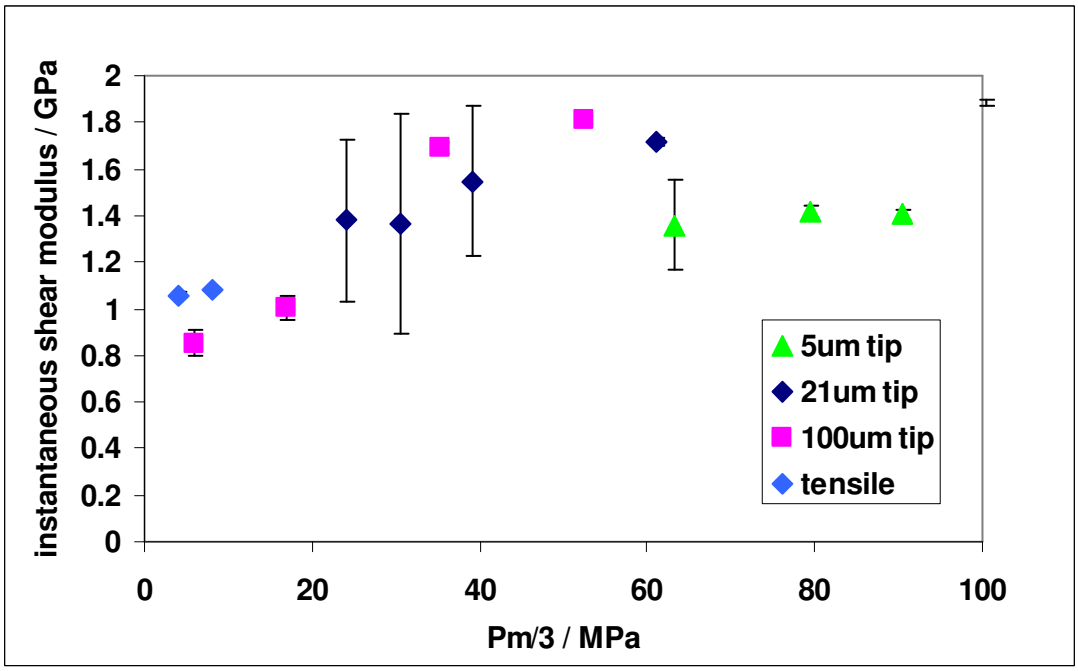

Figure 5.5-5 PMMA: instantaneous shear modulus vs mean pressure/3 : modulus values change with increasing mean pressure

(Error bars at 95% confidence level)

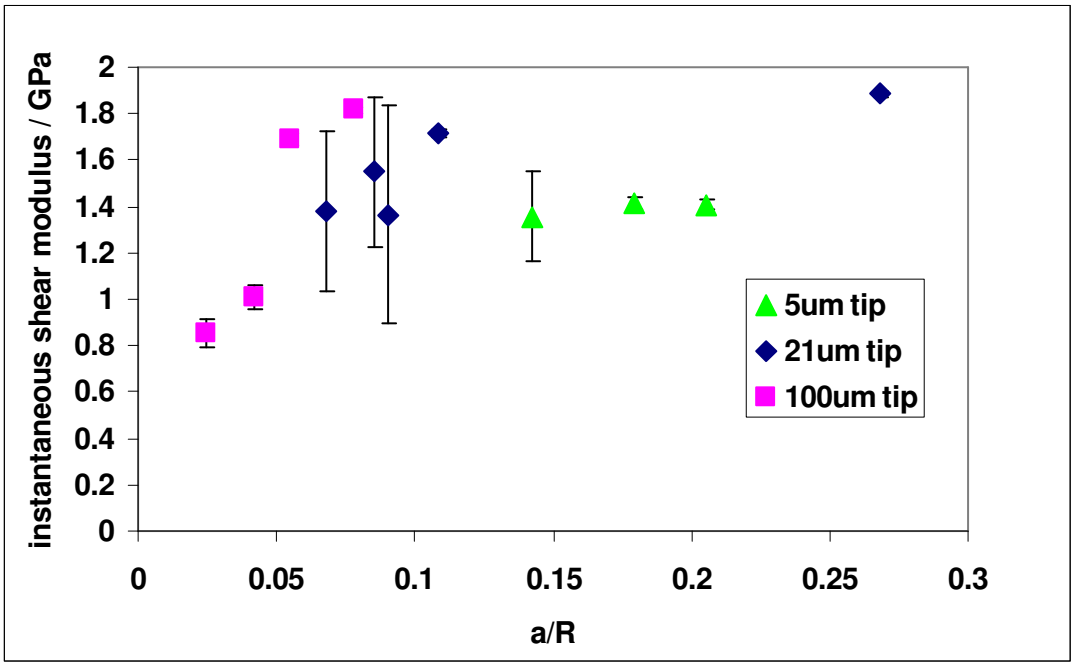

Figure 5.5-6 PMMA modulus value vs. *a/R*: modulus values calculated from nanoindentation with 3 different radius spherical indenters show that the modulus appears to change with increasing strain

(Error bars at 95% confidence level)

It appears from Figures 5.5 -5 and 5.5 -6 that calculated modulus values are strain and pressure dependent. Data resulting from tests using a 21 μm radius tip and 5 μm radius tip suggest that there may be particular value of *a/R* above which the calculated modulus no longer increases.

However this may be because at low strains the surface roughness has a greater influence.

The PMMA results show that in nanoindentation tests scatter is greater at lower loads for each tip size, larger radius tips enable lower strains with less scatter in results.

5.6 Summary

Comparisons between tensile creep and nanoindentation creep showed that whilst observed trends in material behaviour were in agreement, the observed trends in sensitivity to experimental variables were not always the same. Nanoindentation appeared to be the more sensitive technique. Calculated modulus values obtained from the results of nanoindentation creep were approximately twice those obtained from tensile creep.

To further investigate the reasons for these differences and to determine real contact conditions under spherical indentation, an experiment was set up so that *in situ* contact areas under load could be measured at the same time as measurement of penetration depths.

6 Indentation on a macro scale as a means to directly examine the contact area under load

6.1 Introduction

Although nanoindentation using a spherical indenter tip and Hertzian contact analysis has proved to be a valid technique for the determination of the mechanical properties of many materials (Cheng *et al.* 2004, Oyen 2007), for some visco-elastic polymers there appears to be a difference in the moduli values derived from the test results and the literature values determined from other techniques (Oyen 2007).

The comparative studies between tensile testing and nanoindentation (Chapter 5) have also identified a difference in the values of the shear modulus resulting from the two techniques.

It is not clear if this is due to a difference between the contact area calculated from nanoindentation displacement via conventional contact mechanics and the real contact area, *i.e.* the contact conditions may not be Hertzian.

It is therefore necessary to measure the real contact area directly.

Direct observations of spherical contact areas under indentation load have previously been made by Swain and Hagan using an inverted microscope to look at indentation plasticity and fracture of glass using spherical tips in the range of 0.2mm to 0.5 mm radius (Swain and Hagan 1976). Direct observations of contact areas using a Vickers tip to confirm post – indentation measurements of residual impressions (Thurn *et al* 2002) and crack initiation and growth for toughness measurements (Cook & Pharr 1990) on elastic materials have also been made, and more recently on

silicone elastomers using Berkovich and cube cornered indenters where it was found that for shallow penetrations contact areas calculated using the Oliver and Pharr procedure were up to 40% smaller than the *in situ* observations (Deuschle *et al.* 2009).

It is believed that direct observations of contact areas of visco-elastic materials during loading, and during a period of creep under constant load, using spherical indenters have not previously been made.

To examine the actual contact area and to investigate how visco-elastic material is displaced around the contact, the indentation experiment was performed on a macro scale so that *in situ* contact areas could be measured at the same time as indentation depth.

A boundary condition of the Hertzian contact of an elastic half space indented with a rigid sphere (see Chapter 2 Equation 2.3-4 and Figures 2.4-2) is that the contact area is at a depth, h_c, half that of the total displacement, h_{max}, so that $\frac{h_c}{h_{\max}} = \frac{1}{2}$. In this experiment the value of h_c can be determined directly from the contact area and if this boundary condition is satisfied, the experimentally determined value of h_{cA}/h_{max} should be 0.5, where h_{cA} is real h_c determined from the measured contact area and h_{max} from measured displacement. Figure 6.1-1.

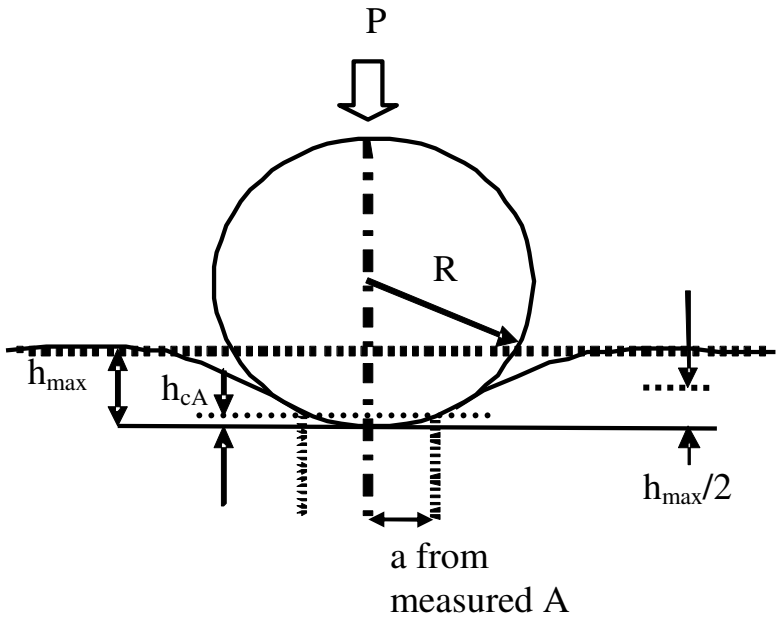

Figure 6.1-1 Contact area is at a depth, h_{cA}, determined from direct measurements of contact area, A

6.2 Methods

The materials tested were:-

glass, as a control; **PMMA** which has been widely tested and found to have a Hertzian contact response (Oyen 2006), (Ramesh Kumar and Narasimhan 2004); and **epoxy**, which from the preceding chapter was found to have a value for shear modulus depending on the method of testing and analysis. The epoxy sample was as detailed in Chapter 3 and mixed as before in the ratio 15:2 resin to hardener.

All samples were approximately 50mm x 60mm x 5mm thick.

Loads were chosen so that average mean pressures and *a/R* ratios in macroindentation were similar to those in the nanoindentation tests.

The loads and rise times are given in Table 6.2-1.

Table 6.2-1 Loading procedures for macroindentation

sample	rise time t_R (s) approx.	load rate; displcmnt rate (N/s) (mm/s)	maximum load P_{max} (N)	comments
glass	20 60	2.5 N/s 7.5 N/s	50 200	under these conditions it was possible to collect a number of measurable images
PMMA	1.5-2 17 14 140	0.01mm/s; 4.5N/s 0.001mm/s;0.5N/s 0.01mm/s;5.5 N/s 0.001mm/s;0.55N/s	8 8 80 80	only 1 or 2 images taken during ramp load for 2s rise time
Epoxy	6-7 16 14 70-90 150 140	0.01mm/s;7N/s 0.01mm/s;10N/s 0.01mm/s;14N/s 0.001mm/s; 0.7N/s 0.001mm/s;1N/s 0.001mm/s;1.4N/s	50 150 200 50 150 200	good images taken

The rise times were chosen so as to be in the region of the rise times resulting from nanoindentation tests in the previous chapter using the 10 increments of load control. The slower rise times were chosen to enable comparisons to be made and investigate the effects of rise time on contact areas and examine the time dependent behaviour.

Tests were repeated and data collected at various times during the ramp and hold load procedure. Together, data provide information throughout the ramp and hold load period and the degree of scatter between repeated tests is evident in the presented plots.

6.3 Results : Measurements

Contact areas It was found that the contact areas in the region of as little as 250 pixels could be measured, equivalent to a contact radius of approximately 63 μm.

Contact areas could be measured to within 6 % error for the smaller areas to 2 % error for the larger areas for all the samples tested.

Displacement The Instron / extensometer resolution was ± 0.0004 % strain. Displacement errors were due to the error in gauge length 13mm ± 0.3mm and subsequent conversion from strain to displacement. The resulting errors in displacement were 2.3 %. It can be seen from $A = \pi a^2 = \pi h_{\max} R$, where A is contact area, a is the radius of the contact area, h_{max} is the displacement and R is the radius of the indenter tip that the uncertainties in the measurement of contact area is similar to the uncertainties in displacement measurement.

However, over a set of 5 tests the scatter in displacement was much greater than the scatter in contact area, as can be seen in all of the results presented. This is most likely due to the repositioning of the clamps holding the extensometer after moving the sample to indent a new area of the surface. Repositioning of the camera between tests was not necessary.

Displacement control of the Instron crosshead was used in preference to load control. This was to minimise overload at peak load observed in the preliminary tests at low loads due to slow feedback of the system during load control. Displacement control also introduced problems as ramp loading was not always at a constant load rate. This was material dependent; it was not seen in glass loading. For the faster loading of PMMA to 80 N, it made the difference between 5.5N/s at start of loading to 6.0 N/s at end of loading and for the epoxy loading the load rate was doubled from start of loading to the end of loading presented in Figure 6.3-1. However, as the method of analysis is based on creep, displacement control was preferred as it gave more precise data at the maximum load and at the start of the hold load period.

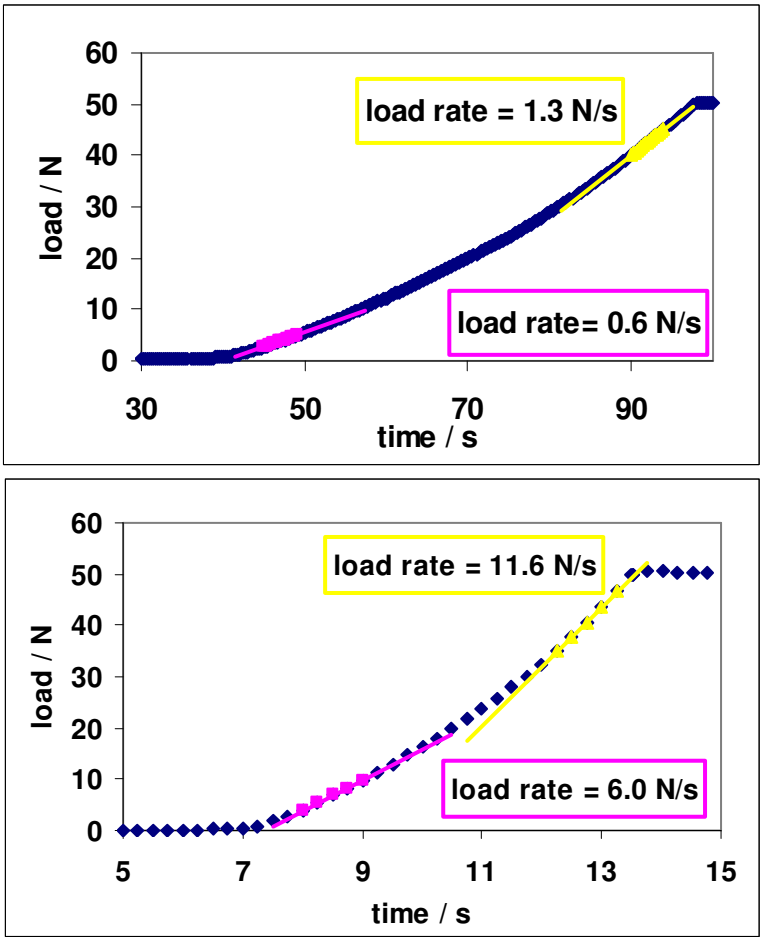

Figure 6.3-1Epoxy load vs. ramp time: load rate is not constant under displacement control

6.4 Results: Glass as validation of method

Figure 6.4-1 shows images of glass under load. The image contrast and clarity is typical of all material samples tested.

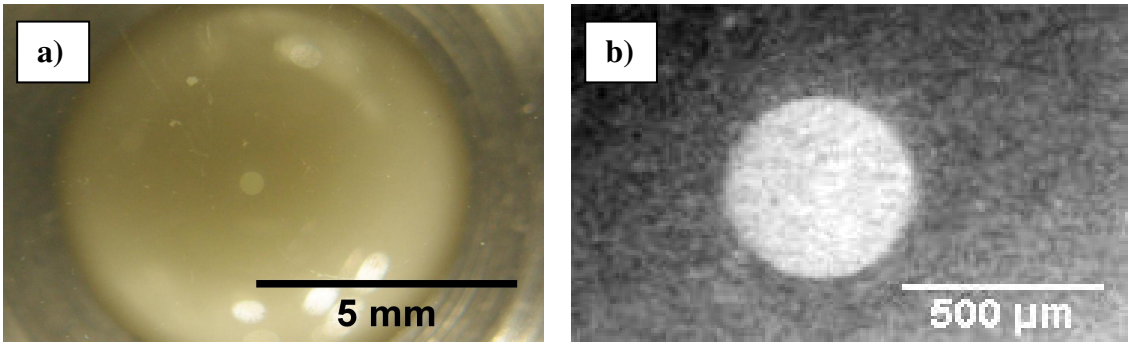

Figure 6.4-1 a) Unprocessed image of contact area indenter on glass under 200N load, b) enlarged and processed image of the same contact area

Contact areas and displacements were measured during the ramp and constant load period and it can be seen in Figure 6.4-2, and Figure 6.4-3 that both contact areas and displacements were as expected according to Hertzian contact mechanics. As expected, throughout the hold at maximum load period contact areas and displacements remain constant.

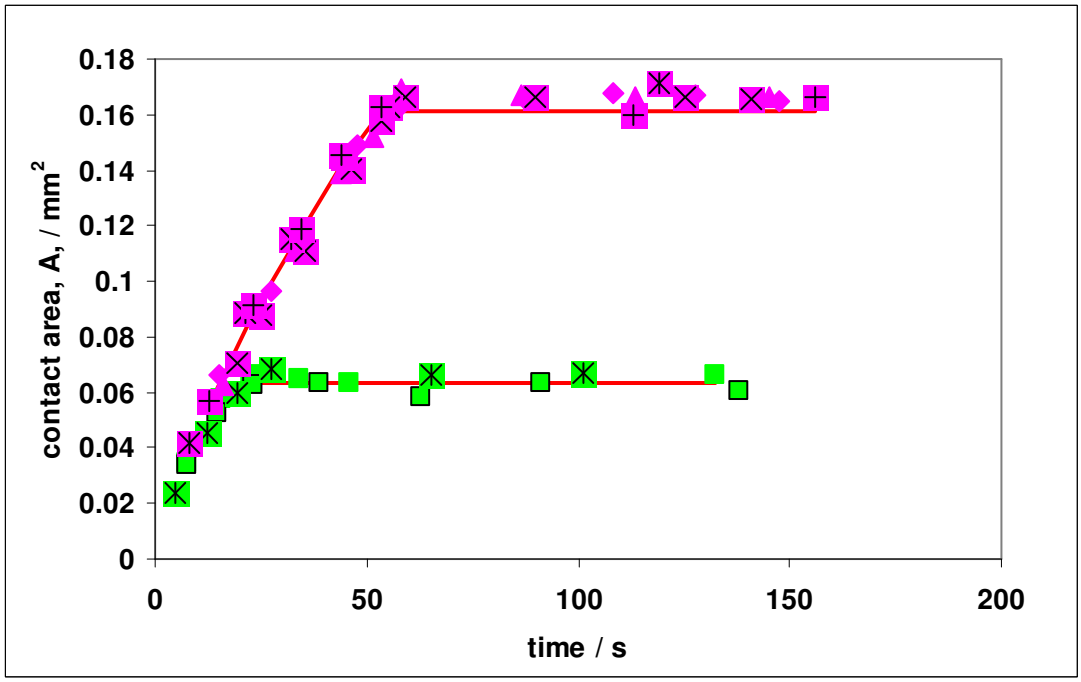

Key : green = load to max. 50 N at approx. 2.5 N/s, pink = 200N at 3.5 N/s, red line = Hertzian prediction

Figure 6.4-2 Glass sample contact areas vs. time : areas can be measured over duration of ramp and hold load period and agree with theoretical values, scatter over repeated tests can be seen

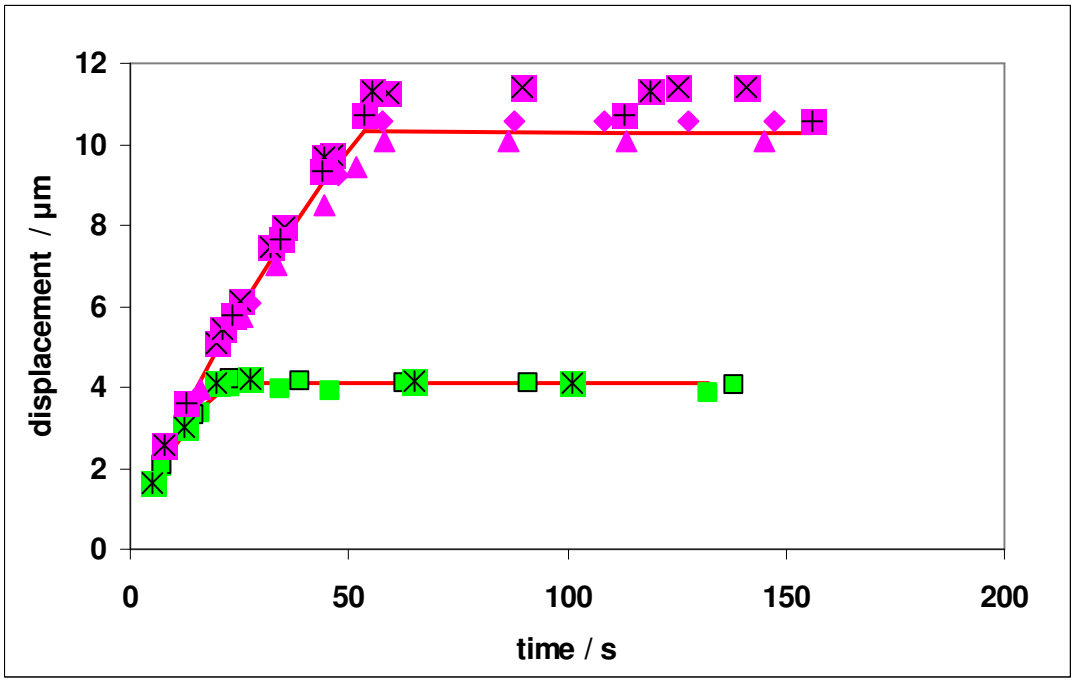

Key : green = load to max. 50N, pink = 200N, red line = Hertzian prediction

Figure 6.4-3 Measured displacement of indenter into glass sample vs. time : displacements can be measured over time period of ramp and hold at maximum load 50 N and 200 N and agree with theoretical values, scatter over repeated tests can be seen.

Using the modulus 73.6 GPa for glass see Chapter 3.1.5 and load frame compliance 0.01 μm/N (Chapter 3.4), measured contact areas on glass plotted against load $^{2/3}$ fall on the theoretical line as predicted by Hertzian contact mechanics. Unsurprisingly, no time dependent behaviour was evident over the various ramp to maximum loads applied in this timescale. Figure 6.4-4 presents the contact area vs. load $^{2/3}$ during ramp and hold load.

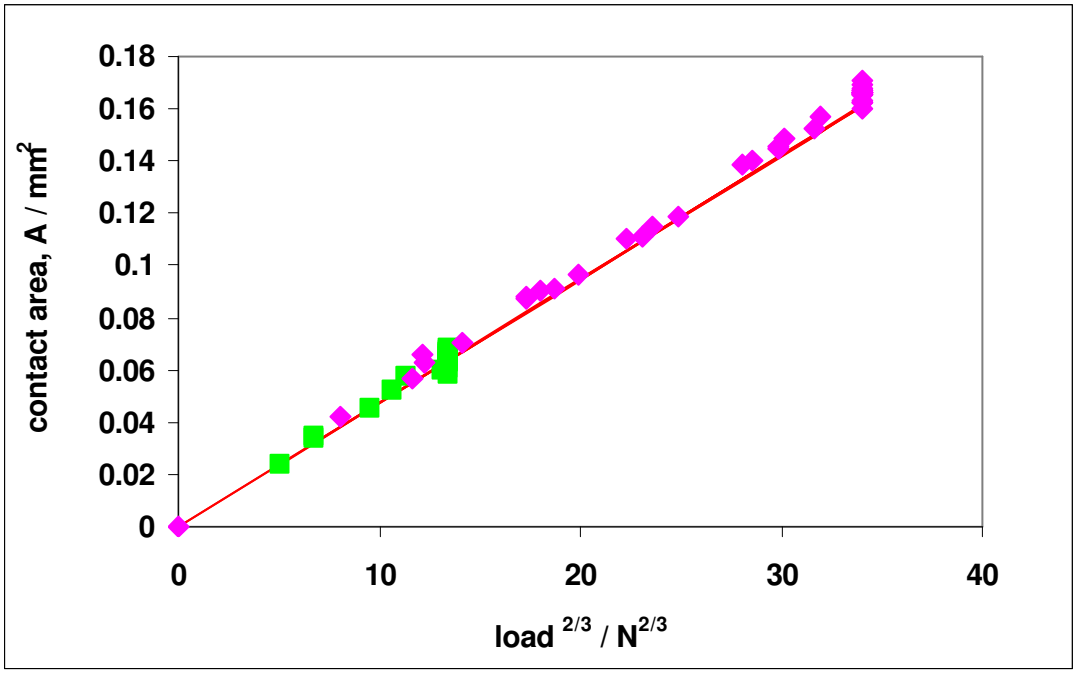

Key: green squares = load to max. 50 N at approx. 2.5 N/s, pink diamonds = 200N at 3.5 N/s, red line = Hertzian prediction

Figure 6.4-4 Glass sample contact areas plotted against load $^{2/3}$ for ramp to maximum load and hold load 120s : tests show a good fit to the Hertzian line

Measured displacement during ramp and constant hold load also lies on the theoretical line when plotted against load $^{2/3}$ as seen in Figure 6.4-5.

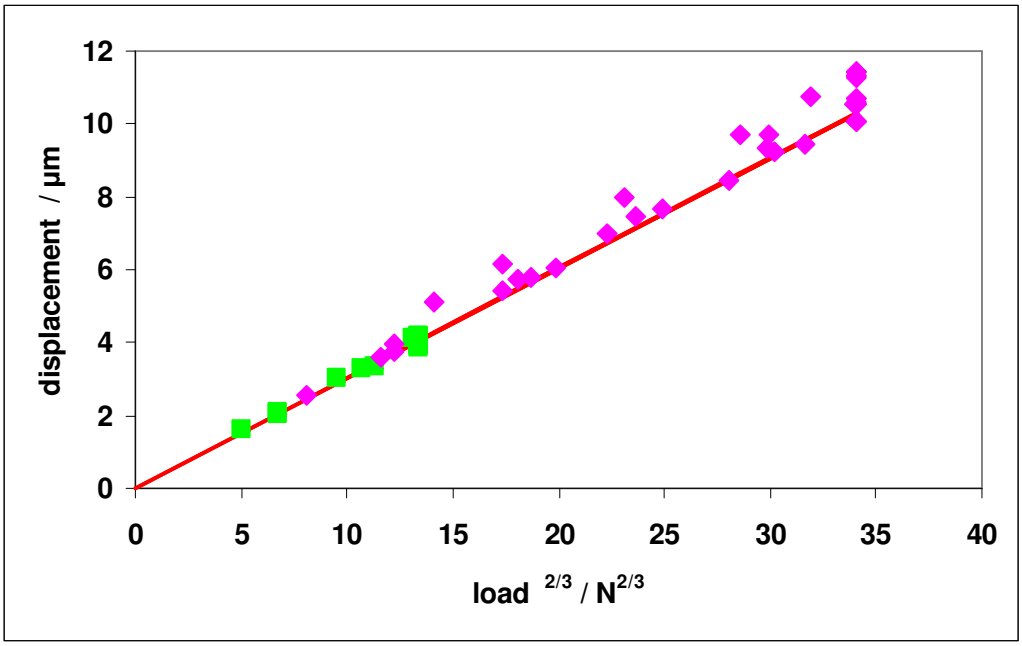

Figure 6.4-5 Displacement of indenter into glass sample plotted against load $^{2/3}$ at 50 N maximum load and 200 N maximum load shows good agreement to Hertzian theory

Key : green squares = load to max. 50N, pink diamonds = 200N, red line = Hertzian prediction

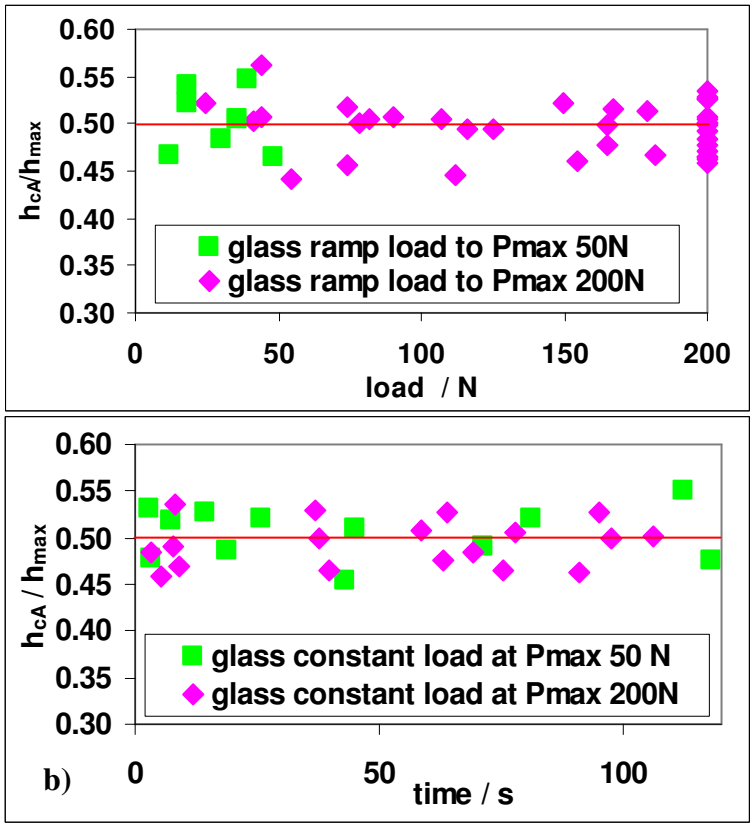

Figure 6.4-6 Glass indentation: h_{cA}/h_{max} shown a) during ramp loading, b) during hold at constant load

When glass was indented under various loads the expected Hertzian response is seen. Additionally, it can be seen that the relationship remains Hertzian over a period of time with no evident creep in displacement or contact area.

The Hertzian boundary conditions of a rigid indenter in contact with an elastic half space are satisfied *i.e.* $h_{cA}/h_{max} = 0.5$, as can be seen in Figure 6.4-6.

These results validate the methods for measurement of contact area and indenter displacement.

6.5 Results: PMMA

The time dependence of the response is evident in both contact areas and displacement. Creep in contact area can be seen in Figure 6.5-1, creep in displacement is seen in Figure 6.5-2. More scatter is evident in the displacement data. Using the modulus value supplied, 3.2 GPa (Chapter 3.1.4) a theoretical data set was produced assuming Hertzian contact conditions. This is shown in the Figures for comparison.

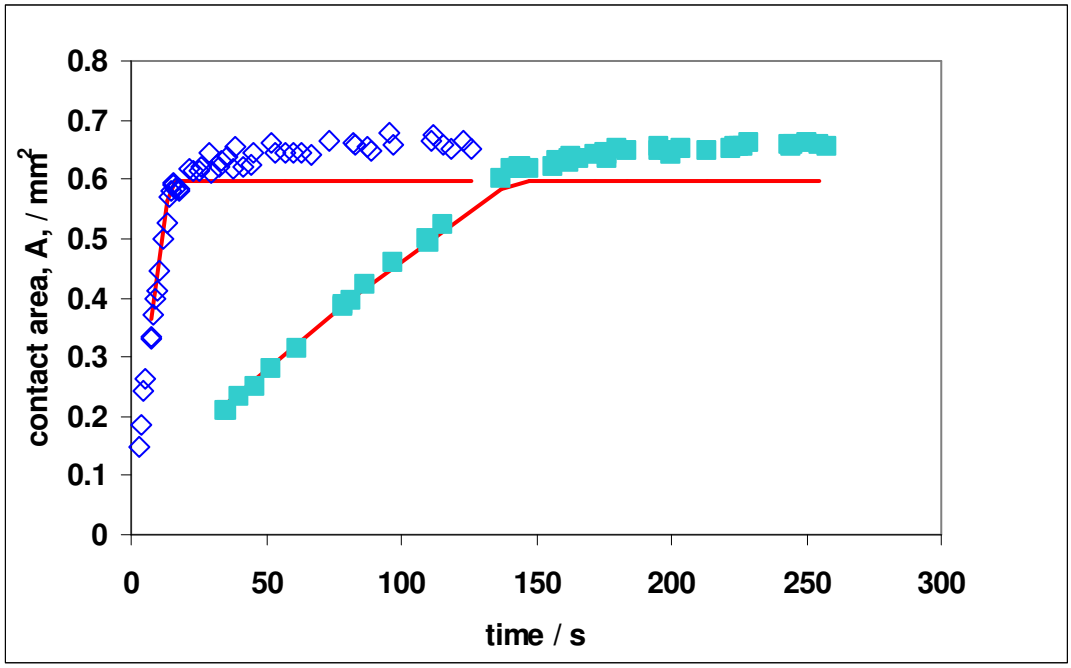

Key : red line = theoretical Hertzian; solid squares =slow load displacement control 0.001mm/s approx. 0.55 N/s; open diamonds = fast load displacement control 0.01 mm/s approx. 5.5 N/s

Figure 6.5-1 PMMA measured contact areas vs time during two ramp load times and 120s constant load of 80N : showing contact area during ramp load and creep during hold load period (results from 6 repeated tests).

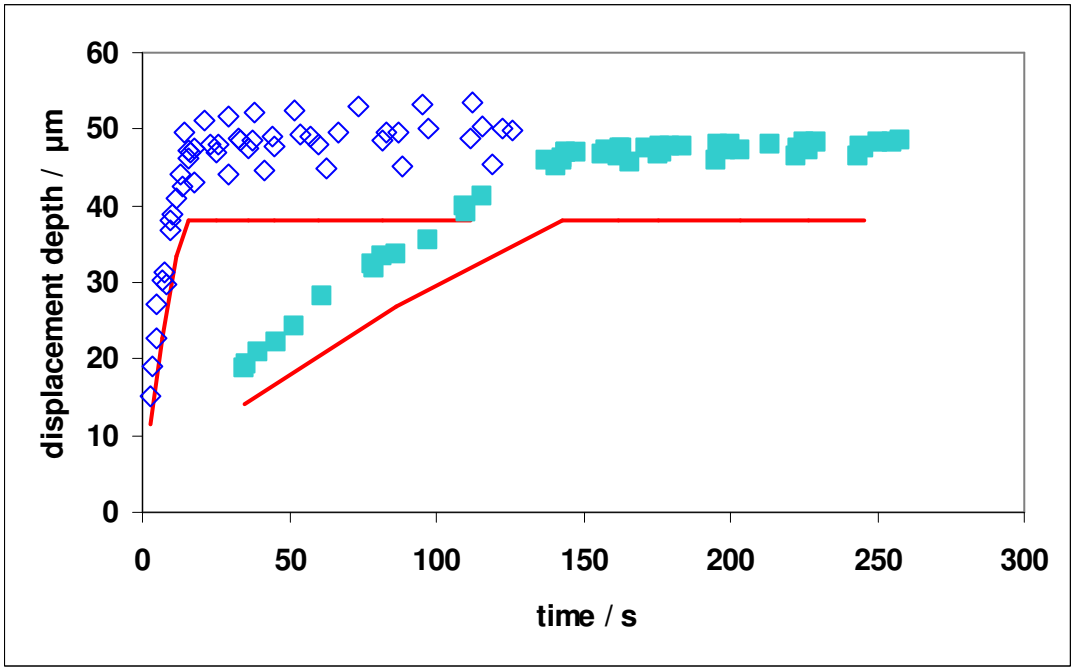

Key : red line = theoretical Hertzian data; solid squares = slow load displacement control 0.001mm/s approx. 0.55 N/s ; open diamonds = fast load displacement control 0.01 mm/s approx. 5.5 N/s

Figure 6.5-2 PMMA displacement vs. time during ramp and hold load constant at 80N after 2 different rise times showing displacement during ramp and hold load (results from 6 repeated tests).

When the PMMA sample was indented (ramp loading up to 80 N maximum) the measured displacement was initially greater than predicted using Hertzian theory Figure 6.5-3. However, after the first 25 µm of displacement the displacement vs. load appeared to have a Hertzian relationship. When PMMA was indented to a lower load, maximum load 8 N, so that displacement was below 25 µm, the displacement was found to be non-Hertzian see Figure 6.5-4.

A second sample of PMMA (Perspex ICI) showed similar behaviour but the initial greater displacement continued to approximately 40 µm. The load rates for the second sample were different as a consequence of the test being under displacement control and the response of the material itself.

Investigations using a profilometer suggest that the initial displacement is not a consequence of surface texture / roughness (surface roughness, Ra = 0.2µm).

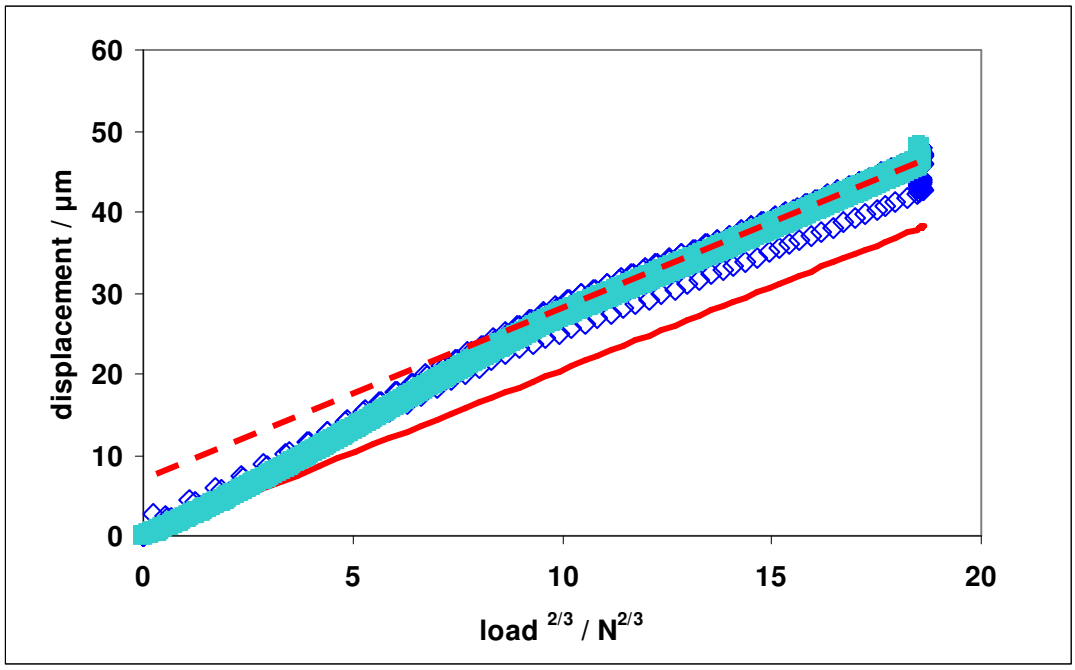

Key : red line = theoretical Hertzian; solid squares = slow load displacement control 0.001mm/s approx. 0.55 N/s to 80 N max.; open diamonds = fast load displacement control 0.01 mm/s approx. 5.5 N/s to 80 N max.

Figure 6.5-3 PMMA displacement vs. load $^{2/3}$: ramp load to 80N shows displacement is initially greater than predicted with subsequent displacement appearing to be Hertzian as indicated by fit to dotted line which is parallel to Hertzian line

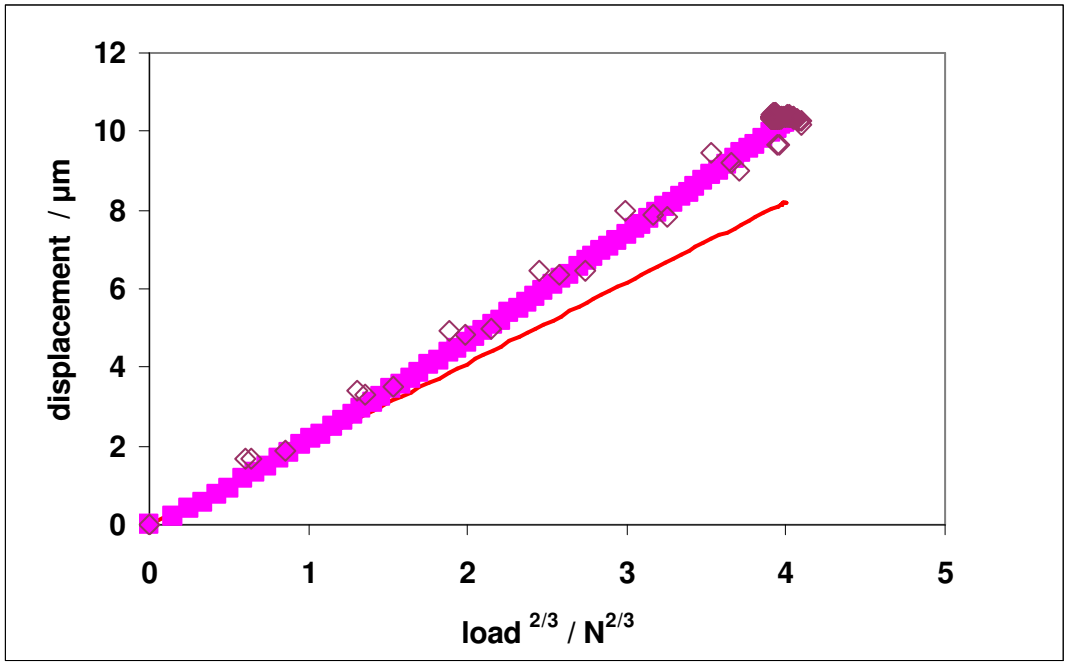

Key : red line = theoretical Hertzian; solid squares = slow load displacement control 0.001mm/s approx. 0.55 N/s to 80 N max.; open diamonds = fast load displacement control 0.01 mm/s approx. 5.5 N/s to 80 N max.

Figure 6.5-4 PMMA displacement vs. load$^{2/3}$ ramp load to 8 N : measured displacement against load $^{2/3}$ showing initial non-Hertzian displacement

The load$^{2/3}$ versus contact area plots at 8 N and 80 N loads are linear and the PMMA sample shows a good agreement to theoretical contact areas predicted by Hertzian theory using the given modulus value, Figures 6.5-5 and 6.5-6. It appears that when the load was applied relatively slowly the contact areas were larger whereas during a faster ramp load time the measured contact areas were slightly less than predicted.

Less contact area data is available for tests in which loading was up to 8 N maximum due to the amount of time necessary to take photographs in the reduced rise time, however combining the data with data from the second PMMA sample (sample with no given modulus value) shows that at these load rates contact areas were as predicted using Hertzian contact mechanics (Figure 6.5-5).

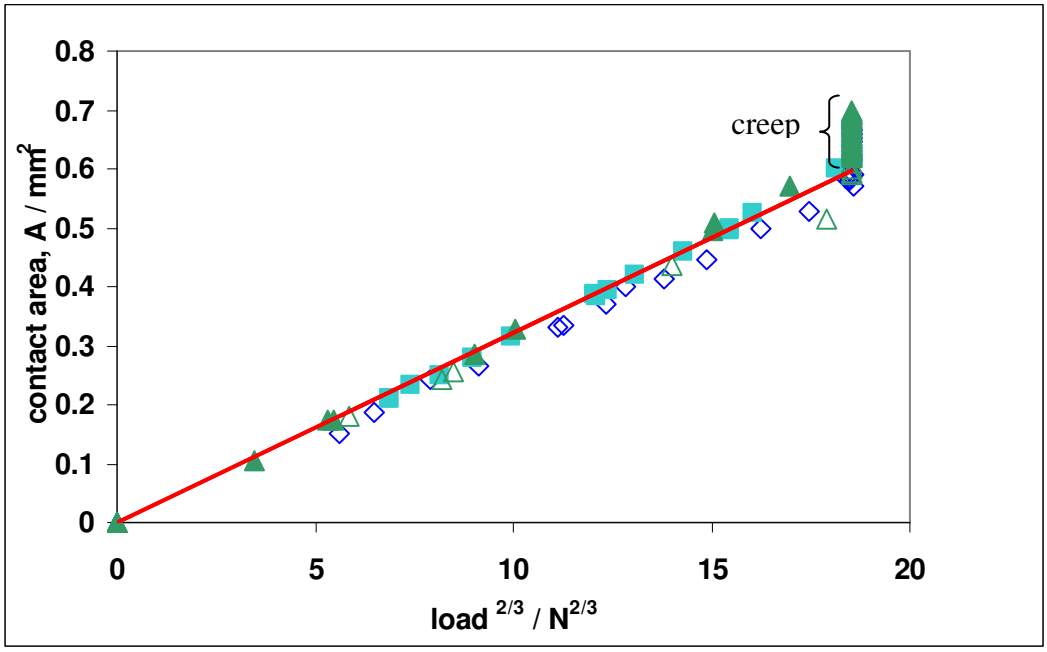

Key : red line = theoretical Hertzian; solid squares = slow load displacement control 0.001mm/s approx. 0.55 N/s; open diamonds = fast load displacement control 0.01 mm/s approx. 5.5 N/s; 2nd PMMA sample green triangles solid =slow load 0.001 mm/s approx. 1.1 N/s and green triangle open = fast load 0.01 mm/s approx. 12 N/s

Figure 6.5-5 PMMA contact areas against load $^{2/3}$ over two rise times to maximum load 80N showing agreement to Hertzian prediction using literature value modulus 3.2 GPa

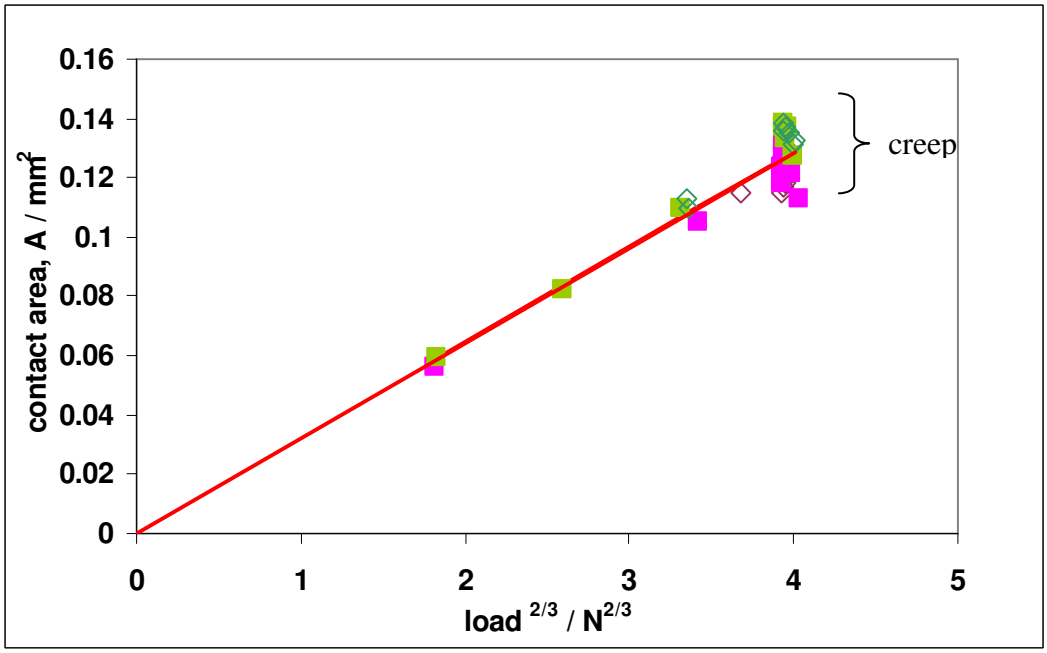

Key: red line = theoretical Hertzian; solid squares pink = load rate approx 0.55 N/s; open diamonds dark pink = load rate approx. 5.5 N/s; 2nd PMMA sample solid squares green = load rate approx.0.15N/s; open triangles green = load rate approx. 0.5N/s

Figure 6.5-6 PMMA contact areas against load $^{2/3}$ during two rise times to maximum load 8N limited results show some agreement to Hertzian predicted areas

During slow ramp loading measured contact areas were 90 to 100% of the areas predicted whereas during fast loading they were 85 to 95 %, Figure 6.5-7. This is evidence of the time dependent viscous flow of material around the indenter tip, it does not necessarily occur at a rate such that contact areas are Hertzian whilst the indenter is pushed into the surface. As loading continues the increase in contact areas also increases and at faster load rates the contact area appears to “catch up” faster.

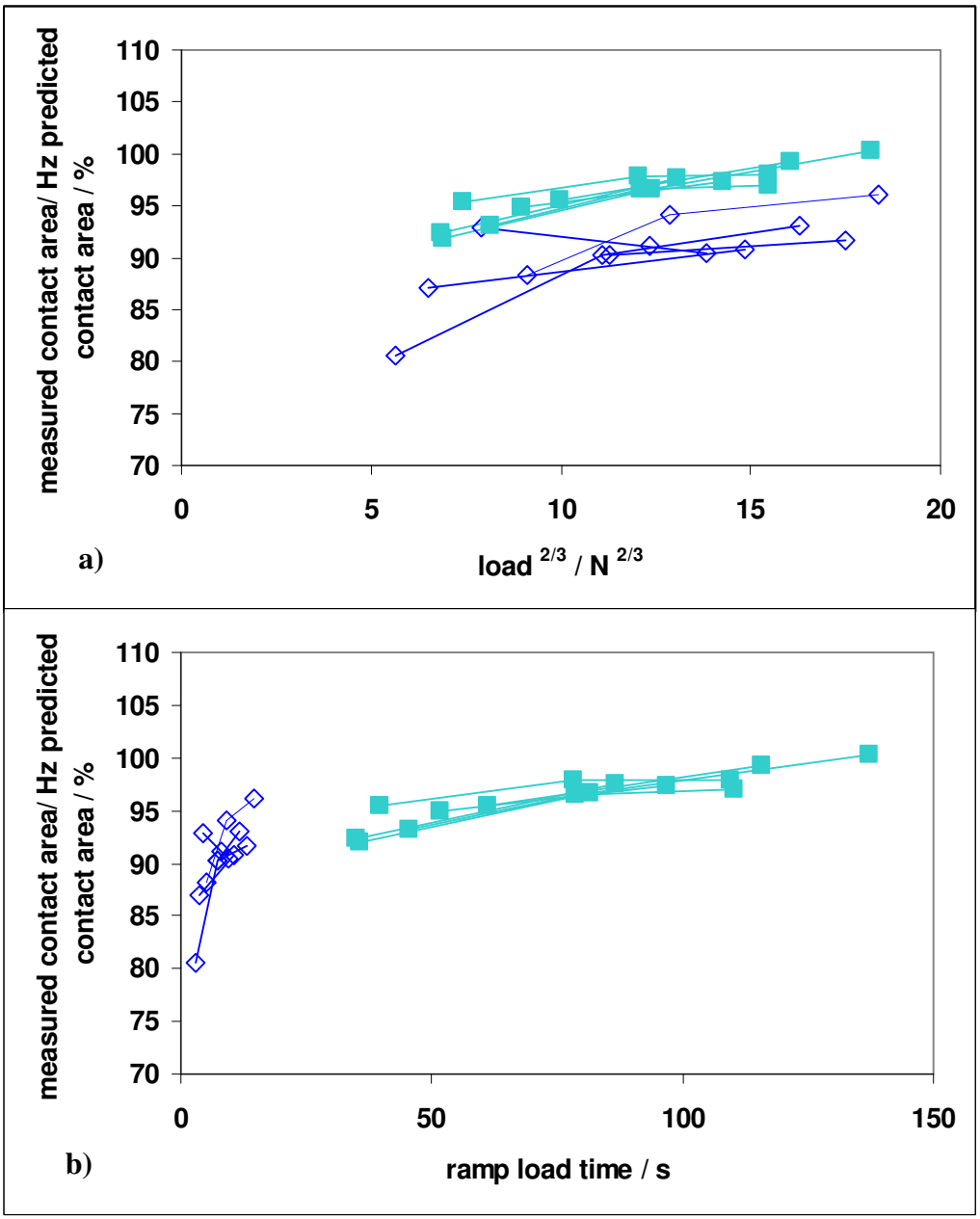

Figure 6.5-7 Measured contact area as a percentage of Hertzian predicted contact area using given literature value for Young's modulus 3.2 GPa during loading to 80 N a) as load increases, b) as rise time increases

Measured contact areas on the PMMA sample appear to increase with the hold load period. There is a greater increase in contact area occurring over the hold period when the load rate to maximum load was faster, this is evident in Figure 6.5-8.

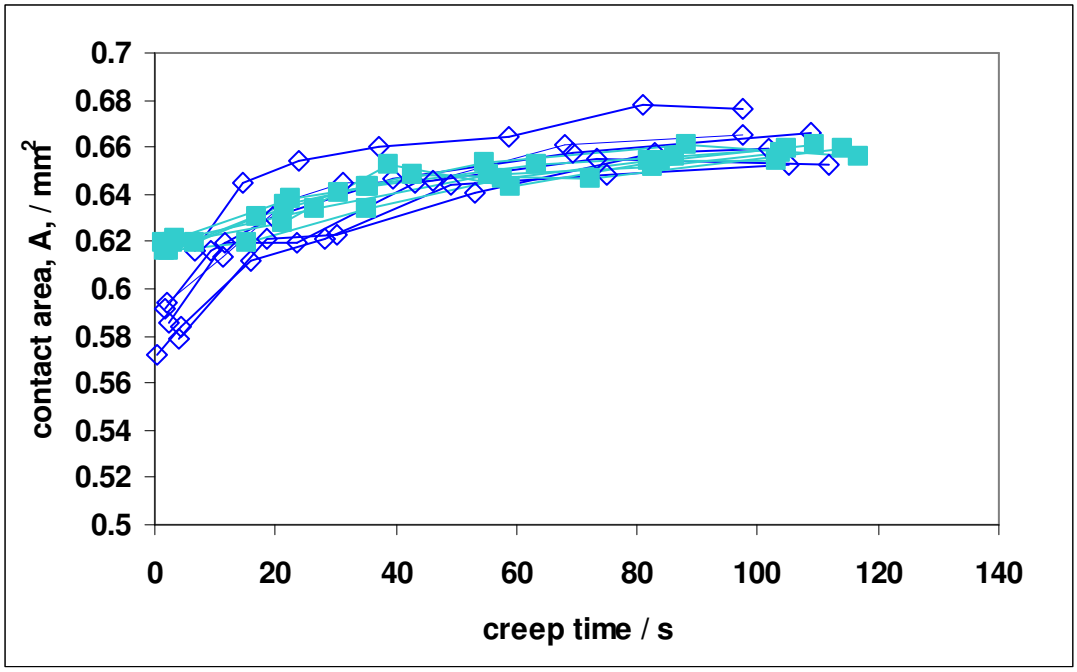

Key : solid squares = contact area at constant 80N load after slow ramp (under displacement control at 0.001mm/s equivalent to approx. 0.55 N/s); open diamonds = contact area at constant 80N load after fast ramp (under displacement control of 0.01 mm/s equivalent to approx. 5.5 N/s)

Figure 6.5-8 PMMA area vs. creep time at constant 80N load : more contact area creep is seen after a faster rise time

(Lines are a guide to the eye)

As can be seen in Figure 6.5-9, creep displacement at 80 N appears similar to creep in contact area in that after a slow rise time to maximum load less creep occurs.

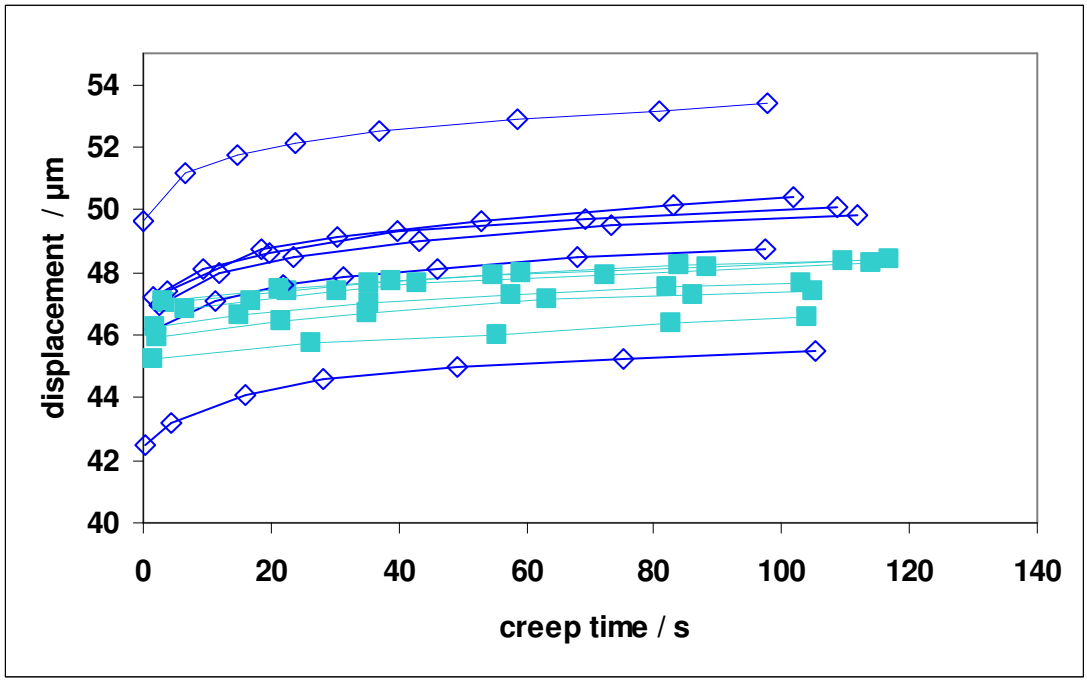

Key : solid squares = slow load displacement control 0.001mm/s approx. 0.55 N/s; open diamonds = fast load displacement control 0.01 mm/s approx. 5.5 N/s

Figure 6.5-9 PMMA displacement vs. creep time at constant 80N load : more displacement creep occurs after faster ramp load

(Lines are a guide to the eye)

The shear modulus determined from the results of the analysis of the displacement creep at 80 N, (assuming a Poisson's ratio of 0.5) as in previous chapters, were corrected using the known Poisson's ratio (Chapter 3.3). Further values were calculated by making an adjustment to the initial depth correction so that the later portion of the displacement data during ramp loading made a good fit to the theoretical line calculated using the given modulus value. The adjustment can be seen in Figure 6.5-10.

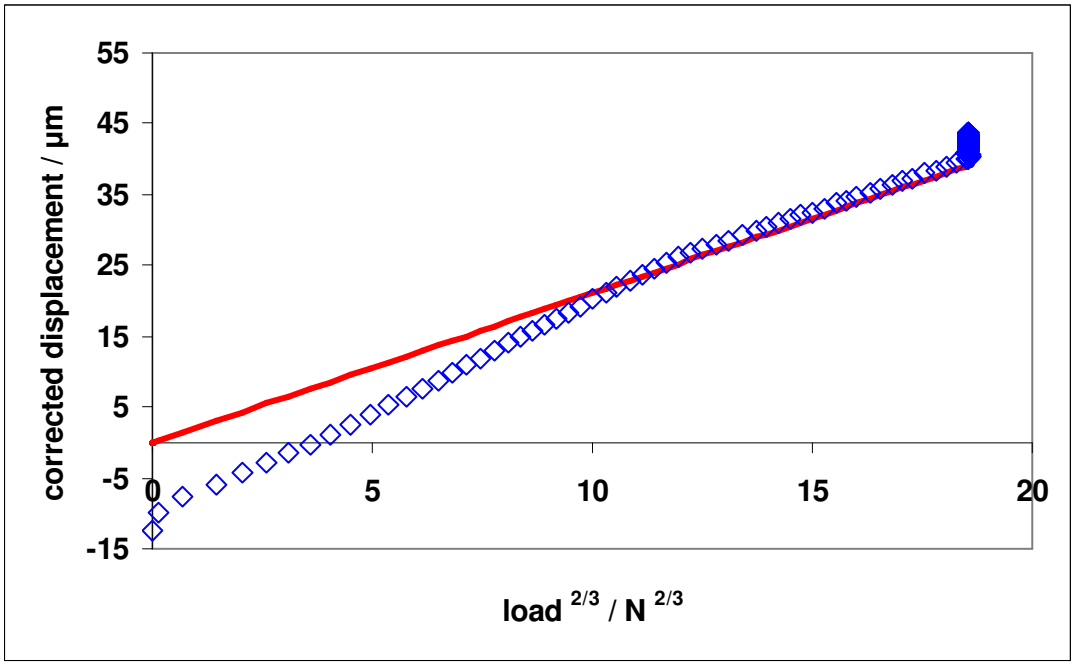

Figure 6.5-10 PMMA displacement vs. load$^{2/3}$ during ramp and hold load to 80 N : displacement data corrected to fit Hertzian prediction using literature value modulus 3.2 GPa

The calculated values are compared to the literature value and to the results from the nanoindentation test in Table 6.5-1.

Table 6.5-1PMMA calculated modulus values

literature value elastic modulus and Poisson's ratio	3.2GPa, $\nu = 0.35$ so G = **1.18 GPa**		
G0 from **nanoindentation creep** corrected for Poisson's ratio	**0.97 GPa** 0.15SD (0.3mN load) a/R =0.06 (from displacement)	**1.07 GPa** 0.19SD (0.6mN load) a/R = 0.07 (from displacement)	**1.20 GPa** 0.18 SD (0.9 mN load) a/R = 0.08 (from displacement)
G0 from **macroindentation creep** results averaged over both rise times and corrected for Poisson's ratio	**0.80 GPa** 0.06SD (8N load) *a/R*= 0.047		**0.94 GPa** 0.06 SD **1.23GPa** 0.10SD (when corrected for initial displacement) (80N load) *a/R* = 0.1
G0 calculated from *E* from **macroindentation displacement** vs ramp load$^{2/3}$ slope, results averaged over both rise times	**0.88 GPa** 0.06 SD (8N load) *a/R*= 0.047		**0.77 GPa** 0.05 SD from initial displacement/ load$^{2/3}$ gradient **1.09 GPa** 0.06SD from later part of displacement/ load$^{2/3}$ gradient (80N load) *a/R* = 0.1
G0 calculated from *E* from **macroindentation contact area** vs load$^{2/3}$ slope	**1.26 GPa** 0.01SD (8N load) *a/R* = 0.047		**1.19 GPa** 0.02SD (80N load) *a/R* = 0.1

A range of modulus values result from both the nanoindentation and the macroindentation test results. Plots were made of calculated modulus value, *G*0 vs.

displacement during ramp and hold load. Figure 6.5-11 presents the results of repeated tests during ramp and hold to 8N maximum load and to 80N maximum load with corresponding *a/R* values indicated. Strain dependence of calculated modulus values was previously seen in nanoindentation tests (Figure 5.5-6). When the modulus values resulting from the 8N tests results are considered together with the results from the 80 N test results, a strain or displacement dependence is not seen and the trend suggested by the 80 N tests alone can be attributed to the initial greater displacement measured at the sample surface. Corresponding modulus values calculated from the measured contact areas are again skewed by the initial greater displacement. No clear trends can be seen in the ramp load to 8 N tests results. But as expected decreasing modulus values can be seen during the period of creep.

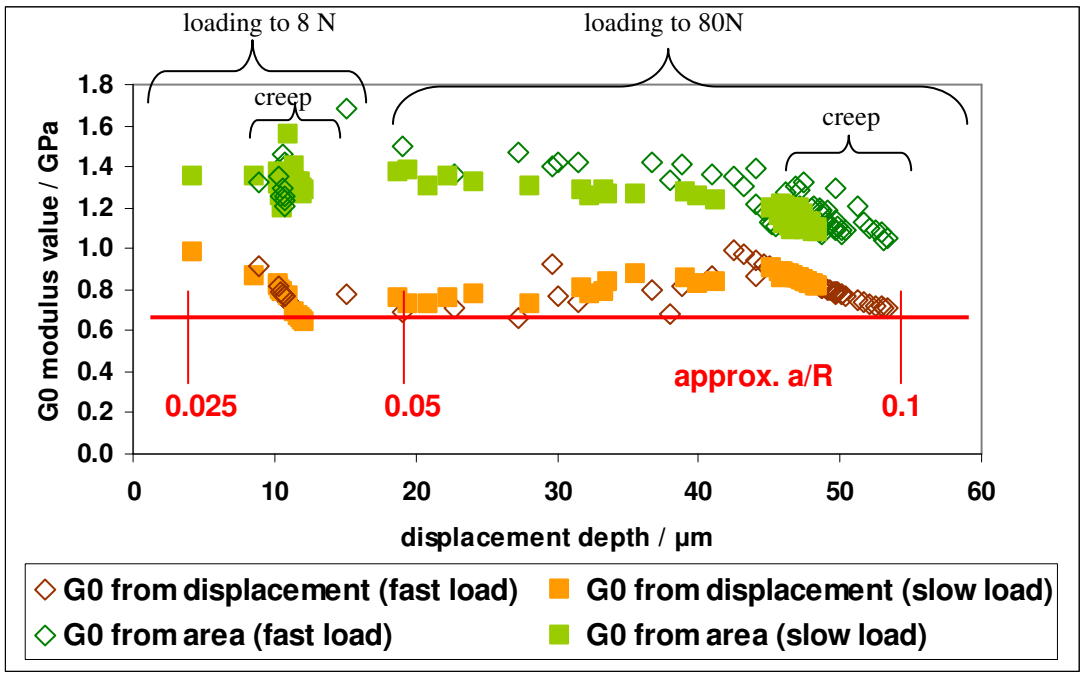

Figure 6.5-11 PMMA shear modulus values calculated from the measured contact area and from displacement during repeated ramp and hold load tests shows some strain dependence during loading to 80N

Figure 6.5-12 shows the relationship between contact area and displacement during the ramp load period. The approximately 10 µm offset in displacement is due to the initially greater displacement mentioned previously (Figures 6.5-3 and 6.5-4). Allowing for the 10µm offset in displacement the gradient of the lines suggest that the relationship is Hertzian during loading.

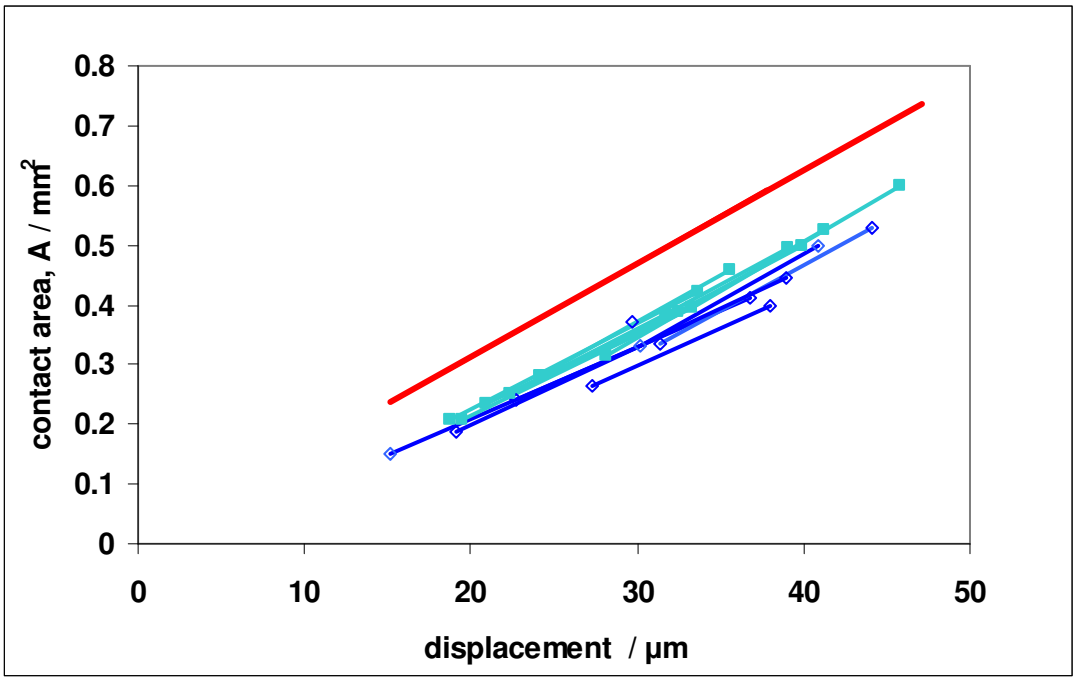

Key : red line = theoretical Hertzian using literature modulus value, solid squares = slow load displacement control 0.001mm/s approx. 0.55 N/s; open diamonds = fast load displacement control 0.01 mm/s approx. 5.5 N/s

Figure 6.5-12 PMMA : relationship between contact area and depth over ramp load period appears Hertzian but displacement is displaced by 10µm

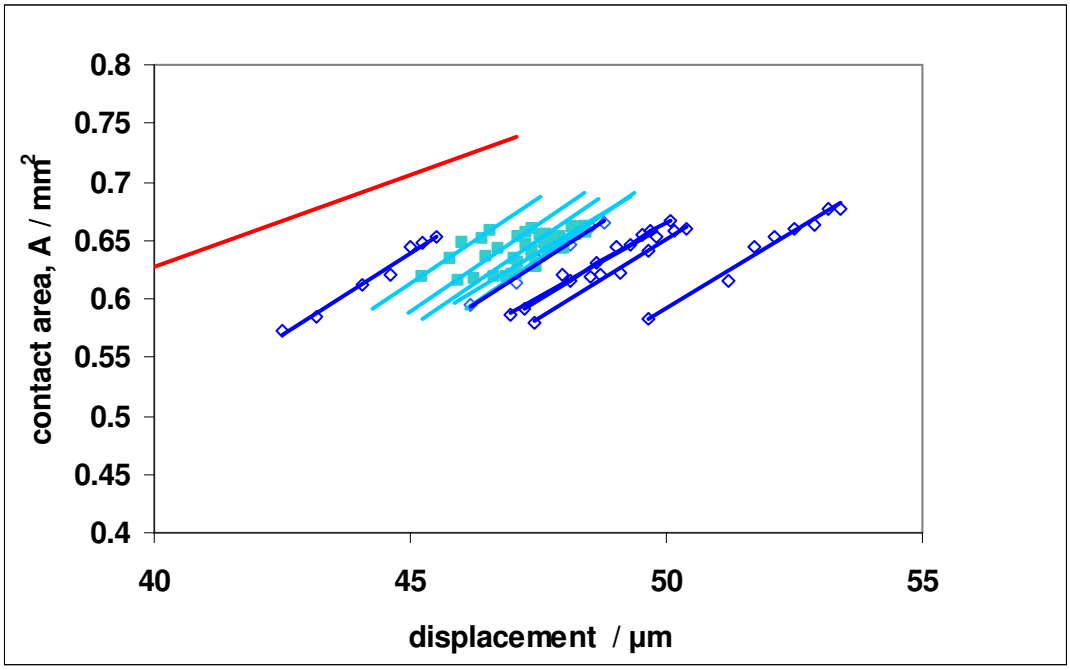

Key : red line = theoretical Hertzian using literature modulus value, solid squares = slow load displacement control 0.001mm/s approx. 0.55 N/s; open diamonds = fast load displacement control 0.01 mm/s approx. 5.5 N/s

Figure 6.5-13 PMMA relationship between contact area and displacement during period of creep time appears non – Hertzian as contact area increases more than displacement.

However, during the corresponding creep period at constant load the relationship between contact area creep and displacement creep appears to change, the contact area appears to increase more rapidly than the displacement, and this can be seen in Figure 6.5-13 as a change in the gradient with lines of data no longer parallel to the Hertzian line predicted using the given literature value.

The change in relationship between contact area and displacement during ramp and hold load is reflected in the change in relationship between h_c/h_{max} Figure 6.5-14. That the relationship is less than 0.5 is due to the greater displacement measured, however it can be seen that the relationship increases slightly with load and during the hold load period continues to creep and then to equilibrate, again there is more creep after the rapid ramp loading figure 6.5-15.

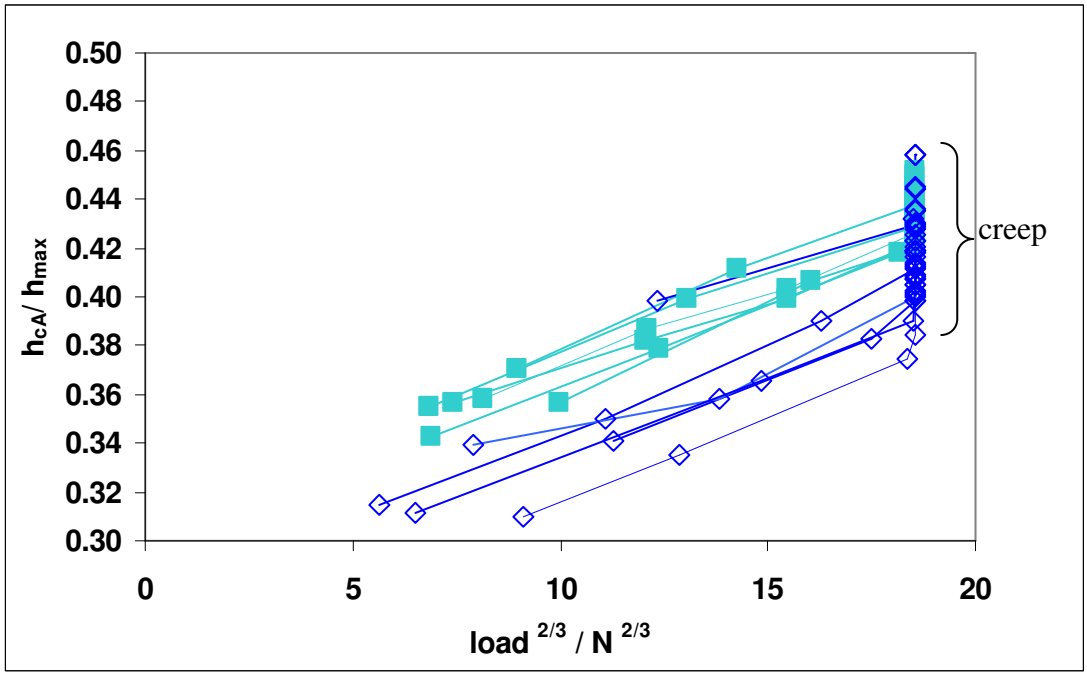

Key : solid squares = slow load displacement control 0.001mm/s approx. 0.55 N/s; open diamonds = fast load displacement control 0.01 mm/s approx. 5.5 N/s

Figure 6.5-14 PMMA shows increase in h_{cA}/h_{max} with load $^{2/3}$ during ramp loading and during creep at constant load 80N

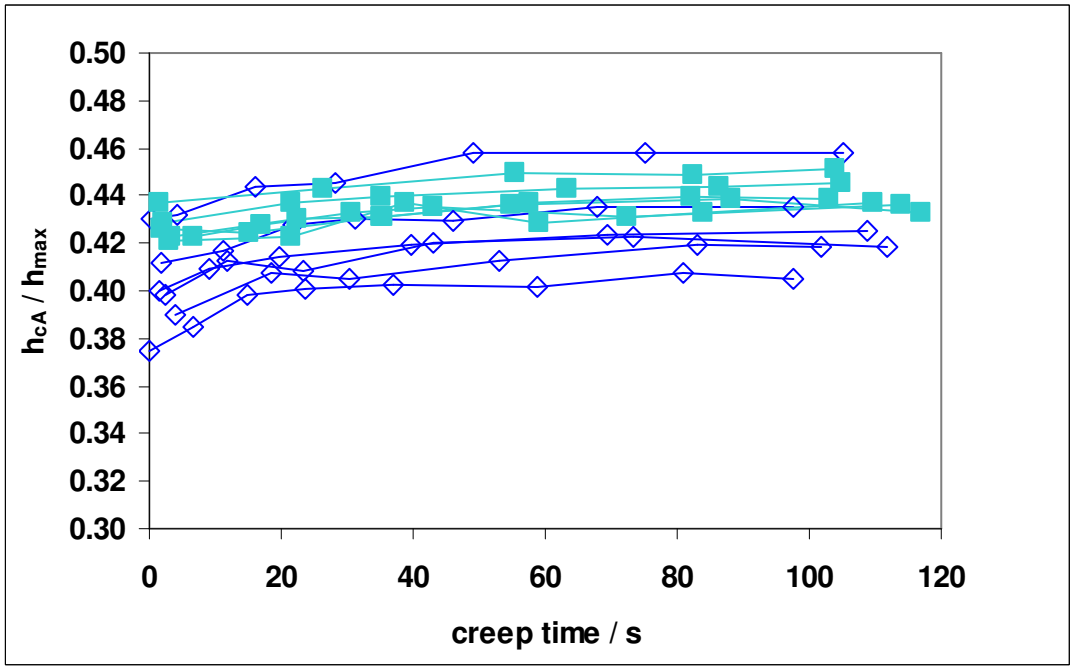

Key : solid squares = slow load displacement control 0.001mm/s approx. 0.55 N/s; open diamonds = fast load displacement control 0.01 mm/s approx. 5.5 N/s

Figure 6.5-15 PMMA shows change in h_{cA}/h_{max} with creep time at constant load 80 N

Measured displacements suggest that the indenter sinks in initially and subsequently the material flows around the indenter so that contact areas approach areas predicted by Hertzian theory. The contact area and displacement relationship seen during the hold load period suggests that contact areas initially creep more than the corresponding displacement until the Hertzian relationship is reached, thereafter both contact areas and displacements creep together in a Hertzian relationship.

6.6 Results : Epoxy

Measured contact areas appear to be smaller that those predicted by Hertzian contact theory and using the tensile modulus value. Measured contact areas range from approximately 60 to 68% of the predicted values during load, whilst during creep they increase to approximately 70 to 75% for the 50 N load and 80% for the 200 N load. In PMMA the measured areas during the faster load rate appeared slightly smaller than those measured when the load rate was slower; this is not so clearly seen in the epoxy. Contact areas over the period of ramp loading appear linear with respect to load $^{2/3}$ over the range of loads applied up to 150 N with possibly some non linearity occurring at 200N. Figure 6.6-1.

The value of the indentation modulus, E^*, was determined from the slope of the contact area versus load$^{2/3}$ plot, data resulting from 3 different loads, Figure 6.6-1. Assuming the Poisson's ratio is 0.5 the calculated value for E is 2.2 GPa and correspondingly the value for G_0 is 0.73 GPa which is approximately 1.6 to 1.8 times higher than the average value calculated from the results of tensile testing, however it is near the low range value for G_0 found in nanoindentation, see Chapter 5.3.

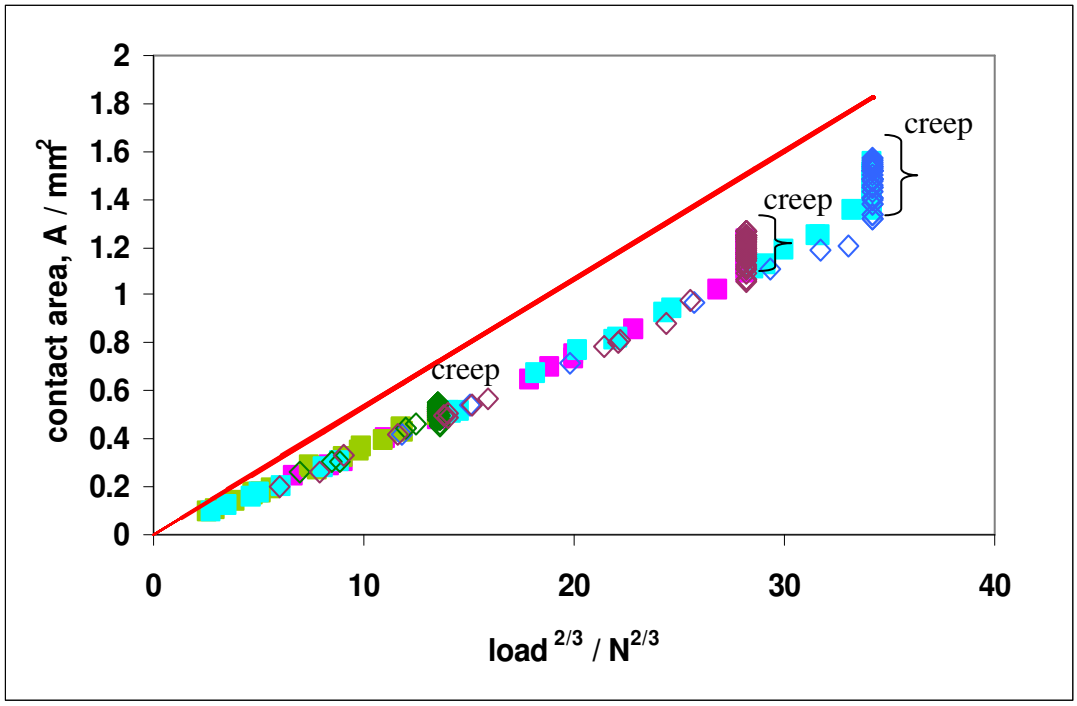

Key: -

red line = Hertzian prediction using experimentally determined tensile modulus

fast load displacement control		**slow load displacement control**	
0.01 mm/s = open diamonds		**0.001mm/s = solid squares**	
dark green	approx. 7 N/s to 50 N max.	light green	approx. 0.7 N/s to 50 N max.
dark pink	approx.10 N/s to 150 N max.	pink	approx. 1 N/s to 150 N max.
dark blue	approx.14 N/s to 200 N max.	light blue	approx.1.4 N/s for 200 N max.

Figure 6.6-1 Epoxy contact areas against load $^{2/3}$ over two rise times to maximum loads 50 N, 150 N and 200 N showing linearity, showing smaller contact areas than predicted using tensile modulus value and showing smaller contact areas during faster loading

Contact areas appear to increase over a period of creep time at constant load. It can be seen that more creep occurs after the faster ramp loading relative to the slower ramp loading at lower loads, 5 N and 50 N, although at higher loads, 150 N and 200 N, this is not seen so clearly. It appears that at higher loads more creep occurs. See Figure 6.6-2.

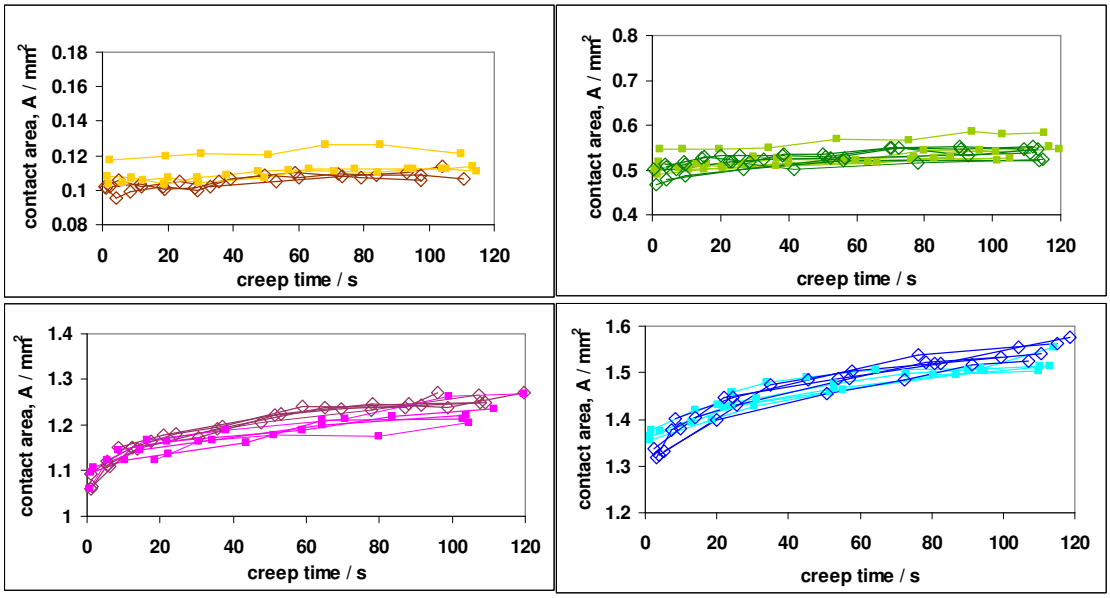

Key: -

red line = Hertzian prediction using experimentally determined tensile modulus

fast load displacement control		**slow load displacement control**	
0.01 mm/s = open diamonds		**0.001mm/s = solid squares**	
brown	approx. 5 N/s to 5 N max.	yellow	approx. 0.55 N/s to 5 N max.
dark green	approx. 7 N/s to 50 N max.	light green	approx. 0.7 N/s to 50 N max.
dark pink	approx.10 N/s to 150 N max.	pink	approx. 1 N/s to 150 N max.
dark blue	approx.14 N/s to 200 N max.	light blue	approx.1.4 N/s for 200 N max.

Figure 6.6-2 Epoxy: contact area during hold load at 4 different maximum loads : showing contact area increases more during a hold period at higher loads.

There is more scatter in the epoxy displacement data, this is most likely due to the difficulty in making perfectly flat samples. Displacements were variable, either on Hertzian line using tensile modulus or below at approximately 80% of the predicted displacement. The scatter in the displacement was such that at the start of the hold load period there was up to 20 μm difference in displacement between tests after the same loading conditions. The scatter and linearity of the tests over the changing loading conditions can be seen in Figure 6.6 -3.

The results show that displacements were proportional to load$^{2/3}$.

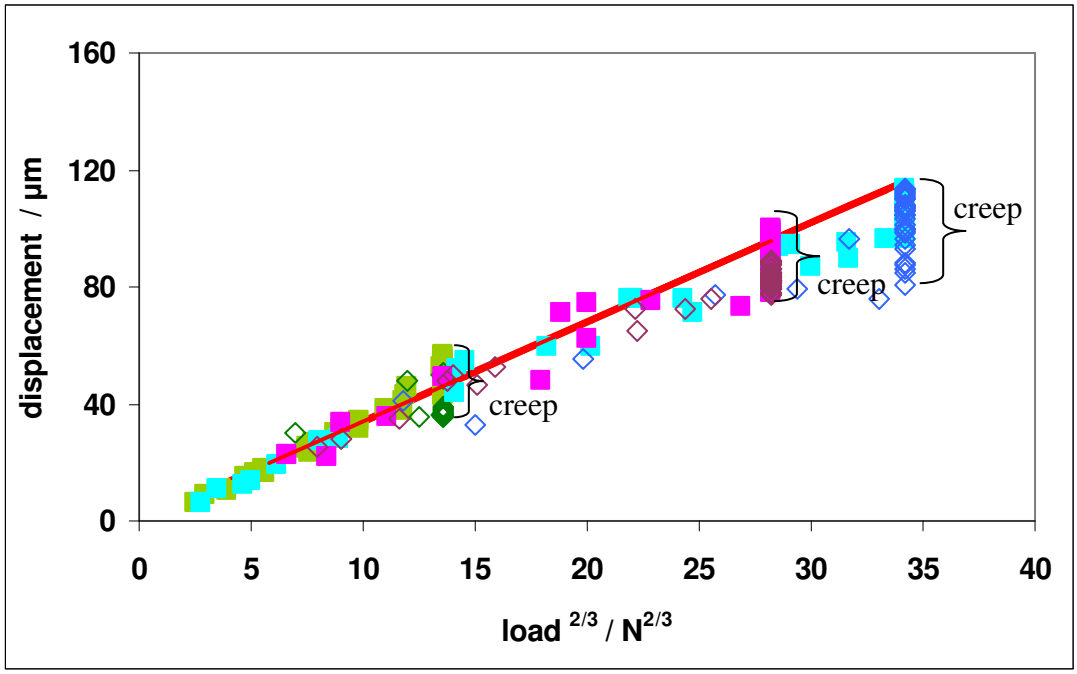

Key: -

red line = Hertzian prediction using experimentally determined tensile modulus

fast load displacement control		**slow load displacement control**	
0.01 mm/s = open diamonds		**0.001mm/s = solid squares**	
dark green	approx. 7 N/s to 50 N max.	light green	approx. 0.7 N/s to 50 N max.
dark pink	approx.10 N/s to 150 N max.	pink	approx. 1 N/s to 150 N max.
dark blue	approx.14 N/s to 200 N max.	light blue	approx.1.4 N/s for 200 N max.

Figure 6.6-3 Epoxy displacement versus load $^{2/3}$ for a range of maximum loads : showing linearity during ramp loading up to 150N approx.

There was possibly some non linearity at 200 N particularly after fast ramp loading as it can be seen that data points at higher loads begin to fall below the line. Generally, displacement was greater at the end of loading after the slower ramp.

Displacement creep shows similar trends to contact area creep; more creep is apparent after a more rapid load rate.

Analysis of the displacement creep curves, Figures 6.6-4 and 6.6-5, gave values for the shear modulus that are close to the values obtained from tensile creep and are at most only10% higher.

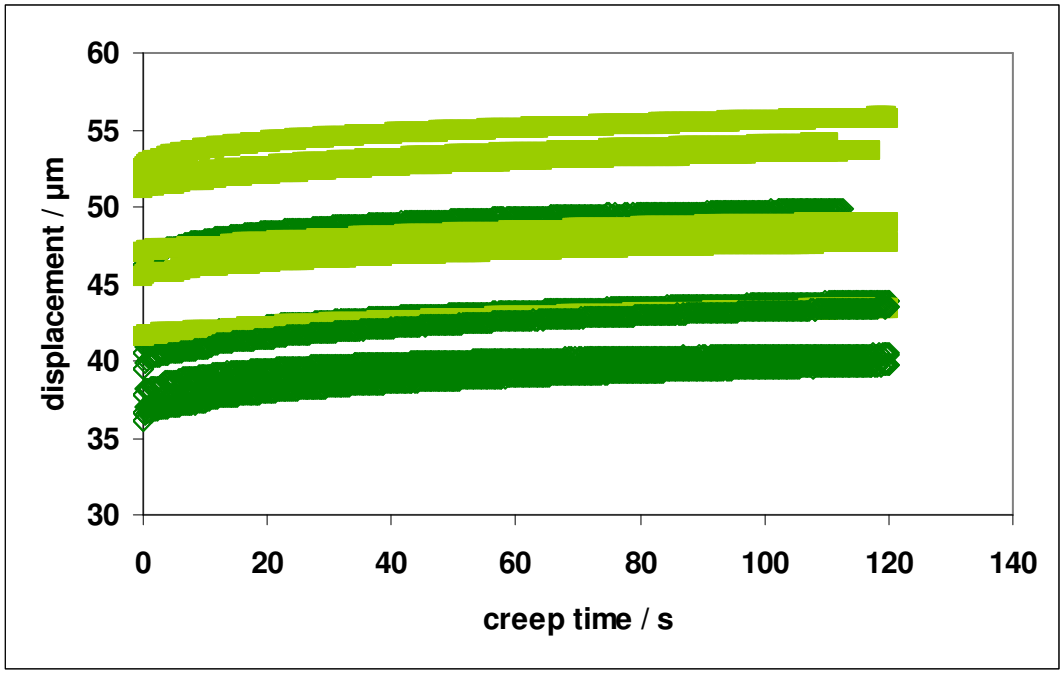

Key : light green = 50N after approx. 0.55 N/s slow loading (displacement control 0.001mm/s)
dark green = 50N after approx. 5 N/s fast loading (displacement control 0.01 mm/s)

Figure 6.6-4 Epoxy displacement creep at 50 N during hold load period of 120s : shows more creep occurs after a faster ramp load

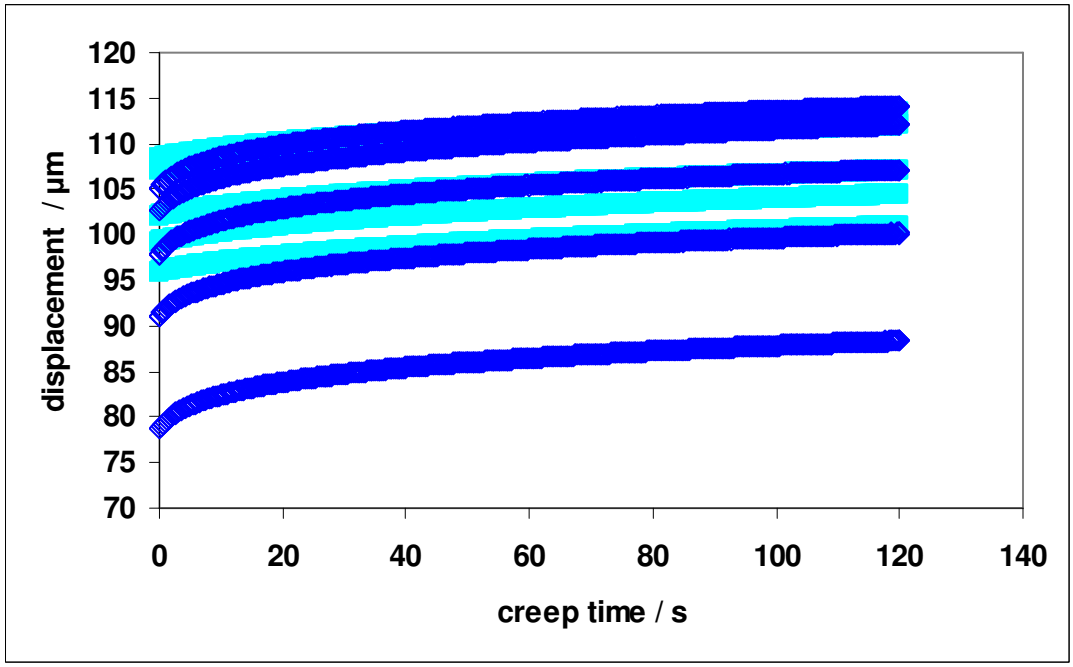

Key : light blue = 200 N after approx. 1.4 N/s slow loading (displacement control 0.001mm/s)
dark blue = 200 N after approx. 14 N/s fast loading (displacement control 0.01 mm/s)

Figure 6.6-5 Epoxy displacement creep at 200N shows more creep occurs after a faster ramp load

Figure 6.6-6 presents the relationship between contact area and depth during loading. During loading to 50 N maximum load the relationship appears non Hertzian, i.e. the relationship is not parallel to the line as predicted by the Hertzian relationship. This is expected due to the reduced contact areas observed. The data from the tests at the 150 N and 200 N maximum loads is variable, although contact areas are also less than predicted the relationship appears Hertzian as displacement is also reduced at higher loads as the displacement response becomes non linear. Differences between the fast and slow ramp load rates are not clear as there is a lack of contact area data in the initial stages of ramp loading due to the time required to record images during a rapid rise time.

However, during the period of hold at constant load the relationship between contact area and displacement is seen to change, this can be seen in Figure6.6-7.

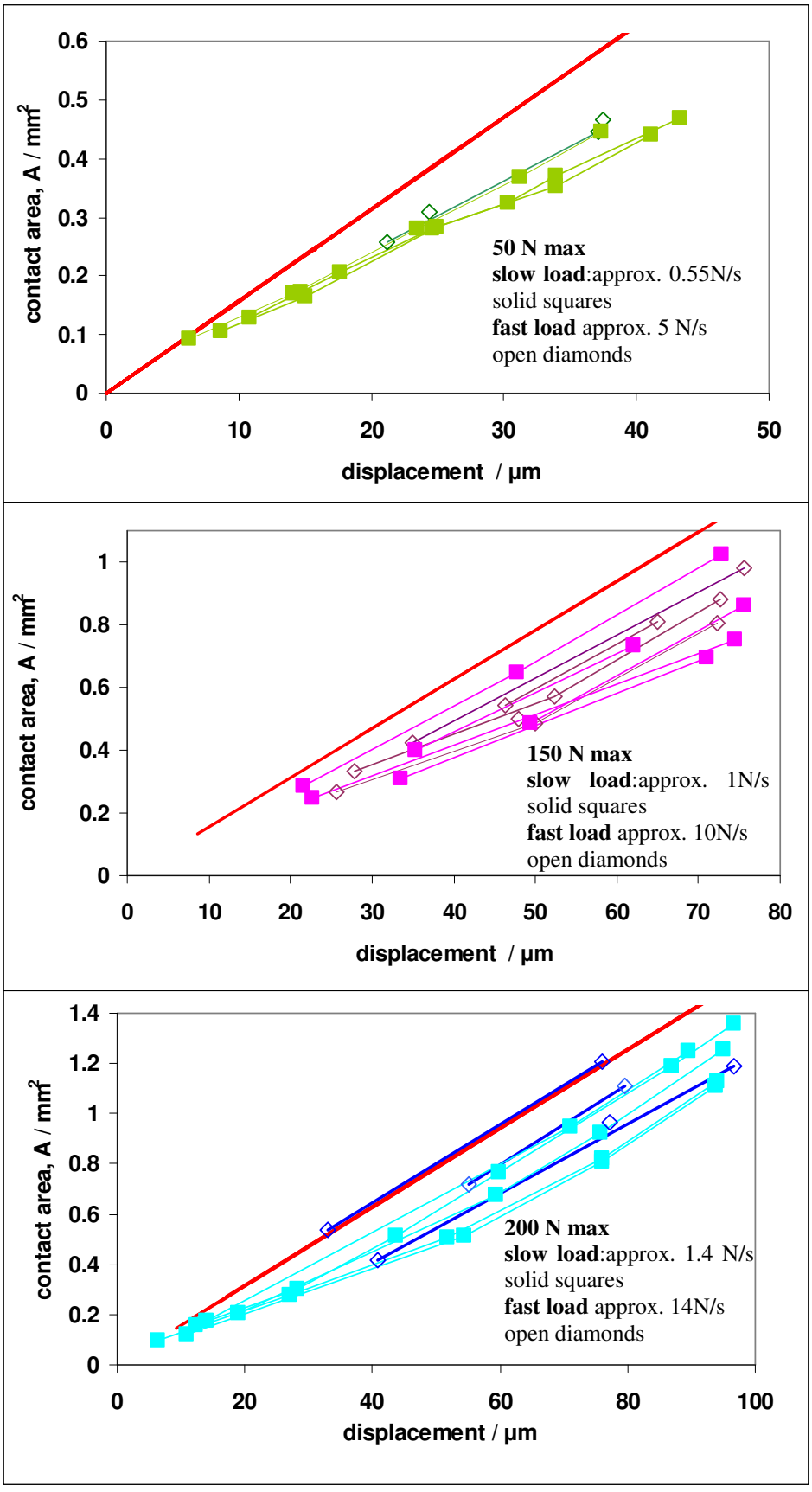

Key : red line Hertzian prediction using tensile modulus

Figure 6.6-6 Epoxy : relationship between contact area and depth during ramp loading to 3 different maximum loads : showing non Hertzian relationship at 50 N

During hold at constant load the relationship appears to change as the contact area appears to increase more than the displacement at the higher loads. Figure 6.6-7.

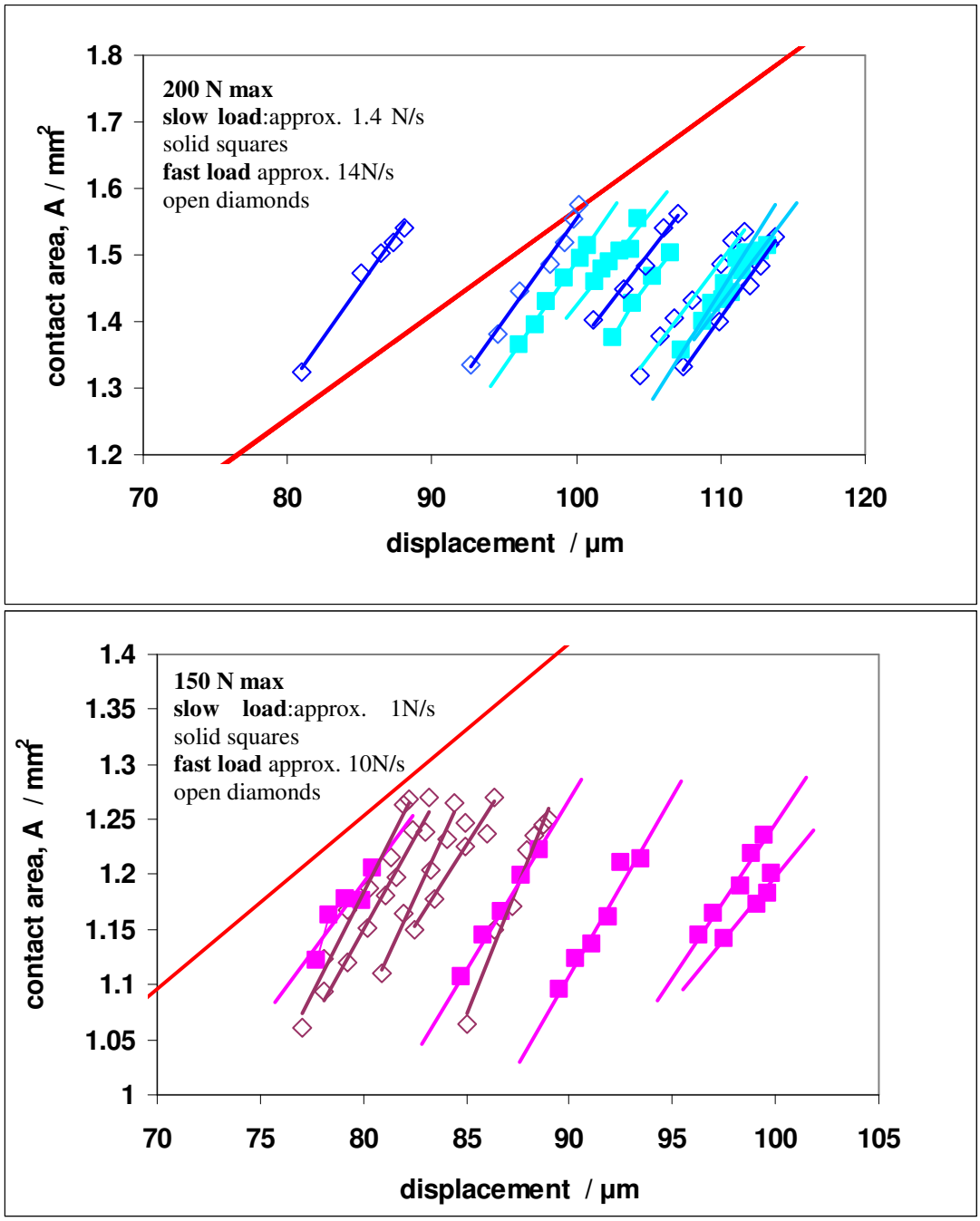

Key : red line Hertzian prediction using tensile modulus

Figure 6.6-7 Epoxy: contact area and depth relationship over a period of creep time is not Hertzian as contact area increases more than displacement increases

Unlike the 150 N and 200N test results the contact area and depth relationship for the 50 N test is parallel to the Hertzian theoretical line as can be seen in figure 6.6-8 suggesting that during creep both contact area and displacement increase together according to Hertzian theory despite the contact areas being smaller than predicted.

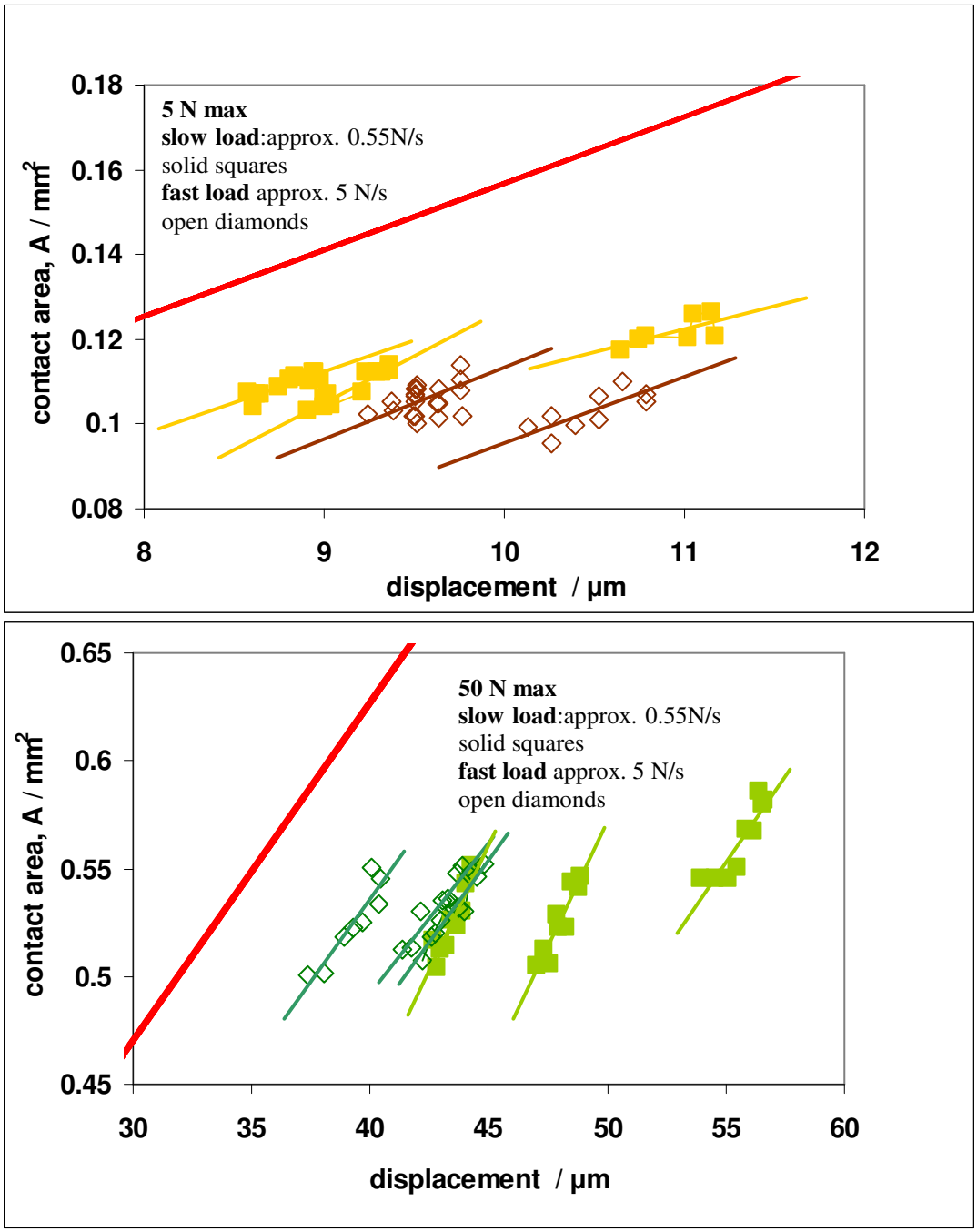

Key : red line Hertzian prediction using tensile modulus

Figure 6.6-8 Epoxy: the relationship between contact area and depth appears Hertzian during creep at constant 5 N and constant 50 N after ramp loading at 5 N/s and at 0.5 N/s

When looking at the ratio of the depth in contact, h_c , to the maximum depth, h_{max} , the relationship between h_c and h_{max} appears to remain constant during the load and hold periods, however some deviations appear during loading but these are due to increased displacement during loading which will be discussed in the next section. Figures 6.6-9 presents the ratio h_c/ h_{max} as a function of load$^{2/3}$ over the ramp and hold load constant period for the tests at 5 N, 50 N and 200 N maximum load. Figure 6.6-10 presents the results during constant load as a function of creep time. During the period of hold load there does appear to be some sink in at the 200 N load.

The variation in load rate during ramp loading under displacement control could account for the "dip" shape seen in the plots of h_c/ h_{max} during loading seen in Figure6.6-9.

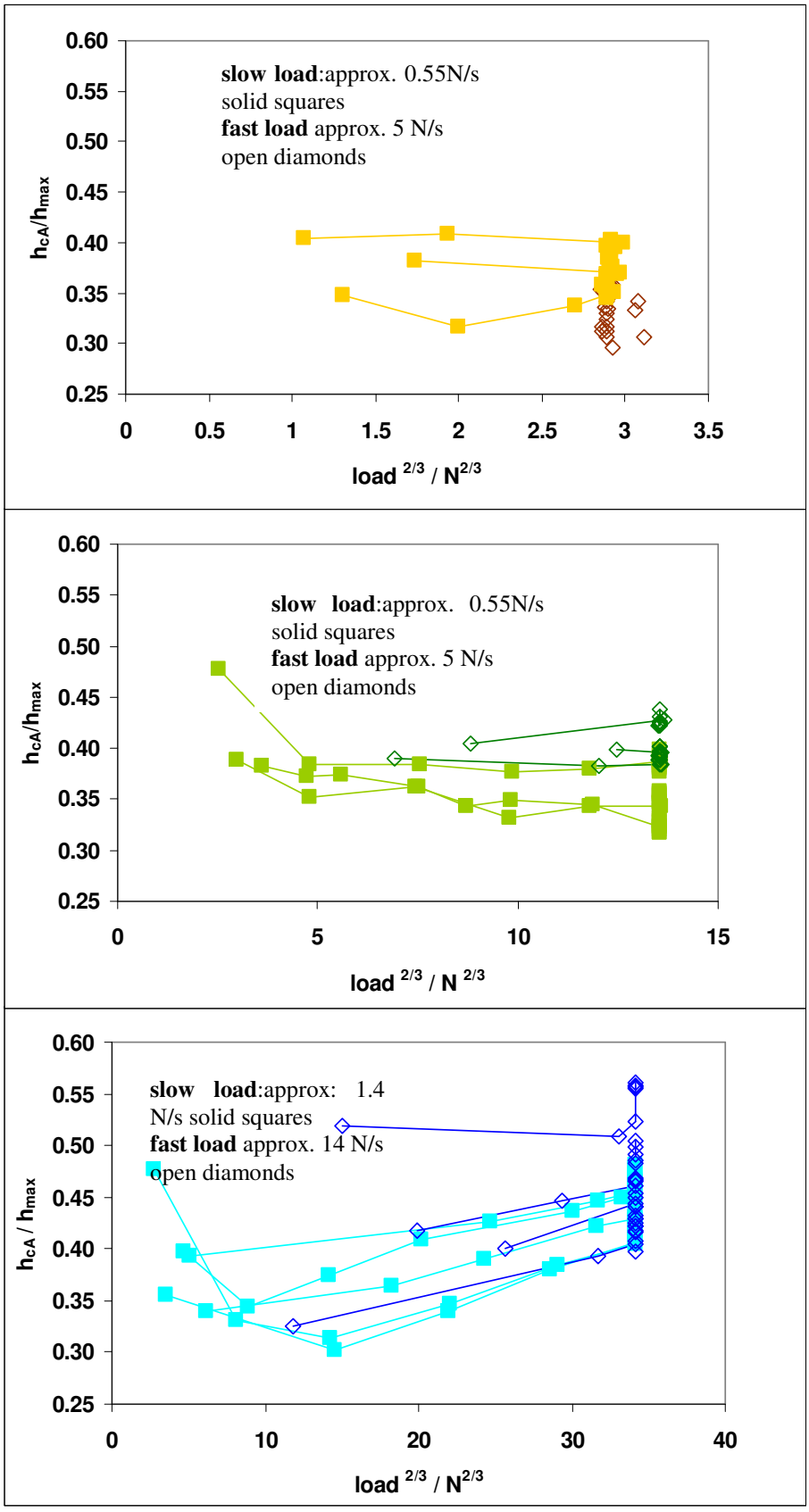

Figure 6.6-9 Epoxy: h_{cA}/h_{max} vs load$^{2/3}$ (top to bottom - 5N load, 50N, 200N) during ramp loading showing that h_{cA}/h_{max} appears constant apart from sink in during loading to 200N

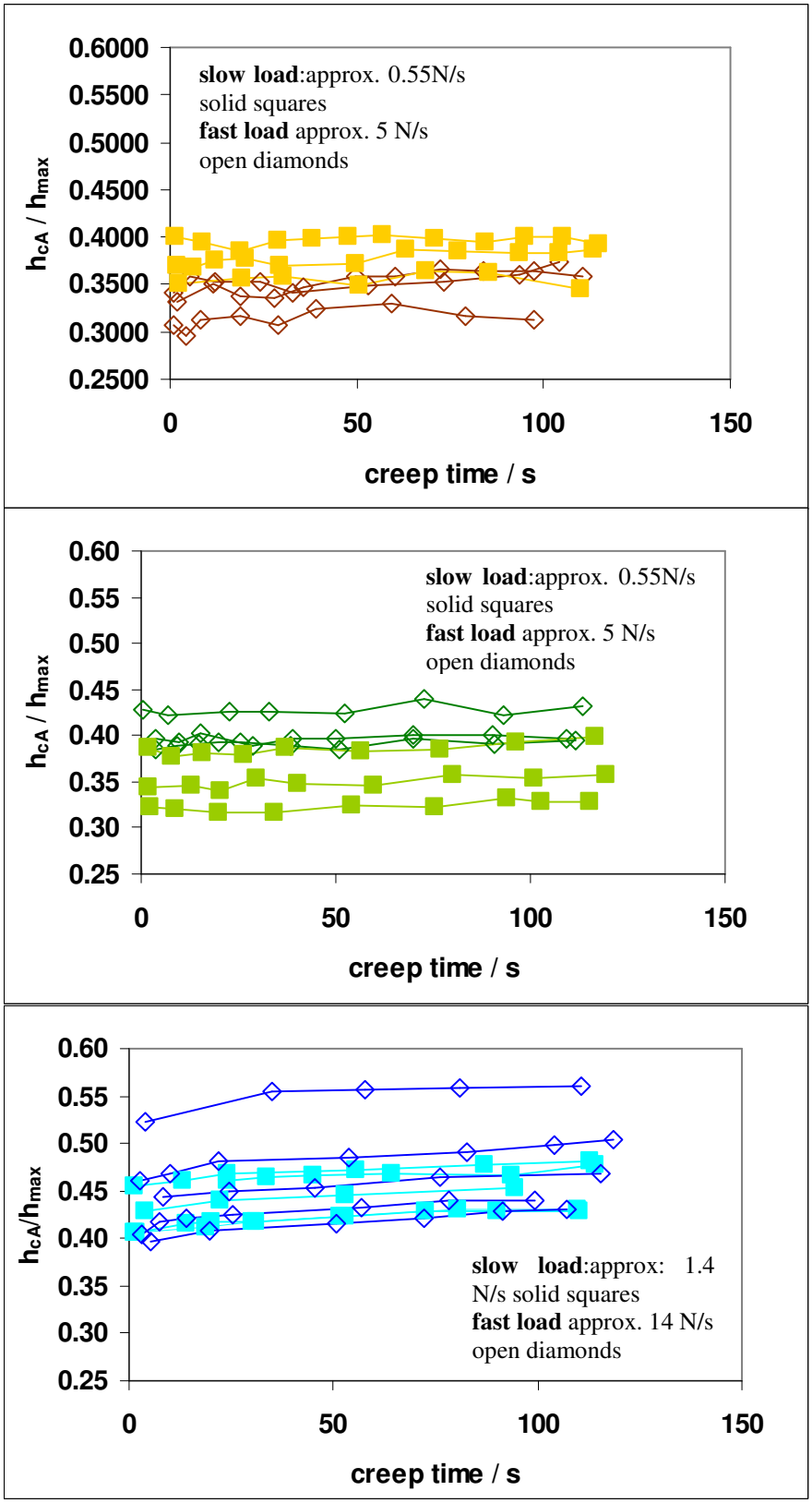

Figure 6.6-10 Epoxy : h_{cA}/h_{max} vs creep time at constant load (top to bottom - 5N load, 50N, 200N) showing that h_{cA}/h_{max} appears to be constant throughout period of creep at 5 N and 50 N with some sink in at 200 N

Table 6.6-1Epoxy : calculated modulus values

average tensile creep value instantaneous shear modulus G0 assuming Poisson's ratio = 0.5 (results averaged over 3 rise times and 3 loads) see Chapter 5.3	**0.43GPa** 0.01SD		
G0 from **nanoindentation creep** (results averaged over all rise times)	**0.80 GPa** 0.04SD (3mN load) *a/R*= 0.15 (from displacement)	**1.0 GPa** 0.02 SD (10mN load) *a/R* = 0.25 (from displacement)	**0.95GPa** 0.03 SD (30mN load) *a/R* = 0.4 (from displacement)
G0 from **macroindentation creep** (results averaged over both rise times)	**0.50 GPa** 0.08SD (50N load) *a/R*= 0.08	**0.56Gpa** 0.07SD (150N load) *a/R*= 0.12	**0.47 GPa** 0.08 SD (200N load) *a/R* = 0.13
G0 calculated from *E* from **macroindentation displacement** vs ramp load$^{2/3}$ slope, results averaged over both rise times	**0.46 GPa** SD 0.08 (50N load) *a/R*= 0.08	**0.46Gpa** 0.07SD (150N load) *a/R*= 0.12	**0.50 GPa** 0.1 SD (200N load) *a/R* = 0.13
G0 calculated from *E* from **macroindentation contact area** vs load$^{2/3}$ slope	**0.73GPa** 0.03SD (50N load) *a/R* = 0.08	**0.73 Gpa** 0 SD (150N load) *a/R*= 0.12	**0.70GPa** 0.04SD (200N load) *a/R* = 0.13

Table 6.6-1 summarises the modulus values calculated from the displacement creep using the creep compliance function in Chapter 2, as well as values calculated from the gradients of contact area versus load$^{2/3}$ and displacement versus load$^{2/3}$ plots. The values calculated from the measured contact areas are approximately 1.5 times higher than those calculated from the measured displacement.

The values of the calculated creep ratios from nanoindentation, tensile testing and macroindentation are presented in Table 6.6-2, only at 200 N is agreement found

with the lower range values resulting from tensile and nanoindentation. The material response to macroindentation at lower loads is more elastic than viscous.

Table 6.6-2 Epoxy : averaged creep ratios calculated from nanoindentation, tensile and macroindentation testing

Cr from nanoindentation creep	range 0.2-0.5
Cr from tensile creep	0.22 - 0.26
Cr from macroindentation creep	0.14 (50 N) 0.16 (150N) 0.2 (200N)

6.7 Summary

It was seen that contact was Hertzian in the macroindentation of glass. However, the contact did not appear to be Hertzian when epoxy and PMMA were indented. The reasons for this were not clear so the contact problem was modelled using finite element analysis in an attempt to clarify the experimental results.

7 Finite element analysis of visco-elastic indentation

7.1 Introduction

Finite element analysis is used to model a continuum broken down into discrete elements connected by nodes. The relationship between forces and displacements for the model is solved by a global system of simultaneous equations. If certain parameters involved in the mechanics are varied in a systematic way it is possible to determine the influence these may have thus minimising experimental work.

Bolshakov and Pharr (1997) have used finite element analysis to investigate pile up effects on contact areas on materials defined as elastic-plastic and indented using conical indenters. Contact profiles in the element mesh were compared with those derived from the load displacement data. They found that contact areas calculated from load – displacement data can be significantly underestimated when pile up is large. However, their work considered the case of conical indenter tips, visco-elastic material response was not included in their study.

Similarly, Deuschle *et al.* (2009) made finite element studies of contact areas with cube corner and Berkovich indenters into elastomers but visco-elastic behaviour was not modelled.

In this work the spherical contact problem was modelled visco-elastically as in the macroindentation experiment to enable contact areas and displacements to be re - examined.

To avoid making the assumption of plane strain indentation modulus of the sample together with an analytical rigid indenter tip, the ball and the sample were both modelled as deformable so that no assumptions were made with regard to the mechanical response of the materials under load.

7.2 Methods

The commercial finite element code ABAQUS version 6.7 (Dassault Systemes Simulia Corp., Providence RI USA) was used to model the contact problem.

The problem was modelled axisymmetrically as a solid deformable spherical indenter under load and in contact with a solid deformable sample section.

To minimise computation only part of the ball indenter and a section of the sample were included in the analysis.

The surface at the top of the ball was coupled to a reference point enabling the load to be evenly distributed over the ball.

The glass material was described using the modulus, E, of glass as 73.6GPa with a Poisson's ratio, ν, of 0.22 , the alumina ball was described using the modulus value 380GPa and Poisson's ratio 0.22 in agreement with the values used previously.

To describe the PMMA material behaviour the modulus, E, 3.2GPa with Poisson's ratio 0.35 was used together with the normalised displacement creep compliance function determined from the macro indentation test results to describe the visco-elastic response.

The epoxy material was described using the modulus calculated from the tensile experimental results and Poisson's ratio equal to 0.4999 was assumed. The creep description put into the model was the averaged normalised displacement creep

function obtained from tensile tests as this was not too dissimilar to the averaged normalised displacement creep function obtained from the macro indentation tests.

Glass was modelled using standard linear quadrilateral axisymmetric elements CAX4 in a static general analysis.

Standard linear quadrilateral axisymmetric elements CAX4 were also used to model the PMMA using a visco-elastic analysis

Hybrid elements CAX4RH were used to model the epoxy in a visco-elastic analysis, reduced integration hybrid elements are preferable to fully integrated elements which can produce shear and volumetric locking in incompressible materials. The problem of "hour-glassing" (a numerical problem due to reduced integration which results in the material being too flexible), is minimised by using hybrid elements.

Preliminary studies were performed to determine the influence of the contact formulation, the element type and the mesh density.

A biased mesh was used to include more elements in the region of contact.

The contact conditions were modelled as "hard contact", frictionless, surface to surface with small sliding.

Boundary conditions applied to the sample were : constraints in the z - direction at the bottom of the sample but freedom of movement in the radial, r – direction., symmetry conditions applied to the tip and the sample along the z – axis.

Loading was applied as a concentrated force to the reference point of the tip. Figure 7.2-1 shows the meshed model geometry. A ramp and hold load constant loading protocol was applied using similar loads and rise times to mimic the loading of the experimental macroindentation tests.

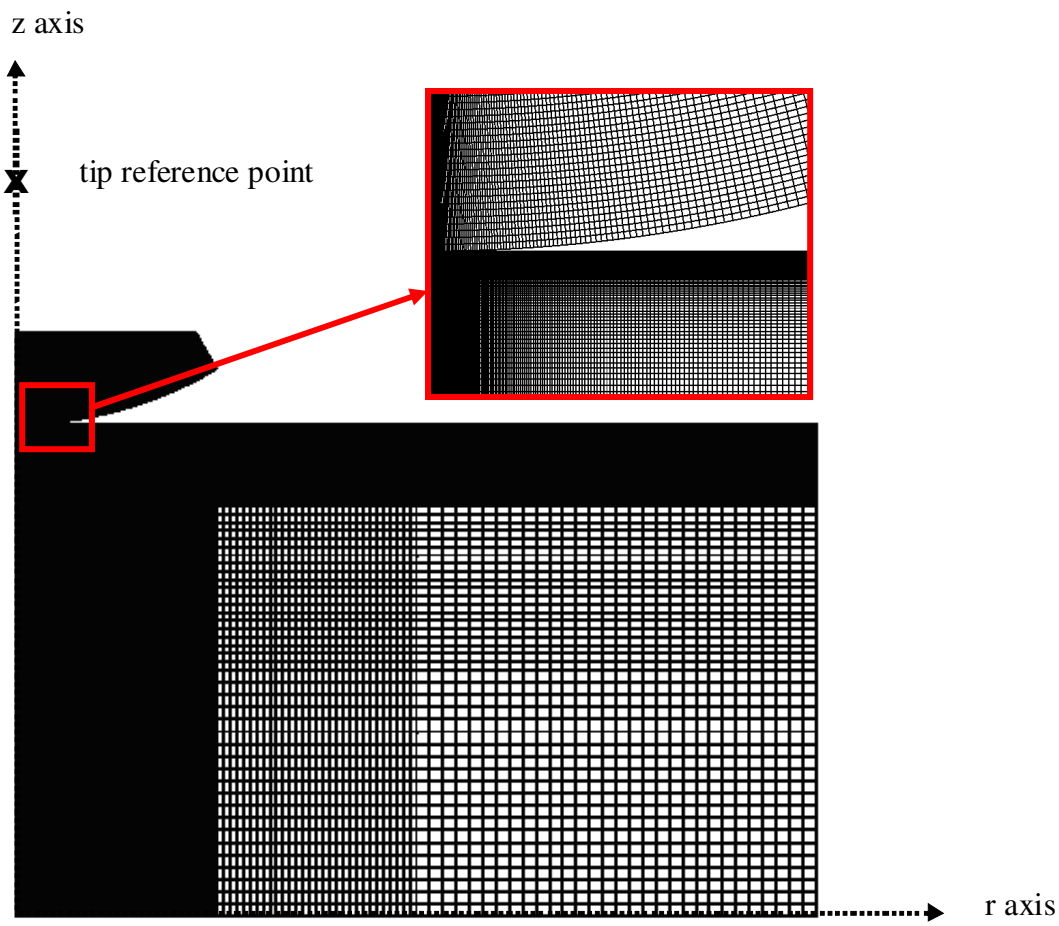

Figure 7.2-1 Biased meshing of axisymmetric model with close up inset

A 6 mm x 10 mm section of the sample was modelled, representing a portion of the sample specimen which was the actual depth of the epoxy sample by a length of at least 100 times the radius of the contact area. This enabled any changes in sample dimensions due to incompressibility to be realised.

The preliminary studies to determine a suitable mesh and contact formulation showed that slight shape changes were still occurring even at the surface edges furthest from the indenter for the epoxy, however, when the complete dimensions of the sample were modelled there was no significant difference in the resulting contact

areas and displacement between the two models. To minimise computational time the 6 mm x 100 mm model was used.

7.3 Results

It is possible to see the extent of the depth of the contact stresses and verify that the substrate does not influence the penetration depth under the particular loads applied. Figure 7.3-1.

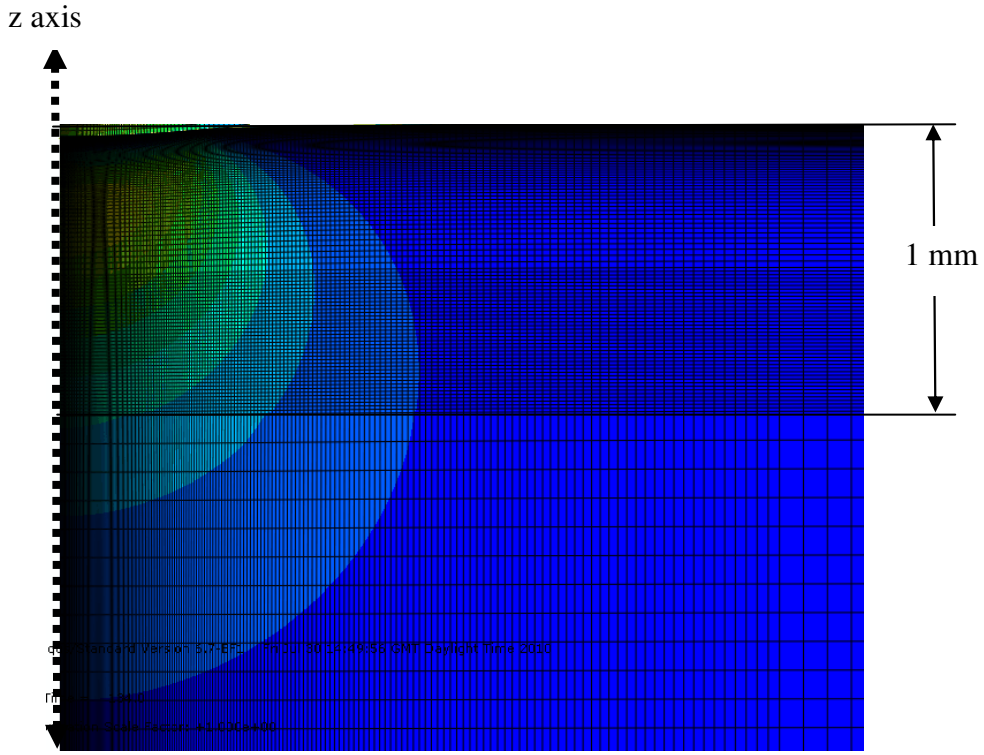

Figure 7.3-1 Finite element analysis stress contour plot : epoxy sample under 50N load spherical indentation showing the depth to which the stress field extends

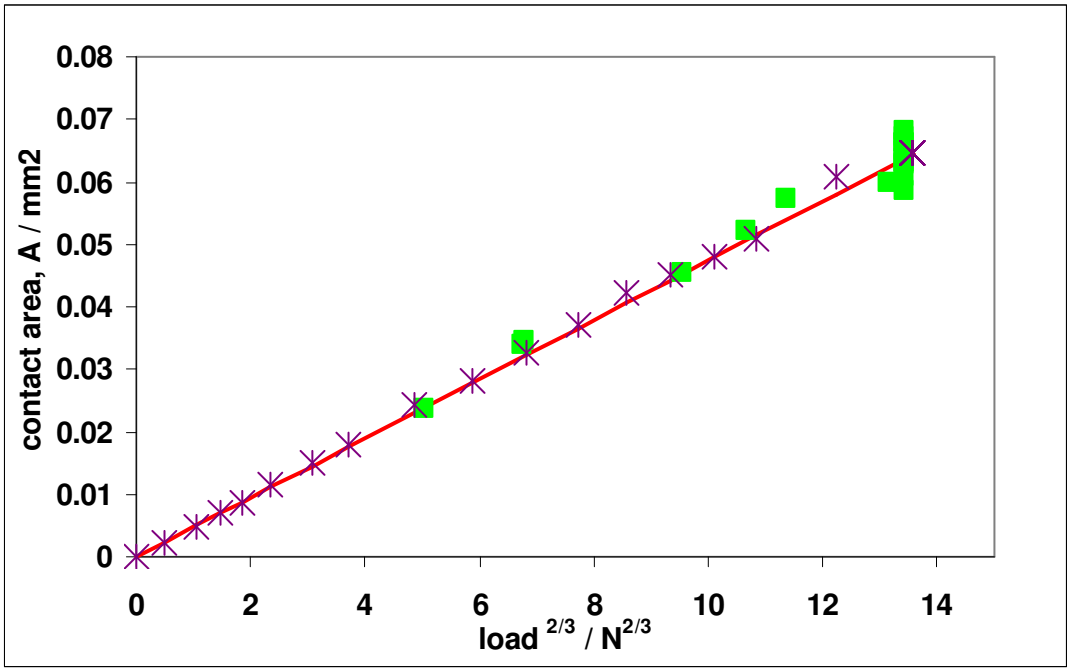

Key: ABAQUS values = stars, experimental values = squares, line = Hertzian theoretical line

Figure 7.3-2 Glass : Finite element analysis results for contact area vs. load $^{2/3}$show results as predicted by Hertzian theory and as in experimental results

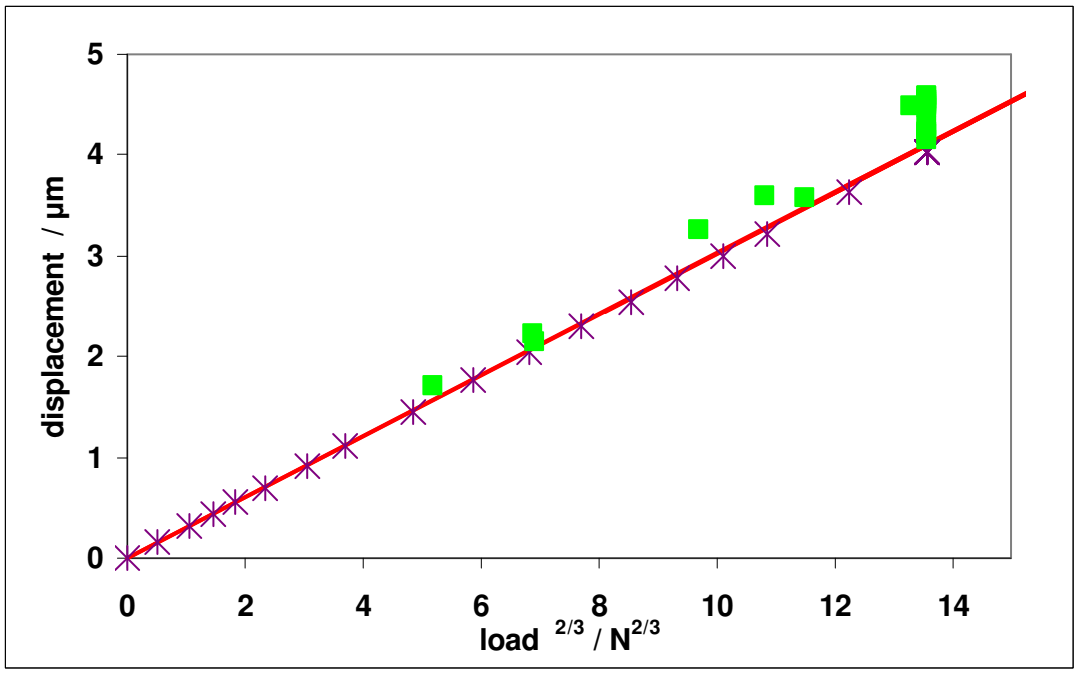

Key: ABAQUS values = stars, experimental values = squares, red line = Hertzian theoretical line

Figure 7.3-3 Glass : Finite element analysis results for displacement vs. load $^{2/3}$show expected displacements

The results for glass were as expected, values for contact areas fit the Hertzian theoretical line for both displacement and contact areas versus load $^{2/3}$. Figures 7.3-2 and 7.3-3.

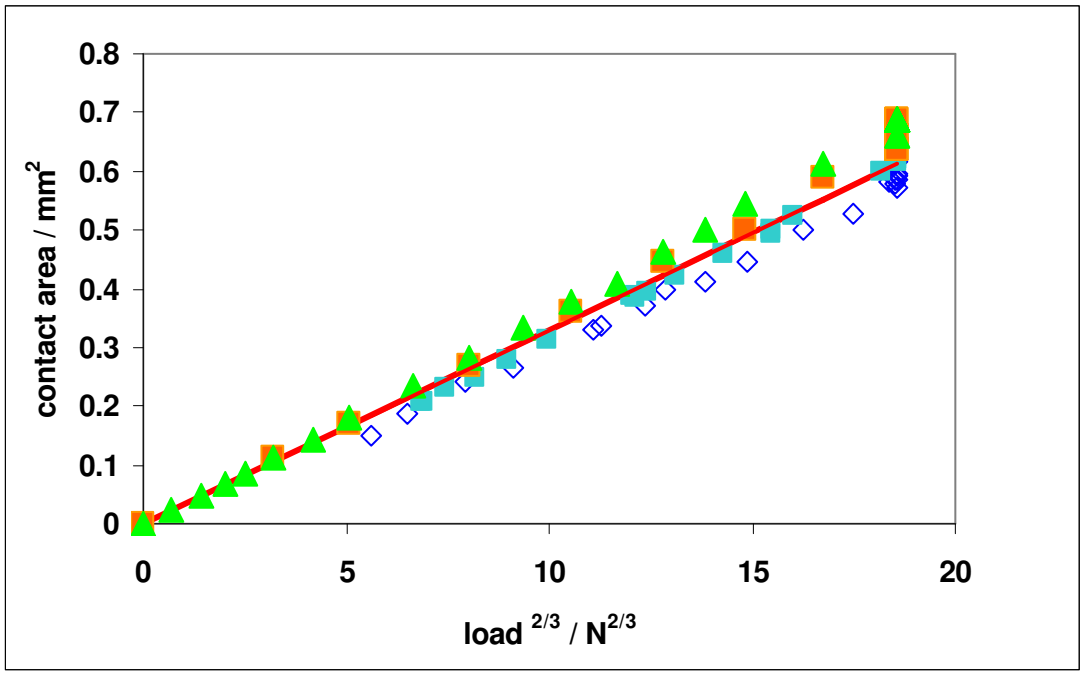

Key: ABAQUS values green triangles = slow ramp load (t_R 140s), orange squares = fast ramp load (t_R 14s), experimental values = blue squares, diamonds red line = Hertzian theoretical line

Figure 7.3-4 PMMA : Finite element analysis results for contact area versus load $^{2/3}$ during ramp load and hold load period appear Hertzian

The results from modelling the contact in PMMA are also as expected, although contact areas increase in jumps according to the mesh refinement they mostly agree with Hertzian theory for the fast ramp load. As in the experimental results seen in the previous chapter contact areas are slightly increased when the load rate is slower. Figure 7.3-4.

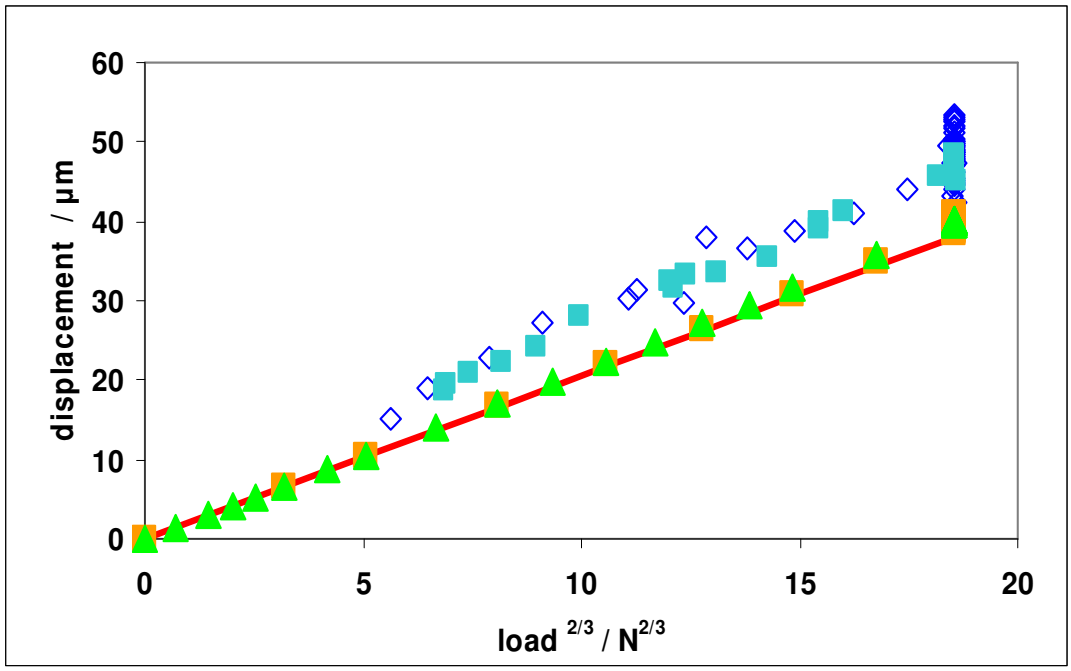

Key: ABAQUS values green triangles = slow ramp load (t_R 140s), orange squares = fast ramp load (t_R 14s), experimental values = blue squares, diamonds red line = Hertzian theoretical line

Figure 7.3-5 PMMA : Finite element analysis results for displacement versus load $^{2/3}$ during ramp load and hold load period show Hertzian contact but do not agree with experimental results

Figure 7.3-5 presents the change in displacements with load, these agree with theory but not with experimental results and this is expected as there appeared to be an increased initial displacement experimentally. Again more creep displacement is seen after the fast ramp load.

The relationship between displacements and contact area appears Hertzian during loading, however as calculations are made at nodes, the refinement of the mesh affects the results such that the calculated contact area is in steps as different elements come into contact. Thus the results for contact areas are coarse over the period of creep time; this is evident in Figure 7.3-6 as the increasing contact area does not appear smooth but increases in steps.

Displacement creep is similar to the experimental data, apart from the initial greater displacement seen experimentally, as expected more creep displacement is seen after a faster ramp load, presented in Figure 7.3-7.

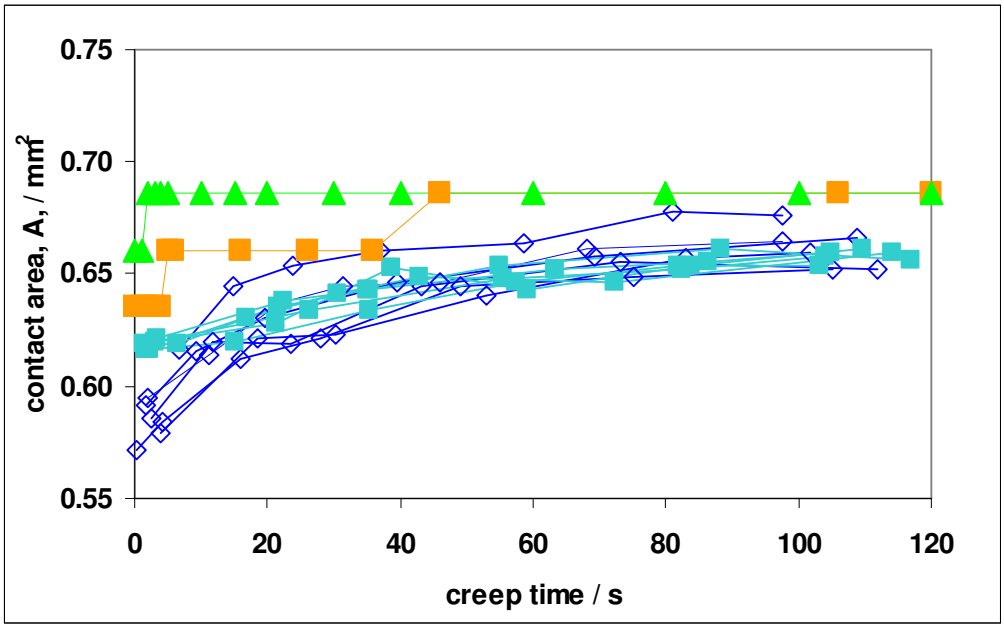

Figure 7.3-6 PMMA: Finite element analysis results for contact area during period of creep over 120 s at constant 80 N load shows contact areas approach the same value and more creep occurs after faster rise times as in experimental results

↕Key: ABAQUS values green triangles = after slow ramp load (t_R 140s), orange squares =after fast ramp load (t_R 14s), experimental values = blue squares, diamonds

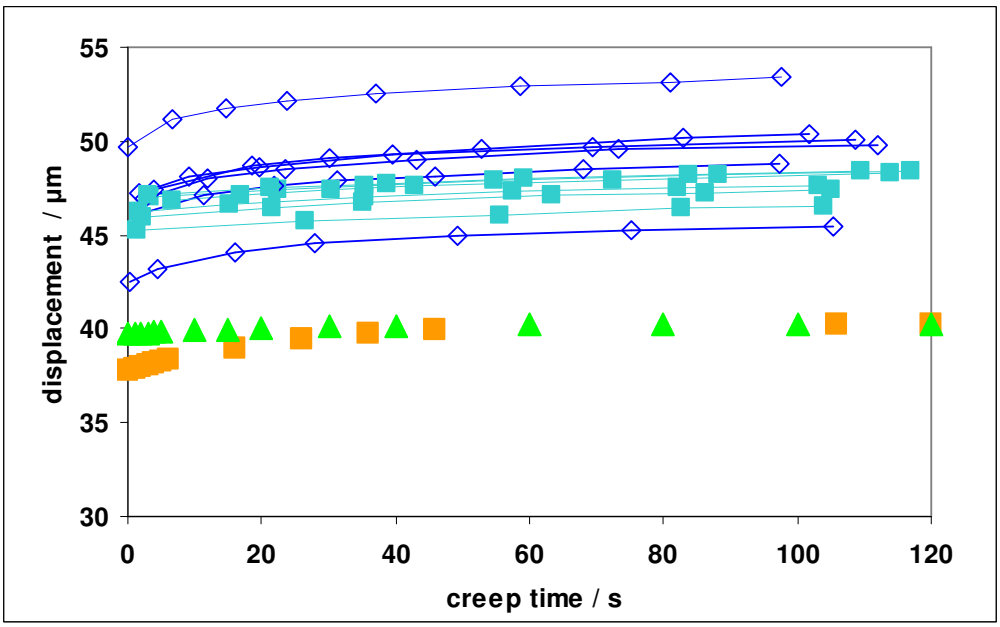

Figure 7.3-7 PMMA: Finite element analysis results for displacement during period of creep over 120s at constant 80 N load show more creep occurs after faster ramp loading as seen in experimental results

The relationship between contact area and depth appears Hertzian during loading as can be seen in Figure 7.3-8, but during the hold load period, Figure 7.3-9, the relationship may change slightly as the contact area increases more than the depth suggesting some "pile up" as creep, this is also seen in the experimental results.

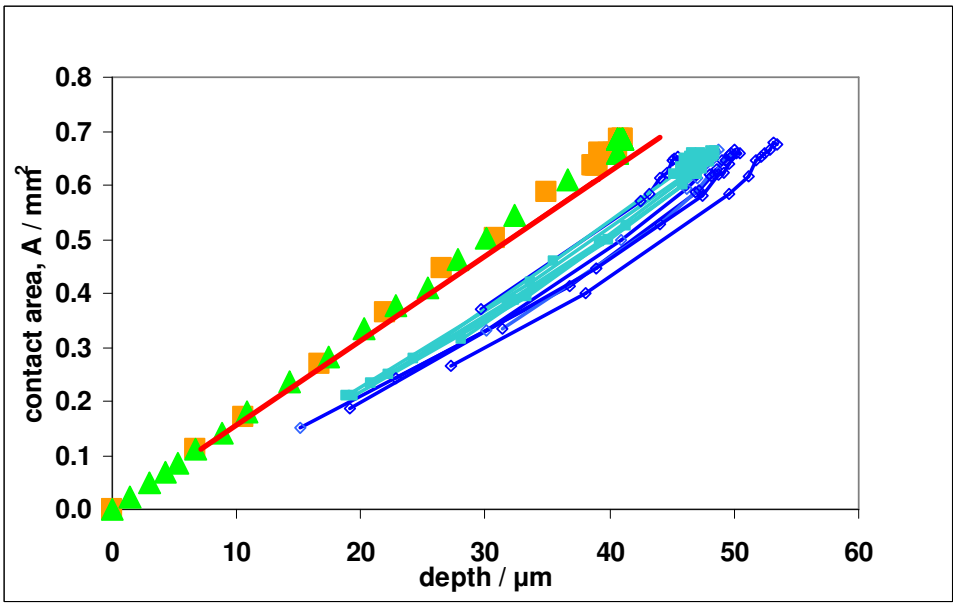

Figure 7.3-8 PMMA : Finite element analysis results for relationship between contact area and displacement agrees with Hertzian theory

Key: ABAQUS values green triangles = slow ramp load (t_R 140s), orange squares = fast ramp load (t_R 14s), experimental values = blue squares, diamonds, red line = Hertzian theoretical line

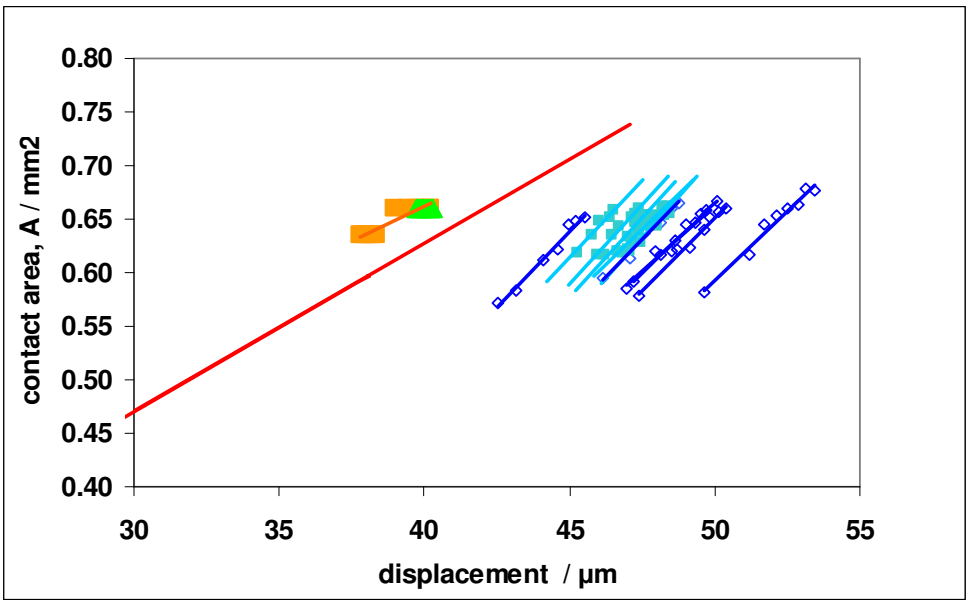

Figure 7.3-9 PMMA : Finite element analysis results for relationship between contact area and displacement over period of creep time at constant load 80N are difficult to see due to the step nature of the analysis, but regression to fast load data appears parallel to Hertzian line

Results when modelling indentation of epoxy approximate Hertzian contact, both contact areas and displacements fit the Hertzian line calculated using the average value for the modulus determined from tensile testing. The contact areas resulting from the model may be slightly larger but this could also be due to the mesh refinement as mentioned previously. Results are presented in Figures 7.3-10 to7.3-14.

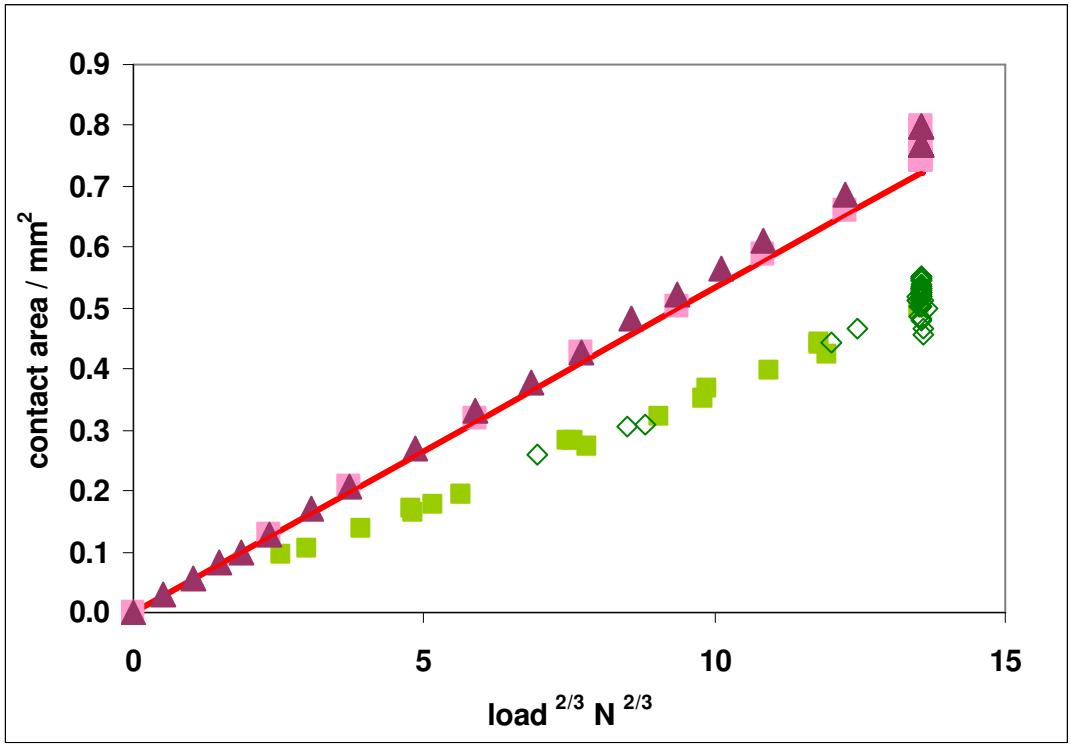

Key : ABAQUS values :- plum triangles=slow ramp load (t_R =140s), pink squares = fast ramp load (t_R =14s)
Experimental values:- dark green =slow ramp load, light green fast ramp load, red line = Hertzian theoretical line

Figure 7.3-10 Epoxy : Finite element analysis results contact areas versus load $^{2/3}$ the model contact areas are Hertzian

Displacements predicted by modelling are Hertzian and are in agreement with the displacements measured experimentally as is to be expected.

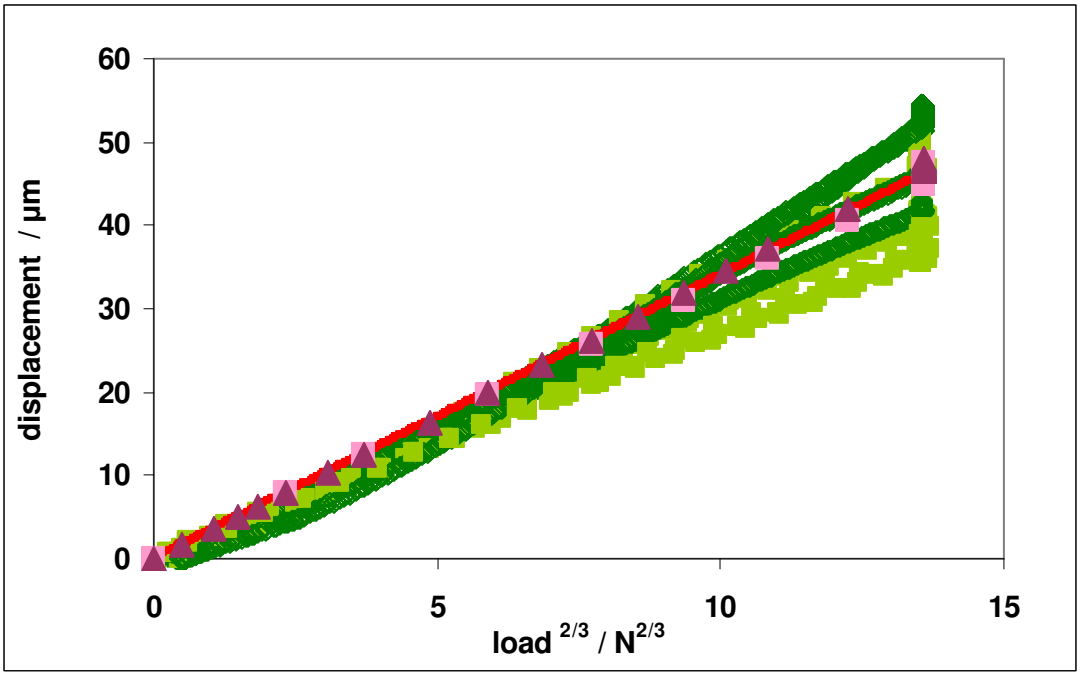

Key : ABAQUS values :- plum triangles=slow ramp load, pink squares = fast ramp load Experimental values:- dark green =slow ramp load, light green fast ramp load, red line = Hertzian theoretical line

Figure 7.3-11 Epoxy : Finite element analysis results for displacement versus load $^{2/3}$agree with theory

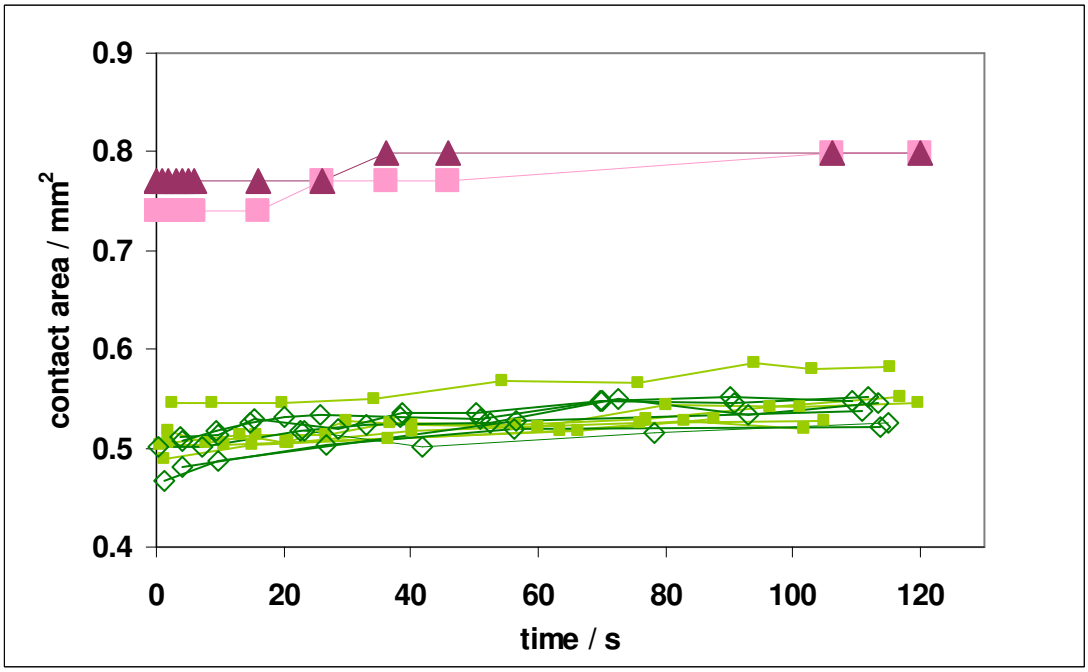

Key : ABAQUS values :- plum triangles = slow ramp load, pink squares = fast ramp load Experimental values:- green squares=slow ramp load, open green diamonds fast ramp load,

Figure 7.3-12 Epoxy model : contact area over creep time at constant load 50 N shows more creep after fast ramp load as does experimental result

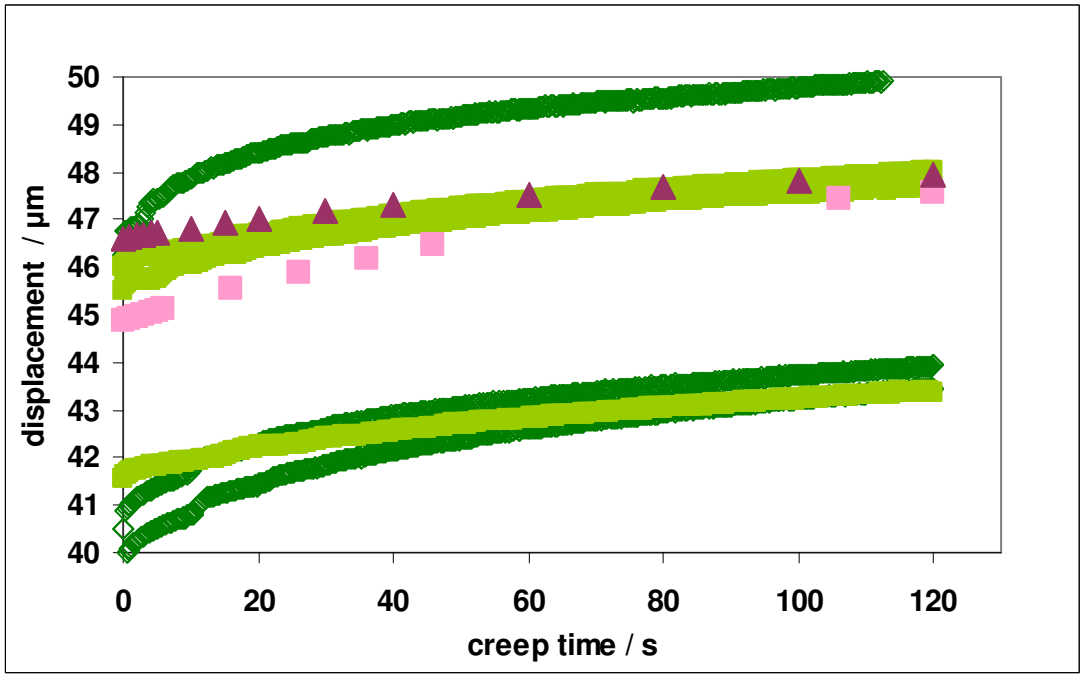

Key : ABAQUS values:- plum triangles = slow ramp load, pink squares = fast ramp load
Experimental values:- green squares=slow ramp load, open green diamonds fast ramp load

Figure 7.3-13 Epoxy : Finite element analysis results for displacement over creep time at constant load 50 N

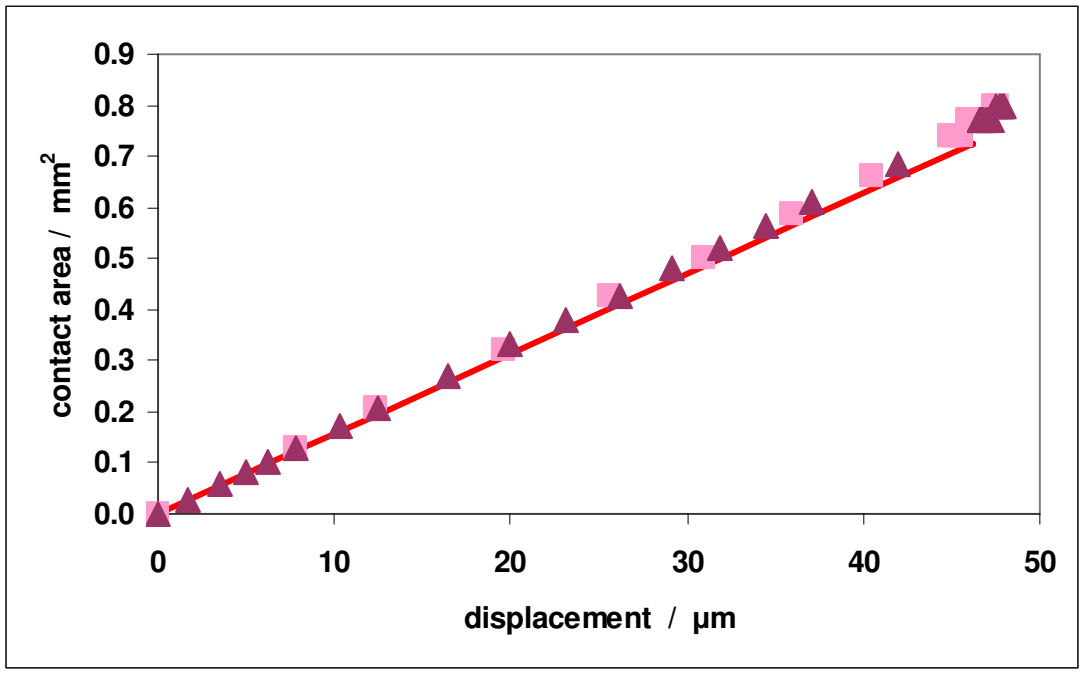

Key : ABAQUS values:- plum triangles = slow ramp load, pink squares = fast ramp load, red line = Hertzian theoretical line

Figure 7.3-14 Epoxy: Finite element analysis results for contact area versus displacement during ramp loading

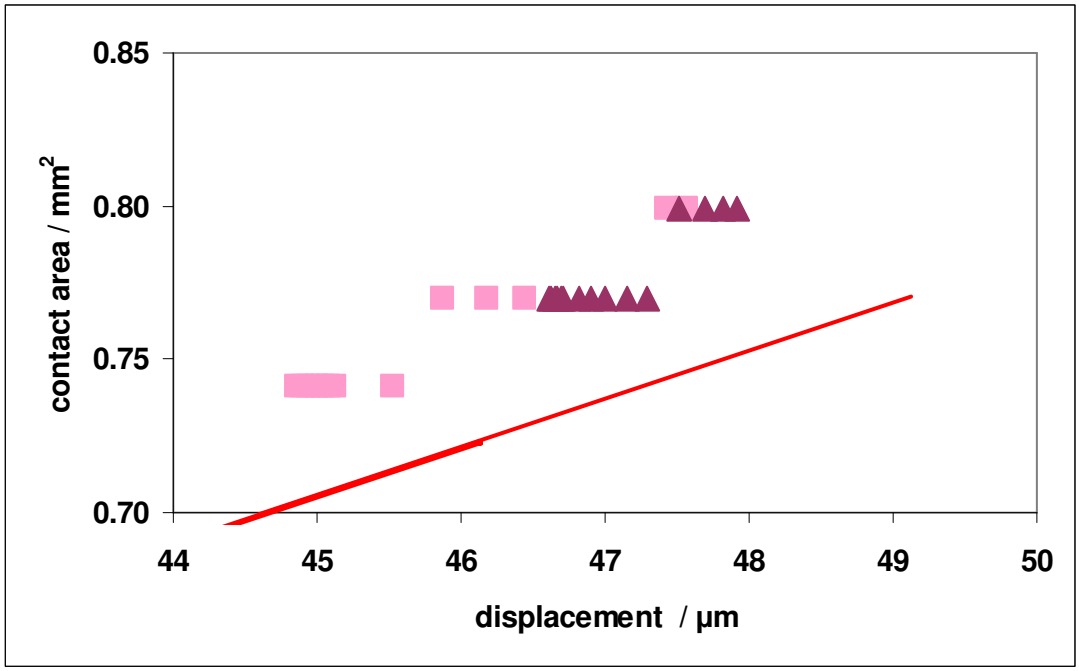

Key : ABAQUS values:- plum triangles = slow ramp load, pink squares = fast ramp load, red line = Hertzian theoretical line

Figure 7.3-15 Epoxy: Finite element analysis results for contact area versus displacement during creep time period of 120 s at constant 50 N load

Due to the steps in the results as each node on the slave surface of the model comes into contact with the master surface, it is not clear from Figure7.3-15 whether the relationship between contact area and depth during the hold load period is Hertzian, however this is presumably the case as much as it is during the loading period as the same material description is applied.

The ABAQUS results for epoxy suggest that both contact areas and displacement should be Hertzian using the tensile modulus. However, when a surface region, corresponding to the top 0.25 mm, of the sample is defined using the modulus value obtained experimentally from nanoindentation tests, the results are closer to those obtained experimentally in the macroindentation experiment. This can be seen in Figures 7.3-16 and 7.3 -17. With a stiffer surface region the contact area is significantly reduced being 50 – 72 % whereas the displacement is only slightly reduced at 70-95% in agreement with experimental observations.

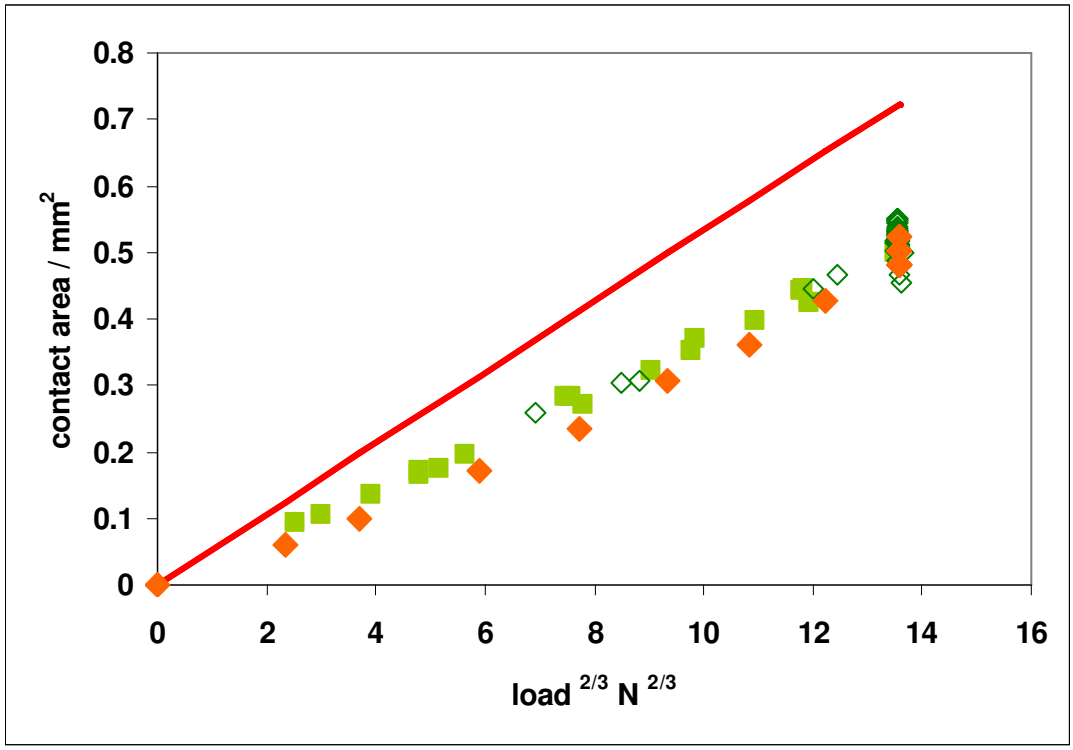

Key : ABAQUS values :- orange diamonds = fast ramp load , red line= Hertzian
Experimental values:- green squares=slow ramp load, open green diamonds fast ramp load

Figure 7.3-16 Epoxy : Finite element analysis results contact areas versus load $^{2/3}$ modelled with stiffer surface layer has good agreement with experimental results

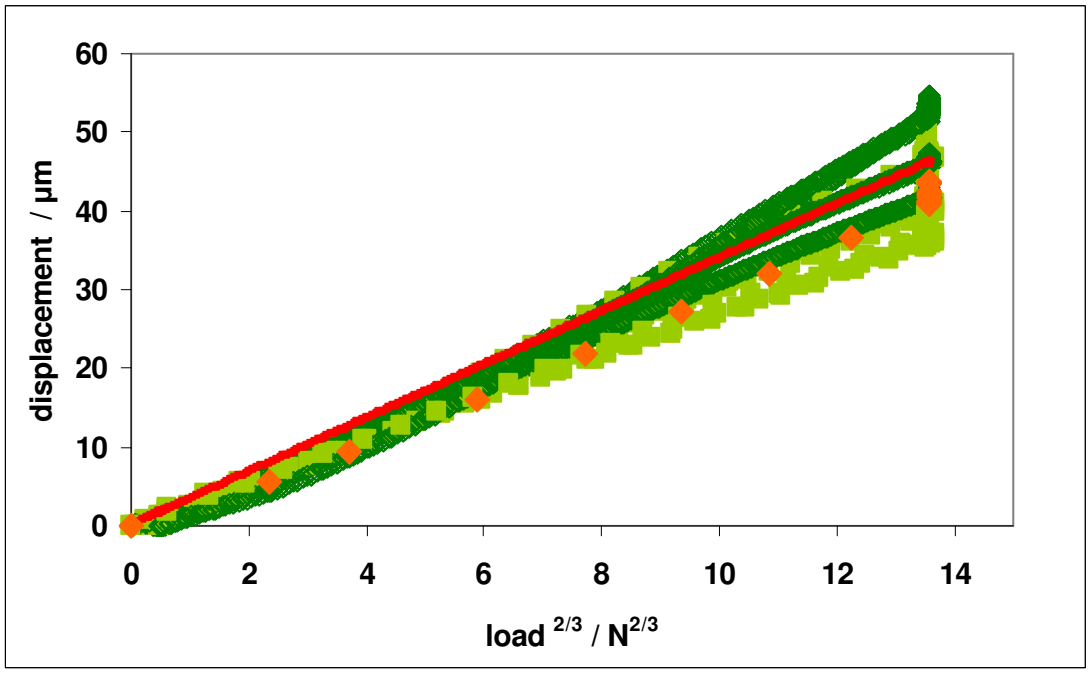

Key : ABAQUS values :- orange diamonds = fast ramp load, red line = Hertzian
Experimental values:- green squares=slow ramp load, open green diamonds fast ramp load

Figure 7.3-17 Epoxy : Finite element analysis results displacement versus load $^{2/3}$ shows some agreement with experimental results

7.4 Summary

Finite element analysis suggests that for amorphous, isotropic, elastic materials (glass) and visco-elastic materials described as amorphous and isotropic, Hertzian contact applies. The modelled glass behaviour was in agreement with the experimental results, however, the modelled PMMA and epoxy behaviour was not. The results of further modelling which included a stiffer skin at the surface of the epoxy did however appear to simulate the experimental results.

8 Discussion

8.1 Advantages of creep response analysis over conventional methods

Nanoindentation testing is widely used to determine the mechanical properties of thin films and small structures. Nanoindentation tests can be easily set up to map over a chosen area, making it possible to observe any changes that may occur locally. In the vast majority of nanoindentation test procedures a single load – unload cycle is used, and a single value for the elastic modulus is obtained from the unloading slope. Hardness, P_{max}/A , values are also derived from these tests, with contact area calculated from displacement assuming particular contact area – displacement relationships dependent on the tip shape. However, hardness values for polymers are not independent of the test conditions, polymers creep under load and actual contact areas may not be as assumed from linear elastic mechanics (Hertz).

Frequently, Berkovich and other pointed indenter tips are used, which, even at low loads, can produce localised regions of high stress resulting in plastic strain. Indentation with a spherical indenter results in elastic displacement initially and it has been seen that spherical indenter tips have the advantage over pointed and sharp tips (Oyen 2003, 2005).

Use of the unloading slope to determine elastic modulus is based on the assumption that the unloading is elastic even though plastic deformation may have occurred. When indenting time dependent materials such as polymers, this method is further complicated by the additional problem of the "nose" (named after the shape of the

force / displacement curve caused by continued forward creep displacement in the initial part of the unloading slope). Methods to overcome this include unloading at times that are 10 to 100 times faster than the relaxation time of linear visco-elastic materials (Cheng 2005), and by holding the load constant for a period to exhaust creep before unloading. Both of these methods eliminate creep and, of course, valuable information regarding the mechanical properties is lost.

In contrast, the ramp and hold load test with a spherical indenter (assuming Hertzian contact as contact areas cannot be measured directly) and the resulting creep analysis gives more information than the single stiffness or modulus value obtained from the unloading slope of the conventionally used test. In a ramp and hold load test additional information is provided by the time response. From the creep compliance function a mechanical characterisation is possible. Instantaneous and long term shear modulus values can be calculated from the creep function parameters, as well as the ratio of these which gives the creep ratio. By monitoring the creep function it is possible to determine changes not only in the immediate stress response such as maximum displacement at a particular load, it is also possible to observe the nature of the creep function and any changes in this that may occur as a result of changes in material properties. (Figures 4.3-10 to -13).

A further advantage of the ramp and hold load test is that relative to the load - unload test in which data is collected during changing load conditions, the creep test is measured under constant load conditions with contact fully established. In the load-unload test the data is taken from the initial unloading slope whilst the load is decreasing, and the assumption is that the contact area is also decreasing, however due to the time dependent nature of polymer materials this is not necessarily the case. During the ramp and hold load test the load is constant and, based on Hertzian

contact and elastic-visco-elastic correspondence, both the displacement and contact area increase with time. Additionally, in the load - unload test measured displacement is more dependent on the initial point of contact as data is collected during loading and unloading, however, in a creep test the initial point of contact is less important as the data is collected at peak load when contact is more established. The ramp and hold load test is therefore a potentially more robust test.

8.2 Creep analysis to distinguish different mechanical properties

The differences in creep response observed between the materials tested were as expected according to the material descriptions. Cool-lok is an amorphous, thermoplastic polymer composed of waxes and petroleum it would be expected to exhibit more viscous flow than the cross-linked epoxy and this was reflected in the trends of calculated instantaneous shear modulus values with increasing creep stress (Tensile values:- Cool-lok = approx. 23 MPa, epoxy15:2 mix. = approx. 430 MPa Tables 5.3-1 and 5.4-1).

The results of both tensile tests and nanoindentation tests show that the instantaneous shear modulus values of the epoxy standard mix show no clear trend in modulus values with increasing creep stress, Figure 5.3-7, whereas over a shorter range of increasing creep stress the modulus values of Cool-lok decrease, Figure 5.4-10. This is evidence of viscous flow in Cool-lok causing an increased strain response to increased stress and suggesting a correspondingly lower modulus value. In nanoindentation tests the Cool-lok appeared to flow more during slow ramp load

times so that less flow occurred during the creep period, Figure 5.4 -8. This gave rise to the observed trend of increasing modulus with rise time, which was not seen clearly in tensile tests; however, the trend was confounded by the strong effect of increasing creep stress Figure 5.4-11.

In addition, creep ratios average between 0.2-0.5 for epoxy 15:2 and between 0.5-0.6 for Cool-lok, which again is as expected as the Cool-lok might be expected to exhibit more viscous flow than the cross – linked epoxy.

It can be seen that the nanoindentation creep analysis enables distinctions to be made between different materials (Figures 4.3-2). It can distinguish between the epoxy resin : hardener ratios in the same way as a tensile test (Chapter 5.3) and is more sensitive to changing loads and load rise times than tensile testing Figures 5.4-10 and 5.4-11.

8.3 Nanoindentation creep analysis to monitor age and exposure related changes in mechanical properties of coatings

Nanoindentation creep was found to be suitable for distinguishing between different materials in terms of their mechanical properties. It was also found to be sensitive enough to be used to monitor changes in mechanical properties with aging and environmental conditioning. Changes such as water permeation or changes resulting from attack by free radicals such as increased cross-linkage or chain scission a result of exposure to sunlight as most resins in coatings contain small peroxide and ketone impurities which absorb sunlight to produce free radicals (Weldon 2001).

The most significant changes in the creep response of the coatings tested appeared as seasonal fluctuations with control samples of coatings 3 and 4 following the same trends as the exposed samples suggesting that seasonal changes in humidity were the major factor (Figures 4.3-10 to-13). (There is no control for relative humidity in the lab, although temperature is controlled.) Relative humidity is known to cause recoverable shifts in T_g (Zhou 2001, Foster *et al.* 2004) and shifts are only non-recoverable after situations with thermal spikes, *i.e.* extreme sudden large temperature changes > 180°C (Karad *et al.* 2002). Moisture absorption is largely due to the affinity that highly polar functional groups have with water, and water movement through the film is dependent on free volume. The aliphatic PUMA should have a higher free volume and have more polar groups than the aromatic PUMA and, notwithstanding the effects of the remaining chemical composition of the film, this together with a possible increased susceptibility caused by sunlight exposure, may account for the differences in the seasonal fluctuations seen in coatings 1 and 2. Similarly, dependent on their chemical composition and structure, humidity affects the other coatings and it is known that acrylic coatings are widely used for their weather resistance (Bentley 1999).

8.4 Use of nanoindentation creep relative to tensile creep for determining shear modulus values

In theory both tensile creep and indentation creep should give the same modulus values, providing the material under test is isotropic and amorphous, and if the Boltzmann superposition principle, BSP, applies. The calculation of the shear modulus from the measured creep function resulting from nanoindentation tests generally gave values which were approximately twice the values calculated from

tensile tests for all of the materials tested in Chapter 5, *e.g*. epoxy standard mix ratio:- G0 tensile = 0.43GPa G0 indentn = 0.7-1.0 GPa, Cool-lok :- G0 tensile = 23MPa, G0 indentn. = 50MPa, PMMA :- G0 tensile = 1.1GPa, G0 indentn. = 1.6GPa. This was apparent even when the BSP was seen to be applicable *i.e.* at the lower loads and faster rise times in the epoxy (Figures 5.3-2 and 5.3-5) and in the faster rise time for the PMMA (Figure 5.5-1a). However, even in the case of the nonlinear indentation response of the Cool-lok the calculated instantaneous shear modulus value was again approximately twice the corresponding tensile shear modulus value.

In the nanoindentation of Cool-lok the ramp displacement was approximately half of the displacement that is predicted using the calculated tensile modulus. Although the displacement was less than expected there was still evidence of creep occurring during ramp loading and this was the most likely reason for the non linearity. This could be seen as increasing displacement with load$^{2/3}$ during ramp load Figures 5.4-5 to -7 which was not seen in the tensile ramp loading Figures 5.4-1 to -3.

The creep function can be normalised to eliminate the effects of ramp load and rise time. The resulting normalised creep provides information regarding the relative creep of the material, it should be a material property, and the results from the two test methods should be in agreement. However, the normalised creep in nanoindentation of Cool-lok was less than the corresponding normalised creep in tensile tests Figure 5.4-9. The pattern in the reduced creep Figure 5.4-8, gave rise to the trend in calculated modulus values seen in 5.4-11 in which the modulus value was seen to increase with rise time in nanoindentation tests, corresponding to a relative decrease in creep during the hold load period as creep was occurring during the load. This trend was not seen in the normalised tensile creep, Figure 5.4-4, creep

became relatively greater at higher stress when the response was non linear. This suggests that, for Cool-lok under indentation, visco-elastic flow was slower as load increased, although this could be due to the increasing displacement with load seen during the ramp loading (Figures 5.4-5 to 5.4-7).

The normalised indentation creep for the epoxy appeared similar to the normalised tensile creep under the lower load and fast ramp conditions only, Figure 5.3-4. At higher indentation loads normalised creep was greater. However, during nanoindentation ramp load the displacement was less than predicted assuming Hertzian contact and using the modulus values calculated from the tensile test, Figure 5.3-5.

The reduced displacement during ramp loading in indentation may be explained by the steep stress gradients in the confined volume of the material under the indenter.

Apparently increased modulus values resulting from indentation tests have been seen before. A comparison of mechanical properties of polytetrafluoroethylene, PTFE, using uni-axial tensile testing, dynamic mechanical analysis, DMA, and nanoindentation with the continuous stiffness measurement option, by Lucas *et al.* found modulus values calculated from indentation test data to be 2.4 to 3 times that obtained from the other two methods (Lucas *et al*. 1998).

Despite the theory suggesting that the modulus value, as a material property should be the same, the viscous response, or the way in which the polymer chain molecules respond to different forms of stress, may be different. It may be that in a tensile test the free volume of the material is not directly reduced in the same way as it is in an indentation test. The pressure of the indenter on the polymer chains would initially reduce the free volume, equivalent to raising the T_g, with subsequent chain movement to release this reduction if possible. It would also affect the position of the

contact area relative to the penetration, the volume directly under the indenter under hydrostatic pressure would be compressed whilst the rest of the material would still be able to flow, possibly resulting in increased penetration relative to contact area. The extent of this would depend on the particular polymer as chain segment movement depends on the polymer configuration; factors include average molecular weight of the polymer chain, steric hindrance and cross – linkage.

8.5 Pressure or strain sensitivity of mechanical response

Nanoindentation results suggested pressure or strain dependence of the calculated modulus in PMMA Figures 5.5-5, 5.5-6. Using conical and spherical indenters Briscoe and Sebastian (1996) also found that calculated elastic modulus values for PMMA increased with increasing representative strain, ε_r, their definition of which is $\varepsilon_r = h_p / R$ where h_p is the intercept of $\frac{dP}{dh}$ on the h axis; and by extrapolating the results to find the modulus value at $\varepsilon_r = 0$, the value was found to be in good agreement with the tensile, literature value. Under the conditions of Briscoe and Sebastian however, using conical indenters the modulus continued to increase with no maximum value seen and their results using spherical indenters were limited again with no maximum value seen; in addition their definition of representative strain includes plastic strain.

The results presented in this work when nanoindenting PMMA also suggest that modulus values increased with increasing *a/R* and that the modulus value could also be in agreement with the literature value if results are extrapolated to *a/R* or $\varepsilon_r = 0$. However, results using 5 μm and 21 μm radius tips suggest that the increasing

modulus value with increasing *a/R* reached a maximum value dependent on tip size Figure 5.5-6.

The initial lower modulus values may be due to the local movement of sections of the polymer chain that are in contact. Initially, such local sections of chain may reposition themselves relatively easily, but as stress is increased and free volume is reduced, chains further into the material, *i.e.* those not in contact with the indenter, have to move cooperatively and this corresponds to the response found as a result of tensile testing.

However, the macroindentation data in the same regions of *a/R* as the nanoindentation tests did not show the same result. There was no such clear trend in Figure 6.5-11. The modulus values calculated from contact area and from displacement were different and the changes in modulus value with *a/R* and mean pressure were slight relative to the changes seen in the nanoindentation test Figure 6.5-6. The *a/R* value of a nanoindentation test may be similar to the *a/R* value from a macroindentation test but the nanoindentation test is probing a small volume at the near surface of the material whereas the macroscaled test will probe further into the material. This suggests that the surface properties were significant and that the reduced modulus values found with reduced *a/R* in the nanoindentation of PMMA were as a result of surface properties such as surface roughness, which become less significant at greater penetration depths.

8.6 Surface properties

In addition to the issue of confinement of the material under an indentation test, the indentation test is a contact test, so the surface properties are significant especially in a nano-scale test in which the near surface is penetrated. On the other hand, a tensile

test is through the bulk of the material and this may account for the differences in the modulus values calculated from the two test methods, and why, in the case of the epoxy, when indenting on a macro scale, in which the elastic stress field can extend further into the material, the modulus value calculated from the creep displacement, $G0$ = 0.43GPa, is close to the modulus value obtained from tensile creep, $G0$ = 0.47GPa.

Surface properties may also explain the changing values modulus calculated from nanoindentation creep seen in the PMMA at lower penetration depths, Figure 8.6 -1. At such low penetration depths contact may not be complete and contact may be made only with peaks of material at the surface due to the surface texture and the indenter itself will also have some surface roughness. The peaks of the material in contact may then compress relatively easily until complete contact between the tip and the sample surface is made. Surface debris, such as that caused by electrostatic attraction of dust particles may also affect the measurements. Furthermore, surface layers may have absorbed water or similar which may affect the material behaviour at the surface and consequently initial displacement measurements.

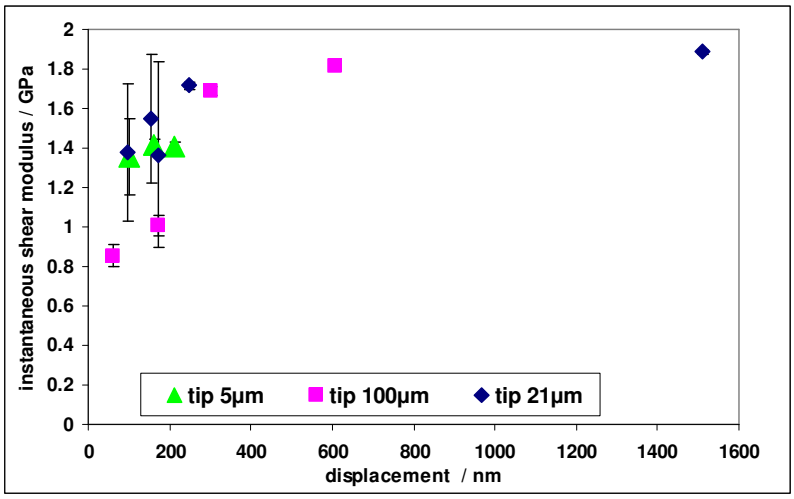

Figure 8.6-1 PMMA nanoindentation at loads 0.3mN, 0.6mN, 0.9mN, 3mN, 10mN 30mN with different radius indenters show that modulus changes with depth

8.7 Validity of assumed Hertzian contact

In an indentation test the contact area is assumed from the measured displacement according to Hertzian contact analysis. The macroindentation studies show that contact was not always Hertzian for the polymers studied; contact areas were smaller relative to displacement. This suggests “sink in” behaviour. In the case of the PMMA this was due to a greater initial displacement, thereafter a Hertzian relationship was seen.

Macroindentation of the epoxy showed that the contact area was less than expected during loading (Figure 6.6-1), however, on this scale the displacement was as predicted using the calculated tensile modulus (Figure 6.6-3). During the period of hold load constant, again contact areas appeared to be less than expected. During hold load periods at 150N and 200N, Figure 6.6-7, contact areas increased more than the displacement increased. At lower loads the contact area and displacement increased together in proportion to the radius of the indenter, as in Hertzian contact Figure 6.6-8.

Reduced contact areas relative to displacement were also seen when indenting PMMA on a macro scale Figure 6.5-12, however, this was due to the increased initial displacement, Figures 6.5-3, 6.5-10, apart from this the relationship between contact area and displacement was constant and Hertzian. Contact areas were generally in good agreement with those calculated from Hertzian theory using the literature value under the test conditions applied, but were slightly smaller during faster loading Figures 6.5-5, 6.5-7. However, Hertzian contact was not satisfied for epoxy and the reduced contact areas are evidence of “sink in”.

The reduced contact areas were not due to surface roughness, the scale of the surface roughness is less significant for macroindentation. Neither were the reduced contact

areas due to adhesion, as adhesion results in contact areas greater than those predicted by Hertzian theory. Also, area values would tend towards a finite value at zero load due to attractive forces which are more significant at low loads (Johnson *et al*. 1971).

It is possible that friction between the indenter and the surface could also be a contributing factor in the observed reduced contact areas. Friction has been seen to have a significant effect in the indentation of iron (Li et al. 1993), and in the elastic-plastic deformation of PMMA under spherical indentation (Kent 1981) where friction was found to be a substantial component of the measured pressure. Other works, predominantly considering finite element analyses on metals suggest that friction does not affect the load-depth curves (Lee *et al.* 2005) (Zhao *et al*. 2005). However as the penetration depths and contact areas in this work were much smaller than the indenter radius as in Hertzian contact the effects of friction were initially assumed to be insignificant.

Together, the reduced nanoindentation penetration depth and reduced contact area in macroindentation and the agreement of the macroindentation penetration depth with the response predicted using the modulus obtained from tensile tests suggest that the epoxy may have a stiffer surface layer, possibly due to increased cross-linking at the surface. Alternatively, the modulus may be approximately as determined from the nanoindentation test (0.8-1.0 GPa) and the macroindentation contact area (0.70- 0.73 GPa) from Table 6.6-1, and increased viscous flow under stress in tensile tests and in macroindentation displacement results in lower modulus values, however, as there is good agreement between normalised creep in tensile tests and nanoindentation tests this is not likely.

The macroindentation study shows that contact was Hertzian for amorphous, time independent glass. The measured contact areas, penetration depths and the relationship between these were all as predicted using Hertzian contact mechanics (Figures 6.4-2 to 6.4-5). However, for the polymers tested in this work, contact was not always Hertzian throughout an indentation test as contact areas were not at a depth predicted by Hertzian theory. The analysis of force-displacement data is based on the assumption that Hertzian contact applies, if the assumption is invalid *i.e*. measured penetration depth does not relate to contact area according to Hertzian theory, then the modulus values calculated only from the measured penetration depth should also be invalid.

8.8 Use of FEA to predict contact response

Finite element modelling confirmed the Hertzian contact in spherical indentation of the elastic and visco-elastic materials described. This is seen as good agreement between the modelled results and the theory. However, as the material behaviour is described by the user this is expected when homogeneous, isotropic elastic and visco-elastic behaviour is defined. Finite element analysis relies on the information given by the user it can not predict any pressure sensitivity or surface effects in the material response unless this has already been defined by the user. It cannot replicate the reduction of free volume that occurs as the polymer is under compressive stress unless this is included in the material description.

The modelled glass results agreed with the experimental results and with the theory. The modelled PMMA and epoxy results agreed with theory only as experimental results appear to be depth and/or pressure sensitive.

However, when the epoxy sample was modelled with a stiffer skin *i.e.* the top 0.25mm with material properties defined using the modulus calculated from nanoindentation results, the model produced results that were closer to those obtained experimentally in the macroindentation tests. Maximum penetration depths resulting from nanoindentation of the epoxy sample at loads up to 30mN and tip radius 21μm were less than 2μm, Figure 5.3-5; therefore it is possible that nanoindentation displacement would have been within the stiffer skin. The presence of a stiffer skin at the surface is possible as crosslink density is likely to be different at the surface than in the bulk.

The finite element modelling which includes a stiffer surface confirms that although contact is Hertzian in a homogeneous and isotropic sample, this is not the case when indentation causes stress fields through both the stiffer surface of the material and the softer bulk material, in which case contact may sink in.

Although the model consists of a stiffer surface skin with uniform mechanical properties described, in reality there may be a gradient in mechanical properties from surface to bulk and this would affect the mechanical response in a similar way.

This skin effect is to be expected in some polymers such as the cross linking epoxy because at the surface or interface the cross-linking bonds cannot be formed equally in all three dimensions. The reduction in molecules available to be linked at the surface in the normal direction results in the cross-linker making more bonds to those

molecules that available laterally and immediately below, so that bonding is increased at the surface.

8.9 Suggested procedure for nanoindentation creep

Polymers are sensitive to rise time and to maximum applied load. Nanoindentation is particularly sensitive to the changing polymer response to these and is able to distinguish between polymers in the same way as tensile tests.

As nanoindentation is suitable for probing small volumes of material and nanoindentation creep tests provide more information than conventional nanoindentation tests, (although values also depend on unknown contact areas), it appears that the nanoindentation creep test and analysis is ideal for characterising the mechanical response of coatings.

However, it is not always possible to determine a valid modulus value from a single test due to the sensitivity of the nanoindentation test. In this work calculated modulus values and creep ratios were seen to vary as a result of changing ramp load conditions. *E.g.* epoxy standard mix calculated modulus and creep ratios varied as much as 40 - 50% as rise times changed from 8 to 30 seconds over the various maximum loads.

It is evident from the work presented that a single test is not suitable and at least the test should be repeated over a range of loads to determine linearity and the applicability of the Boltzmann super position principle, BSP. The BSP should be seen to apply to the results to justify the use of the creep analysis to calculate shear modulus values.

The effects of ramp load time should also be considered. The analysis is based on step loading with corrections made for the ramp loading seen in practice. In this work the effects of reduced creep as a result of slower ramp load times has been seen, the loading should therefore be as short as possible but good data collection is also required. The best ramp load rate will be dependent on the nanoindentation instrument due to factors such as feedback in the load and displacement control. Tests should be performed with tips of different radii over a similar range of loads, or to the same depth such that strains remain small, and resulting calculated modulus values plotted against average mean pressure or a/R or with depth. Results may indicate any pressure or strain or depth dependence of the calculated modulus values.

The resulting modulus values should then be considered as modulus values describing the surface properties of the material which should not necessarily be representative of the bulk material properties for all polymers.

However, for very thin films, ~ 100nm, mechanical properties can be expected to be consistent throughout the film thickness due to the confinement during curing. The mechanical properties can also be expected to be different to the mechanical properties of a bulk sample of the same material.

9 Conclusions and Future Work

In this work the theory describing the visco-elastic mechanical response of polymers and the associated contact mechanics with regard to spherical nanoindentation have been examined. Nanoindentation creep and analysis as a technique to monitor age and environmental conditioning on polymer coatings has been investigated.

The visco-elastic mechanical response of selected polymers under spherical nanoindentation has been compared to the response to traditional tensile testing.

The parameters of contact loading have been directly measured for polymers under spherical indentation and the results have been compared with tensile testing and literature values. Finite element analysis of visco-elastic contact has been used to help interpret the results.

The results of this work suggest the following:-

9.1 Conclusions

- A nanoindentation ramp and hold load method and creep analysis provides more information about the mechanical properties than the conventional load – unload test cycle as well as being more robust.
- The nanoindentation creep function can be used to calculate modulus values and in addition the creep function itself provides a means to distinguish between different materials with different mechanical properties.
- The nanoindentation creep response is particularly sensitive and is therefore suitable to be used to monitor any associated age and exposures related

changes in mechanical properties even if simply used as relative creep displacement.

- If comparisons need to be drawn between tensile testing, nanoindentation may not always provide the same results in terms of modulus values.
- Examination of contact areas under macro indentation suggests that contact - depth relationships are not always Hertzian in spherical indentation of visco-elastic polymers. The reasons for this are not clear but possibly due to pressure sensitivity, or to the volume of the material being tested as a near surface volume is probed in an indentation test.
- Finite element analysis can be used only when material behaviour can be accurately described in the model.
- Procedures for nanoindentation of polymers should not be based on a single test and should include checks for linearity and the applicability of the BSP as well as checks into a possible changing response with penetration depth or pressure.

9.2 Future Work

To investigate the effects of near surface mechanical properties, nanoindentation could be made along a cross section of the sample from bulk to surface, providing the material does not reconstruct during the cutting of a section. This may be possible by fracturing at low temperature.

Any differences in the moduli calculated across the material from bulk to surface should be evident. Results should clarify whether the differences in modulus values

calculated from direct measurement of contact areas compared to those calculated from displacement are due to different mechanical properties at the polymer surface.

It may also be possible to investigate the surface – bulk effect by tensile testing samples of various cross sections such that bulk cross sectional surface area to skin cross sectional surface area are varied, *e.g.* a wide strip of material of very small thickness relative to a sample having the same width but with thickness equal to width.

The effects of tip - sample friction could be investigated by lubrication of the surface. More glassy polymers as well as polymers with varying degrees of cross-linking could be indented to build up a library of the mechanical properties of visco-elastic polymers. The results may suggest that a correction factor to the Hertzian contact analysis is possible.

Nanoindentation of polymers with increasing degrees of cross links could also be done over a cross-section of the samples from bulk to surface to investigate the effects cross-linking has on the surface mechanical properties compared to those of the bulk.

10 References

Agilent Technologies, Inc. (2009) Agilent Nano Indenter G200 Data Sheet http://cp.literature.agilent.com/litweb/pdf/5990-4172EN.pdf

Auerkari, P., (1996) Mechanical and physical properties of engineering alumina ceramics, *VTT Tiedotteita Meddelanden Research Notes* 1792 Technical Research Centre of Finland (VTT)

Bentley, J., (1999) Ch. 2 Organic film formers, *Paint and Surface Coatings : Theory and Practice* Eds. Lambourne, T., Scrivens, T. A., Woodhead Publising Ltd.

Boersma ,A., Soloukhin, V.A., Brokken-Zijp. J.C.M., De With, G., (2004) Load and Depth Sensing Indentation as a Tool to Monitor a Gradient in the Mechanical Properties across a Polymer Coating : A Study of Physical and Chemical Aging Effects. *Journal of Polymer Science: Part B: Polymer Physics*, Vol.**42**, 1628-1639 Wiley Periodicals, Inc.

Bolshakov, A., Pharr, G. M., (1998) Influences of pileup on the measurement of mechanical properties by load and depth sensing indentation techniques, *Journal of Materials Research*, Vol. **13** No. 4 pp.1049-1058

Briscoe, B. J., Sebastian, K. S., (1996) The elastoplastic response of poly(methyl methacrylate) to indentation, *Proceedings: Mathematical Physical and Engineering Sciences* Vol.**452** No. 1946 pp.439-457

Briscoe, B. J., Fiori, L., Pelillo, E., (1998) Nanoindentation of Polymeric Surfaces. *Journal of Physics D : Applied Physics* **31**, pp2395-2405 IOP Publishing Ltd.

Burch, D., Martin, J. W., VanLandingham, M.R., (2002) Computer Analysis of a Polymer Coating Exposed to Field Weather Conditions. *Journal of Coatings Technology* Vol.**74** No.924 pp75-86

Bushby, A. J., (2001) Nano-indentation using spherical indenters, *Nondestructive Testing and Evaluation,* Vol. **17** pp.213-234 Overseas Publishers Association N.V.

Bushby, A. J., Jennett, N. M., (2001) Determining the area function of spherical indenters for nanoindentation, *Materials Research Society Symposium Proceedings* Vol. **649**

Carre, A., Gamet, D., Schultz, J., Schreiber, H. P., (1986) Nonuniformity in thin polymer films, *Journal of Macromolecular Science – Chemistry A* **23** (1) pp1-18.

Cheng, L., Xia, X., Scriven, L. E., Gerberich, W. W., (2004) Spherical tip indentation of visco-elastic material, *Mechanics of Materials* **37** pp213-226

Cheng, Y-T., Cheng, C-M., (2005) General relationship between contact stiffness, contact depth,and mechanical properties for indentation in linear visco-elastic solids using axisymmetric indenters of arbitrary profiles. *Applied Physics Letters*, **87**, 111914 Elsevier B.V.

Cheng, Y-T., Cheng, C-M., (2005) Relationships between initial unloading slope, contact depth, and mechanical properties for conical indentation in linear visco-elastic solids. *Journal of Materials Research* Vol. **20** No.4 pp 1046-1053

Chima - Okereke, C., Bushby, A. J., Reece, M. J., Whatmore, R. W., Zhang, Q., (2006) Experimental, analytical and finite element analyses of nanoindentation of multilayer PZT/Pt/SiO2 thin film systems on silicon wafers. *Journal of Materials Research*, **21**, 2. pp.409-419.

Cook, R. F., Pharr, G. M., (1990) Direct observation and analysis of indentation cracking in glasses and ceramics *Journal of the American Ceramic Society* **73** 4 pp.787-817

Cowie, J. M .G., (1991) *Polymers : Chemistry and Physics of Modern Materials*, CRC Press p 330 p 272

Deuschle, J. K., Deuschle, H. M., Enders, S., Arzt, E., (2009) Contact area determination in indentation testing of elastomers *Journal of Materials Research* Vol. **24** No. 3 March 2009 Materials Research Society

Doerner, M.F. and Nix, W.D., (1986) A method for interpreting the data from depth-sensing indentation instruments. *Journal of Materials Research*, **1**, pp 601-609

Fabes, B. D., Oliver, W. C., McKee, R. A., Walker, F. J., (1992)The determination of film hardness from the composite response of film and substrate to nanometer scale indentations, *Journal of Materials Research* Vol. **7**, No. 11 pp. 3056-3064

Ferry, J. D., (1980) Visco-elastic properties of polymers *John Wiley & Sons Inc*. Ch. 2 p40

Field, J. S., Swain, M. V., (1993) A simple predictive model for spherical indentation *Journal of Materials Research* Vol.**8** No. 2

Findley,W.N., Lai, J.S., and Kasif Onaran, (1976) *Creep and Relaxation of Nonlinear Visco-elastic Materials*, North Holland Publishing Co.. p3, p.81, p.87, p.68

Foster, G. M., Ritchie, S., Evans, K. E., Lowe, C., (2004) Controlled relative humidity testing for the characterisation of the brittle-tough and glass transition temperatures of coil coating paint films, *Progress in Organic Coatings* **51** 3 pp.244-249

Gacoin, E., Fretigny, C., Chateauminois, A., Perriot, A., Barthel, E., (2006) Measurement of the mechanical properties of thin films mechanically confined within contacts, *Tribology Letters* , **21** 3

Gao, S.L., Habler, R.,Mader, E., Bahners, T., Opwis, K., Schollmeyer, E., (2005) Photochemical surface modification of PET by excimer UV lamp irradiation. *Applied Physics B*, **81**, 681-690 Springer-Verlag

Hay, J. C., Bolshakov, A.,Pharr, G. M., (Jun 1999) A critical examination of the fundamental relations used in the analysis of nanoindentation data *Journal of Materials Research* Vol. **14**, No. 6, pp2296-2305 Materials Research Society

Herbert, E. G., Oliver, W. C., Pharr, G. M., (2008) Nanoindentation and the dynamic characterisation of visco-elastic solids, *Journal of Applied Physics D : Applied Physics*, **41** pp1-9

Johnson, K.L., (1985) *Contact Mechanics*. Cambridge University Press.

Johnson, K. L., Kendall, K., Roberts, A. D.,(1971) Surface energy and the contact of elastic solids, *Proceedings of the Royal Society of London* **324** pp.301- 313

Karad, S. K., Jones, F. R., Attwood, D. A., (2002) Moisture absorption by cyanate ester modified epoxy resin matrices. Part 1. Effect of spiking parameters, *Polymer* **43** pp.5209-5218

Kent, R. J. (1981) Indentation processes in poly(methyl methacrylate): I. ball indentation, *Journal of Physics D: Applied Physics*, **14** pp.601-611

Kourtesis, G., Renwick, G. M., Fischer-Cripps, A.C., Swain, M.V., (1997) Mechanical property characterisation of a number of polymers using uniaxial compression and spherical tipped indentation tests, *Journal of Materials Science* **32** 1997 pp4493-4500 Chapman & Hall

Lakes R.S. (1999) *Visco-elastic Solids* CRC Press p.140

Larsson, P.-L., Carlsson, S., (1998) On microindentation of visco-elastic polymers, *Polymer Testing* **17** pp 49 -55

Lee, E.H., Radok, J.R.M. (1960) The Contact Problem for Visco-elastic Bodies, *Journal of Applied Mechanics* pp 438-444

Lee, H., Lee, J.H., Pharr, G. M., (2005) A numerical approach to spherical indentation techniques for material property evaluation, *Journal of the Mechanics and Physics of Solids* **53** 2037–2069

Li, H., Gosh A., Han Y. H., Bradt, R. C, (1993) The frictional component of the indentation size effect in low load microhardness testing, *Journal of Materials Research* Vol. **8**, No. 5 pp.1028-1032

Loubet, J. L., Oliver, W. C., Lucas, B. N., (May 2000) Measurement of the Loss Tangent of Low-density Polyethylene with a Nanoindentation Technique. *Journal of Materials Research.*, Vol. **15** No.5 pp 1195-1198 Materials Research Society

Lu, H., Wang, B., Ma, J., Huang, G., Viswanathan, H., (2003) Measurement of Creep Compliance of Solid Polymers by Nanoindentation, *Mechanics of Time-Dependent Materials* **7** 189-207 . Kluwer Academic Publishers

Lucas, B. N., Rosenmayer, C. T., Oliver, W.C., (1998) Mechanical Characterization of Sub-micron Polytetrafluorothylene (PTFE) Thin Films. *Materials Research Society Symposium Proceedings* Vol.**505** pp 97-102 Materials Research Society

McCrum, N.G., Buckley, C.P., Bucknall, C.B., (1997) *Principles of Polymer Engineering,* Oxford Science Publications p104

Mencik, J., Munz, D., Quandt, E., Weppelmann, E. R., Swain, M. V., (1997) Determination of elastic modulus of thin layers using nanoindentation, *Journal of Materials Research*, Vol.**12** No.9 pp2475 - 2484

Miller, J. A., Lin, S. B., Hwang, K. K. S., Wu, K. S., Gibson, P. E., Cooper, S. L., (1985) Properties of polyether-polyurethane block copolymers : effects of hard segment length distribution, *Macromolecules* **18** pp.32-44

O'Connor, J. J., and E F Robertson (December 1996) http://www-history.mcs.st-andrews.ac.uk/Biographies/Volterra.html

Oliver, W.C., Pharr, G.M., (June 1992) An improved technique for determining hardness and elastic modulus using load and displacement sensing indentation experiments. *Journal of Materials Research* Vol **7** No.6 Materials Research Society

Oliver, W.C., Pharr, G. M., (2004) Measurement of hardness and elastic modulus by instrumented indentation advances in understanding and refinements to methodology *Journal of Materials Research* Vol **19** No 1 pp 3-20

Oyen, M. L., Cook, R. F., (2002) Load-displacement behaviour during sharp indentation of viscous-elastic-plastic materials, *Journal of Materials Research*, Vol. **18** No.1 pp.139-150

Oyen, M. L., (Aug 2005) Spherical indentation creep following ramp loading, *Journal of Materials Research*, Vol.**20**, No.8, Materials Research Society

Oyen, M. L. (2006) Analytical techniques for indentation of visco-elastic materials, *Philosophical Magazine.* Taylor & Francis

Oyen. M.,L., (2007) Sensitivity of polymer nanoindentation creep measurements to experimental variables. *Acta Materialia Inc*. **55** 3633-3639 Elsevier Ltd

Oyen, M. L., Ferguson, V. L., Bembey, A. K., Bushby A. J., Boyde, A. , (2008) Composite bounds on the elastic modulus of bone, *Journal of Biomechanics* Vol **41**, 11 pp.2585-2588

Puttick, K. E., Smith, L. S. A., Miller, L.E., (1977) Stress fields round indentations in poly(methyl methacrylate), *Journal of Physics D: Applied Physics*, Vol. **10**, pp. 617-632

Ramesh Kumar, M. V., Narasimhan, R., (2004) Analysis of spherical indentation of visco-elastic materials, *Current Science* **87** 8 pp1088 – 1095

Sakai, M., (2009) Substrate-affected indentation contact parameters of elastoplastic coating/substrate composites, Journal of Materials Research Vol. **24** No.3

Saha, R., Nix, W. D., (2002) Effects of the substrate on the determination of thin film mechanical properties by nanoindentation. *Acta Materialia* **50** p23-38 Elsevier Science Ltd.

Sneddon, I. N., (1965) The relation between load and penetration in the axisymmetric Boussinesq problem for a punch of arbitrary profile *International Journal of Engineering Science* Vol. **3** pp. 47-57

Sperling, L.H., (1992) Glass - rubber transition behaviour, *Introduction to Physical Polymer Science* John Wiley & sons, inc. p310

Strivens, T. A., (1999) Mechanical Properties of Paints and Coatings, Lambourne, R., & Strivens T.A., eds. *Paints and Surface Coatings Theory and Practice,* Woodhead Publishing Ltd. p599

Struik, L.C.E., (1980) *Physical Aging in Amorphous Polymers and Other Materials*, Elsevier Scientific Publishing Co. Amsterdam, The Netherlands. pp8,9

Swain, M. V., Hagan, J. T., (1976) Indentation plasticity and the ensuing fracture of glass, *Journal of Physics D: Applied Physics* Vol. **9** pp.2201- 2214

Tabor, D., *The Hardness of Metals*, Clarendon Press, Oxford. 1951

Thurn, J., Morris, D. J., Cook, R. F., (Oct 2002) Depth - sensing indentation at macroscopic dimensions. *Journal of Materials Research*, Vol. **17**, No. 10, Materials Research Society

Tweedie, C. A., Van Vliet, K. J., (2006) Contact creep com,pliance of visco-elastic materials via nanoindentation. *Journal of Materials Research* Vol**.21**, No. 6, 1576-1589

UMIS 2000 (ultra micro-indentation system) Operating Manual, Division of Applied Physics, Institute of Industrial Technologies. CSIRO Australia. March 1996

Van Landingham, M.R.,Villarrubia, J.S.,Guthrie,W.F. Meyers,G.F., (August 2000) Nanoindentation of polymers: An overview, from Recent Advances in Scanning Probe Microscopy. *Proceedings.220th American Chemical Society National Meeting* NIST

Van Landingham, M. R., (July-August 2003) Review of Instrumented Indentation, *Journal of Research of the National Institute of Standards and Technology* Vol. **108**, No. 4 pp 249-265

Ward, I. M., Hadley, D. W., (1996) *An Introduction to the Mechanical Properties of Solid Polymers* John Wiley & Sons

Weldon, D. G., (2001) *Failure Analysis of Paints and Coatings*, John Wiley & Sons Ltd.,

White, C. C., Drzal, P. L., VanLandingham, M. R., (2005) Visco-elastic Characterization of Polymers Using Dynamic Instrumented Indentation, *Materials Research Society Symposium Proceedings*, Vol. **841** Materials Research Society

Yang, S., Zhang, Y-W., Zeng, K., (2004) Analysis of nanoindentation creep for polymeric materials, *Journal of Applied Physics* **95** (7) pp.3655-3666

Zhang, C. Y., Zhang, Y. W., Zeng, K. Y., (October 2004) Extracting the mechanical properties of a visco-elastic polymeric film on a hard elastic substrate, *Journal of Materials Research*, Vol. **19** No.10 pp. 3053-3061

Zhao, M., Ogasawara, N., Chiba, N., Chen, X., (2006) A new approach to measure the elastic–plastic properties of bulk materials using spherical indentation, *Acta Materialia* **54** 23–32

Zhou, S.-M., Tashiro, K. and Ii, T. (2001), Confirmation of universality of time–humidity superposition principle for various water-absorbable polymers through dynamic visco-elastic measurements under controlled conditions of relative humidity and temperature. *Journal of Polymer Science Part B: Polymer Physics*, **39**: 1638–1650.

Zhu, T. T., Bushby, A. J., Dunstan, D. J. (2008), Size effect in the initiation of plasticity for ceramics in nanoindentation, *Journal of the Mechanics and Physics of Solids*, Vol. **56**, Iss. 4 pp 1170-1185

11 Appendix

11.1 Analysis of creep curves

Analysis of strain / time creep curves from tensile tests and depth ^(3/2) / time creep curves from spherical indentation tests :-

For tensile tests:- strain versus time data during the period of hold load is copied to a worksheet in Origin 7 scientific graphing and analysis software (OriginLab Corporation USA)

For nanoindentation:- raw data from the UMIS operating system is compiled with corrections made for compliance, initial contact depth, time and indenter radius into an Excel workbook using an in-house macro compiled by Bushby, Oyen and Fergusson. Data for depth $^{3/2}$ versus time during the creep hold is then copied to an Origin worksheet.

For macroindentation:- corrections are made as described in the main work and depth$^{3/2}$ versus time is copied to an Origin worksheet.

Origin 7 scientific graphing and analysis software (OriginLab Corporation USA) is then used to fit creep curves obtained during the hold load period to the 2 parameter exponential decay function $y = y_0 + A_1 \exp\left[\frac{-x}{t_1}\right] + A_2 \exp\left[\frac{-x}{t_2}\right]$. The fitting process uses a non linear least squares fitting process based on Levenberg - Marquardt iterations, the number of which can be controlled by the user until the chi- squared value is no longer reduced.

The 2 parameter exponential decay function $y = y_0 + A_1 \exp\left[\frac{-x}{t_1}\right] + A_2 \exp\left[\frac{-x}{t_2}\right]$ to which the experimental creep curves are fitted corresponds to :-

$$h^{3/2}(t) = \frac{3}{8}\left(\frac{1}{R}\right)^{1/2} C_0 k t_R - C_1 k \tau_1 \exp\left(\frac{-t}{\tau_1}\right)\left[\exp\left(\frac{t_R}{\tau_1}\right) - 1\right] - C_2 k \tau_2 \exp\left(\frac{-t}{\tau_2}\right)\left[\exp\left(\frac{t_R}{\tau_2}\right) - 1\right]$$

for indentation creep (Equation 2.47 in Chapter 2.4-2)

and for tensile tests

$$d_{ij}(t) = \frac{2}{3}\left[C_0 k t_R - \sum C_1 k \tau_1 \exp\left(\frac{-t}{\tau_1}\right)\left[\exp\left(\frac{t_R}{\tau_1}\right) - 1\right] - C_2 k \tau_2 \exp\left(\frac{-t}{\tau_2}\right)\left[\exp\left(\frac{t_R}{\tau_2}\right) - 1\right]\right],$$

to Equation 2.27 described in Chapter 2.3-7

The amplitude coefficients of the creep function,

$J(t) = C_0 - C_1 \exp\left[\frac{t}{\tau_1}\right] - C_2 \exp\left[\frac{t}{\tau_2}\right]$, for the spring in series with two Kelvin, or Voigt, units as described in Chapter 2.3.3 – 2.3.4 can then be determined from the coefficients from the Origin function $y = y_0 + A_1 \exp\left[\frac{-x}{t_1}\right] + A_2 \exp\left[\frac{-x}{t_2}\right]$.

$C_0 = \frac{y_0}{k t_R}\left(\frac{8\sqrt{R}}{3}\right)$ for indentation testing

$C_0 = \frac{y_0}{k t_R}\left(\frac{3}{2}\right)$ for tensile testing;

for indentation testing $C_1 = \frac{A_1}{k t_R (RCF_1)}(TGF)$ where *TGF* is tip geometry factor

$= \left(\frac{8\sqrt{R}}{3}\right)$ and RCF_1 is ramp correction factor $= \frac{\tau_1}{t_R}\left[\exp\left(\frac{t_R}{\tau_1}\right) - 1\right]$, and

for tensile testing $C_1 = \frac{A_1}{k t_R (RCF_1)}\left(\frac{3}{2}\right)$;

Similarly,

for indentation testing $C_2 = \frac{A_2}{kt_R(RCF_2)}(TGF)$ and $RCF_2 = \frac{\tau_2}{t_R}\left[\exp\left(\frac{t_R}{\tau_2}\right) - 1\right]$ and

$C_2 = \frac{A_2}{kt_R(RCF_2)}\left(\frac{3}{2}\right)$ for tensile testing.

11.2 Measurement of contact areas using Image J

Open **Image J**

select **File** – **Open** – photo file no.

1. Use selection tool to select relevant area of photo then select **Image** – **Crop**

Zoom in on selection using **control +**

2. Select **Image – Type – 32 bit** then **Process – Enhance contrast – OK**

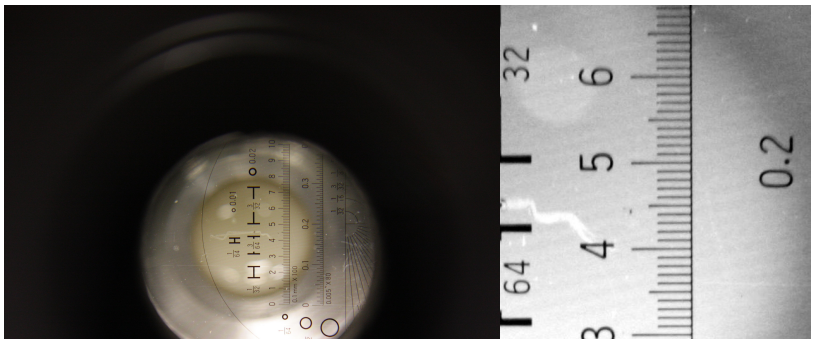

Figure 11.2-1 Left: unprocessed image; right processed image for scale setting

3. To calibrate pixels/mm choose line tool measure along known distance select **Analyze – Set Scale** enter known distance in box, record given value for p/mm repeat to get average p/mm in both x and y directions

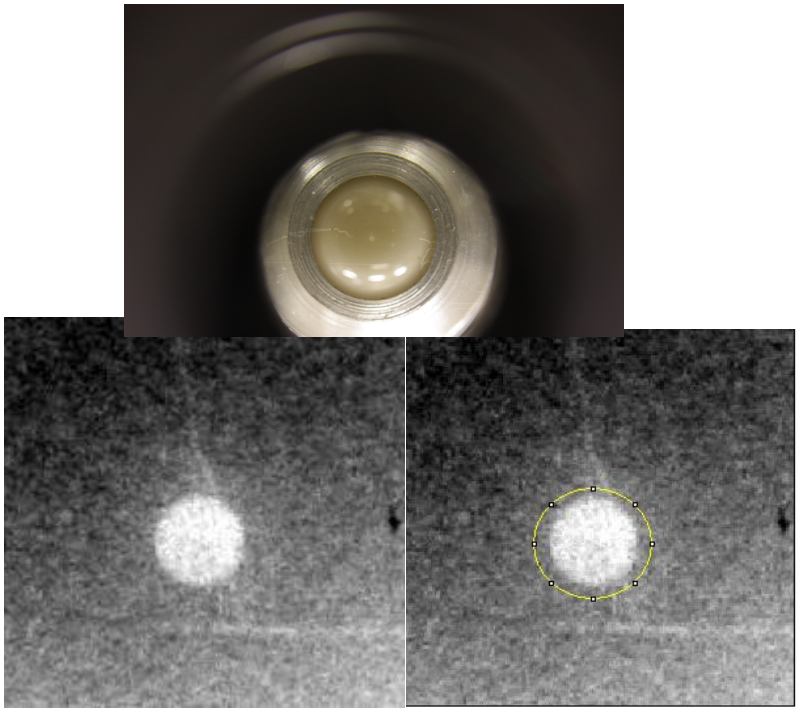

Figure 11.2-2 Top: unprocessed image; bottm left: processed image; bottom right processed image showing circular measurement tool

4. To measure area : - use circle selection tool to outline area of contact select **Analyze – Measure** record area in pixels from **Results** box, repeat to obtain upper and lower limits of the observed contact area from which the contact radius can be calculated.

11.3 Initial Statistical tests for coated glass slides

11.3.1 t-test of modulus ratio between samples

t-Test: Two-Sample Assuming Equal Variances
1 exposed and 1control (coating R11080/18/1)

	Cr	*Cr*
Mean	0.619095	0.607639
Variance	0.009285	0.011146
Observations	22	22
Pooled Variance	0.010216	
Hypothesized Mean Difference	0	
df	42	
t Stat	0.375936	
P(T<=t) one-tail	0.354428	
t Critical one-tail	1.681952	
P(T<=t) two-tail	0.708857	
t Critical two-tail	2.018082	

t-Test: Two-Sample Assuming Equal Variances
2 exposed and 2 control (coating R11080/18/2)

	Cr	*Cr*
Mean	0.405481	0.437397
Variance	0.009264	0.011244
Observations	32	40
Pooled Variance	0.010367	
Hypothesized Mean Difference	0	
df	70	
t Stat	-1.32167	
P(T<=t) one-tail	0.095291	
t Critical one-tail	1.666914	
P(T<=t) two-tail	0.190582	
t Critical two-tail	1.994437	

t-Test: Two-Sample Assuming Equal Variances
3 exposed and 3 control (coating R11080/18/3)

	Cr	*Cr*
Mean	0.463678	0.434178
Variance	0.016682	0.009466
Observations	20	26
Pooled Variance	0.012582	
Hypothesized Mean Difference	0	
df	44	
t Stat	0.884247	
P(T<=t) one-tail	0.190685	
t Critical one-tail	1.68023	
P(T<=t) two-tail	0.38137	
t Critical two-tail	2.015368	

t-Test: Two-Sample Assuming Equal Variances
4 control and 4 exposed (coating R11080/18/4)

	Cr	*Cr*
Mean	0.898185	0.886974
Variance	0.001824	0.001906
Observations	26	26
Pooled Variance	0.001865	
Hypothesized Mean Difference	0	
df	50	
t Stat	0.936018	
P(T<=t) one-tail	0.176881	
t Critical one-tail	1.675905	
P(T<=t) two-tail	0.353763	
t Critical two-tail	2.008559	

For all sample pairs coated with the same material, t Critical two-tail is greater than the t Stat, which means that the difference in calculated creep ratios between pairs is statistically insignificant.

11.3.2 Analysis of variance to test for differences between coatings

Anova: Single Factor to test for differences between coatings
null hypothesis = no variation between creep ratios of coatings
SUMMARY

Groups	*Count*	*Sum*	*Average*	*Variance*
R11080/18/1	40	24.81365	0.620341	0.010188
R11080/18/2	40	17.04646	0.426162	0.0112
R11080/18/3	40	17.90998	0.44775	0.013725
R11080/18/4	40	36.02014	0.900503	0.001427

ANOVA

Source of Variation	*SS*	*df*	*MS*	*F*	*P-value*	*F crit*
Between Groups	5.764368	3	1.921456	210.345	1.35E-54	2.662569
Within Groups	1.425027	156	0.009135			
Total	7.189395	159				

The F value is larger than the F crit value therefore the null hypothesis can be rejected at 95% confidence level, there is a significant difference between coatings. However, the mean values of creep ratio for coatings 2 (R11080/18/2) and 3

(R11080/18/3) appear very similar, another analysis of variance test was applied to the modulus for these two coatings separately.

Anova: Single Factor
null hypothesis = no variation between creep ratios of coatings R11080/18/2 and R11080/18/3
SUMMARY

Groups	*Count*	*Sum*	*Average*	*Variance*
R11080/18/2	40	17.04646	0.426162	0.0112
R11080/18/3	40	17.90998	0.44775	0.013725

ANOVA

Source of Variation	*SS*	*df*	*MS*	*F*	*P-value*	*F crit*
Between Groups	0.009321	1	0.009321	0.74792	0.389788	3.963472
Within Groups	0.972071	78	0.012462			
Total	0.981392	79				

These results suggest that the apparent differences between the creep ratios obtained for coatings 2 (R11080/18/2) and 3 (R11080/18/3) could be due to chance. It is possible that these coatings could be the same.

11.4 Statistical tests after exposure

11.4.1 1 week

t-Test: Paired Two Sample for Means
1 exposed (coating R11080/18/1)

	Cr	*Cr*
Mean	0.619095	0.61069
Variance	0.009285	0.010231
Observations	22	22
Pooled Variance	0.009758	
Hypothesized Mean Difference	0	
df	42	
t Stat	0.282208	
P(T<=t) one-tail	0.389585	
t Critical one-tail	1.681952	
P(T<=t) two-tail	0.77917	
t Critical two-tail	2.018082	

t-Test: Paired Two Sample for Means
1 control(coating R11080/18/1)

	Cr	*Cr*
Mean	0.614917	0.700572
Variance	0.011205	0.004839
Observations	20	30
Pooled Variance	0.007359	
Hypothesized Mean Difference	0	
df	48	
t Stat	-3.45888	
P(T<=t) one-tail	0.000574	
t Critical one-tail	1.677224	
P(T<=t) two-tail	0.001147	
t Critical two-tail	2.010635	

t-Test: Paired Two Sample for Means
control 2 (coating R11080/18/2)

	Cr	*Cr*
Mean	0.44757	0.418441
Variance	0.021381	0.007008
Observations	24	24
Pearson Correlation	-0.07077	
Hypothesized Mean Difference	0	
df	23	
t Stat	0.822218	
P(T<=t) one-tail	0.209698	
t Critical one-tail	1.713872	
P(T<=t) two-tail	0.419395	
t Critical two-tail	2.068658	

t-Test: Paired Two Sample for Means
exposed 2 (coating R11080/18/2)

	Cr	*Cr*
Mean	0.4538042	0.419691
Variance	0.0076287	0.013343
Observations	19	19
Pearson Correlation	-0.027889	
Hypothesized Mean Difference	0	
df	18	
t Stat	1.0132963	
P(T<=t) one-tail	0.1621733	
t Critical one-tail	1.7340636	
P(T<=t) two-tail	0.3243466	
t Critical two-tail	2.100922	

t-Test: Paired Two Sample for Means
3 control (coating R11080/18/3)

	Cr	*Cr*
Mean	0.456907	0.463678
Variance	0.006217	0.016682
Observations	20	20
Pearson Correlation	-0.53886	
Hypothesized Mean Difference	0	
df	19	
t Stat	-0.16451	
P(T<=t) one-tail	0.435532	
t Critical one-tail	1.729133	
P(T<=t) two-tail	0.871065	
t Critical two-tail	2.093024	

t-Test: Paired Two Sample for Means
3 exposed (coating R11080/18/3)

	Cr	*Cr*
Mean	0.512153	0.434178
Variance	0.006553	0.009466
Observations	26	26
Pearson Correlation	-0.34713	
Hypothesized Mean Difference	0	
df	25	
t Stat	2.712377	
P(T<=t) one-tail	0.005956	
t Critical one-tail	1.708141	
P(T<=t) two-tail	0.011912	
t Critical two-tail	2.059539	

t-Test: Paired Two Sample for Means
4 exposed (coating R11080/18/4)

	Cr	*Cr*
Mean	0.929362	0.904712
Variance	0.003725	0.00161
Observations	22	22
Pearson Correlation	-0.21451	
Hypothesized Mean Difference	0	
df	21	
t Stat	1.446927	
P(T<=t) one-tail	0.08134	
t Critical one-tail	1.720743	
P(T<=t) two-tail	0.162681	
t Critical two-tail	2.079614	

t-Test: Paired Two Sample for Means
4 control (coating R11080/18/4)

	Cr	*Cr*
Mean	0.866922	0.885737
Variance	0.001288	0.002006
Observations	24	24
Pearson Correlation	0.079007	
Hypothesized Mean Difference	0	
df	23	
t Stat	-1.671659	
P(T<=t) one-tail	0.054072	
t Critical one-tail	1.713872	
P(T<=t) two-tail	0.108144	
t Critical two-tail	2.068658	

It can be seen from above that there is a significant difference in the means of the creep ratios obtained for exposed coating 1, and exposed coating 3 after 1weeks exposure.

.

11.4.2 7 weeks

t-Test: Paired Two Sample for Means
1exposed (coating R11080/18/1)

	Cr	*Cr*
Mean	0.713989	0.607639
Variance	0.010048	0.011146
Observations	22	22
Pearson Correlation	0.285091	
Hypothesized Mean Difference	0	
df	21	
t Stat	4.051325	
P(T<=t) one-tail	0.000287	
t Critical one-tail	1.720743	
P(T<=t) two-tail	0.000575	
t Critical two-tail	2.079614	

t-Test: Paired Two Sample for Means
1 control (coating R11080/18/1)

	Cr	*Cr*
Mean	0.594145	0.619095
Variance	0.01319	0.009285
Observations	22	22
Pearson Correlation	0.244701	
Hypothesized Mean Difference	0	
df	21	
t Stat	-0.896	
P(T<=t) one-tail	0.190204	
t Critical one-tail	1.720743	
P(T<=t) two-tail	0.380408	
t Critical two-tail	2.079614	

t-Test: Paired Two Sample for Means
2 control (coating R11080/18/2)

	Cr	*Cr*
Mean	0.377085	0.413342
Variance	0.011921	0.008343
Observations	27	27
Pearson Correlation	0.084409	
Hypothesized Mean Difference	0	
df	26	
t Stat	-1.38207	
P(T<=t) one-tail	0.089355	
t Critical one-tail	1.705618	
P(T<=t) two-tail	0.178709	
t Critical two-tail	2.055529	

t-Test: Paired Two Sample for Means
2 exposed (coating R11080/18/2)

	Cr	*Cr*
Mean	0.315735	0.429677
Variance	0.023556	0.014635
Observations	20	20
Pearson Correlation	0.284522	
Hypothesized Mean Difference	0	
df	19	
t Stat	-3.06582	
P(T<=t) one-tail	0.003181	
t Critical one-tail	1.729133	
P(T<=t) two-tail	0.006361	
t Critical two-tail	2.093024	

t-Test: Paired Two Sample for Means
3 control (coating R11080/18/3)

	Cr	*Cr*
Mean	0.485425	0.463678
Variance	0.00689	0.016682
Observations	20	20
Pearson Correlation	-0.12906	
Hypothesized Mean Difference	0	
df	19	
t Stat	0.599245	
P(T<=t) one-tail	0.278044	
t Critical one-tail	1.729133	
P(T<=t) two-tail	0.556088	
t Critical two-tail	2.093024	

t-Test: Paired Two Sample for Means
3 exposed (coating R11080/18/3)

	Cr	*Cr*
Mean	0.509945	0.431821
Variance	0.010158	0.010956
Observations	20	20
Pearson Correlation	0.128154	
Hypothesized Mean Difference	0	
df	19	
t Stat	2.574965	
P(T<=t) one-tail	0.009274	
t Critical one-tail	1.729133	
P(T<=t) two-tail	0.018549	
t Critical two-tail	2.093024	

t-Test: Paired Two Sample for Means
coating 4

4 exposed	*Cr*	*Cr*
Mean	0.953749	0.89956972
Variance	0.003244	0.00184845
Observations	25	25
Pearson Correlation	-0.05902	
Hypothesized Mean Difference	0	
df	24	
t Stat	3.692885	
P(T<=t) one-tail	0.00057	
t Critical one-tail	1.710882	
P(T<=t) two-tail	0.00114	
t Critical two-tail	2.063899	

t-Test: Paired Two Sample for Means

4 control	*Cr*	*Cr*
Mean	0.999629	0.886974
Variance	0.00122	0.001906
Observations	26	26
Pearson Correlation	0.17381	
Hypothesized Mean Difference	0	
df	25	
t Stat	11.27478	
P(T<=t) one-tail	1.35E-11	
t Critical one-tail	1.708141	
P(T<=t) two-tail	2.7E-11	
t Critical two-tail	2.059539	